HEAT TRANSFER IN SEPARATED FLOW

Michael Stephen Holden, B.Sc.(Eng).

November, 1963.

A thesis for the Degree of Doctor of Philosophy in the Faculty of Engineering of the University of London

SUMMARY

This thesis describes an experimental study of the heat transfer distribution developed in regions of separated flow, on bodies travelling at hypersonic speeds. The investigation was carried out in the Imperial College Gun Tunnel at Mach numbers of 7, 10 and 15.

A multi-channel apparatus utilising thin film resistance thermometers together with electrical analogues, was developed for the direct recording of heat transfer rates of between 0.02 and 100 Btu.ft^{-2}sec^{-1}. This apparatus was used initially to measure the heat transfer distributions over bodies in unseparated flow, and these measurements were compared where possible with existing theoretical and experimental information.

Measurements of the heat transfer distribution were made in regions of adverse pressure gradient and flow separation, induced both by forward facing wedges and externally generated shocks. From an examination of the detailed heat transfer distributions obtained, the separation phenomena was shown to be independent of the mechanism by which it was induced, and a separation criteria in terms of the form of the heat transfer distribution, was suggested to distinguish between separated and unseparated flows.

A detailed study was made of the heat transfer distribution developed in the reattachment region of a separated shear layer. Both two-dimensional and axisymmetrical models were used in experiments which sought to investigate the effects of reattachment angle, Mach number, downstream expansion and boundary layer thickness at separation, on the reattachment heat transfer.

The final experimental investigation, the study of heat transfer over spiked bodies, was designed to study the parameters which influenced the protection of aerodynamic surfaces by the use of controlled regions of separated flow. In this investigation the flow pattern and distribution of heat transfer were measured

over spiked spheres, flat ended cylinders, and a family of cones, at Mach numbers of 10 and 15.

The work concludes with a comparison between the experimental separated flow measurements and theoretical calculations based on simple approximations for the separated flow field.

ACKNOWLEDGEMENTS

The author wishes to thank Mr. J. L. Stollery and Mr. B. J. Belcher for their help and guidance. Thanks are also due to members of the gun tunnel group and workshop staff, and in particular to Mr. D. A. Needham with whom the investigation into incipient separation was performed conjointly. Lastly I should like to thank my sister Anne for her help with the typing of this thesis and previous papers.

LIST OF CONTENTS

LIST OF ILLUSTRATIONS

LIST OF NOTATION

A	defined by the equation $U_e = AX$
A	open loop gain of an amplifier
A_G	gauge area
A_F	gain of an amplifier with feedback
a	speed of sound
C	capacitance
C	defined by the equation $\sqrt{\frac{t_w}{t_o}} \cdot \frac{(t_o + 200°F)}{(t_w + 200°F)}$
c	specific heat
c_f	skin friction coefficient
c_p	specific heat at constant pressure
D	body diameter
$E(t)$	voltage change across the thin film gauge
E_o	steady voltage across the thin film gauge
f	frequency
f	u/u_e
$f_{f(P)}$	transform of surface temperature
g	dimensionless total enthalpy H/H_e
H	total enthalpy
H_{1+2}	boundary layer form factor $(\delta^*/\theta)_{1+2}$
h	specific enthalpy
I_o	steady current through the thin film
j	$\sqrt{-1}$
K	thermal conductivity
k	thermal diffusivity
$\mathcal{L}( )$	Laplace transform
L	spike length
L_e	Lewis - Semenov number
l	gauge thickness
l	length of shear layer
M	Mach number
N	pressure gradient parameter defined in section 4.6.3.
N	$\rho\mu/\rho_e\mu_e$
N	reattachment parameter $(P_R - P_2 / P_3 - P_2)$
Nu	Nusselt number
n	θ_2/θ_1
P_r	Prandtl number
P	pressure
p	Laplace transform variable
Q	total heat transfer
q	heat transfer rate
R	resistance
R_o	steady resistance of the thin film gauge
R	radial distance
R_e	Reynolds number
r_o	radial co-ordinates.
S	$\left(\frac{h}{h_o} - 1\right)$
S_t	Stanton number
s	surface dimension

T temperature
t time
U transformed velocity component in X direction
u velocity component in the x direction
V voltage
V transformed velocity components in Y direction
v velocity component in the x direction
X transformed x co-ordinate
x rectangular cartesian co-ordinate in the free stream direction
Y transformed y co-ordinate
y rectangular cartesian co-ordinate normal to the surface

α temperature coefficient of resistance
α angle of the shock generator relative to the free stream
β reattachment angle
β pressure gradient parameter in the boundary layer momentum equation
γ specific heat ratio for a perfect gas
δ boundary layer thickness
δ^* boundary layer displacement thickness
η transformed y co-ordinate in the boundary layer
θ wedge angle relative to the free stream
μ coefficient of viscosity
ν kinematic viscosity
ξ transformed x co-ordinate in the boundary layer
ρ density
τ dummy time variable
τ time constant t/RC
τ wall shear stress
ϕ u/u_2
ψ stream function
ω angular velocity
ω defined by the equation $\frac{\mu}{\mu_0} = \left(\frac{T}{T_0}\right)^{\omega}$

SUBSCRIPTS

0 zero time or position
1 values in the inviscid flow before separation
2 values in the inviscid flow above mixing region
3 values in the inviscid flow after reattachment
B backing material
e conditions at the outer edge of the boundary layer
f sensor
i conditions on the dividing streamline
i incipient separation conditions
l conditions below the dividing streamline
o stagnation conditions
r, AW recovery conditions
R reattach conditions
s conditions immediately downstream of a shock
u conditions in the shear layer above the dividing streamline
$*$ reference conditions

INTRODUCTION

1.1. Scope and Purpose of the Investigation

At low speeds, regions of separated flow are often unsteady and generally their effect is detrimental to the performance of the aerodynamic surface upon which they occur. At supersonic and hypersonic speeds however, such regions become increasingly stable, which together with the increased stability of the laminar boundary layer at high Mach numbers, has produced a situation in which there exists a strong possibility of accurately predicting the occurrence, extent and properties of these regions.

The predominance of laminar boundary layers at hypersonic speeds, and the comparative ease with which such boundary layers will separate, has made separation criteria and the properties of separated zones of great importance. An accurate knowledge of data relating to the separation and properties of laminar separated regions, is essential for the design of compression surfaces such as intakes, nozzles, flaps and flared junctions.

Flared and flapped surfaces are often used to control the drag and stability of hypersonic vehicles. The adverse pressure gradients induced at the junctions between the surfaces often causes flow separation, and the heat transfer developed in the reattachment region of the separated shear layer may cause serious heating problems. Very little is known about the parameters which influence the heating in the reattachment region, and there is almost a complete absence of theoretical and experimental information, even relating to characteristics of an unseparated flow passed a body-flap junction.

In recent years there have been suggestions that controlled regions of laminar separated flow may be used to obtain desired heat transfer, skin friction and pressure characteristics over aerodynamic surfaces. Theoretical studies have shown that the

total heat transfer to the boundaries of a laminar separated cavity flow, is less than the heat transfer to the boundary of an equivalent attached flow bridging the cavity. This study has initiated experiments which have centred around the use of spiked blunt bodies to investigate the practical significance of such results.

The following work was undertaken to investigate the general topic, heat transfer in separated flows, but with particular emphasis on the subjects mentioned briefly above. When the work was commenced, there was no record of a successful technique to measure accurately the large range of heat transfer rates which occur in regions of separated flows in a gun tunnel. After a study of various heat transfer measurement techniques had been made, the thin film technique was selected and used successfully to measure the heat transfer to models in unseparated flow. The mechanism of heat transfer to regions of adverse pressure gradient and moderately separated flows was investigated, and an attempt was made to distinguish between flow separation and boundary layer thickening. A study was then made of the heat transfer distribution in regions of shear layer reattachment, and measurements were made on two-dimensional and axisymmetric models to investigate the effect of Mach number and body shape on this phenomena. Spiked sphere and cone models were used to investigate the protection of aerodynamic surfaces by the use of controlled regions of separated flow. These experimental results were compared, where possible, with existing experimental data and approximate theoretical calculations.

1.2. A Review of Literature Relevant to the Study of Heat Transfer in Separated Flows

The shape and size of a separated flow is controlled primarily by the flow mechanism in the separation and reattachment regions and by the wall geometry. In the simplest cases, such as the flow past a cut-out, the wall geometry determines the size and shape of the separated region by fixing the separation and reattachment points on the lip of the cavity. The geometry of separated regions caused by a shock incident on a flat plate, or induced by a flared junction, is however determined by the conditions in the separation and reattachment regions, together with mass balance conditions in the mixing region. Flows in which either the separation or reattachment points are fixed geometrically, such as in forward or backward facing steps, constitutes a mixture of the two types of flow. Rogdonoff (1962) identified the two basic types of separated regions as "cavity flows", and "wedge separated flows", with the third type classed as a "mixed separated flow".

The most important single characteristic, which has been found to influence the occurence, extent and properties of a separated flow, is the condition of the boundary layer; that is to say whether it is laminar, turbulent or a combination of both during the interaction. The importance of this factor prompted Chapman, Kuhen and Larson (1957) to further classify separated flows into three types; (1) pure laminar in which the separated shear layer is laminar, with transition occurring well downstream of reattachment; (2) transitional separated flow, where transition from laminar to turbulent flow occurs in the separated shear layer between the separation and reattachment points, and (3) wholly turbulent flow where the transition point occurs upstream of the point of separation.

At supersonic and hypersonic speeds the separation of a boundary layer is associated with the phenomena of shock wave-boundary layer interaction. Both the experimental and theoretical work in this

field has been concerned with the investigation of the shock wave-boundary layer interaction, resulting from an external shock incident on a tunnel wall or flat plate, or induced by a forward facing wedge or compression surface. Early experimental work in this field was made by Liepmann, Roshko and Dhawan (1951), Gadd, Holder and Regan (1954), Gadd and Holder (1957) and Chapman, Kuehn and Larson (1957). The primary objects of these investigations was the study of the mechanism of boundary layer separation, and the criteria which governed the incipient separation of both laminar and turbulent boundary layers. The results from these experiments showed that boundary layer transition had a large effect on both the pressure rise to cause incipient separation, and on the size, shape and properties within the separated region. Turbulent boundary layers were found to withstand far larger adverse pressure gradients before flow separation occurred, and whilst laminar interactions were found to occupy regions of the order of a hundred boundary layer thicknesses in length, a turbulent interaction occupied a region of the order of ten boundary layer thicknesses, for the same agency inducing separation.

The properties within separated regions, such as pressure, skin friction and heat transfer, were found to be entirely different for laminar and turbulent flows. The heat transfer, which was found to decrease in a laminar separation region, was found to increase in a turbulent separated flow. An examination of the schlieren photographs and pressure distributions, obtained from the experimental study of flow separation, induced both by forward facing wedges and externally generated shocks, revealed that the phenomena of boundary layer separation was a "free interaction", i.e. independent of the mechanism by which it had been induced.

The effect of Reynolds number and Mach number on the shock strength and pressure coefficient to cause the incipient separation of laminar boundary layers has been investigated more recently by Hakkinen, Greber, Trilling and Abarbanel (1959) and Sterrett and

Emery (1960). Hakkinen et.al examined the interaction of an externally generated shock with a boundary layer on a flat place, with pressure and skin friction measurements. The incipient separation condition, which was determined by measuring the skin friction and pressure distribution, was found when the skin friction at one point only was zero. Sterrett and Emery found the incipient separation point by observing an inflection in the pressure profiles over wedges. Both Hakkinen et.al and Sterret and Emery found their experimental results in good agreement with the separation criteria deduced in a theoretical study by Chapman et.al (1957). Sterret and Emery also found that for curved compression surfaces, much greater adverse pressure gradients could be withstood before flow separation occurred.

The effect of heat transfer on the separation of a boundary layer has been examined experimentally by Gadd (1960), Gadd and Attridge (1961) and Ferguson and Schaefer (1962). In these experiments the wall-to-free stream temperature was varied to effect a change in heat transfer, and separation was promoted by a step or flare. These experiments have demonstrated that the pressure gradient needed to cause separation increases with wall cooling, and that the length of the separated region decreases with wall cooling. Although pressure and skin friction measurements have been made in small regions of wedge separated flows, there is almost a total absence of detailed heat transfer data for both unseparated flows in regions of adverse pressure gradient and moderately separated flows.

The theoretical study of wedge separated regions is complicated by the fact that the boundary layer approximations to the Navier-Stoke's equations, ignore the existence of a pressure gradient normal to the flow in the boundary layer. In the separation and reattachment regions of a separated shear layer this assumption is badly in error. Recently the classical momentum - integral method of Von Karman has been used to investigate the properties in regions

of shock induced boundary layer separation. Two forms of this relationship are embodied in the Crocco-Lees (1952) method and the Pohlhausen method as used by Curle (1960). A modified form of Crocco-Lees was developed by Glick (1960) to investigate thin regions of shock-induced wedge separated flows. Although this method gave good agreement with the experimental results of Chapman et.al for the pressure distribution in a separated region, the complexity of the numerical calculations required to analyse a separated flow field were lengthy. The Crocco-Lees method was compared with a Pohlhausen solution for the case of shock induced separation by Bray, Gadd and Woodger (1960). Bray et.al concluded that the relative complexity in applying the Crocco-Lees method compared with the Pohlhausen method, did not justify the slightly more accurate solution obtained. The Pohlhauson method has also been used to examine pressure and skin friction distribution in moderately separated flows by Bloom (1961) and Curle (1962). There are no solutions for the distribution of heat transfer in wedge separated flows.

The size and shape of a wedge separated region is controlled primarily by the flow mechanism in the reattachment region. A knowledge of the pressure rise to reattachment, the pressure distribution in the reattachment region, and the condition of the reattaching shear layer is essential before the shape and size of a free separated zone can be predicted. The basic flow mechanism in the reattachment region of a separated shear layer was described by Chapman (1956). Briefly, Chapman considers the recirculating flow in the separated region to be confined between the external flow and the body surface, by a dividing streamline which stretches between the separation and reattachment points. The external flow can only influence the flow in the separated region by momentum and energy transfer. The fluid flowing in the shear layer experiences a pressure rise as it approaches the reattachment region. The part of the shear layer below the dividing streamline does not possess sufficient kinetic energy to negotiate the reattachment pressure

rise and is reversed into the separated region, whilst the flow above the dividing streamline continues downstream. Chapman assumes the compression process in isentropic, and thus the flow will reattach when the total pressure on the dividing streamline is equal to the static pressure just downstream of the point of reattachment. The pressure rise from ahead of the separation point to a point just downstream of reattachment is determined by the wall geometry and the conditions in the free stream. Further experimental work has indicated that reattachment may take place at a pressure between the plateu pressure and the final downstream pressure. Cooke (1963) makes the assumption, (based on experimental evidence of Hakkinen et.al), that for a laminar shear layer the reattachment takes place midway between the plateu pressure and the pressure just downstream of the end of the reattachment pressure rise. Nash (1962) suggests that the reattachment point for a turbulent shear layer occurs one third of the way up the reattachment pressure rise. Precise experimental data on this important problem has yet to be obtained.

An important method for the prediction of the scale of a wedge separated region and mixed interaction, was made in a theoretical study by Cooke (1963). Cooke, by considering the development of the velocity along the dividing stream, from its initial value of zero at separation, to a value sufficient to make its total pressure equal to the reattachment static pressure, was able to predict the scale of the interaction. Good agreement was obtained with the results of Ginoux (1960).

The reattachment region is also of the greatest importance in the study of heat transfer in separated flows, for it is in this region that the highest heat transfer rates in the separated zone are developed. Chung and Viegas (1961) have derived a theory for the heat transfer rate in the reattachment zone of a two-dimensional laminar boundary layer in a cavity separated flow. An interesting result of their investigation is the prediction that the heat transfer rates developed at the reattachment point of a reattaching

shear layer could be greater than twice those found at the stagnation point of a body, whose radius of curvature at this point is equal in length to the shear layer. There was very little experimental evidence with which this result could be compared, but it is clear that the development of large heat transfer rates at reattachment points would have an important bearing on the design of hypersonic vehicles, where laminar separated regions may occur either by accident or design.

The heat transfer to a separated cavity flow was analysed theoretically by Chapman (1956). Using the mixing theory which he developed earlier, (Chapman 1949), Chapman predicted that the total heat transfer to the boundaries of a laminar separated cavity flow, was approximately 0.56 of the heat transfer to the boundary of an equivalent attached flow bridging the cavity. This ratio was found to be practically independent of both Mach number and Reynolds number. Chapman based this analysis on four main assumptions; the shear layer at separation has zero thickness, the shear layer thickness is small compared with the depth of the cavity, the pressure throughout the mixing region is constant, and wall temperature is constant and equal to the temperature at the inner edge of the mixing layer. The analysis was extended to turbulent flow, for which it was found that the overall heat transfer was increased for Mach numbers below four, whilst at high Mach numbers it was slightly diminished. Chapman also considered analytically the case of fluid injection in the separated flow, and concluded that both the heat transfer and skin friction in the cavity could be substantially reduced by moderate rates of fluid injection.

Chapman's predictions for the heat transfer to laminar cavity flow without fluid injection were verified experimentally be Larson (1958). Larson investigated the laminar heat transfer to the walls of both two-dimensional and axisymmetric cavities at a Mach number of 4. He found the experimental results to be in good agreement with Chapman's theoretical results. Further work in

turbulent flow verified Chapman's prediction that a turbulent separated layer would cause an increase in total heat transfer to the cavity, but this increase was less than the predicted value.

The detailed structure of a turbulent separated cavity flow was investigated experimentally by Charwat, Dewey, Roos and Hitz (1961). In this work the pressure and velocity fields in two-dimensional notches of various geometries were examined at a Mach number of 2.4. It was discovered that, depending on the geometry of the notches, the flow either bridged the cavity (defined as an open cavity) or the shear layer would reattach on the base of the cavity and then separate again (defined as a closed cavity). An empirical relationship was obtained to predict the type of flow for a given notch geometry. These experiments indicated the complex structure of cavity flows and showed that such flows may be unsteady. Similar studies on the turbulent flow in notches were made by Thomann (1958) and Johannsen (1955) confirm and amplify the experimental work of Charwat et.al.

Bogdonoff (1962) has investigated experimentally the laminar heat transfer to an annular cavity in the surface of a cone, at a Mach number of 11.7. The results from the heat transfer distribution inside the cavity agreed with Chapmans analysis, but an increase in the heat transfer downstream of the cavity caused the total heat transfer to the cone was increased. Bogdonoff noted that a large increase in heat transfer above the corresponding cone value occurred in the reattachment region at the back of the cavity.

The flow past forward or rearward facing right angle steps cannot be classified into either the free interaction or cavity flows which have been previously discussed. In these cases either the separation or reattachment point is fixed geometrically, whilst the size and shape of the separated region is determined by the separation or reattachment criteria previously discussed. Heat

transfer measurements in the separated region induced by a two-dimensional forward facing step have been made in turbulent flow by Gadd and Holder (1959) and Thomann (1958) at Mach numbers of 4 and 1.8 respectively. In direct contrast to the laminar flow case Gadd et.al and Thomann found that the presence of the step caused an increased in the heat transfer to the flat plate, in the region of boundary layer separation. Naysmith (1962), Thomann (1958), and Seban, Emery and Levy (1959) at Mach numbers of 4, 1.8 and 1.2 respectively, investigated the turbulent heat transfer distribution in the separated region behind a rearward facing step. All these experiments indicated that low heat transfer rates were developed in the separated region just behind the step. Naysmith, using a densely instrumented model, and taking precautions to minimise the conduction along the skin of the model, detected a very sharp and pronounced peak at reattachment, while the other experiments indicated that the heating rates in the reattachment region were not severe. By this investigation Naysmith underlined the importance of dense instrumentation and the minimisation of surface conduction in an experimental study of separated flows.

The heat transfer distribution in regions of separated base flows over axisymmetric blunt bodies has been investigated by Rabinowicz (1955) and Powers, Stetson and Adam (1959). Rabinowicz measured the turbulent heat transfer over the flat base of a pedestal mounted body and found large heat transfer rates to occur in the centre of the base, as might be anticipated because of the existence of a stagnation point in this region. Powers et.al measured the heat transfer rates in a separated region developed on a hemisphere-cylinder followed by a step down to a cylinder of smaller diameter, the axisymmetrical counterpart of the two dimensional step. The form of the heat transfer distribution was similar to those obtained for the equivalent two dimensional configuration, but the model was insufficiently instrumented to give the heat transfer profile in the reattachment region.

Carlson (1959) has used the momentum - integral method to obtain an approximate theoretical analysis of the heat transfer in a constant pressure separated wake region. The theoretical results were in good agreement with the experimental results of Powers et.al. However, the experimental velocity and temperature distributions obtained by Hitz et.al for rearward facing steps, indicated that Carlson's polynomial model for the separated velocity profiles was seriously in error. Carlson's method therefore rests on its agreement with Powers et.al. It is the only theoretical method yet available to predict the distribution of heat transfer in a constant pressure separated region.

The study of the separated flow over axisymmetric spiked bodies has been designed primarily to investigate the possibility of using such flows to obtain desirable aerodynamic and heat transfer characteristics. Early experimental work in this field by Moeckel (1951), Beastall and Turner (1952), Mair (1952), and Jones (1952), at Mach numbers between 1.2 and 2 was concerned primarily with the measurement of pressure and drag over spiked hemispherically capped and flat-ended cylinders. The additon of the spike caused a large reduction in drag to these bodies and the magnitude of this drag could be varied by varying the spike length. In the investigations of the flow over the spiked flat ended cylinders both Beastall and Turner, and Mair discovered an oscillational instability of the flow for short spike lengths. The instability of the separated flow past a spiked flat-ended cylinder was further investigated by Maull (1960), at a Mach number of 6.8 and Reynolds number of 0.85×10^5. Maull investigated the effect of model configuration in the reattachment region on the stability of the separated zone. He suggested an empirical criteria for the prediction for the onset of instability, as well as discussing the mechanism of the oscillation which then results.

The separated flow over spiked cones at Mach 10 was examined in a photographic investigation by Wood (1960). Wood found that five different types of flow occurred over the spiked cone configuration, depending on the cone angle and length of spike. For blunt cones with short spikes, Wood confirmed, (with some reservations on the interpretation of the photographic results), Mudl's conclusions on the occurrence and mechanism of the oscillatory instability. For slender cones Wood found that spikes were unable to induce flow separations. The remaining intermediate flow configurations induced flow separation on the spike with reattachment on the conical face or at the cone - cylinder junction. Wood suggested that the configuration with shoulder reattachment might be of the most practical importance for the reduction of drag and heat transfer. Using a modified form of the separation relationship developed by Hakkinan et.al, with a correction term for spike transverse curvature, Wood developed a semi-empirical relationship between the separation angle and spike length, which can be used to predict the flow geometry for configurations with shoulder reattachment.

Stalder and Nielson (1954) were the first to investigate the heat transfer characteristics over a hemisphere sylinder equipped with flow separation spikes. In these experiments, which were conducted at a Mach number of 2.67 and Reynolds number of 0.5 x 10^6 the boundary layers were purely turbulent. It was found that the total heat transfer to the hemisphere was approximately doubled by the presence of the spike regardless of its length. Later Crawford (1959) also investigated the heat transfer to a spiked sphere but at a Mach number of 6.8. By varying the Reynolds number (based on body diameter) from 012 to 1.5 x 10^6 Crawford was able to investigate the pressure and heat transfer distribution for laminar, transitional and fully turbulent shear layer conditions. Crawfords measurements in turbulent flows were in good agreement with Stalder's results, whilst the completely

laminar separated results indicated that the total heat transfer to the spike hemisphere was reduced regardless of spike length. For transitional flow, Crawford found that both the heat transfer and pressure distributions over the hemisphere were markedly affected by the position of the point of transition in the shear layer. Further measurements of pressure and heat transfer to spiked hemisphere-cylinders were made in purely laminar flow by Bogdonoff and Vas (1959) at M = 14 and Re = .36 x 10^6 and by Wagner and Pine (1961) at M = 19.4 and Re = .23 x 10^6. Bogdonoff found that for short spike lengths the total heat transfer to the hemisphere was increased inspite of a fully laminar flow. These experiments reveal an interesting trend for the effectiveness of a spiked in reducing the total heat transfer. At M = 6.8 the ratio of the minimum total heat transfer to the unspiked value was 0.5, at M = 14 this factor was 0.3 and at M = 19.4 the ratio was reduced to 0.1. The drag of the spiked hemisphere (for L/D = 3) was found to be approximately independent of Mach number and constant at approximately one tenth of the unspiked value.

Bogdonoff and Vas also investigated the total heat transfer to the front face of a spiked flat-ended cylinder. Their results indicated that the addition of the spike caused a 50% reduction in the total heat transfer to the front face of the cylinder. In an investigation by Zakkay (1961), the heat transfer distribution over a hemispherically capped cone was measured in regions of separated flow promoted by a blunt spike. Heat transfer coefficients of three times the stagnation point value were recorded in the reattachment zone on the conical surface. Unfortunately Zakkay did not state the condition of the reattaching shear layer, but from the Reynolds number and Mach number of the tests (M = 7.9 and Re = 0.3 - 0.5 x 10^6) it seems probable that the layer was laminar.

Recently Centolanzi (1963) has investigated the heat transfer to blunt concial bodies with cavities to promote separation. These tests, which were carried out at Mach numbers from 4 to 6 and

Reynolds numbers from 0.12 to 0.19 x 10^6, showed that the presence of the cavities changed the distribution of heat transfer considerably from the basic cone value. The large heat transfer rates developed in the reattachment regions caused total heat transfers greater than the unseparated value both in laminar and turbulent flow. For certain configurations the separated flow over the cavity was found to be unsteady.

2. Heat Transfer Instrumentation and Experimental Techniques

2.1. Introduction

All the previous investigations on the subject of separated flows in the Imperial College hypersonic gun tunnel have been confined to photographic studies using shadowgraph and schlieren techniques, which require the minimum of complex electronics. Whilst these methods yield a good qualitative description of the flow it is difficult to deduce quantitative results from these techniques. Even the deduction of the main features of the pressure distribution from schlieren photographs is inaccurate because of the small angles inherent in a high Mach number flow. To examine the flow mechanism of separated flows in more detail, flow properties such as pressure, heat transfer and skin friction distributions must be measured.

The magnitude and distribution of heat transfer is an important factor in the design of vehicles travelling at hypersonic speeds. It is also of particular interest in the study of hypersonic separated flows, as indicated in the previous section. The experimental measurement of heat transfer in regions of separated flow creates special problems implicit in the nature of the separated regions themselves. The large heat transfer gradients in reattachment regions require instrumentation techniques permitting a high density of individual measurements on a surface which will not distort the distribution so obtained, by longitudinal heat conduction. Whilst the instrumentation must be capable of recording a large range of heat transfer rates, it must also be able to make accurate measurements of small differences in heat transfer distribution, as characterised by the study of heat transfer in regions of incipient separation. The stability of separated regions in high Mach number flow is of great interest, particularly with regard to the possibility of the controlled use of these regions. Thus it is essential that the instrumentation technique should be capable of detecting and

following any instability that may arise, and in particular the gross instability which is inherent in the flow about some spiked blunt body configurations.

When this work was begun there was no record of a successful technique for the measurement of heat transfer in a gun tunnel, and so a study was made of the methods available. In this section, a brief review is presented of the heat transfer measurement techniques which have been developed for use in the diverse conditions encountered in a number of short duration hypersonic facilities. The theory and performance of these techniques are discussed.

The major part of this section is devoted to a description of the development of the thin film resistance thermometer, together with an electrical analogue and calibration system for the direct measurement of heat transfer rates between 0.02 and 100 Btu./ft^{2}sec. in a gun tunnel.

2.2. Review of Heat Transfer Instrumentation

2.2.1. Introduction

The advent of intermittent hypersonic testing facilities such as Shock tubes, Shock tunnels, Hot-Shot tunnels and Gun tunnels brought the need for the development of new heat transfer measuring techniques which have response times sufficient to cope with running times of the order of 0.1 to 100 milliseconds. During the period from 1956, to the present day, a number of heat transfer transducers have been developed. Although these transducers are mechanically different, they may all be classified into one of two groups; (a) Surface temperature thermometers or thin-film gauges and (b) Calorimeter or thick-film gauges.

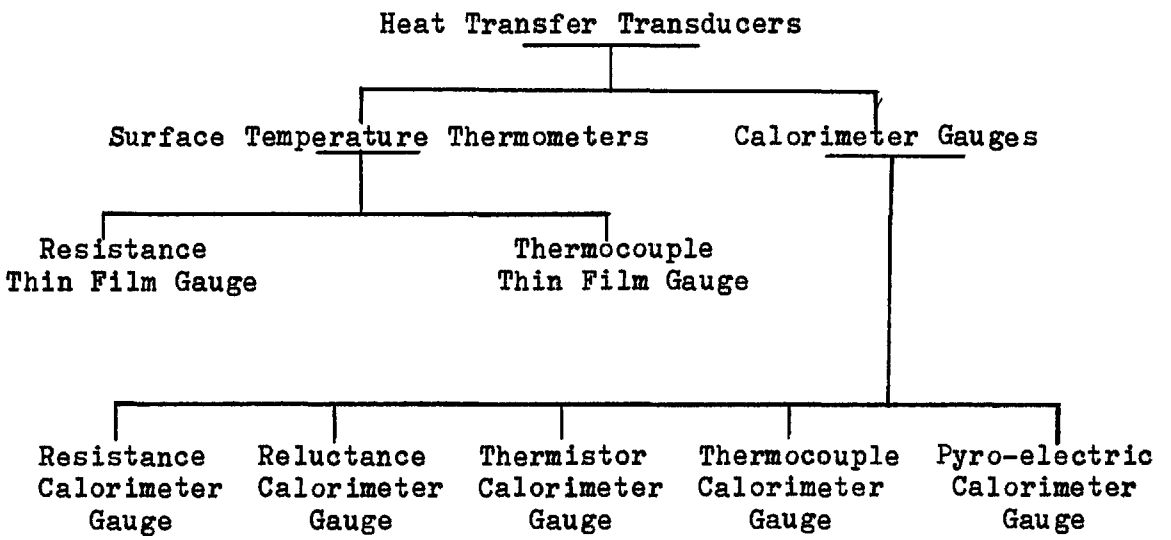

2.2.2. Surface temperature thermometer or thin film gauge

The surface temperature thermometer is composed of a thin film of a good thermal conductor (usually a metallic conductor) deposited on a poor conductor usually of glass or ceramic. The metallic conductor, which must not influence the thermal diffusion through the backing material, must change its physical or electrical

properties with change in temperature so that these properties can be used to indicate the surface temperature of the backing material.

The potential of the thin film thermometer for measuring heat transfer was recognised almost simultaneously at a number of American aeronautical laboratories. Vidal (1956) at Cornell, Emrich and Chabai (1955) at Lehigh, Bershader (1956) at Princeton and Rabinowicz at C.I.T. (1956) all approached the problem of transient heat transfer measurement via the measurement of surface temperature.

Prior to the initiation of these programmes, two successful designs for surface temperature transducers with response times of the order of a microsecond had been developed. Mier (1939) perfected a resistance thermometer comprising of a 2 micron thick gold film deposited on a backing material of aluminium oxide which had a response time of 1 microsecond. Later Hackmann (1941) designed a thermocouple surface temperature thermometer, which was constructed by the deposition of a 2 micron thick film of nickel on a steel wire and had a response time of 1 microsecond. A more refined version of the Hackmann thermocouple was produced by Bendersky (1953), who, by reducing the thickness of the nickel to one micron reduced the response time to a quarter of a microsecond. The thin film resistance thermometer and the thin film thermocouple have remained the basic sensing elements of thin film transducers, and their relative merits are discussed below.

The thermocouple has not proved to be a very successful sensing element and it is not often used as a thin film gauge. Vidal (1956) constructed thermocouples by using two overlapping films of nickel and platinum deposited on a pyrex substrate, but unfortunately they were difficult to construct and gave erratic outputs. Later however, Sabol (1958) successfully developed a thin film thermocouple gauge made by the deposition of overlapping films of nickel and silver on a pyrex substrate.

The resistance thermometer has featured prominently in transient temperature thermometry and heat transfer research for the last five years. The resistance element, which comprises of a single layer of metallic film, is deposited on a substrate which has good electrical and thermal insulation properties. This transducer, which has a good sensitivity and response time, has been successfully used in shock tubes and shock tunnels to measure heat transfer rates between 0.1 and 1,000 Btu./ft^{2}sec.

The thermocouple thin film gauge has the following advantages over the resistance thermometer; (1) The calibration factor is constant for all gauges constructed on backing materials with the same thermal properties, and is unaffected by flow abrasion. (2) The thermocouple does not require an external power supply and hence no energy is generated by power dissipation in the gauge.

The resistance thermometer possesses two main advantages over the thermocouple. (1) It is easier to construct a reliable resistance gauge. (2) A typical resistance thermometer has a sensitivity of ten times that of a corresponding thermocouple gauge.

Surface temperature thermometers have two main disadvantages. (1) The gauges cannot be used to measure heat transfer rates in conditions for which the temperature rise of the backing material causes a change in its thermal properties. This rules out the thin film gauges for measuring typical stagnation heat transfer rates under re-entry conditions in shock tubes (see Rose (1958). (2) Resistance and thermocouple thin film gauges are sensitive to flow abrasion, which may cause errors in the indicated surface temperature and finally lead to the destruction of the gauge. It was because of the failure of the thin film gauge for one or both of the above reasons that the calorimeter gauge was developed.

2.2.3. The calorimeter gauge

The calorimeter gauge consists of a calorimeter element which is backed by a good thermal insulator and equipped with a sensing mechanism which indicates the average temperature of the element. In direct contrast to the surface temperature thermometer, which theoretically has zero thermal capacity, the thermal capacity of the calorimeter element must be such that it retains the heat transferred to it during the recorded running time.

All calorimeter gauges work on the same basic principles and differ only in the mechanism for sensing the average temperature. Consider a calorimeter element of thickness ℓ and thermal properties ρ_F, c_F, K_F (see figure 1). The heat transfer to the gauge is then given by:-

$$q = \rho_F c_F \ell \cdot \frac{d\bar{T}}{dt} + q_B + q_S$$

where

$$\bar{T} = \frac{1}{\ell} \cdot \int_0^{\ell} T \, dy$$

The gauge is designed so that the heat losses q_B and q_S from back and sides respectively are negligible. The sensitivity of the gauge is a function of the thermal capacity of the calorimeter element and the mechanism of the temperature sensing devise. For a given sensing mechanism, the choice of the gauge thickness ℓ is a practical compromise between the accuracy, sensitivity, frequency response and running time of the gauge. In the following paragraphs the performance of a number of calorimeter gauges using different sensing mechanisms are reviewed.

A platinum resistance calorimeter gauge was developed by Rose (1958) to measure high heat transfer rates in a shock tube. Under the conditons encountered in these experiments (heat transfer rates of 10,000 Btu./ft^{2}sec and flow durations 50 microseconds) the large surface temperature rise caused thin film gauges to yield erroneous results because of changes in the properties of gauge and substrate materials. By increasing the thickness of the platinum film from the case where $\ell \ll \sqrt{k_F t}$ to where $\ell \gg \sqrt{k_F t}$ when the film behaves as a

calorimeter element. The change in the electrical resistance of the gauge was used to indicate the average temperature of the calorimeter element. This transducer can measure heat transfer rates greater than 100 Btu./ft^{2}sec, but cannot be used for running times (set by the minimum practical resistance of the calorimeter element) of longer than 1 millisecond.

Platinum thick and thin film gauges were used by Morgan (1961) in attempts to measure heat transfer in a Hot-shot facility. Both these gauges proved unsuccessful; the thin film gauge was melted or erroded away, whilst the resistance calorimeter was of insufficient sensitivity for accurate measurements. Subsequently Morgan developed a calorimeter gauge which utilised the change in the magnetic reluctance of a copper calorimeter situated in a magnetic field to indicate the average temperature of this element. This transducer was used to measure heat transfer rates between 10 and 400 Btu./ft^{2}sec for running times from 25 to 100 milliseconds.

Another form of calorimeter gauge, described by Morgan (1960), was used to measure heat transfer rates below 10 Btu./ft^{2}sec. This gauge is a thermistor bead (a cermic resistance element) which acts both as a calorimeter and temperature sensing element. The thermistor has an output which varies exponentially with temperature and thus its useful range is confined to a small region over which it is approximately linear. Thermistor gauges have been used to measure heat transfer rates between 0.1 and 10 Btu./ft^{2}sec. with an accuracy of $\pm$ 10%, for running times of approximately 10 milliseconds. These gauges have also been used with great success by Miller et.al. (1962) in the Boeing Hot-shot tunnel.

Two laboratories have developed calorimeter gauges which use a thermocouple as the average temperature sensing element. These transducers were developed for use in facilities in which the magnitude of the heat transfer, length of running time, or flow abrasion, precluded the use of the platinum thick or thin film gauge,

or the thermistor gauge. Thermocouple calorimeters are also easier to construct and use than the reluctance gauge. The gauge is constructed by welding or swaging a thermocouple into the back of a calorimeter element, which may form a separate segment or an integral part of the shell of the model. Ledford (1962) developed a transducer which consisted of a copper disc of 0.5 inches in diameter and 0.010 inches thick, supported in a nylon insulator, with a chromel-constantin thermocouple sensing element. This transducer can measure heat transfer rates between 1 and 1,000 Btu./ft^{2}sec for running times for 5 to 80 milliseconds. R.A.R.D.E. have also developed thermocouple calorimeter gauges which form an integral part of the metallic shell of the model, Cox (1960) and Cox and Winter (1961). Although these transducers are easy to construct they cannot be used to make accurate closely spaced measurements in regions of large heat transfer gradients typically found in the reattachment region of a separated shear layer.

A calorimeter gauge which uses a pyro-electric material as both the calorimeter and temperature sensing element has been developed recently by Perls and Hartog (1961). The mechanism of the gauge is slightly different from the calorimeter gauges reviewed above, for when the pyro-electric material is heated it generates an electrical charge which is proportional to its temperature change. When the gauge is connected in series with an external resistor, the current which flows through the resistor, and hence the voltage generated across it, is directly proportional to the heat transfer rate to the gauge. This transducer has been used to record heat transfer rates from 0.1 to 100 Btu./ft^{2}sec for running times of 10 to 50 milliseconds. Unfortunately the gauge is also sensitive to both pressure and acceleration, and further development is in progress to perfect this instrument to obtain an accuracy comparable with other techniques.

2.2.4. Comparison of techniques

The surface temperature thermometer has an inherently higher sensitivity and frequency response than a calorimeter gauge. Although the deduction of the heat transfer from the direct output of the

surface temperature thermometer is more difficult than the corresponding data reduction for a calorimeter gauge, the introduction of analogue networks (see section 2.8.) has made the surface temperature gauge the most sensitive and accurate technique for the flow conditons under which it can be used.

Although resistance calorimeter gauges have been used successfully to measure large heat transfer rates in shock tubes, these transducers cannot be used to measure heat transfer rates below 100 Btu./ft^{2}sec, or for running times of greater than 1 millisecond. Thermistor calorimeter gauges have been used in errosive flows to measure heat transfer rates down to 0.1 Btu./ft^{2}sec for running times up to 20 milliseconds, but as a result of their inherently non linear characteristics these gauges cannot be used to measure heat transfer rates above 15 Btu./ft^{2}sec with an accuracy of better than $\pm$ 10%. A comparison between the performance of the reluctance and thermocouple calorimeter gauges indicates that inspite of the relative complexity of the instrumentation required for the reluctance gauge, the thermocouple gauge has both a larger range (1 - 5,000 Btu./ft^{2}sec) and a faster response. However to achieve this complete range . requires a series of calorimeter elements with different thicknesses. When the design problems have been solved, the pyro-electric gauge will prove extremely useful, for not only does this gauge give an output which is directly proportional to the heat transfer rate, it will also span the range of heat transfer rates from 0.1 to 200 Btu. /ft^{2}sec. which at present requires a series of separate calorimeter gauges.

2.3. Theory of the Thin Film Gauge

2.3.1. Response of a thin film gauge

The thermal response of a thin film backed by a semi-infinite insulator can be determined from classical one-dimensional heat transfer theory, detailed solutions of this problem have been given by Carslaw and Jaeger (1947) and Vidal (1956). The characteristic time for heat to diffuse from the front to the rear surface of a film of thickness l (see figure 1) is a measure of the response time, and may be estimated by replacing the film by an equivalent element composed of discreet thermal capacitance $C_F = \rho_F c_F l$ and thermal resistance $R_F = l/K_F$ (see section 2.8.2). The thermal time constant t_t is then given by

$$t_t = \frac{l^2}{(K_F/\rho_F c_F)} = \frac{l^2}{K_F}$$

where ρ_F, c_F, K_F are respectively the density, specific heat and thermal conductivity of the film material. For film thicknesses typical of those used in the experimental work ($l \doteq 0.2$ microns), t_t was approximately 10^{-9} seconds. This time is far shorter than the shortest times of interest and therefore the temperature gradient through the film can be neglected. Thus the temperature through the film is uniform and equal to the instantaneous surface temperature of the substrate.

2.3.2. Calculation of q from the variation of surface temperature

The problem is analysised by considering the one-dimensional diffusion of heat through a uniform semi-infinite slab. The heat transfer rate q at a depth y and time t is

$$q(y,t) = -K \frac{\partial T}{\partial y}$$

The heat transfer across a parallel plane at $(y+dy, t)$ is given by

$$q(y+dy, t) = -K \frac{\partial}{\partial t}\left[T + \frac{\partial T}{\partial y} dy\right]$$

The difference in the flow across the plane is the rate of absorption of the heat by the element of thickness dy thus

$$q_y - q_{y+dy} = K \frac{\partial^2 T}{\partial y^2} dy = \rho c \, dy \frac{\partial T}{\partial t}$$

$$\therefore \quad \frac{\partial T}{\partial t} = \left(\frac{K}{\rho c}\right) \frac{\partial^2 T}{\partial y^2} \quad \text{the thermal diffusion equation} \qquad \ldots\ldots 2.3.1.$$

To obtain q in terms of the surface temperature rise T_s we have to solve equation 2.3.1., where T is the temperature rise from the initial value at time $t = 0$. The appropriate boundary conditons are:

$$T(0,t) = T_s$$

$$T(y,0) = 0$$

$$\lim_{y \to \infty} T(y,t) = 0$$

Using the Laplace transform technique equation 2.3.1. becomes

$$pT(y,p) = \frac{K}{\rho c} T_{yy}(y,p)$$

where $\quad T(0,p) = f(p)$

and $\quad q(0,p) = K T_y(0,p)$

then $\quad q(p) = \sqrt{\rho c K} \cdot \sqrt{p} \cdot f(p) \qquad \ldots\ldots 2.3.2.$

since $\quad \mathcal{L}\left(\frac{1}{\sqrt{\pi t}}\right) = \frac{1}{\sqrt{p}} \qquad p f(p) = \mathcal{L}\left[T'(t) + T(0)\right]$

therefore $\quad q(p) = \sqrt{\rho c K}\left[\frac{T(0)}{\sqrt{p}} + \mathcal{L}\left\{T'(t) + T(0)\right\}\right]$

This may be transformed into

$$q(t) = \frac{\sqrt{\rho c K}}{\sqrt{\pi}}\left[\frac{T(0)}{\sqrt{t}} + \int_0^t \frac{T'(t-\tau)\,d\tau}{\sqrt{\tau}}\right]$$

or inverting the second term

$$q(t) = \frac{\sqrt{\rho c K}}{2\sqrt{\pi}}\left[\frac{2\,T_s(t)}{\sqrt{t}} + \int_0^t \frac{T_s(t)^{1/2} - T_s(\tau)^{1/2}}{(t-\tau)^{3/2}} d\tau\right]$$

$\ldots\ldots 2.3.2.$

Thus by recording the variation of surface temperature $T_s(t)$ with time during a run, it is possible to deduce the heat transfer q at any time during the run, by the graphical or numerical integration of equation (2.3.3.). For a constant heat transfer rate equation (2.3.3.) simplifies to:-

$$q = \sqrt{\rho c k} \cdot \frac{\sqrt{\pi}}{2} \cdot \frac{T_s(t)}{\sqrt{t}} \qquad \ldots\ldots 2.3.4.$$

which may be evaluated immediately from the temperature - time history.

2.4. Preparation of Thin Film Gauges

The metallic resistance element is commonly made from a thin film, of gold, platinum, rhodium or chromium; the relative merits of the properties of films produced from these metals are discussed by Winding, Topper and Baus (1955). In the present work resistance elements of platinum were used. Suitable backing materials which are in common use are soda glass, quartz and Pyrex (bora-silica) glass. A Pyrex substrate was used for all gauges in this investigation because of the consistency of its thermal properties and the ease with which it could be blown, moulded and ground.

There are three methods in common use for the deposition of metallic films; these are evaporation (Chabia 1955), sputtering (Rabonowicz 1956) and the painting technique, (Vidal 1956). Although the sputtering technique produces a gauge with a better metal-to-glass bond than evaporation deposition, neither method produces a gauge with good resistance to abrasion. Improved abrasion characteristics are achieved by heating the gauges to the softening temperature of the substrate, thereby allowing a certain amount of diffusion of the film material into the substrate. Evaporation and sputtering techniques have the advantage that they produce metallic films of accurately controlled thickness and surface dimensions, but masking problems make their use difficult on sharply curved surfaces. Film deposition by the use of the painting technique is a simple and effective method in which a metallic powder held in suspension in an organic solvent,

is applied to the model with a brush, air spray or ruling pen. The painting technique was used to prepare all the resistance elements used on the models in the present experimental work. A detailed description of the preparation of the gauges and models used in this investigation is given in Appendix 1.

2.5. Electronic Instrumentation

2.5.1. Introduction

A great deal of time and effort was devoted to the development of the electronic measuring and calibration equipment. Heat transfer measurements in the range 0.02 - 100 Btu./ft^{2}sec were made during the experimental investigation. The measurement of low heat transfer rate (< 0.5 Btu./ft^{2}sec) required particularly refined instrumentation.

The electronic instrumentation is based on a completely "differential system", and thus electrical noise resulting from common mode electrical interference or mechanical vibration is reduced to a minimum.

The instrumentation is divided into the following sections.

A. Signal Circuits

(a) The energising circuit for the thin film resistance element (figure 5)

(b) Amplification circuit (figure 6)

(c) Analogue and recording circuits (figure 10).

B. Calibration Circuits

(a) Pulse calibrator circuit (figure 7)

(b) Electronic calibrator circuit (figure 13)

2.5.2. Signal Circuits

(a) The energising circuit for the thin film resistance element

The thin film gauge is used in a Wheatstone bridge network as shown in figure 5. The resistance element is energised by a constant current of between 5 and 20 milliamps, depending on its resistance, so that a standing potential of between 0.5 and 1 volt is established across the gauge. A large resistance in series with the film maintains a constant current through the gauge.

The stabilised power supply had a terminal voltage of 250 volts and noise content of approximately 200 μV. For a standing potential across the gauge of 1 volt the electrical noise across the film is therefore 0.8 μV , a figure which is comparable with the Johnson noise for a typical film of approximately 0.7 μV ..

The resistance of the film can be assumed to vary linearly with temperature over the range of application, thus

$$R = R_o [1 + \alpha (T - T_o)]$$

Hence the increase in resistance ΔR for a change in gauge temperature T_s is given by $\Delta R = \alpha . R_o . T_s$

and the change in voltage across the thin film gauge E(t)

$$E(t) = I_o \Delta R = \alpha E_o T_s \qquad \ldots . \text{ 2.5.1.}$$

The voltage E(t) appears as an out-of-balance voltage across the arms of the Wheatstone bridge.

For the lowest heat transfer rates measured(0.02 Btu/ft^{2}sec) a standing voltage of approximately 0.5 volts was applied to the gauge (film resistances were approximately 100 Ω). The effect of the electrical power dissipation on the heat transfer indicated by the gauge was checked by doubling the standing voltage across the gauge and found to be negligible.

(b) Amplification circuits

For low heat transfer rates the output of the heat transfer gauges required additional amplification before they could be displayed upon the oscilloscope. The Tektronix 502 oscilloscope used to record the output of the gauges had a maximum sensitivity of 200 $\mu V/cm$. An overall sensitivity of 8$\mu V/cm$ was required for a system using electrical analogues, to record heat transfer rates down to 0.02 Btu./ft^2sec.

As the purchase of commercial low noise differential amplifiers of the required specifications was not possible, a considerable amount of time and effort was devoted to the development of a suitable differential amplifier. After a large number of both valve and transistor circuits had been designed and tested, a transistor differential amplifier, (shown in figure 6), was developed and successfully tested. The amplifier, which has a gain of 25 and a bandwidth 0 to 50 Kc/s was designed specifically for use in the heat transfer apparatus. The input to the amplifier is directly connected to the Wheatstone bridge and can be used at a D.C. potential between 0 and -2 volts relative to earth. The output of the amplifier, which was at earth potential, was matched so that it could be directly connected to the input of the analogue network. All the transistors in the amplifier were mounted in a copper block and the electrical drift and noise level at the output was minimised by packing the space between the circuit board and the metallic screening with an insulation material.

The experience so far obtained with the transistor amplifiers indicates that they are extremely stable, and the maximum change in gain over a period of 4 months was only 2%.

c. Analogue networks

To evaluate the heat transfer to the thin film gauge directly from its output a lengthly integration has to be performed either graphically or numerically at each selected time interval (see

section 2.7.). The integration is tedious and time consuming and even if carried out by a computor there is an undesirable delay between testing and data reduction. The problem has been solved by the use of electrical analogues. By feeding the out-of-balance voltage from the signal bridge, directly or via a pre-amplifier, into an analogue network, an instantaneous and continuous record proportional to the heat transfer is obtained from the analogue output. The two types of analogue networks used in the electronic instrumentation are shown in figure 10.

2.5.3. B. Calibration Circuits

(a) The pulse calibration apparatus

The pulse calibration apparatus is used to determine $\alpha/(\rho c K)^{1/2}$ the calibration constant of the heat transfer gauge and A* the calibration constant of the analogue. The circuit of the pulse calibrator is shown in figure 7.

The gauge, which is situated in one arm of a Wheatstone bridge network, is heated by electrical dissipation from the discharge of a large capacitor in series with the bridge. The time constant of the circuit is sufficiently long for the current through the gauge to be sensibly constant for 2 milliseconds. With the switch K in position A (see figure 7), a small current is passed through the bridge network to enable the bridge to be carefully balanced. Upon switching to position B, the power supply is switched out of the bridge circuit to prevent 50 cycle interference, and then a mercury switch is activated so that it discharges the large capacitor through the bridge circuit. The circuitry was carefully designed to eliminate initial transients when the capacitor was discharged. A description of the data reduction to determine $\alpha/(\rho c K)^{1/2}$ and A* from the pulse apparatus is given in section (2.6.1.) and (2.9.1.) respectively.

(b) Electronic calibrator unit

The Electronic Calibrator was designed to simulate electronically the response of a thin film gauge to a constant heat transfer rate. A circuit diagram of the apparatus is shown in figure 9. The physical properties of the film, its resistance and temperature coefficient, and the thermal constant of the substrate, can be simulated together with the gauge current and required heat transfer rate, so that the apparatus generates an output voltage equal to that obtained from the signal bridge in which the simulated gauge is situated. The calibrator unit is used to calibrate the entire heat transfer recording system, so that the magnitude of the deflection on the face of the oscilloscope obtained from a tunnel run, can be interpreted directly in terms of a calibration trace obtained from the calibrator unit. A description of the design and operation of the calibrator is given in section (2.9.3.).

2.6. Calibration of Thin Film Gauges

The expression $\alpha/(\rho c K)^{1/2}$ is known as the calibration constant of the thin film gauge and must be determined for each gauge before the heat transfer rate can be evaluated from the gauge output. The calibration constant can be determined by evaluating $\alpha/(\rho c K)^{1/2}$ as a complete factor by using the pulsing technique, or by determining α and $(\rho c K)^{1/2}$ separately.

2.6.1. Determination of $\alpha/(\rho c K)^{1/2}$ by the pulsing technique

The gauge is calibrated by discharging a constant current through it and thereby subjecting it to a constant heat transfer rate. For a gauge of resistance R_o subjected to a constant current I_o, the heat dissipated in the film is $I_o^2 R_o/1.13$ Btu./ft^2 sec. The heat transfer to a gauge of area A_g is therefore $q = I_o^2 R_o/1.13 A_g$. The gauge is situated in a Wheatstone bridge, as described in section 2.5.2. and therefore the heating causes an out-of-balance voltage to appear across the bridge. For the resistances as shown in figure 7

the out-of-balance voltage is given by

$$\Delta V = \frac{V \cdot R_3 \cdot \Delta R_0}{(\Delta R_0 + R_0 + R_3)(R_3 + R_0)}$$

therefore since ΔR is small compared with R_0

$$\Delta R = \frac{\Delta V}{V} \cdot \frac{(R_0 + R_3)(R_2 + R_1)}{\left[R_2 - \frac{\Delta V}{V}(R_2 + R_1)\right]}$$

also $$I_0 = \frac{V_c^2}{\left[R_0 + R_2 + R_c\left(\frac{R_0 + 3R_2}{2R_c}\right)\right]}$$

and $$q = \frac{I_0^2 R_0}{1.13 A_G} = \frac{V_c^2}{\left[R_0 + R_2 + R_c\left(\frac{R_0 + 3R_2}{2R_2}\right)\right]^2} \frac{R_0}{A_G}$$

For a linear resistance - temperature relationship

$$\Delta R = \alpha R_0 (T - T_0)$$

From equation (2.3.4.)

$$q = \frac{\sqrt{\pi}}{2} \left(\frac{\sqrt{\rho c K}}{\alpha}\right) \frac{\Delta R_0}{R_0 \sqrt{t}}$$

Therefore $$\frac{\alpha}{\sqrt{\rho c K}} = \frac{\sqrt{\pi}}{2} \cdot \frac{1.13}{I_0^2 R_0^2} \cdot \frac{\Delta R_0}{\sqrt{t}}$$

For $R_0 = R_1 = R_2 = R_3$: $\Delta R_0 = \frac{4 R_0 \Delta V}{V}$

and $$\frac{\alpha}{\sqrt{\rho c K}} = \frac{1.13}{2 V_0^3} \left(\frac{4}{R_0}\right)\left(\frac{\Delta V}{\sqrt{t}}\right) \cdot (R_0 + 3R_c)^3 A_G$$

. . . . 2.6.1.

The variation of the out-of-balance voltage ΔV is displayed on an oscilloscope and recorded on Land-Poloriod film. The factor $\Delta V/\sqrt{t}$ is evaluated by measurements of the slope of the graph of ΔV^2 versus t deduced from the oscilloscope trace, which, since the output of bridge varies parabolically with time, is a straight line.

The area of gauges mounted upon flat or slightly curved surfaces were determined from planimeter measurements from enlargements of photographs of gauges situated beneath a graticule.

Since a great number of the models which were used in the experimental work had curved surfaces upon which the gauges were mounted, the pulsing technique was found on average to give an answer which was less accurate for routine calibration than by deducing $\alpha/(\rho cK)^{1/2}$ from values of α and $(\rho cK)^{1/2}$. The pulsing technique was however used to deduce $\alpha/(\rho cK)^{1/2}$ of specially large gauges, the area of which could be accurately measured, mounted on sample specimens of pyrex. The object of these experiments was to determine $\sqrt{\rho cK}$ from the measurement of $\alpha/(\rho cK)^{1/2}$ by the pulsing technique and from the measurement of α described below.

2.6.2. Determination of α

The temperature coefficient of resistance α of thin films is a function of film thickness and differs markedly from the corresponding bulk values. Winding et.al (1955) found that the value of α decreased with decreasing film thickness and finally became negative for very small film thicknesses. Since the sensitivity of the gauges is directly proportional to α, it is desirable to have the thickest film compatable with abrasion and response properties. Measurements described in Appendix 1 showed that typical gauges used in our experiments were between 0.2 and 0.7 microns in thickness. The temperature coefficient of resistance of the gauges used in the tunnel tests were measured by immersing the models in an oil bath and measuring the gauge resistances at a series of equally spaced temperatures from 15° to 120°C.

2.6.3. Determination of the thermal constant $\sqrt{\rho cK}$

In the preparation of the thin film gauge it is possible that there is some penetration of film material into the substrate during the baking process. Thus it is by no means certain that the value of $\sqrt{\rho cK}$ can be determined from the bulk properties of the

backing material. Experiments were made to determine the gauge calibration factor $\alpha/(\rho c K)^{1/2}$ and the resistance coefficient α of a number of sample gauges, as described above. For all cases $(\rho c K)^{1/2}$ was found to be within $\pm$ 5% of the bulk property value of 0.0740 Btu./ft^{2}sec$^{1/2}$F.

An accurate method for the direct determination of $(\rho c K)^{1/2}$ has been developed by Skinner (1961). Skinner's method eliminates the necessity of measuring the gauge area, by determining the thermal constant in terms of the known thermal properties of distilled water. The pulsing technique was used to obtain the ratio $\frac{(\rho c K)^{1/2}_{\text{water}}}{(\rho c K)^{1/2}_{\text{pyrex}}}$ by pulsing the gauge in air and then water.

This technique could not be applied to the gauges used in the present experimental work because they were not coated with an insulating layer of silicon dioxide, however Skinners experimental results for pyrex, $(\rho c K)^{1/2} = 0.743 \pm 5\%$ are in good agreement with the values found in the present investigation.

The value of $(\rho c K)^{1/2}$ is a weak function of temperature. Figure 13 gives the variation of this factor as determined by Bogdon (1963) using the above technique.

2.7. Data Reduction

Although the majority of the data from the experimental work were reduced using the electrical analogue technique, all the data from the early tunnel tests were reduced by the graphical and numerical integration of data obtained directly from the gauge output. The performance of the electrical analogue circuits were also checked by direct comparison with numerically processed data.

The platinum gauge is used in a Wheatstone bridge circuit as explained in section 2.5.1. The out-of-balance voltage E (t) across

the bridge caused by an increase in gauge temperature $T_s(t)$ is

$$E(t) = \alpha E_o T_s(t)$$

Therefore substituting for $T_s(t)$ in equation 2.3.2.

$$q = \frac{1}{2\sqrt{\pi} E_o} \left(\frac{\sqrt{\rho c k}}{\alpha}\right)\left[\frac{2E(t)}{\sqrt{t}} + \int_o^t \frac{E(t) - E(\tau)}{(t-\tau)^{3/2}} d\tau\right] \quad \ldots .2.7.1.$$

and for a constant heat transfer rate

$$q = \frac{\sqrt{\pi}}{2E_o} \left(\frac{\sqrt{\rho c k}}{\alpha}\right)\left(\frac{E(t)}{\sqrt{t}}\right) \quad .. 2.7.2.$$

The initial tests with the heat transfer apparatus were made with the tunnel in the original of the two conditions described in Section 2.11. For this tunel configuration the starting process of the tunnel was extremely severe. The heat transfer trace could not be analysed with any accuracy by using the simple constant heat transfer formula (equation 2.7.2.) and so equation (2.7.1) was used in the reduction of all the data from the gauge output. To evaluate the heat transfer - time history equation (2.7.1.) has to be integrated numerically or graphically at each time (t). The records of the oscilloscope traces were measured using a travelling microscope.

For the graphical integration of equation (2.7.1.) the factor $\frac{E(t)-E(\tau)}{(t-\tau)^{3/2}}$ is evaluated from the gauge output and plotted for values of between $0 \leq \tau = t$ A typical curve is shown in figure 8. By using D'Alemberts rule it can be shown that $\frac{E(t)-E(\tau)}{(t-\tau)^{3/2}} \to \infty$ as $\tau \to t$. Thus an approximate procedure must be adopted to evaluate the integral where $\tau \fallingdotseq t$. An approximation for the evaluation of the integral for $\tau \fallingdotseq t$ is shown in figure 8, where the curve is stopped at $\tau = 0.95.t$ and the area of the curve above $\tau = 0.95.t$ is evaluated from the area of the triangle as shown in figure 8. The total integral is evaluated by adding this value to the area under the rest of the curve, which is measured with a planimeter. This procedure is repeated for a series of values for t to obtain the heat transfer time history.

A numerical method which was subsequently developed to evaluate equation (2.7.1.) was designed for use with a desk machine and automatic digital computor; it includes a more accurate method for the evaluation of the integral in the region where $\tau \doteqdot t$. The factor $\frac{E(t)-E(\tau)}{(t-\tau)^{3/2}}$ is integrated in two parts. The curve is split into $n+3$ ordinates where n is chosen according to the complexity of the starting process, and in this work $n \fallingdotseq 40$.

The integral up to n^{th} ordinate is performed by Simpson's rule, with $\frac{E(t)-E(\tau)}{(t-\tau)^{3/2}} = z$ & $t = (n+4)h$

thus $$\int_0^h z\,d\tau = \left(\frac{2h}{3}\right)\left[z_0+z_n+4(z_1+z_3\cdots)+2(z_2+z_4\cdots)\right] \quad \ldots\ 2.7.3.$$

To evaluate the integral in the region $\tau \fallingdotseq t$ putting

$$f'(\tau') = E(t)-E(\tau) \quad \& \quad (t-\tau) = \tau'$$

and letting $$\int_0^{4h} \frac{f'(\tau')}{\tau'^{3/2}} = \frac{1}{(4h)^{1/2}} \sum C_i f(ih)$$

we find by putting $f(\tau') = T^n$ and solving for n = 1, 2, 3, 4

$$\int_0^{4h} \frac{f(\tau')}{(\tau')^{3/2}} = \frac{1}{315}\frac{1}{\sqrt{4h}}\left[3776f(h)-1988f(2h)+1088f(3h)-146f(4h)\right] \quad \ldots\ 2.7.4.$$

Thus the total integral is obtained by the addition of expression (2.7.3.) and (2.7.4.), which is then substituted in equation 2.7.1. to evaluate the heat transfer rate q.

2.8. Analogue Theory and Operation

2.8.1. Introduction

One of the disadvantages of the heat transfer measurement technique using the thin film thermometer is the considerable amount of time and effort involved in the numerical reduction of data. Even if the results are processed by an automatic digital computor, the time delay between tunnel testing and the final reduction of data is inhibiting; particularly in an exploratory experimental programme, such as the present investigation, where the results of many of the tests are required before further work can be embarked upon.

The problem, by its very nature, lends itself to solution by electrical analogue techniques, for both the transport of heat and electrostatic charge are governed by the diffusion equation (2.3.1.). The general analogy between electrical and thermal diffusion has often been used; Lawson and McGuire (1953), Robertson and Cross (1958) and numerous other authors have investigated the solution of the transient heat flow problems, for example, the kinetic heating of aircraft, using electrical analogue techniques. Recently Skinner (1960) and Meyer (1960) have studied the electrical analogue technique for its specific application in conjunction with the thin film thermometer to give a direct indication of the heat transfer rate to the gauge. Although the two approaches differ, they are complementry and together give a good insight into the design parameters and performance of the electrical analogues.

2.8.2. The analogue design method proposed by Meyer

Meyer uses the direct analogy between the thermal and electrical systems in a similar treatment to that of Lawson and McGuire. The analogy is drawn between the equation of the one dimensional diffusion of heat by conduction

$$\frac{\partial T}{\partial t} = \left(\frac{K}{\rho c}\right) \cdot \frac{\partial^2 T}{\partial y^2} \qquad \ldots\ldots 2.8.1.$$

and the corresponding equation for the electrical diffusion of electric charges through a medium of uniformly distributed resistance and capacitance.

$$\frac{\partial V}{\partial t} = \left(\frac{1}{RC}\right) \cdot \left(\frac{\partial^2 V}{\partial y^2}\right) \quad \ldots \quad 2.8.2.$$

Here V the voltage potential in the electrical system is analogous to the temperature T; the electrical capacitance C is analogous to the thermal capacity ρc and the electrical conductivity $\frac{1}{R}$ is analogous to the thermal conductivity K. Pursuing the analogy, it can also be seen that $\frac{1}{RC}$ the "time constant" of an electrical medium is analogous to $\frac{K}{\rho c}$. In an ideal system the electrical analogue would be composed of distributed resistance and capacitance, but the technical difficulty in producing such a system is prohibitive and so it is replaced by a series of "lumped components" each composed of a discreet capacitance and resistance.

Meyer studied the response of three common electrical networks composed of lumped components which approximate to a system of distributed capacitance and resistance. These networks are called the L, T and Pi section networks and are shown in figure 9. The problem which he studied is which one of the three networks is the best analogue for use with the thin film apparatus.

The Pi section must be ruled out immediately, for the current into this circuit (a measure of the heat flow) cannot be easily measured; whereas in both the L and T section networks the voltage across the first resistor in the network gives a measure of this quantity. The relative merits of the L and T section networks were examined by calculating their response times and outputs to a series of different inputs which are commonly met in heat transfer measurements, namely,

$V = \text{constant}$	heat input proportional to $\frac{1}{\sqrt{t}}$
$V = V_o\sqrt{\frac{t}{RC}}$	constant heat input
$V = V_o \frac{t}{RC}$	heat input proportional to $\sqrt{t}$

It can be shown from Meyers work that for L and T networks with identical high frequency responses, the T section network will have approximately 3.5 times the sensitivity of the equivalent L section. Therefore the T section network was chosen.

The remaining parameters to be determined are "lump size" and length of the network. The "lump size" of the electrical system must be chosen so that the response of the analogue is similar to the thermal system for the shortest times of interest; whilst the network must be sufficiently long as to appear to represent a semi-infinite slab for the measured duration of the tests.

Meyer considers the modified analogy

$$C = \frac{\rho c}{n} \quad : \quad R = \frac{1}{mK} \quad : \quad t_e = \frac{t_t}{m.n}$$

Considering the lump component as equivalent to a slab of insulation material Δy thick, then

$$C = \frac{\rho c}{n} \quad : \quad R = \frac{\Delta y}{mK} \quad : \quad RC = \frac{\Delta y^2}{K m n}$$

For the electrical system to operate on the same time scale

therefore $\quad mn = 1 \quad$ & $\quad RC = (\Delta y^2/K)$

The performance of the analogue is characterised by the product RC and whilst the output voltage of the analogue is proportional to $\sqrt{RC}$, the frequency response is inversely proportional to $\sqrt{RC}$. Thus the value of RC is decided upon as a compromise between the magnitude of the output and the maximum frequency response required of the system.

The minimum length of the network, such that it will appear infinite during the useful running time of the experiments, was investigated by considering the ratio:-

$$\frac{\text{heat transfer to a slab of finite thickness}}{\text{heat transfer to a semi-infinite slab}}$$

The ratio τ/P^2 characterised the performance of the network, where $\tau = \frac{t}{\sqrt{RC}}$ and P is the total number of stages. Meyer found unity by 1.4 percent for $\tau/P^2 = 0.2$. Therefore, when RC has been

selected the running time t_r is related to the number of sections by

$$P = \left(\frac{0.2\, t_r}{\sqrt{RC}}\right)$$

The number of lumps may be reduced by increasing the lump size progressively along the network. Thus the small lumps near the surface will give a fast response time, whilst the larger lumps away from the surface achieve the same effective slab thickness with fewer components. For a network where the lump size is increased in size arithmetically, h the number of sections required is given by

$$P = \frac{h(h+1)}{2}$$

Output of the Analogue

The output of the film gauge from equation (2.5) is

$$E(t) = \alpha \cdot \bar{T}_s(t) \cdot I_o R_o$$

From the analogy

$$V_A = I(t.)\frac{R}{2} = I_o R_o \alpha m q \frac{R}{2}$$

Also $$R = \frac{\Delta y}{mK} \quad \& \quad \Delta y = \sqrt{kRC}$$

Therefore $$V_A = I_o R_o \frac{\alpha}{(\rho c K)^{1/2}} \cdot \frac{\sqrt{RC}}{2} \cdot q$$

or $$q = \frac{2}{\sqrt{RC}} \left(\frac{\sqrt{\rho c K}}{\alpha}\right) \frac{V_A}{I_o R_o}$$

or more generally $$q = A^* \left(\frac{\sqrt{\rho c K}}{\alpha}\right) \frac{V_A}{I_o R_o} \quad \ldots . 2.8.5.$$

where A* is defined as the analogue calibration factor.

2.8.3. The analogue design method proposed by Skinner

Skinner treats the analogue network as a filter which is designed to create a transfer function which transforms the transient output of the thin film gauge into a signal proportional to the heat transfer flux to the gauge. He adopts the rather

more practical approach of considering the frequency range which the filter has to handle to give an accurate performance. The function which relates the surface temperature to the heat flux to the gauge, is given in section (2.3.1.) by

$$q(p) = \sqrt{\rho c k}.\sqrt{p}.f(p)$$

thus the required transfer function $g(p)$ is

$$g(p) = \sqrt{\rho c k}\ \sqrt{p} \qquad \ldots .2.8.6.$$

Skinner chooses the network shown in figure 9, which is equivalent to the T network, to approximate to this transfer function. The transfer function of this network is

$$g^*(s) = \frac{V_o}{V_i} = \frac{R_o}{R_o + \sum_1^n z_k}$$

$$= \frac{1}{1 + \sum_1^n \frac{1}{\tau_k(p+a_k)}}$$

where Zk is the impedence of R and C in parallel and $\tau_k = \frac{1}{R_k C_k}$

He then compares the transfer function g (p) and g*(p) for a sinusoidual input. For a sinusoidual input we can replace p by $j\omega$ the equation (2.8.6.) then becomes

$$g(t) = \sqrt{\rho c k}.\sqrt{j\omega}.e^{\omega t}$$

Thus the amplitude $|g(t)| = N$ is

$$|g(t)| = \sqrt{\rho c k}\ \sqrt{\omega}$$

and phase angle $\phi = 45^\circ\ (\sqrt{j})$

As in conventional filter theory we express the attenuation N in decibels (dbs) [db = 20 $\log_{10}$ (attenuation)]

therefore $N = 20 \log \sqrt{\rho c k} + 10 \log_{10} \omega$

then $\frac{dN}{d(\log \omega)}$ = 10 dbs per decade or 3 dbs per octave.

Thus the required analogue is nothing more than a filter with a linear attenuation of 3 dbs per octave and a phase shift of 45°.

Skinner showed that $g^*(p) = g(p)$ for a circuit with n sections in the frequency range $f_A > f > f_B$ where $\frac{f_A}{f_B} \doteqdot (2n-1)$ octaves. Thus the frequency range can be made arbitrarily large by the appropriate choice of the number of sections. The operational range of the analogue can be moved along the frequency scale by scaling the capacitors in the circuit. Although the frequency response of the analogue may be made arbitrarily high, this is done at the expense of the sensitivity of the analogue. As a consequence the signal to noise ratio is inversely proportional to the maximum design frequency.

Skinner designed three analogues to investigate the frequencies which must be covered for an accurate response. These three analogues were designed to operate over frequency ranges of (a) 3 - 190,000 c.p.s. (b) 8 - 8,000 c.p.s. and (c) 10 - 1,000 c.p.s. Although analogue (a) worked well in shock tubes when it was used in shock tunnels to measure large heat transfer rates (> 50 Btu./ft^{2}sec), when it was used in shock tunnels to measure heat transfer rates of the order of 1 Btu./ft^{2}sec, the signal to noise ratio was approximately 2. By reducing the upper frequency to 8,000 c.p.s. the analogue was used successfully to measure heat transfer rates of 1 Btu./ft^{2}sec with a signal to noise ratio of 20. The further lowering of the high frequency limit to 1,000 c.p.s. once again improved the signal to noise ratio, but errors introduced by the large variation of heat transfer in the starting process were carried over the remainder of the run to yield inaccurate results.

Thus it can be concluded from this work that the choice of the magnitude of the upper frequency required is governed both by the severity of the starting process and the length of running time of the tunnel for which the analogue is designed.

2.8.4. Analogue design

Two analogues were designed and tested. Both of these analogues were developed from the design patterns suggested by

Meyer, because these were found to be the most easily adapted to obtain analogues with long running times. Although Meyer's basic patterns were used, it was found best to base the maximum design frequency of the analogue on Skinner's experience, and to examine and extend the performance of the analogue by viewing the problem in a similar manner to that set out by Skinner.

Skinner's work indicates that the analogue for use in a shock tunnel with a running time from 2 to 10 milliseconds should have linear frequency response to an upper frequency of 8 Kc/sec. For a gun tunnel where measurements are required between 10 and 40 milliseconds, but the starting process is inherently worse than in a shock tunnel, a maximum frequency between 5 Kc/s and 8 Kc/s should be adequate. The two analogues which were tested were the uniform T section and the arithmetically increasing T network, with the same basic time constant of 100 microseconds. The frequency response characteristics of these two analogues are shown in figure 11. It can be seen that both analogues have a frequency response which results in a linear attenuation of 3 db/octave and although the uniform section network has a higher frequency response than that of arithmetic analogue, both analogues are accurate to within 2% up to 5 Kc/s.

The low frequency characteristics were calculated from equation (2.8.4.) for a maximum running time of 70 milliseconds. A 60 section uniform T section analogue and a 10 section arithmetic analogue were chosen. The 60 lump T section analogue was used as the feedback network in the electronic calibrator unit (see section 2.10). By plotting the square of the voltage output from this unit against time, it was found that the unit could simulate the response of the thin film gauge with an accuracy of better than 5% for approximately 110 milliseconds. The performance of the arithmetic analogue was tested by feeding the output of the analogue calibrator through it. The analogue responded within 1 millisecond to give a good step function, the top of which was flat to

within 5% for the initial 80 milliseconds. The running time of the analogue of 80 milliseconds compares with 60 milliseconds deduced from equation (2.8.4).

For analogues designed by the methods of both Skinner and Meyer, the frequency response of the filter networks is such that at high frequencies the attenuation tends asymptotically to zero. This means that any high frequency aerodynamic or electrical noise is passed through the analogue almost unattenuated, and results as mentioned earlier, in a poor signal to noise ratio at low signal levels. There is no reason why, once the analogue has covered the range of frequency to give the required transfer function, the analogue should not attenuate the high frequency components.

In this work we have added a second filter network to the basic arithmetic analogue, which modifies its performance at high frequencies. This second network, which is shown in Figure 10, is an L.R.C. filter which fits across the output from the basic analogue unit. The L.R.C. network was designed so that when it was used in conjunction with the arithmetic analogue the combination gave a linear performance up to 7 Kc/sec and marked attenuation of 12 dbs/octave for frequencies above 10 Kc/sec, as shown in figure 11. This combined network was used to measure heat transfer rates down to 0.02 Btu/ft^{2}sec with a signal to noise ratio of approximately 10.

The pulse calibration and tunnel tests on the analogue are described in the following section.

2.9. Analogue Calibration

2.9.1. Pulse calibration

The pulse calibration apparatus described in section (2.5.2.) was used to examine the performance of the analogue for times up to several milliseconds. The calibration factor A* of the analogue, was determined by comparing the output of the analogue connected to

the calibration bridge, with the value calculated directly from the out-of-balance voltage appearing across the bridge. The out-of-balance voltage ΔV for a constant heat transfer rate q is given from equation (2.7.2.) by

$$q = \frac{\sqrt{\rho c k}}{\alpha} \cdot \frac{\pi}{2} \cdot \frac{1}{I_o R_o} \cdot \frac{\Delta V}{\sqrt{t}}$$

and from analogue theory the relationship between the heat transfer and the analogue output V_A is given by equation (2.8.2.) and is

$$q = \frac{\sqrt{\rho c k}}{\alpha} \cdot A^* \cdot \frac{V_A}{I_o R_o}$$

therefore eliminating q from the above equations we obtain

$$A^* = \frac{\sqrt{\pi}}{2} \cdot \frac{1}{V_A} \cdot \left(\frac{\Delta V}{\sqrt{t}}\right)$$

The analogue calibration factor A* can easily be found with an accuracy of better than 5% from the slope of a plot of ΔV^2 versus t and the output of the analogue.

The value of A* was found to be in good agreement with the theoretical value of 2×10^{-2}. From these tests the uniform section analogue was found to have the slightly faster response (as indicated from the frequency versus attenuation curve) but both analogues produced traces which were flat after 100 micro-seconds.

2.9.2. Tunnel tests on analogues

Extensive tunnel tests were made in which the output from the analogue was compared with data obtained from the numerical reduction of the gauge output. Most of these tests were carried out with the tunnel in its initial configuration (see section 2.11.) and with its inherently poor starting process it provided a good test of the ability of the analogue to follow the starting process of the tunnel. From equation (2.7.1.) the non-constant heat transfer q is related to the gauge output E(t) by

$$q = \left(\frac{\sqrt{\rho c k}}{\alpha}\right) \frac{1}{2\sqrt{\pi}\, E_o} \left[\frac{2\, E(t)}{\sqrt{t}} + \int_0^t \frac{E(t) - E(\tau)}{(t-\tau)^{3/2}} d\tau \right]$$

and again from analogue theory

$$q = A^* \left(\frac{\sqrt{\rho c K}}{\alpha}\right) \cdot \frac{V_A}{E_o}$$

Thus the calibration factor may be determined by eliminating from the above equations

$$A^* = \frac{1}{V_A} \cdot \frac{1}{2\sqrt{\pi}} \cdot \left[\frac{2E(t)}{\sqrt{t}} + \int_0^t \frac{E(t) - E(\tau)}{(t-\tau)^{3/2}} d\tau \right]$$

A^* should be constant for all q and t. The value of A^* evaluated from the above equation for a variety of heating conditions and for running times of between 10 and 60 milliseconds was found to be constant within $\pm$ 7% of the nominal value obtained for pulsing tests. This scatter was within the errors due to data reduction and tunnel repeatability.

2.10. The Electronic Calibrator

The electronic calibrator unit was designed to calibrate the electronic recording apparatus so that the heat transfer to the gauge could be interpreted directly in terms of the deflection of the trace on the oscilloscope. The apparatus was used initially to examine the performance and design characteristics of the two analogues based on design principles suggested by Meyer.

Design Principles.

The electronic calibrator apparatus was designed to simulate electronically the response of a thin film gauge to a constant heat transfer rate. The thermal and electrical properties of the gauge together with heat transfer to the gauge, are simulated on precision attenuators, whilst the function representing the form of the temperature versus time output of the gauge is generated by an operational amplifier.

Simulated Properties

The response of the thin film gauge E(t) is related to the calibration factor $\frac{\alpha}{\sqrt{\rho c K}}$ the steady voltage across the gauge $I_o R_o$ and the constant heat transfer to the gauge q by the expression

$$E(t) = 2.\left(\frac{\alpha}{\sqrt{\rho c K}}\right).I_o R_o.q\sqrt{\frac{t}{\pi}}$$

From a survey of thermal and electrical properties of materials commonly used in gauge construction, the following range of properties were chosen for simulation.

Property		Maximum	Minimum
$\frac{\alpha}{\sqrt{\rho c K}}$	$\frac{ft^2 sec^{1/2}}{B.t.u.}$	0.03	0.01
$I_o R_o$	Volts	1.5	0.25
q	$\frac{B.t.u.}{ft^2 sec}$	100	0.1

Basic Operation of the Analogue Calibrator

A block diagram showing the operation of the calibrator is shown in figure 12. The calibrator simulates the response of the gauge in the following ways:-

(i) A square wave of magnitude $I_o R_o$ volts is produced by switching the voltage across the gauge in the signal bridge into the calibrator with a mercury relay.

(ii) The pulse is multiplied by a factor proportional to $\left(\frac{\alpha}{\sqrt{\rho c K}}.Y_1\right)$ using a precision potentiometer.

(iii) A factor proportional to $2\sqrt{\frac{t}{\pi}}$ is introduced by passing the pulse through an operational amplier, the output from the amplifier is then equal to $\left(\frac{\alpha}{\sqrt{\rho c K}}Y_1\right).I_o R_o.\left(2\sqrt{\frac{t}{\pi}}Y_2\right)$

(iv) Finally a factor proportional to q is introduced by a second potentiometer, and the final output is then

$$(I_o R_o)\left(\frac{\alpha}{\sqrt{\rho c k}} Y_1\right)\left(2\sqrt{\frac{t}{\pi}} Y_2\right)(q Y_3)$$

The scaling factors Y_1, Y_2, Y_3 are chosen so that $Y_1 \times Y_2 \times Y_3 = 1$
The output of the calibrator is therefore

$$E(t) = \frac{\alpha}{\sqrt{\rho c k}} \cdot I_o R_o \cdot 2\sqrt{\frac{t}{\pi}} \cdot q.$$

Potentiometer Design

$\alpha/\sqrt{\rho c k}$ Potentiometer

The design of the $\alpha/(\rho c k)^{1/2}$ potentiometer is shown in figure 13 A scaling factor $Y_1 = 2$ was chosen and so the range of the attenuator is from 0.02 to 0.06 in steps of 0.004 so that the mid-range calibration factor may be set with an accuracy of 1%.

q Potentiometer

The design of the q poteniometer is shown in figure 13. A scale factor of $Y_3 = \frac{1}{400}$ was chosen, and heat transfer rates of 100, 50, 20, 10, 5, 2 and 1, 0.5, 0.2 Btu./ft^{2}sec can be simulated with an accuracy of better than 1%. The output impedence of the potentiometer was between 20 and 100 ohms to simulate the output impedence of a typical gauge.

Operational Amplifier Design

The function $2\sqrt{\frac{t}{\pi}}$ is generated by conventional feedback operational amplifier techniques. The amplification factor A_F of an amplifier with a feedback ratio β and an open loop gain A (gain without feedback) of A is given by

$$A_F = \frac{A}{1 - \beta A}$$

for a high gain amplifier $\beta A >> 1$

$$A_F = \frac{-1}{\beta}$$

To generate the function $2\sqrt{\frac{t}{\pi}}$ we must find a circuit element with a transfer function proportional to $\frac{1}{2}\sqrt{\frac{\pi}{t}}$ From section 2.8. the transfer function of an analogue network is given by

$$\frac{V_A}{V_0} = \frac{\sqrt{RC}}{4}\sqrt{\frac{\pi}{t}} = \left(\frac{1}{Y_2}\right)\frac{1}{2}\sqrt{\frac{\pi}{t}}$$

Therefore introducing an analogue circuit into the feedback circuit we have $-\beta = \frac{2}{Y_2}\sqrt{\frac{\pi}{t}}$ and the gain of the amplifier is

$$A_F = Y_2 2\sqrt{\frac{t}{\pi}}$$

For a 1% simulation of the function $2\sqrt{\frac{t}{\pi}}$ the open loop gain A of the operational amplifier must exceed the maximum feedback β by a factor of over 100. The maximum value of β , its D.C. value, is approximately 130, the open loop gain of the amplifier used was over 20,000.

Calibration and Gain Adjustment

The analogue calibrator is calibrated by injecting a sinusoidual signal to the input attenuator. The output V_Q of the calibrator is related to the input voltage Vs by the equation

$$\frac{V_Q}{V_S} = \left(\frac{\alpha}{\sqrt{\rho c K}}\right) q \frac{1}{\sqrt{\omega}}$$

setting $\alpha/\sqrt{\rho c K} = 0.02$ and $q = 10$, for a 1 Kc/s sinusodual input we have

$$\frac{V_Q}{V_S} = 0.038\angle 45^\circ$$

A diagram of the calibrating oscillator circuit is shown in figure 13. The signal generated from the oscillator circuit which is past through the calibrator circuit is compared with 0.038 of the input at a phase angle of 45° generated by a resistance - capacitance network coupled to the oscillator. The overall gain of the calibrator is adjusted until these two signals are identical, which can be found with high accuracy by subtracting the signals on a differential oscilloscope.

2.11. The Gun Tunnel

All the experimental investigations were carried out in the Imperial College Gun Tunnel. The facility which is essentially a blow-down tunnel with a shock compression heater was used in two configurations, the performance and calibration of which are described by Stollery, Maull and Belcher (1960), and Needham (1963) respectively.

The first series of tests were carried out at a stagnation pressure of 500 p.s.i.a. and stagnation temperature of approximately 1000°K, corresponding to a 650 p.s.i.g. driver pressure and an atmospheric barrel pressure. The Mach number at the model position was 10 and the free stream Reynolds number was 0.7×10^5/per inch. The naturally bursting single diaphragm gave a repeatability of heat transfer readings of approximately $\pm$ 7%. Therefore a reference gauge was necessary, the heat transfer to which was always recorded, to correlate data from these tests. One undesirable feature of the performance of the tunnel in this configuration was the extremely poor starting process. This resulted from the position of the second diaphragm being at the downstream end of the nozzle. Typical surface temperature and heat transfer traces indicated unsteadiness lasting 20 milliseconds after the bursting of the second diaphragm. Unsteady heat transfer rates greater than twice the steady value were recorded during this time.

The modified form of the tunnel had the second diaphragm station at the upstream end of the nozzle. For this configuration the starting process was far less severe and steady heat transfer readings were established in less than 10 milliseconds after the bursting of the second diaphragm. Experimental studies were conducted at Mach numbers of 7, 10 and 15 by changing the throat diameter of the conical nozzle. The drive pressure was maintained constant at 2000 p.s.i.g. for all these tests, whilst the barrel pressure was varied to obtain the required Reynolds number

conditions. At Mach 10 barrel pressures of 14.7 and 100 p.s.i.a. were used to obtain Reynolds numbers of 1.35×10^5/inch and 2.7×10^5 respectively. At Mach 7 a barrel pressure of 14.7 p.s.i.a. gave a Reynolds number of 2.7×10^5/inch whilst at Mach 15 the barrel pressure was 72 p.s.i.a. to obtain a Reynolds number of 1.35×10^5/inch. The use of the double diaphragm rig to give controlled bursting of the first diaphragm improved the repeatability of the heat transfer results, and the variation of the heat transfer readings resulting from the run to run variation of the aerodynamic free stream conditions was less than 3%.

Stagnation Temperature

The stagnation temperature of the gas flow in the gun tunnel was estimated by comparing the experimental measurements of the stagnation point heat transfer to a hemispherically capped cylinder with the theoretical predictions of Cohen and Reshotko (1955) and Fay and Riddell (1957). For a Mach number 10 and bursting pressure ratio of 140 this temperature was calculated to be 1275°K. This value is in good agreement with estimates made from pressure and running time measurements by Needham (1963) and with the stagnation temperature measurements of Stollery (1960).

The decay of the stagnation temperature during a run was estimated from the heat transfer versus time profiles. The mean value of the temperature decay as measured from a large number of heat transfer profiles between 10 and 40 milliseconds from the start of the run was approximately 2500°K per second. This value compares with values of 1000°K/sec obtained by Cox (1960) and Stollery (1960) and 8000°K/sec by Merritt (1961).

Flow Abrasion

The erosion of heat transfer gauges resulting from the impingment of particles contained in the air flow was found to be a serious problem. One advantage of the gun tunnel is that the

piston prevents any particles of dust or rust from the drive vessels directly contaminating the flow, so that all the particles which impinge on the models must have come from the barrel, the second diaphragm, or the nozzle. Regular and meticulous cleaning of both the barrel and the nozzle block reduces the number of particles to a minimum,but sellotape particles from the second diaphragm together with aluminium particles scraped from the piston in its retarding motion, still cause a small amount of damage to the gauges. The careful preparation of thin film gauges can increase the abrasion resistance properties of gauges enormously as explained in Appendix 1.

3. Heat Transfer Measurements in Unseparated Flow

3.1. Introduction

All the measurements made while the instrumentation was being perfected, were to determine the heat transfer to models in unseparated flows. The models used in these tests were shapes for which reliable theoretical data already existed, namely the stagnation point solutions for the two-dimensional cylinder and hemispherically capped cylinder.

Subsequent measurements were made on models in unseparated flow which formed the basic configurations over which separated flows were later promoted. Although there were a number of theoretical solutions for the distribution of heat transfer over these shapes, there was little experimental data. The data which was available came mostly from high-enthalpy low-Mach-number facilites such as shock tubes, or high-Mach-number, low-enthalpy facilities such as helium tunnels.

In this section the stagnation point heat transfer measurements are compared with existing theoretical and experimental data. The heat transfer distribution over the blunt body configurations of the hemispherically capped and flat ended cylinder are compared with two theoretical solutions for this problem. The heat transfer measurements to a flat plate are compared with the constant pressure solutions of Van Driest (1952) and Eckert (1955), and also with the solution of Hall et.al (1961) which takes into account viscous interaction effects. Finally the heat transfer measurements to a number of cones with different apex angles are compared with theoretical results derived from the flat plate solutions.

3.2. Stagnation Point Heat Transfer

3.2.1. Theory

The theory of stagnation point heat transfer, which was originally derived for low speed flow by Squire (1939), has been developed in recent years by Sibulkin (1952), Cohen and Reshotko

(1955) and Fay and Riddell (1957) to successfully predict the stagnation point heat transfer to blunt bodies travelling at hypersonic speeds.

The solution of the stagnation point heat transfer is obtained from the Stewartson transformation (see section 4.6.2.) of the compressible laminar boundary layer equations:-

$$f''' + ff'' = \beta(f'^2 - 1 - S) \quad \ldots .3.1.1.$$

$$S'' + Pr.fS' = 0 \quad \ldots .3.1.2.$$

putting $\beta = 1$ for two dimensional stagnation point flow and $\beta = 1/2$ for axisymmetrical stagnation point flow. The two-dimensional solution by Squire and the extension to axisymmetric flow by Sibulkin assumed a Prandtl number of unity, but they extended their analysis for constant Pr other than unity by multiplying the heat transfer coefficient for Pr = 1 by an empirical factor $(Pr)^{0.4}$.

Cohen and Reshotko solved equations (3.1.1.) and (3.1.2.) for Prandtl numbers of 0.6 to 1.1. They found these exact solutions were in good agreement with the results of Squire and Sibulkin modified to include the empirical correction factor.

Fay and Riddell extended the solution of the boundary layer equations to take into account both the variation of the product $\rho\mu$. (taken as constant by Cohen and Reshotko as the result of using the Stewartson transformation) and also the dissociation of oxygen and nitrogen through the boundary layer. They found the laminar heat transfer coefficient at the stagnation point of a sphere to be

$$\frac{N_u}{\sqrt{R_e}} = 0.763\,(P_r)^{0.4}\left(\frac{\rho_w\mu_w}{\rho_e\mu_e}\right)\left[1 + (L_e^{0.52} - 1)\frac{h_e}{H_e}\right] \quad \ldots . 3.1.3.$$

Romberg (1956) showed that the "reference enthalpy" method could be used to account for the variation of $\rho\mu$ through the boundary layer by evaluating the heat transfer coefficient at the

"reference enthalpy". (see section 3.4.1.). For $L_e = 1$ Romberg found

$$\frac{Nu}{\sqrt{R_e}} = 0.763(P_r)^{0.4}\left(\frac{\rho^*\mu^*}{\rho_e\mu_e}\right) \quad \ldots\ldots 3.1.4.$$

3.2.2. Experimental results and discussion

The stagnation point heat transfer was measured at a Mach number of 10 to both cylinders and spheres.

The stagnation point heat transfer to the two dimensional stagnation point along the axis ofacircular cylinder was measured on two cylinders with different diameters one of which is shown in figure 18. The results from these measurements are plotted in non-dimensional form in figure17. Also included in this diagram are the results of Hertzberg and Witliff (1960) from shock tunnel measurements. These results are also compared with theoretical calculations from Cohen and Reshotko, and Fay and Riddell. In these calculations the stagnation point velocity gradient was taken as the Newtonian value, namely $\left(\frac{du}{dx}\right)_{x=0} = \frac{\sqrt{2}.u_s}{R}$ where u_s is the velocity just behind the normal shock.

The stagnation point heat transfer was measured on the hemispherically capped cylinder shown in figure 18. The results of these measurements, which are shown in figure 19, were compared with calculations made using the theoretical results of Cohen and Reshotko, Fay and Riddell, and also Lees (1956). In all these calculations the stagnation point velocity gradient was taken from Cohen and Reshotko, and is

$$\left(\frac{du}{dx}\right)_{x=0} = \frac{3u_s}{2R}(1 - 0.252M_s^2 - 0.0175M_s^4) \quad \ldots\ldots 3.2.1.$$

Both the two dimensional and axisymmetrical stagnation point heat transfer measurements are in good agreement with the theoretical calculations.

3.3. The Distribution of Heat Transfer over Blunt Bodies

3.3.1. Theory

The study of the heat transfer distribution over blunt bodies has attained importance because such shapes are often used as leading edge surfaces on hypersonic vehicles. Two theoretical methods for the prediction of the heat transfer to blunt bodies were advanced by Lees (1956) and Kemp, Rose and Detra (1958). These theories assume that the velocity and enthalpy profiles are a function of a single variable, thereby reducing the basic set of partial differential equations to a system of ordinary differential equations. To solve these equations they also assume the external flow conditions to vary slowly along the surface of the body - the local similarity concept. With these assumptions the boundary layer equations reduced to the form

$$(Nf'')' + ff'' + \beta\left(\frac{\rho_e}{\rho} - f'^2\right) = 0 \qquad \ldots\ldots 3.3.1.$$

$$\left(\frac{N}{P_r} g'\right)' + fg' + \frac{u_e^2}{H_e}\left[N\left(1 - \frac{1}{P_r}\right)\right] = 0 \qquad \ldots\ldots 3.3.2.$$

where the co-ordinate system is given in section (4.6.2.). Lees found that for blunt bodies the dissipation term $\frac{u_e^2}{H_e}\left[N\left(1 - \frac{1}{P_r}\right)\right]$ could be neglected and for a highly cooled wall the effect of the pressure gradient parameter β on the enthaply gradient factor at the wall $\frac{g'_\eta}{1-g_w}$ was negligible and thus this factor was equal to $0.47 Pr^{1/2}$

The heat transfer coefficient

$$\frac{Nu}{\sqrt{R_e}} = \frac{\sqrt{\rho_w \mu_w u_e r}}{\sqrt{2\xi}} \left(\frac{g_\eta}{1-g_w}\right)\left(\frac{H_e - h_w}{h_{AW} - h_w}\right)$$

also $$q = \frac{\rho_w \mu_w u_e r}{\sqrt{2\xi}} \cdot \left(\frac{g_\eta}{1-g_w}\right)(H_e - h_w)$$

therefore $$\frac{q}{q_0} = \frac{\rho_w \mu_w u_e r}{2\sqrt{\xi}\sqrt{(\rho_w \mu_w)_0}} \left(\frac{du_e}{dx}\right)^{-1/2}_{x=0} \left(\frac{g'_\eta}{g'_{\eta_0}}\right)_{\eta=0} \qquad \ldots\ldots 3.3.3.$$

for $$\frac{g'_r}{1-g_w} = \frac{g_{r_0}}{1-g_w} = 0.47\,P_r^{1/2}$$

hence $$\frac{q}{q_0} = \frac{\left(\frac{P}{P_0}\right)\sqrt{1-\left(\frac{P}{P_0}\right)^{\frac{\gamma-1}{\gamma}}}\cdot r\left(\frac{1}{u_e}\cdot\frac{du_e}{dx}\right)^{1/2}}{\left[\int_0^s \left(\frac{P}{P_0}\right)^{\frac{\gamma\omega+(1-\omega)}{\gamma}}\sqrt{1-\left(\frac{P}{P_0}\right)^{\frac{\gamma-1}{\gamma}}}\cdot r^2 ds\right]^{1/2}} \quad \ldots\ldots 3.3.4.$$

Rose showed that while this formula may be used for smoothly curved surfaces such as a sphere, on sharply radiused surfaces the assumption that the enthalpy gradient $\frac{g'_r}{1-g_w}$ remains constant is no longer valid. By solving the boundary layer equations (3.3.1.) and (3.3.2.) Rose found that the wall enthalpy gradient $\frac{g'_r}{1-g_w}$ could be expressed as a function of β thus:-

$$\frac{g'_r}{1-g_w} = 0.458\left(1+0.096\sqrt{\beta}\right)\left[\frac{\rho_0\mu_0}{(\rho_w\mu_w)_0}\right]^{0.438}$$

where $$\beta = 2\left(\frac{\xi}{u_e}\right)\left(\frac{du_e}{d\xi}\right) = 2\left(\frac{du_e}{dx}\right)\frac{\int_0^x \left(\frac{\rho_e}{\rho_{w0}}\right)u_e r^2 dx}{\left(\rho_e/\rho_{w0}\right)u_e r^2}$$

3.3.2. Experimental results and discussions

A. Heat transfer to a hemisphere cylinder

The heat transfer distribution to a hemisphere cylinder was measured at a free stream Mach number of 10 and Reynolds number based on body diameter of 0.225×10^6. The models used in the tests are shown in figure 18. The theoretical distribution was evaluated from equation (3.3.4.) using the Newtonian pressure distribution shown in figure 42, the stagnation point heat transfer was taken as the experimental value. Both the experimental and theoretical values of the heat transfer distributions are shown in figure 19 and are in good agreement.

B. Heat transfer to flat-ended cylinder

The heat transfer distribution to a flat ended cylinder was measured at a Mach number of 10 and Reynolds number of 0.21×10^6. Figure 18 shows the models used in the experiment.

The stagnation point heat transfer to a flat ended cylinder may be calculated by noting

$$q_{F.E.C} = q_{SPHERE} \cdot \left(\frac{du_e}{dx}\right)_{\substack{x=0 \\ F.E.C}} \times \left(\frac{du_e}{dx}\right)^{-1}_{\substack{x=0 \\ SPHERE}}$$

From Lees (1957)

$$\left(\frac{du_e}{dx}\right)_{F.E.C.} = \frac{4u_s}{3\pi R}\left[K(2-K)\right]^{1/2}$$

where $M >> 1$ & $K \doteq 0.66$

From Cohen and Reshotko

$$\left(\frac{du_e}{dx}\right)_{SPHERE} = \frac{3u_s}{2R}\left(1 - 0.252\,M_s^2 - 0.0175\,M_s^3\right) \doteq \sqrt{\frac{\gamma-1}{\gamma}}\left(\frac{u}{R}\right)$$

hence $$\frac{q_{FEC.}}{q_{SPHERE}} = \left[\frac{4}{3\pi}\left(\frac{\gamma}{\gamma-1}\right)^{1/2}\left[K(2-K)\right]^{1/2}\right]^{1/2} = 0.66$$

This compares with 0.7 obtained from the experimental results, see figures 19 and 20.

The heat transfer distribtuion to the flat ended cylinder was calculated using equations (3.3.4.), (3.3.5.) and 3.3.6.). The pressure distribution around the body was assumed to be that given by Lees (1957) which is shown in figure 21. Figure 20 shows the theoretical and experimental distributions of heat transfer to the flat-ended cylinder.

3.4. Heat Transfer to a Flat Plate

3.4.1. Constant pressure solutions

The theoretical prediction of the skin friction and heat transfer to an isothermal flat plate with zero pressure gradient in compressible flow has been the subject of many studies. The early solutions of the compressible boundary layer equations were based on the assumption of unity Prandtl number or a linear temperature - viscosity relationship, thereby allowing the independent integration of the energy or momentum equations. Other solutions employed the Stewartson transformation to reduce the equations to their incompressible forms. However the most accurate solutions for the constant pressure compressible boundary layer equations were obtained by Hantzsche and Wendt (1940) and Van Driest (1952). Van Driest used the Crocco transformation in a numerical scheme which incorporated the Sutherland viscosity relationship, to obtain solutions of the boundary equations for a Prandtl number of 0.75, wall to free stream temperature ratios from 0.25 and 6 and Mach numbers from 0 to 20.

A number of simple empirical solutions have been derived which are based on approximate expressions which fit the results obtained from computer solutions of the boundary layer equations. Young (1949) analysed the results of Hantzsche and Wendt (1940) and found a simple formula which agreed with their results to within one percent.

This expression, together with use of the Reynolds analogy becomes

$$S_t\sqrt{Re_\infty} = 0.332\left[0.45 + 0.55\left(\frac{T_w}{T_o}\right) + 0.09(\gamma-1)M_\infty^2 P_r^{1/2}\right]^{\frac{\omega-1}{2}} P_r^{-2/3} \quad \ldots\ldots 3.4.1.$$

Further work by Chapman and Rubesin (1949) adopts a slightly different approach by introducing the concept of a "reference temperature", being the temperature at which the friction factor $\frac{C_f}{\sqrt{Re}}$ is independent of the Mach number and Reynolds number

variation. Chapman et.al found the reference temperature could be expressed by

$$T_* = T_\infty + 0.58(T_w - T_e) + 0.19(T_{AW} - T_\infty) \quad \ldots 3.4.2.$$

Eckert (1955) using the results of Young expressed the reference conditions in terms of a "reference enthalpy" which he expressed as

$$h_* = 0.5(h_e - h_w) + 0.22(h_{AW} - h_\infty) \quad \ldots 3.4.3.$$

where $h_{AW} = h_\infty + 1/2\sqrt{P_r^*}\,u_\infty^2$

The heat transfer coefficient is therefore

$$S_t\sqrt{R_{ex}} = 0.332\sqrt{\frac{\rho_*\mu_*}{\rho_e\mu_e}}\,(P_r^*)^{-2/3} \quad \ldots 3.4.4.$$

and hence the heat transfer rate is

$$q = \frac{0.332\,\rho_{ue}^*(P_r^*)^{-2/3}(h_{AW}-h)}{\sqrt{R_e^*}} \quad \ldots 3.4.5.$$

3.4.2. Boundary layer displacement and leading edge bluntness effects

There are two important features of the hypersonic flow over a flat plate which causes the flow phenomena to be different from the low speed case, even when real gas effects and non continuum flow effects can be neglected. These are the displacement effect of the boundary layer and the influence of leading edge bluntness.

For the hypersonic flow over a flat plate with a sharp leading edge the viscous boundary layer and the shock wave formed at the leading edge interact. The interaction, which is caused by the displacement of the external stream by the growth of the viscous layer near the leading edge, causes the pressure over the surface of the plate to increase. In high Mach number flows, the induced pressure caused by the interaction causes pressures on the plate many times greater than free stream values, and this increase in surface pressure is reflected in the increase of skin friction and heat transfer over the plate.

The effect of leading edge bluntness is manifest in two ways; firstly it influences the pressure field around the body independant of the existance of the boundary layer; and secondly the large curvature of the leading edge shock associated with a blunt leading edge in high Mach number flows, creates a vorticity field external to the viscous flow associated with the boundary layer, which influences the growth of the boundary layer and hence the heat transfer characteristics.

The theoretical work of Hall, Cheng, Golian and Hertzberg (1961) takes into account both these effects and also the transition states between the two cases. They also give experimental evidence which supports their predictions. From Hall et.al the expression for the heat transfer to a sharp edged flat plate is given by:-

$$M^3 C_H = 0.219\sqrt{\epsilon\gamma\left(0.664 + 1.73\frac{H_w}{H_\infty}\right)}\cdot\bar{\chi}^{3/2} \qquad \ldots\ 3.4.6.$$

where $$C_H = \frac{q}{\rho_\infty U_\infty (H_\infty - H_w)}$$

$$\bar{\chi} = M^3\sqrt{C}/\sqrt{R_{ex}}$$

C = constant in linear viscosity - temperature relationship

$$\epsilon = (\gamma-1)/(\gamma+1)$$

3.4.3. Experimental results and discussion

The heat transfer to a flat plate model was measured for a free stream Mach number of 10 and Reynolds number of 0.136×10^6/inch. The flat plate model used in the investigation had a leading edge thickness of 0.0015 inches, so the plate may be considered sharp from criteria of Hall et.al, and only the displacement effect need be included. Figure 22 shows a comparison between the experimental results and the theoretical curves calculated using the methods of Van Driest and Eckert which ignore viscous interaction, together with the results from equation (3.4.6.). As often shown before the reference enthalpy method of Eckert is in remarkably close agreement with the more exact method of Van Driest. Close to the

leading edge the experimental data is in good agreement with the work of Hall et.al and confirms the importance of considering viscous interaction effects.

3.5. Heat Transfer to a Cone

3.5.1. Theory

The heat transfer distribution to the surface of a cone can easily be predicted by applying the Mangler transformation to the flat plate results discussed in the previous section. For cones with attached shocks the Mangler transformation (see section 4.6.2.) gives

$$\frac{(St\sqrt{Re})_{CONE}}{(St\sqrt{Re})_{FLAT\ PLATE}} = \sqrt{3}$$

The distribution of heat transfer to a cone is therefore given by

$$q = \frac{0.322\sqrt{3}\,\rho^{*}u_e(P_r^{*})^{-2/3}(h_{AW}-h_w)}{\sqrt{R^{*}_{ex}}} \quad \ldots .3.5.1.$$

Where the reference conditions are evaluated over the face of the cone.

For the case where the cone has an apex angle greater than the conical detactment angle the heat transfer distribution may be calculated approximately by using the blunt body solution of Kemp et.al (1958) in section 3.3.

3.5.2. Experimental results

The heat transfer distributions to cones with vertex semi-angles of 30° and 45°, were determined at Mach numbers of 10 and 15 at a Reynolds number based on body diameter of 0.27×10^{6}. Figure 46 shows the models used in the experiments. The experimental results together with theoretical calculations from equation (3.5.1.) are shown in figures 47 and 49 and show good agreement.

4. Heat Transfer in Separated Flow

4.1. Introduction

This section of the report is devoted to a description of an experimental study of the distribution of heat transfer over aerodynamic surfaces which promote wedge separated flows. The experimental work was divided into three main parts.

The first study was designed to investigate the heat transfer distribution to a flat plate in regions of adverse pressure gradient and moderately separated flow, induced by both forward facing wedges and externally generated shocks. In this study emphasis was placed on the difference between a flow in which the boundary layer had been merely thickened by an adverse pressure gradient, and one in which the adverse pressure gradient has caused the boundary layer to separate, thus causing a region of reverse flow. The similarity between the shock wave-boundary layer interaction induced by different flow mechanisms was also studied.

The second study was designed to investigate the heat transfer distribution in large regions of separated flow induced by large angle forward facing two dimensional wedges, and also by axisymmetrical spiked cones. In these experiments the separation and reattachment regions were well separated and the emphasis of this investigation was placed on the mechanism of the heat transfer distribution in the reattachment region of the shear layer. The main parameters varied in these tests were reattachment angle and Mach number.

The third investigation, the study of the heat transfer distribution over spiked bodies, was designed to investigate the parameters which influenced the protection of aerodynamic surfaces by controlled regions of separated flow. In this investigation the basic parameters varied in the tests were model geometry and Mach number. These experiments were also extremely useful in

establishing a reference "unseparated value", the heat transfer to the unspiked body, with which the peak heating in the reattachment region on the spiked body can be compared, as well as yielding data on the reattachment phenomena itself.

4.2. Experimental Technique

There are a number of features in the experimental study of separated flow regions which emphasises the importance of certain experimental techniques. The first important feature of wedge separated flows is their extreme sensitivity to the aligment of the model. This is particularly significant in the study of the heat transfer distribution in the reattachment region on spiked bodies, where it is essential that each configuration should be carefully set up and checked with schlieren photographs. Separated flows are often unsteady, an extreme example of this is the gross instability characterised by the oscillatory flow encountered over spiked blunt bodies. For the correct interpretation of the experimental measurements it is therefore important that the response time of the transducer and associated electronics should be an order of magnitude faster than the fluctuation in the flow under investigation.

It is particularly important, in experiments on separated flows, to examine the effect arising from a finite span of two dimensional models. The two dimensionality of the flow over the flat plate and wedge models was checked by measuring the spanwise distribution of heat transfer across the centre sections of these models. Side plates were initially fitted to the models to prevent cross flows. From flow observations using talcum powder it was found that the side plates themselves caused a three dimensional flow by generating vortices between the side plates and the wedge. The flow observations through the schlieren side plates were also distorted by the growth of the separated flow on these side plates. The heat transfer distribution across the

centre section of the model indicated that the flow was essentially two dimensional both with and without the side plates, and the removal of the side plates had no effect on the magnitude of the heat transfer rates recorded. The two dimensionality of the flow on the face of the wedge without side plates was examined by a flow visualisation technique in which a thin layer of wax was spread along the model in the reattachment region. The heat generated by the reattaching flow caused the molten wax to follow the flow in the boundary layer, and the patterns generated showed that the flow over the wedge was two dimensional over four fifths of the span. This latter observation was confirmed by burn marks on a layer of sellotape which was laid across the face of the wedge. These burn marks, in the reattachment region, formed a straight line parallel to the upper shoulder of the wedge indicating the flow over the wedge was again two dimensional over four fifths of the span. After these observations had been made all the experiments were conducted without side plates, but the span-wise heat transfer distribution was always measured on all the two dimensional models as a check.

4.3. Heat Transfer in Regions of Laminar Separation

4.3.1. Introduction

The predominance of laminar boundary layers at hypersonic speeds and the comparative ease with which such boundary layers will separate, has made separation criteria and the properties of separated regions of great importance. A knowledge of the properties of wedge separated regions is of importance for the design of compression surfaces such as intakes, control surfaces and flared junctions.

At supersonic and hypersonic speeds the pheneomena of wedge boundary layer separation is associated with the phenomena of shock-wave boundary-layer interaction. Experimental and theoretical work has been devoted to the study of this phenomena

resulting from a shock incident on a tunnel wall or flat plate, and induced by a forward facing wedge or compression surface. From the pressure distributions obtained in these experimental studies the separation phenomenon was shown to be a free interaction i.e. independent of the mechanism by which it was caused. Although a number of experimental investigations have been carried out at supersonic speeds, there has been very little experimental work on the boundary layer separation phenomena in hypersonic flow. Detailed experimental information on the distribution of heat transfer in laminar regions of adverse pressure gradient and boundary layer separation, in both supersonic and hypersonic flows is almost completely absent.

In this section we study the heat transfer distribution in regions of adverse pressure gradient and flow separation, induced by both forward facing wedges and externally generated shocks. The object of this work was to measure the distribution of heat transfer in an adverse pressure gradient but no separation, and in flows in which the adverse pressure gradient causes flow separation with a region of reversed flow, and distinguish them i.e. formulate a separation criteria in terms of the heat transfer distribution. It was also of great interest to compare the distribution of heat transfer for flows in which the adverse pressure gradients and flow separation had been induced in different ways.

4.3.2. Apparatus

The flat plate+wedge model which is shown in figure 23 consisted of two plates, the second of which could be inclined at any angle from 0 to 30° to the first plate. The model was engineered so that the second plate rotated about a virtual hinge located at the junction of the two faces, and great care was taken to see that this junction was both "clean" and pressure tight. The flat plate model which was used with an external sharp edged shock generator is shown in figure 24. As can be

seen from the photographs, the distribution of gauges were "graded" on both models so that there was a high density of intrumentation in the region of shock wave boundary layer interaction. The models were also equipped with side gauges to measure the spanwise distribution of heat transfer. Both the wedge model and the flat plate model were fitted with side curtains to prevent interference from flow beneath the plates.

4.3.3. Flat plate+wedge study

The heat transfer distribution to the flat plate+wedge configuration was measured for wedge angles from 0 to 15 degrees at intervals of 2.5 degrees. All these tests were conducted at a Mach number of 10 and free stream Reynolds number of 1.34×10^5.

The length of the plate before the interaction, was chosen so that the shock wave developed from the leading edge did not intersect with the face of the second wedge, and the Mach cones developed from the tips of the plate did not envelop any of the region under investigation. With this length of plate, the viscous interaction effect associated with the growth of the boundary layer from the leading edge is shown in figure 22 to be confined to within the first 2 inches, and the entropy gradient associated with leading edge bluntness (section 3.4.2.) did not influence the interaction which was being studied.

The schlieren photographs and heat transfer distributions obtained from these tests are shown in figure 25. Figures 25(a) and (b) show the heat transfer distributions and flow patterns for boundary layers which have merely been thickened by the adverse pressure gradient caused by the wedge. The heat transfer starts to dip below the level of the flat plate values in front of the wedge as the adverse pressure gradient causes the boundary layer to thicken faster than under flat plate conditions. Whilst the boundary layer is thickened by the pressure feeding forward, its

density is also increased and eventually this causes the heat transfer to the plate to start to increase again, ahead of the wedge. The heat transfer increases along the wedge as the boundary layer is thinned and its density is increased by the compression process. Finally at the end of the compression process the boundary layer starts to grow again under constant pressure and in consequence the heat transfer rates begin to fall. As the adverse pressure gradient caused by an increase in wedge angle becomes more severe, so the magnitude of the dip in heat transfer below the flat plate value increases. However, it will be observed that the form of the curve is in each case in the same, and the portion of the curve in the region of the minimum heat transfer is cusp-like in form as redepicted in figure 27.

Figures 25c, d and e show the schlieren and heat transfer patterns for flow conditions which vary from the case in which the boundary layer is fully separated as in figure 25e to the case depicted in figure 25c where it is difficult to determine whether the boundary layer has been thickened or whether separation has taken place. The fully separated flow is characterised in the schlieren photographs by two distinct shock formations. The first springs from the separation region, and is followed by a constant pressure zone which is bounded by a straight shear layer. The second shock springs from the end of the shear layer and compresses the flow to its final wedge pressure value. As the adverse pressure gradient is decreased by decreasing the wedge angle the two shock systems gradually converge, until they finally collesce to form a single shock at the point at which the boundary layer just separates - the incipient separation point. The difference between the heat transfer distribution in separated and unseparated regions are characterised by two important features. As the wedge angle is increased from 7.5 degrees through to 12.5 degrees the shape of the heat transfer distribution curve in the region of minimum heat transfer undergoes a distinct change. Although the form of the initial decrease in heat transfer is similar, the

junction between decreasing and increasing heat transfer changes from a cusp shaped form for the unseparated case, to a rounded concave form in the case of the separated flow (see figures 25d,e). The comparison can be more easily made by non-dimensionalising the results with respect to the flat plate values as shown in figure 27. The heat transfer distribution in which the cusp shape is just rounded at the point of minimum heat transfer represents the incipient separation condition. From figure 27 we also notice that as the curve changes in form, the rate at which the mimimum value of heat transfer decreases with increasing wedge angle is considerably decreased when the flow becomes separated. By plotting the minimum value of heat transfer against wedge angle (figure 27) it can be seen that a distinct change in slope occurs. This point of change is taken as in the incipient separation region. Additional confirmation of this criterion may be obtained by plotting the wedge angle against shear layer length as shown in figure 27. The value of the wedge angle to cause incipient separation is obtained by extrapolating the curve to zero shear layer length. These criteria predict that the incipient separation condition occurs at a wedge angle of 8.5 degrees.

Looking now at the heat transfer distribution in the compression region on the face of the wedge it can be seen both in separated and unseparated flows there is a sharp but uniform rise along the face of the wedge. For the unseparated flows the heat transfer distribution levels off at the end of the compression process and starts to slowly decrease again. The greater severity of the recompression process in the reattachment region of the separated flows over the 12.5° and 15° wedges causes a pronounced peaking of the heat transfer distribution. The maximum value is coincident with the end of the reattachment compression process and the minimum boundary layer thickness as observed from the schlieren photographs, which is downstream of the point of shear layer reattachment.

4.3.4. Studies of the interaction between an externally generated shock and a flat-plate boundary layer

In this investigation we study the heat transfer distribution on a flat plate in regions of adverse pressure gradient and flow separation induced by the interaction of an externally generated oblique shock wave with the laminar boundary layer on a flat plate. The tests were carried out at a Mach number of 10 and Reynolds number of 1.35×10^5/inch. The position of the shock generator was adjusted so that the shock impingement caused the interaction to occur at approximately the same Reynolds number based on the distance from the leading edge to the interaction as in the previous study. Once again the boundary layer displacement and vorticity effects associated with the leading edge of the plate can be ignored.

The heat transfer distribution, in the interaction regions on the flat plate, were measured for shock strengths corresponding to shock generator angles α of 2.1°, 3.1°, 5.2°, 8.3° and 10.4°. The schlieren photographs and heat transfer distributions obtained from these tests are shown in figure 26.

Figures 26a and 26b show the heat transfer distributions to the flat plate for the cases where the adverse pressure gradient induced by the impingment of the oblique shock was insufficient to cause separation. The heat transfer decreases as the boundary layer thickens under the adverse pressure gradient, but rising pressure and hence density causes a sharp but uniform rise in the heat transfer through the compression region, finally decreasing again as the boundary layer thickens downstream of the interaction. The heat transfer distribution in the region of mimimum heat transfer is once again characterised by its cusp-like profile.

Figures 26e, d anc c show the flow conditions which vary from the case where it is obvious that the boundary layer is fully separated as in figure 26e, to the case close to the

incipient separation condition as shown in figure 26c. The presence of a large region of separated flow is clearly indicated in the schlieren photographs by a well defined shock springing from the separation region. As the external shock becomes weaker so the separation shock becomes less distinct, finally disappearing altogether when separation does not occur. The first appearance of the upstream shock marks the incipient separation condition. The form of the heat transfer distribution in the region of minimum heat transfer in separated flow contrasts sharply with the form for the unseparated case. The curves which are plotted for comparison in figure 28 are again non-dimensionalised with respect to the flat plate value. It can be seen that in direct contrast to the cusp-like unseparated heat transfer profiles, the heat transfer distribution for the separated flow is rounded in the region of minimum heat transfer and the heat transfer begins to increase from the minimum value in a concave profile as compared with the convex form of the unseparated curve. If we plot the minimum heat transfer against the angle of the shock generator (see figure 28) we again find a discontinuity in slope which we use as an indication of the incipient separation condition. From this graph it can be seen that the incipient separation condition is induced by a shock strength which corresponds to a shock generator angle of 4.3°. Additional confirmation of this value is obtained by extrapolating the plot of shear layer length versus shock-generator angle, shown in figure 28, to zero shear layer length.

The heat transfer in the reattachment region of the flow increases almost linearly through the reattachment compression process reaching a maximum at the end of this process, which again coincides with the maximum thinning of the boundary layer. The pronounced peak in the reattachment heat transfer profiles for large separated regions is coincident with the end of the reattachment compression rise and is downstream of the reattachment point of the shear layer as deduced from schlieren photographs.

4.3.5. Comparison of wedge and externally generated shock results

The heat transfer distribution in regions of shock-wave boundary-layer interaction induced by a forward facing wedge and by externally generated shocks are very similar. For the case of unseparated flow in an adverse pressure gradient, the form of the heat transfer profiles from both wedge and external shock results are characterised by the cusp-like profile in the region of minimum heat transfer and a uniform rise in heat transfer through the compression process to a comparatively uniform level in the constant pressure region downstream of the interaction. The heat transfer profiles for wedge and shock induced separation are also very similar and are characterised by concave profile in the separation region followed by an almost linear rise to a peak value at the end of the reattachment compression process.

It is easily shown that for an inviscid flow, a wedge angle of 2α will cause the same pressure rise as a shock wave generator set at an angle of α. Thus if a wedge of angle $2\alpha_i$ causes incipient separation, if the separation phenomena is independent of the mechanism by which it is induced, i.e. a free interaction, the angle at which shock wave generator should be set under identical free stream conditions to obtain incipient separation should be α_i. From the experimental results the wedge angle to cause incipient separation was 8.4° whilst the shock generator angle to cause incipient separation was 4.3°. The similarity between heat transfer profiles together with the latter information indicates that for the configurations studied the separation phenomena is independent of the mechanism by which it is induced.

It is also of great interest to compare the maximum heat transfer generated in the compression region of both wedge and shock induced interactions for configurations which cause the same final pressure rise. Figure 32 shows the graph of wedge angle against maximum heat transfer at the end of the compression region,

upon which both shock and wedge results are plotted. The diagram indicates that the heat transfer generated at the end of the compression process is independent of whether this pressure rise was caused by a wedge or by an external shock.

There are almost no experimental studies with which these results can be compared. Bogdonoff (1962) has investigated the heat transfer distribution to a flat plate with a 10^{o} wedge at $M = 11.7$. The form and magnitude of the heat transfer profile in the separated region is very similar to the results obtained in the present experimental work. Bogdonoff found a large scatter of the results in the reattachment region. Although many measurements were made in the reattachment regions of both shock and wedge induced separation in the present experimental work, no trace of an instability was found and the maximum scatter could be attributed to experimental error.

4.4. Heat Transfer in the Reattachment Region of a Separated Shear Layer

4.4.1. Introduction

The study of the reattachment region has attained prominence because the high heat transfer rates generated in this region may cause serious heating problems to compression surfaces such as flaps or flared junctions on hypersonic vehicles over which the flow may be separated. There is very little information on the parameters which influence either the magnitude or the distribution of heat transfer in the reattachment region of a shear layer in either supersonic or hypersonic flows.

In this investigation we study the effect of the reattachment angle and free stream Mach number on the heat transfer developed in the reattachment region of a separated shear layer. Two-dimensional flat plate wedge models, with various wedge angles and step heights are used to study the effects of reattachment angle and downstream expansion on the heat transfer developed in the

reattachment region on the face of the wedge. The heat transfer developed in conical regions of reattachment were investigated by measuring the distribution of heat transfer over a series of spiked cones. These experiments were conducted at Mach numbers of ten and fifteen.

4.4.2. Flat Plate+Wedge Studies

The heat transfer distribution to wedge separated flows over two dimensional step models were measured at Mach number of 10 and free stream Reynolds number of 0.135×10^6 per inch.

Three sets of models were used in this investigation. The variable angle wedge model (shown in figure 23), which was used to study boundary layer separation, was also used to extend the experimental data up to wedge angles of 30°. A smaller second plate, which is shown below the main model, was fitted in place of the second face of the model so that it could be used up to wedge angles of 30° without blocking the tunnel. The fixed angle step models shown in figure 30 had a common step height of 0.75 inches and fixed wedge angles of 30, 45, 60, 75 and 90 degrees. The third model - the variable angle step model, which is shown in figure 29 was used to obtain measurements for wedge angles between 35 and 90 degrees. The model has a constant wedge length of 1 inch and is so designed that the angle of the wedge is continously variable, with this face rotating about a virtual hinge at the base of the step. The upper face of the model is supported so that it can follow the movement of the second face of the model. All these models were fitted with side curtains (not shown in the photographs) to prevent interference from flow beneath the models.

The length of flat plate ahead of the steps was chosen to ensure that the shock wave developed at the leading edge did not intersect with the face of the wedge,and was not long enough for the tip Mach cones to influence the reattachment process. For

this length of plate the separation of the boundary layer on the flat plate was not controlled by the leading edge, thus the angle of the separated shear layer was approximately constant for all wedge angles.

The variable angle wedge model was used to extend the data obtained in the previous section to wedge angles of 22.5° and 30°. The schlieren photographs of these flows are shown in figures 33a and 33b and the heat transfer distributions in figures 31a and 31b. The results of the heat transfer distribution in the reattachment region show very pronounced peaking. The point of maximum heat transfer coincides with the point of minimum boundary layer thickness (as observed from the schlieren photographs) which is slightly behind the reattachment point of the shear layer. It can be seen from the schlieren photographs that the point of maximum heat transfer moves nearer to the reattachment point as the angle of the wedge is increased. The approximate theoretical results obtained in section 4.6.4. for the distribution of heat transfer in the reattachment region are shown in figures 31a and 31b. By assuming the boundary layer to grow from the reattachment point, an assumption which is not strictly valid in these cases, quite good agreement is obtained downstream of the point of maximum heat transfer. The heat transfer at the end of the reattachment process calculated from equation (4.6.10) is also shown and can be seen to be in good agreement with the experimental results.

The distribution of heat transfer to the 30, 45, 60, 75 and 90 degree fixed angle step models is shown in figures 35a, 35b, 35c, 35d and 35e respectively. The schlieren photographs of the flow are shown in figures 33c, 34b, 34c and 34d. Spanwise distributions of heat transfer indicate that the flow over all the step models is essentially two-dimensional within the region tested.

A comparison between the results obtained from the 30° variable angle wedge model and the 30° fixed angle step model shows that,

within the accuracy of the experiment, the distribution of heat transfer in the reattachment region and throughout the separated flow is uninfluenced by the effect of the downstream expansion at the shoulder of the step model.

The most important feature of these flows is the magnitude and severity of the heat transfer and heat transfer gradient developed in the reattachment region. This feature serves once again to point out the importance of having adequate instrumentation on a non-conducting surface in the reattachment region. A graph of the variation of the maximum heat transfer recorded in the reattachment region against reattachment angle is shown in figure 38b. From this diagram it can be seen that the maximum heat transfer varies almost linearly with reattachment angle for the configurations with face reattachment. Observations from the schlieren photographs show that the reattachment point and the point of maximum heat transfer are almost coincident from wedge angles greater than 35°. Theoretical calculations based on the assumption of zero boundary thickness at reattachment are shown in figures 35a, 35b and 35c and are in good agreement with the experimental results downstream of the reattachment point.

For wedge angles from 30° to 75° the heat transfer to the upper face of the step model remains almost constant. The heat transfer to this face may be calculated approximately by assuming the boundary layer to grow from the junction of the top of the wedge with the upper face. The comparison between this approximation shown in figure 35a, 35b, 35c and 35d and the experimental results indicates reasonable agreement. The heat transfer to the upper face of the 90° wedge model for which shoulder reattachment occurs, differs from the previous distributions and is not in agreement with this approximate calculation.

Further experimental data on the variation of the heat transfer in the reattachment region with reattachment angle was

obtained using the variable angle step model. The heat transfer distribution over this model was measured for wedge angles of 35, 40, 45 and 52.5 degrees. Heat transfer distributions and schlieren photographs are shown in figures 36 and 37 respectively. The variation in step height as the step angle is changed from 30° to 90° is from 0.5 to 1 inch. The variation of the maximum heat transfer in the reattachment region with reattachment angle is shown in figure 38b. The good agreement between the reattachment heat transfer rates for the 45° wedges together with the general trend in the results for the models with different step heights, indicates that the effect of the downstream expansion may be neglected in these tests for wedge angles below 60°. The experimental distributions of heat transfer downstream of the reattachment point are again in good agreement with calculations based on the assumption that the boundary layer grows from the reattachment point. The heat transfer to the upper face changes very little with either wedge angle or step height, and calculations based on the assumption that the boundary layer grows from the junction of this surface with the top of the wedge are again in close agreement with the experimental results.

All these results may be compared with the low angle wedge and shock interaction results by plotting the total angle through which the flow is turned (the wedge angle) against maximum heat transfer in the reattachment region. Figure 38a shows this plot which indicates an almost linear variation of maximum heat transfer with flow angle.

In all the above tests as the angle of the wedge was increased the separation point moved forward, and thus the boundary layer thickness at separation varied for each wedge angle. To investigate the effect of boundary layer thickness on the heat transfer distribution over the models and particularly in the reattachment region, a single wedge configuration (the 45° wedge) was chosen, and the heat transfer distribution to the flat plate+wedge

configuration was measured for three lengths of flat plate. The model configurations and heat transfer distribution to these configurations are shown in figure 39. Schlieren photographs of the flow over these configurations were given in Holden (1962). The form of the heat transfer distribution in the separation region is in each case similar, with the ratio of the minimum heat transfer to the corresponding flat plate value of approximately 0.6 Ahead of the step the results from the three models combine to form a single curve which fits all the experimental points from 2 inches in front of the step, through the reattachment region and along the upper face of the step. These results indicate that the heat transfer distribution in the reattachment zone is only slightly dependent on the boundary layer thickness at separation. This conclusion is substantiated by results from the axisymmetrical spiked-body models.

The study of the heat transfer distribution in reattachment regions on axisymmetric bodies is described in the following chapter in section 4.5.4.

4.5. Heat Transfer to Axisymmetric Spiked Bodies

4.5.1 Introduction

The study of laminar separated regions in hypersonic flow, with the intention of using such regions to obtain favourable heat transfer characteristics, was basically inaugurated by a theoretical study by Chapman (1956). Chapman predicted that the total heat transfer to the boundaries of a laminar separated cavity flow was approximately one half the total heat transfer to the boundary of an equivalent attached flow bridging the cavity. Experimental work to investigate the practical use of controlled regions of laminar separated flows has been concentrated on the measurement of heat transfer around spiked blunt bodies. The configurations for which such studies have been made have been confined to hemi-spherically capped and flat-ended cylinders.

The geometry of such bodies does not allow a simple investigation into the parameters which influence the basic mechanism of heat transfer both in the separated flow region and in the region behind the point of reattachment. For it is the flow mechanism and heat transfer in and downstream of the reattachment region which constitutes the most important single influence in spiked body flow. The spiked cone allows a simple investigation to be made of the effect of body geometry in the reattachment region on the heat transfer to spiked bodies.

The following investigation was designed to study the heat transfer characteristics of spiked bodies in hypersonic flow. The main parameters varied in this study were body shape and free stream Mach number. Initial studies were made to determine the heat transfer distribution to spiked spherically capped and flat-ended cylinders at a Mach number of 10. The results from these measurements were compared with existing experimental data at different Mach numbers. The main study was devoted to an investigation of the heat transfer characteristics of a series of spiked cones with different apex angles, at free stream Mach numbers of 10 and 15.

4.5.2. Spiked spherically-capped cylinder

The distribution of heat transfer to a spiked spherically capped cylinder was measured at a Mach number of 10 and free stream Reynolds number based on body diameter of 0.225×10^6. The models used in the experiments are shown in figure 18. Heat transfer profiles for L/D ratios of 0, 0.5, 1, 2, 3 and 4 are shown in figure 40. The corresponding schlieren pictures are given in figure 41.

The pressure distribution over the spiked hemisphere was estimated from measurements from the schlieren photographs. The

conditions at the outer edge of the separated shear layer were calculated from cone tables. The pressure rise to reattachment was calculated from the relationship developed by Chapman, Kuehn and Larson (1957) but with the assumption that the temperature in the dead air region was equal to the wall temperature rather than the recovery temperature as they had assumed. Figure 42 shows the pressure distributions obtained from the calculations. These results are similar to those of Crawford (1959) and Bogdonoff (1958) but with the notable exception that for the configurations L/D = 0.5 and 1.0 the reattachment pressure rise exceeds the stagnation point value. This result is directly associated with the assumption that the temperature in the dead air region is at wall temperature rather than the recovery temperature. This is probably more realistic for our experiments in an intermittent facility, as opposed to those of Chapman et.al whose tests were carried out in a continuous facility where wall temperatures approaching the recovery temperature were obtained.

The heat transfer profiles on the spiked spheres exibit one point of great interest. For spike lengths of 0.5 and 1.0D the peak heat transfer rates, which occur in the reattachment region of the separated shear layer, exceed the stagnation point value for the unspiked sphere. The laminar results of Crawford at $M = 6.9$ and $Re_b = 0.15 \times 10^6$ do not indicate that reattachment heat transfer rates larger than the stagnation point value occur at reattachment, but as the result of the lower Reynolds number, reattachment occurred further back on the sphere. The only other results, those of Wagner (1961) who obtained an equivalent distribution at $M = 19.4$ and $Re_D = 0.23 \times 10^6$, are not sufficiently detailed for conclusions to be drawn. Although Bogdonoff (1958) did not obtain a detailed distribution of laminar heat transfer to the hemisphere, he did measure the total heat transfer to the hemisphere for spike lengths from 0 to 6 body diameters at a Reynolds number of 0.36×10^6 and $M \doteq 14$. The graph of the total heat transfer against spike length obtained by Bogdonoff is shown

in figure 43. Also plotted on this graph are the results of the present investigation together with those of Wagner and Crawford. There is excellent agreement between the results of the present investigation of those of Bogdonoff for short spike lengths. The laminar results of Crawford and Wagner do not indicate that values of total heat transfer exceeding the unspiked value occur for any body-spike configurations. The transitional results of Crawford indicate that total heat transfer rates well in excess of the unspiked value occur if transition occurs in the shear layer.

For our experiments the length of the reattachment was small compared with the radius of the reattachment circle, and thus the flow in the reattachment region may be regarded as locally two dimensional. With this approximation the results of Chung and Viegas (see section 4.6.) were applied to calculate the reattachment heat transfer for L/D = 0.5 and 1. The results of these calculations, which are plotted in figure 40, are in good agreement with the experimental values and lends support to the conclusions of Chung and Viegas, who predicted that the heat transfer rate in the laminar reattachment region could be greater than that at a stagnation point if the length of the separated shear layer is equal to or less than the nose radius of the body.

4.5.3. Spiked flat ended cylinder

The distribution of heat transfer to a spiked flat-ended cylinder was measured at a Mach number of 10 and Reynolds number based on body diameter of 0.225×10^6. The models used in these tests are shown in figure 18. Heat transfer profiles were obtained for spike lengths of 0, 3, 4 and 4.5 body diameters. Figure 44 shows the distribution of heat transfer obtained for each of the four configurations, and the schlieren photographs of the flow about the models are shown in figure 45.

The flow about the spiked configurations and the heat transfer measurements were found to be extremely sensitive to model alignment and very careful adjustment was required to obtain symmetrical heat transfer profiles in the shoulder reattachment region. For spike lengths of 4D and 4.5D the heat transfer distributions to the cylinder were almost identical, and the total heat transfer to the front face was reduced to less than one half the value in the absence of the spike. This value is in agreement with the results of Bogdonoff (1959) who investigated the total heat transfer to the face of a flat-ended cylinder at a Mach number of 14 in helium. For the configuration L/D = 3 the heat transfer rates measured over the front face indicated that the flow about the body was unstable. An examination of the heat transfer results in the region of the shoulder of the cylinder together with schlieren photographs revealed that a lateral oscillation of the flow occurred with the shear layer flicking across the gauges at the shoulder. A further reduction in spike length promoted a longitudinal oscillation the mechanism of which is described in Maull (1959).

4.5.4. Spiked cones

The tests on the spiked sphere and spiked flat-ended cylinder have shown that for some configurations the total heat transfer to a spiked body may be considerably reduced by the separated flow promoted by the spike whilst in others the total heat transfer may be increased by the presence of separated flow, even when the flow is entirely laminar. The large heat transfer rates and gradients developed in the reattachment region of the shear layer whilst being important in their own right are clearly the key factor which influences the total heat transfer characteristics of spiked bodies. From the tests on the spiked sphere it is also clear that the reattachment flow geometry is an important parameter which influences the heating in this region. The effect of the reattachment flow geometry on both the heat transfer profiles in a region of shear layer reattachment and on the total heat transfer characteristics

of spiked bodies may most easily be studied by an investigation of the flow pattern and distribution of heat transfer over a series of spiked cones with different apex angles. An examination of the total heat transfer versus spike length profiles shown in figure 43 for the spiked spheres also suggests that an increase in free stream Mach number increases the effectiveness of the spike in reducing the total heat transfer to the body.

In this series of experiments, the heat transfer and flow pattern over 4 spiked cones shown in figure 46 was measured at Mach numbers of 10 and 15 for a Reynolds number based on body diameter of 0.27×10^6.

Separated flow geometry

The separated flow past a spiked cone may be divided into a number of distinct flow patterns which depend both on the free stream conditions and the spike length and cone angle of the model. A photographic study of the separated flow over spiked cones at a Mach number of 10 and Reynolds number of 0.50×10^5 was made by Wood(1960) During the present investigation a similar study of flow geometry at a different Reynolds number, and Mach numbers of 10 and 15 was made and thus it is possible to deduce the effect of Mach number and Reynolds number on the flow configuration by comparing these results.

Six regions of different flow patterns were found and are shown in figure 51. The first type of flow (type A) occurs when the adverse pressure gradient induced by the body-spike junction is insufficient to cause flow separation. From the three diagrams in figure 51 it can be seen that the size of region A is directly proportional to the free stream Mach number and inversely proportional to the unit Reynolds number, a result which is in agreement with both the previous two dimensional work and also with the separation criteria of Chapman et.al (1957).

Separated flow type B is characterised by a flow in which separation occurs on the spike and is followed by reattachment on the face of the cone. As the size of th region increases this reattachment point of the shear layer moves nearer to the shoulder until eventually the expansion process at the shoulder controls the reattachment mechanism so that the reattachment point lies on or close to the cone-cylinder junction. The position of the boundary between face and shoulder reattachment (region B and C), which as shown by Wood is sensitive to the temperature of the body, is also influenced by the free stream Reynolds number and Mach number. As can be seen from figure 51 and as verified by selective tests, the region C increases in size at the expense of region B, as the unit Reynolds number increases and the free stream Mach number decreases.

Two distinct oscillatory flow regions were observed and are shown in figure 51 as regions D and E. The unsteady flow in region D has not been observed in any previous investigations and hence is not shown in Woods results. Schlieren photographs of the D oscillation are shown in figure 50d. It is clear from these photographs that the mechanism of this regular oscillation is associated with a cyclic movement of the separation point between the tip and the shoulder of the spike.

The E oscillation, the oscillatory flow which was observed and explained by Maull (1960), occurs when the separation and reattachment flow mechanisms cannot be satisfied simultaneously by a straight shear layer joining these two points. The oscillation appears as a series of violent longitudinal expansions and contractions of the "dead air region". An important and interesting feature of the flow in the boundary region between C and E is that there is not an abrupt breakdown from the steady flow to the longitudianl instabilty; but as observed in section (4.5.3.) the E oscillation is preceeded by a weak but regular lateral oscillation of the flow, which appears in the schlieren photographs as a small misalignment, (and hence was not detected in previous photographic studies) but changes the heat transfer to the separated region by a factor of two during one cycle.

Finally the flow type F, which causes heat transfer rates very similar to those to a cone with a detached shock but without a spike, occurs when the spike does not protrude sufficiently to penetrate the detached shock wave ahead of the cone.

Heat transfer distributions

The heat transfer distributions to the four cone configurations were measured for spike lengths ranging from 0.5 to 4 body diameters at Mach numbers of 10 and 15 and at a Reynolds number based on body diameter of 2.7×10^6. These heat transfer profiles, and the schlieren photographs of the flow patterns over the spiked cones are shown in figures 47, 49 and 48, 50 respectively.

Heat transfer to a conical reattachment region

The spiked cone is the axisymmetric equivalent of the two-dimensonal step models discussed previously in section (4.4.)

The use of axisymmetric models to study the reattachment phenomena has the virtue that there exists no problems which correspond to the finite span effects in the "two dimensional flow", and the heat transfer to the basic unspiked configurations may be used to compare and non-dimensionalise the heat transfer to the spiked bodies.

The heat transfer profiles of the flow over the spiked cones (shown in figure 47 and 49) show once again the large heat transfer rates and gradients associated with the reattachment of a shear layer. The importance of the heat transfer generated in the reattachment region is emphasised by comparing the measurements made on spiked and unspiked bodies. The maximum heat transfer rates in the reattachment region are non-dimensionalised with respect to the local heat transfer rate and the average heat transfer to the basic cone in figures 53 and 54 respectively. These results again show that heat transfer in the reattachment region is strongly dependent on the reattachment angle.

One interesting feature of the heat transfer distribution over a cone with face reattachment, is that the magnitude of the maximum heat transfer is relatively uninfluenced by the spike length or the position of the reattachment point. Although the magnitude of the maximum heat transfer decreases as the reattachment point approaches the expansion at the cone cylinder junction, the upstream influence of this expansion on the heat transfer is small and for the 30 and 45° cones the maximum heat transfer in the shoulder reattachment region differs only slightly from the value with face reattachment.

Although there is no great difference between the non-dimensionalised maximum heat transfer to the corresponding spiked cone configurations with face reattachment at Mach 10 and 15, one noticeable feature is the relatively larger heat transfer gradients in the reattachment region of the Mach 15 flow as compared with the corresponding distribution at Mach 10.

For the spiked cones with $L/D \geq 3$ the heat transfer distribution generated in the steady separated region over the face of the cone changes very little with increased boundary layer thickness at separation, resulting from an increase in spike length. This is in agreement with the previous measurements on spiked hemispheres and flat-ended cylinders, and supports the conclusions of the two-dimensional study on this topic.

As in section (4.4.2) an approximate estimate of the distribution of the heat transfer downstream of the point of face reattachment can be calculated by assuming the boundary layer to grow from the point of reattachment. As the surface is conical, the Mangler transformation must be applied to relate the two-dimensional solution the axisymmetric form (see section 4.6.5.). The results of these calculations are compared with the experimental distributions in figures 47 and 49. In general there is reasonable agreement between the experimental result and the calculations downstream of the point of reattachment.

For shoulder reattachment the theoretical method of Chung and Viegas (see section 4.6.5.) can be applied to calculate the heat transfer in the reattachment zone. The results of these calculations are compared with the experimental results for the 30°, 45°, 60° and 75° spiked cone for an L/D = 3 at a Mach number of 10 in figure 47a, b, c and d and at M = 15 in figures 49b, c and d. Although the reattachment heat transfer calculations are in general agreement with the experimental results for 45° and 60° cones at Mach numbers of 10 and 15, the theory over estimates the reattachment heat transfer on 30° and 75° cones. Because of the extreme sensitivity of the measurements in the reattachment zone to the alignment of the model, the accurate verification of this theory is difficult, but the results obtained for the spike cones together with those on the spiked sphere and flat-ended cylinder do indicate that in general this theory does constitute a valuable method (and the only method published to date) for calculating the heat transfer in the shoulder reattachment zone.

One of the weak points in the theoretical analysis of Chung and Viegas is the use of Lees heat transfer theory, in which the enthalpy gradient is assumed constant despite the large pressure gradient calculated in the reattachment zone. A more accurate solution would be obtained if the effect of the pressure gradient on the enthalphy gradient were taken into account by using the method of Rose, Kemp and Detra (see section 3.3.1.).

Total heat transfer

The total heat transfer to the spiked cones was calculated by integrating the detailed heat transfer distributions shown in figures 47 and 49. The variation of total heat transfer with cone angle and spike length at Mach numbers of 10 and 15 is shown in figures 54a and 54b. These figures indicate that the total heat transfer to the cones varies markedly with cone angle, spike length and Mach number. The most important factor which influences the

total heat transfer to the cones is the position of the point of shear layer reattachment. From figure 52a and 52b it can be seen that as the length of the spike is initially increased, the reattachment point moves away from the spike - cone junction and the large heat transfer rates generated in the reattachment region act over a larger area, and consequently the total heat transfer to the cone is increased. When the reattachment point approaches the cone cylinder junction the expansion at this corner decreases the reattachment pressure levels and hence the local heat transfer, and consequently the total heat transfer to the cones decreases.

For face reattachment the maximum total heat transfer to the cones increases with apex angle, and for the worst case (the 60° cone at M = 10) the total heat transfer is more than doubled by the presence of the spike. The larger heat transfer gradients in the reattachment region of the Mach 15 flows are reflected in the relatively lower increase in total heat transfer caused by the short spikes.

For the configurations with shoulder reattachment the total heat transfer to the cones decreases with increasing spike length, until for spike lengths of greater than 3 body diameters the total heat transfer is approximately constant at its minimum value. In all cases the minimum total heat transfer to the spiked cone is reduced below the basic cone value without presence of the spike.

One interesting feature of the "D" oscillatory flow over the 60° and 75° spiked cones, is that the variation of local heat transfer caused by the oscillation causes the magnitude of the total heat transfer to vary between the steady values which correspond to the L/D values marking the extremities of the oscillation. The E oscillatory flow causes total heat transfer rates which vary between one and one half of the corresponding unspiked values.

It is clear from these experimental results that under optimum conditions a considerable reduction in heat transfer can be effected by the use of controlled regions of separated flows. Also under these conditions there are no local heat transfer rates in excess of the values without the presence of the spike.

The effectiveness of the spiked induced separated flow in the reduction of the minimum total heat transfer to a body (i.e. for long spike lengths) increases with the bluntness of the body. At a Mach number of 10 the minimum total heat transfer for the 30°, 45°, 60° and 75° cones were 0.66, 0.50, 0.33 and 0.25 of the basic cone value respectively. A similar trend is shown in the Mach 15 results.

The effectiveness of the use of separated flows to protect aerodynamic surfaces increases with an increase in free stream Mach number. For the spiked 75° cone the ratio of the minimum total heat transfer to the unspiked value was 0.25 at a Mach number of 10 and 0.15 at a Mach number of 15.

Despite these large heat transfer reductions it is difficult to foresee the use of spike promoted separated flows in any but the most carefully controlled condition. Spiked body flows are extremely yaw sensitive. An asymmetric flow will result in face reattachment which will generate heat transfer rates many times the local unspiked value, thus creating a serious heat transfer problem. The severity of this heating increases with the bluntness of the body, thus the configuration which under optimum conditions gives the greatest reduction in total heat transfer, will in yawed flow be most adversely affected by the large heat transfer rates generated in the reattachment region. The drag and stability characteristics of spiked bodies also vary markedly with the incidence of the model.

4.6. Prediction of Heat Transfer to Separated Flow

4.6.1. Introduction

The theoretical study of heat transfer in hypersonic separated flows is probably one of the most difficult and interesting subjects in the heat transfer field. Even discounting real gas effects, there are as yet no proven solutions for the distribution of heat transfer to the walls of a separated flow region.

Basically the problem of the prediction of the heat transfer to surfaces which promote separated flow is split into two problems, namely (1) the prediction of the size and shape of the separated region and (ii) given the separated flow geometry, to determine the distribution of heat transfer to the surfaces exposed to the flow. For the cavity flow the problem is somewhat simplified as both the separation and reattachment points are defined by the geometry of the cut out. But for wedge separated flow, the flow geometry must be determined before any attempt can be made to determine the distribution of heat transfer.

In this section we are concerned primarily with the prediction of the heat transfer distribution to a wedge separated region when the flow geometry has been established, in our case by experiment.

4.6.2. General theory

The general solution of the boundary layer equations for the case of both pressure gradient and heat transfer in hypersonic flow even if viscous interaction and real gas effects are ignored represents a formidable task. In general, the methods which are used to obtain a simple solution to the boundary layer equations are based first on a transformation which reduces the compressible boundary layer equations to a form which is similar to the corresponding incompressible equation. These incompressible boundary layer equations, which are a set of simultaneous non-linear partial differential equations, are then reduced to a set of ordinary

differential equations by; (i) the introduction of an independent variable upon which the properties of the boundary layer depend exclusively - similar solutions: or (ii) by an "approximate method" which satisfies the differential equations of the boundary layer only in the average over the boundary layer thickness, rather than satisfying the boundary layer conditions for each individual particle - momentum and energy integral techniques.

Boundary layer equations

Continuity $$\frac{\partial}{\partial x}(\rho u r) + \frac{\partial}{\partial y}(\rho v r) = 0$$

Momentum $$\rho u \frac{\partial u}{\partial x} + \rho v \frac{\partial u}{\partial y} = \frac{\partial}{\partial y}\left(\mu \frac{\partial u}{\partial y}\right) - \frac{dp}{dx}$$

Energy
$$\rho u \frac{\partial H}{\partial x} + \rho v \frac{\partial H}{\partial y} = \frac{\partial}{\partial y}\left(\frac{\mu}{P_r}\frac{\partial H}{\partial y}\right) + \frac{\partial}{\partial y}\left[\mu\left(1 - \frac{1}{P_r}\right)\frac{\partial}{\partial y}\left(\frac{u^2}{2}\right)\right] \quad \ldots . \quad 4.6.1.$$

Stewartson - Illingworth transformation

A transformation which converts the compressible boundary layer equations into the incompressible form was derived independently by Stewartson (1949) and Illingworth (1949). This transformation consists essentially of stretching the co-ordinate system both normal and parallel to the wall. The viscosity is assumed to be directly proportional to temperature and given by

$$\frac{\mu}{\mu_0} = C \cdot \frac{T}{T_0} \qquad \text{where} \qquad C = \sqrt{\frac{t_w}{t_0}}\left(\frac{t_0 + 200^\circ F}{t_w + 200^\circ F}\right)$$

Stewartson introduces the new co-ordinate system

$$X = \int_0^x \frac{C\, P_e a_e}{P_0 a_0}\, dx$$

$$Y = \frac{a_e}{a_0}\int_0^y \frac{\rho}{\rho_0}\, dy$$

Applying these transformations to the above boundary layer equations we obtain

$$U_x + V_Y = 0$$

$$UU_x + VU_Y = U_e U_{ex}(1+\beta) + \nu_o U_{YY}$$

$$US_x + VS_Y = \nu_o \left[\frac{S_{YY}}{P_r} - \frac{1-P_r}{P_r}\left(\frac{\frac{\gamma-1}{2}M_e^2}{1+\frac{\gamma-1}{2}M_e^2}\right)\right]\left[\left(\frac{U}{U_e}\right)^2\right]_{YY} \quad \ldots .4.6.2.$$

where the enthalpy function S is defined as

$$S = \frac{h}{h_o} - 1$$

and the velocity in the transformed plane is

$$U = \psi_Y = \frac{a_o}{a_e} u \quad \& \quad V = -\psi_x$$

For the case of constant free stream conditions the transformation simplifies to

$$Y = \int \frac{\rho}{\rho_e} dy \quad \& \quad X = -\psi_x$$

which is used in section (4.6.5.).

The equations may be reduced to a set of ordinary differential equations by choosing the independent variables

$$\zeta = Y\sqrt{\frac{m+1}{2}\frac{U_e}{\nu_o X}}$$

and $$\psi = f(\zeta).\sqrt{\frac{2\nu_o U_e X}{m+1}} \quad \text{where} \quad U_e = AX^m$$

on substituting for ζ the incompressible equations become

Momentum $$f''' + ff'' = \beta(f^2 - 1 - \beta)$$

Energy $$S'' + P_r.fS' = (1-P_r).\left[\frac{(\gamma-1)M_e^2}{1+\frac{\gamma-1}{2}M_e^2}\right](ff'f''' - f''^2)$$

where the pressure gradient parameter β is given by

$$\beta = \frac{2m}{m+1} \quad \& \quad f' = \frac{u}{u_e}$$

for the case of zero external velocity the equations become

$$f''' + ff'' = \beta(f'^2 - 1 - g)$$

$$g''' + Pr.f.g' = 0 \qquad \ldots\ldots 4.6.3.$$

which are the stagnation point equations considered in section (3.2.1.)

The Mangler transformation

A transformation which relates the two-dimensional boundary layer flow passed a surface of dimensions s to the flow past the contour of dimensions $\bar{s}$ of the axisymmetric body is given by

$$\bar{s} = c^2 \cdot \int_0^s \frac{r_0^2}{d^2}\, ds$$

where d is a characteristic length and c is an arbitary scale factor. The transformation which was originally discovered by Mangler (1939) is valid for oompressible viscous and thermal boundary layers in laminar flow. Applying this transformation to derive the relation between skin friction coefficient for two-dimensional and axisymmetric flow we obtain

$$\frac{\bar{c}_f \sqrt{\bar{R}_{ey}}}{c_f \sqrt{R_{ey}}} = \left[\frac{\int_0^s r_0^2(s)\, ds}{s\, r_0^2(s)}\right]^{1/2}$$

Using the Reynolds analogy $\left(S_t = \frac{c_f}{2} = \frac{Nu}{Pr.Re}\right)$ we also obtain:-

$$\frac{\bar{S}_t \sqrt{\bar{R}_{ey}}}{S_t \sqrt{R_{ey}}} = \left[\frac{\int_0^s r_0^2(s)\, ds}{s\, r_0^2(s)}\right]^{1/2} \qquad \ldots\ldots 4.6.4.$$

for a cone r_0 is directly proportional to s and equation 4.6.4.

becomes:- $$\frac{\bar{S}_t \sqrt{\bar{R}_e}}{S_t \sqrt{R_e}} = \sqrt{3} \qquad \ldots\ldots 4.6.4.a.$$

The Levy, Lees transformation

A transformation which combines the essential features of the Stewartson - Illingworth transformation with the similarity parameter η was devised by Levy (1949) and is

$$\bar{s} = \int_0^s \rho_e u_e \mu_e \, ds$$

$$\eta = \frac{\rho_e u_e}{(2\bar{s})^{1/2}} \int_0^s \frac{\rho}{\rho_e} \, dy$$

This was extended to include the Mangler transformation by Lees (1956) and becomes

$$\bar{s} = \int_0^s \rho_e \mu_e u_e \, ds$$

$$\eta = \frac{\rho_e u_e r_0^k}{(2\bar{s})^{1/2}} \int_0^y \frac{\rho}{\rho_e} \, dy$$

and the momentum and energy equation now becomes

$$(Nf'')' + ff'' + \frac{2\bar{s}}{u_e} \cdot \frac{du_e}{d\bar{s}} \left(\frac{\rho_e}{\rho} - f'^2 \right) = 0$$

and $$\left(\frac{N}{P_r} g' \right)' + fg + \frac{u^2}{H_e} \left[N \left(1 - \frac{1}{P_r} \right) f' f'' \right]' = 0 \qquad \ldots . \; 4.6.5.$$

where $$\frac{2\bar{s}}{u_e} \frac{du_e}{d\bar{s}} = \beta \quad \text{and} \quad N = \left(\frac{\rho \mu}{\rho_e \mu_e} \right)$$

and also $$g = \frac{H}{H_e} \; : \; \frac{\partial f}{\partial z} = \frac{u}{u_e}$$

which are equations discussed in the problem of blunt body heat transfer in section (4.6.5.).

4.6.3. Heat transfer in regions of adverse pressure gradient

The calculation of the distribution of heat transfer to the wedge compression surfaces may be treated by an approximate analysis based on momentum integral methods. To adopt these methods it is necessary to replace the sharp discontinuity in the region of the flat plate-wedge intersection by a smooth curve connecting the

surfaces. In so doing, as will be seen later, we cannot predict the dip in heat transfer in the region of adverse pressure gradient in front of the wedge, however in this analysis we are primarily interested in the heat transfer distribution to the face of the wedge.

The flat plate reference enthalpy method has often been used to calculate the heat transfer to a surface with small adverse pressure gradients. The variation of the velocity and pressure along surfaces, can, to a first approximation be taken into account by using the local rather than the free stream values when calculating the heat transfer rate. At hypersonic speeds this method becomes extremely inaccurate. An approximate method which retains the simplicity of the reference enthalpy method whilst taking into account the pressure gradient was proposed by Monaghan (1960). This method embodies simplifications and improvements to the theory of Cohen and Reshotko (1956) which has been shown to be in agreement with experimental work. Monaghan bases the expressions for momentum thickness, skin friction and heat transfer on the transformed co-ordinate X instead of x, and the modified "flat plate solutions" become

$$R_\theta = 0.66\, R_X^{1/2}$$

$$c_f . R_x = 0.664 . \frac{l}{0.22}$$

$$St . R_x = 0.332 . \frac{h}{0.22}$$

where X is given by

$$X = \frac{\int_0^x u_1^{g_1} T_1^{g_2} dx}{u_1^{g_1} T_1^{g_2}}$$

or in terms of local Mach number distribution

$$X = \frac{\int_0^x \left(\frac{T_1}{T_a}\right) M_1^{g_1} dx}{\left(\frac{T_1}{T_a}\right) M_1^{g_1}}$$

where g_1 and g_2 are defined by

$$g_1 = 3 + 2\frac{T_w}{T_{AW}}$$

$$g_2 = \frac{5}{2} - \frac{T_w}{T_{AW}}$$

and the pressure gradient parameter m is given by

$$m = 0.44\left(\frac{T_w}{T_o}\right)\frac{X}{M}\cdot\frac{dM}{dx}$$

the values of ℓ and h are function of m , and defined by

$$\frac{\ell}{0.22} = 1 - 7.45m$$

$$\frac{h}{0.22} = 1 + 2.7m$$

where for adverse pressure gradient ℓ is a funtion of $\frac{T_w}{T_o}$ and m, but h remains constant at a value of approximately 0.225. The heat transfer is therefore given by

$$q = 0.332\,(h_{AW} - h_w)\cdot\frac{\rho_1 u_1}{\sqrt{\frac{\rho_1 u_1 x}{\mu_1}}}\cdot\frac{h(m)}{0.22}$$

where the values of ρ_1, μ_1 & u_1 are based on-local conditions.

For our purposes we introduce two modifications to this formula to take into account the variation of the product $\rho\mu$ through the boundary layer and also the effect of non-unity Prantdl number. As in section (3.4.2.) the variation of $\rho\mu$ can be taken into account by evaluating $\rho\mu$ at the reference enthalpy conditions, and the effect of a non-unity Prantdl number may be taken into account by multiplying the equation above by an empirical factor $(P_r)^n$ as in the correction for the stagnation point heat transfer. However as in the flat plate solution we choose $n = -\frac{2}{3}$ The modified form of the heat transfer equation is

$$q = 0.332\,(h_{AW} - h_w)\frac{\rho^* u_e}{\sqrt{R_{ex}}}\cdot(P_r^*)^{-2/3}\cdot\frac{h(m)}{0.22} \quad \ldots .4.6.7.$$

where R_{ex} is evaluated at reference conditions.

The heat transfer distribution determined using the above relationship was evaluated for comparison with two cases investigated experimentally. The first, the 7.5° wedge at Mach 10 on which no separation occurs, and the second, the 12.5° wedge at Mach 10 in which a small separated region is present. The junction between the flat plate and wedge surface was flared in with a smooth curve as shown in figure 55a and 55b which corresponded to the bottom of the boundary layer as indicated in the schlieren photographs shown in figures 25b and 25d.

The heat transfer distributions to these surfaces are shown in figure 55a to 55b. Whilst these distributions do not indicate the dip in heat transfer to the flat plate ahead of the wedge, they do represent both the form and the magnitude of the heat transfer to the face of the wedge to a reasonable degree of accuracy, this indicates the method constitutes a valuable aid for the prediction of the heat transfer distributions for small flap angles and flared junctions.

4.6.4. Heat transfer in the constant pressure region of a separated flow

A theoretical study of the distribution of heat transfer in the constant pressure region of a separated flow was made by Carlson (1958). This method is based on the simplification of the boundary layer equations using the momentum integral technique together with the assumption of a uniform pressure throughout the region under study. The recirculating flow within the separated region is assumed to be represented by sixth and fifth degree polynomials in velocity and enthalpy respectively. A typical velocity distribution is shown in figure 57. By substituting these profiles into integral forms of the momentum energy equation which had been considerably simplified by assuming $\frac{dp}{dx} = 0$ the problem was reduced to the solution of three simultaneous ordinary differential equations. These equations cannot be solved simultaneously in a closed form and numerical methods of solution are required.

The solutions for the distribution of heat transfer in a separated wake region were compared with the experimental results of Powers et.al (1958) and Bloom and Pallone (1958), and shown to be in general agreement. Charwat, Dewey, Roos and Hitz (1961) however found the arbitary assumption of polynomial profiles for the velocity in the separation region was seriously at variance with their experimental measurements.

A typical distribution of heat transfer from Carlsons analysis is shown in figure 55. It is sufficient here to not the qualitative agreement between this theoretical profile and the heat transfer distributions obtained in the constant pressure regions of the large angle wedge flow shown in figures 35 and 36. One important weakness of this particular theoretical method is its inability to predict heat transfer rates either in the separation region, or in the most important region in the separated flow - the reattachment region.

4.6.5. Heat transfer in the reattachment region

The heat transfer distribution in the reattachment zone of a separated shear layer is of the greatest interest for it is in this zone that the largest heat transfer rates in the separated region are developed. We can divide the reattachment phenomena into two groups (i) free or wedge reattachment and (ii) shoulder or cavity reattachment. The first case - wedge reattachment is characterised by the reattachment of a shear layer on the face of a wedge or cone, followed by a compression process to a constant pressure region uninfluenced by the proximity of an expansion corner. Shoulder or cavity reattachment occurs when the reattachment point of the separated shear layer is controlled to lie on or close to a shoulder where the compression process is partially canoelled by the expansion fan springing from the discontinuity in slope.

Wedge reattachment

The experimental work has shown that for face reattachment the point of maximum heat transfer lies slightly behind the reattachment point and the distance between the reattachment point and the point of maximum heat transfer decreases with the increased severity of the reattachment compression process. The point of maximum heat transfer rate was found to be almost coincident with the point of minimum boundary layer thickness as indicated from schieren photographs, which again coincided with the end of the compression process. The flow mechanism in the reattachment region is extremely complicated and the solution of the boundary layer equations in this region are further complicated by the fact that terms involving the normal pressure gradient, vorticity generated in the shear layer, and interaction between the reattachment shock and growth of the boundary layer behind reattachment can no longer be ignored. An exact solution of the boundary layer equations to calculate the distribution of heat transfer in the reattachment region cannot be easily envisaged.

For wedge reattachment, at reattachment angles of greater than 35°, the distance between the reattachment point and the point of maximum heat transfer rates is very small and at this point the compression process causes the boundary layer to thin violently. As a first approximation therefore, we can assume that the boundary layer grows from the reattachment point. Thus the heat transfer distribution in the reattachment region on the face of a two-dimensional wedge is given simply by:-

$$q_R = \frac{0.332 \rho_R^* u_R \cdot (P_r^*)^{-2/3} \cdot (h_{AW} - h_w)}{\sqrt{Re_{x_R}}} \quad \ldots . \; 4.6.7.$$

where x_R is the distance measured from the reattachment point, and the properties in the constant pressure region behind reattachment are evaluated at the "reference conditions" as defined in section (3.4.1.)

The experimental distribution of heat transfer in the reattachment regions of the two-dimensional wedge models are compared with calculations from the above method in figures 25, 31, 32. There is close agreement between the experimental results and the calculations.

This same technique may be used to calculate the heat transfer in the conical regions of reattachment on spiked cones. However, in this calculation the conicity of the flow must be taken into account by introducing the Mangler transformation (see section 4.6.2.). Assuming the boundary layer to grow from a radius r_R on the face of a conical surface of apex semi-angle α, then to take into account the conicity of the flow we may re-define Re_{x_R} as $Re_{\bar{x}_R}$ where $\bar{x}_R$ is defined by

$$\bar{x} = \int_0^x \frac{r_i^2 dx}{r_i} = \int_0^x \frac{(r_R + x\sin\alpha)^2 dx}{(r_R + x\sin\alpha)^2}$$

Then the heat transfer to the reattachment region on the conical face is given by

$$q_R = \frac{0.332 \rho_R^* u_R (P_r^*)^{-2/3}(h_{AW} - h_w)}{\sqrt{R_{e\bar{x}}^*}}$$

$$\text{or } q_R = \frac{0.332 \rho_R^* u_R (h_{AW} - h_w)(P_r^*)^{-2/3}}{\sqrt{R_{e\bar{x}}^*}} \cdot \left(\int_0^x \frac{(r_R + x\sin\alpha)^2 dx}{(r_R + x\sin\alpha)^2} \right)^{-1/2} \quad \ldots\ldots 4.6.8.$$

Figures 47 and 49 shows a comparison between the experimental and the values calculated using the above equation. Again there is reasonable agreement between the experimental and theoretical distributions behind the reattachment point.

Although the approximation of zero boundary layer thickness at reattachment is in good agreement with the experimental results behind the reattachment point for large reattachment angles, this method of course predicts an infinite heat transfer rate at the point of reattachment. To obtain a solution for the maximum heat

transfer at the end of the reattachment compression process, at a theoretical estimate of the boundary layer thickness in this region is required.

Reattachment heat transfer in moderately separated flows

To obtain an expression for the boundary layer thickness at the end of the reattachment compression process we shall adapt and extend calculations by Lock (1951) and Cooke (1963). The separated flow is divided into three regions; the separation region, the mixing region, and the reattachment region. The velocity profiles ahead of the separation region and in the reattachment region are assumed to be sinusoidal in form whilst those in the mixing region are of the form proposed by Lock. The solution of the boundary layer equations, as in earlier sections, makes use of the momentum integral method.

We first use the Stewartson- Illingworth transformation (section 4.6.2.) thereby reducing the compressible boundary layer equations to the incompressible form. For constant external pressure and velocity these reduce to the form

$$Y = \int \frac{\rho}{\rho_e} dy$$

and $X = Cx$ where $C = \sqrt{\frac{t_w}{t_o}} \left(\frac{t_o + 200°R}{t_w + 200°R} \right)$

The velocity profile in the boundary layer upstream of the separation point and away from the leading edge may be represented by:-

$$\frac{u}{u_e} = \sin \frac{\pi}{2} \eta \quad \text{where} \quad \eta = Y/\delta$$

The displacement and momentum thickness are therefore given by

$$\delta_1 = 4.795 \left(\frac{\nu_1 C x_1}{u_1} \right)^{1/2}$$

$$\theta = 0.655 \left(\frac{\nu_1 C x_1}{u_1} \right)^{1/2} \quad \ldots . \quad 4.6.9.$$

To obtain an estimate of the thickness of the shear layer above the dividing streamline we assume a velocity profile in the mixing region given by Lock, namely:-

Above the dividing streamline

$$\phi_u = \frac{u_u}{u_2} = \phi_i + (1-\phi_i)\sin\frac{\pi}{2}\eta_u, \quad \eta_u = Y/\delta_u$$

where ϕ_i equals the velocity ratio on the dividing streamline $(\phi_i = \frac{u_i}{u_2})$

Below the dividing streamline

$$\phi_l = \frac{u_l}{u_2} = \phi_i(1 - \sin\frac{\pi}{2}\eta_l), \quad \eta_l = Y/\delta_l$$

To obtain a relationship between the momentum thickness before and after separation we use the relationship due to Young and Kirby (1955)

$$\frac{\theta_2}{\theta_1} = \frac{\rho_1 u_1^2}{\rho_2 u_2^2}\left[\frac{1 + \frac{H_1}{2}(1-\frac{u_2}{u_1})}{1 + \frac{H_2}{2}(1-\frac{u_1}{u_2})}\right] = n$$

Just after separation the intial form of the profile in the mixing region is sinusoidual and hence

$$\delta_2 = 7.39\,\theta_2 = \delta_u$$

hence $$\frac{\delta_2}{\delta_1} = \frac{\theta_2}{\theta_1} = n$$

and thus $$\delta_2 = \delta_u = \frac{1}{n}(4.795)\left(\frac{\nu_1 C x_1}{u_1}\right)^{1/2}$$

By using the mixing layer equations we first wish to determine the velocity profile and boundary layer thickness at the beginning of the reattachment compression process.

First equating the shear forces on the dividing streamline we have

$$\frac{\partial \phi_u}{\partial Y} = \frac{\partial \phi_l}{\partial Y} \quad \text{at } Y = 0$$

therefore $$\delta_l(1-\phi_i) = \delta_u \phi_i$$

thus $$\phi_i = \frac{\delta_l}{\delta_u + \delta_l}$$

putting $$W = \delta_u + \delta_l$$

$$\delta_u = W(1-\phi_i) \quad \& \quad \delta_l = W\phi_i$$

Using the momentum integral relationship

above the dividing streamline $$\rho_2 \frac{\partial u_u}{\partial Y} = \frac{\partial}{\partial X}\int_0^{\delta_u}(u_2 - u_u)u_u dY$$

below the dividing streamline $$\rho_2 \frac{\partial u_l}{\partial Y} = -\frac{\partial}{\partial X}\int_{-\delta_l}^{0}(u_2 - u_l)u_l dY$$

thus $$\delta_u\int_0^1(\phi_u - \phi_u^2)d\eta_u + \delta_l\int_0^1(\phi_l - \phi_l^2)d\eta_l = \text{constant}$$

substituting for ϕ_u and ϕ_l and putting $\phi_u = \phi_l$ where

therefore $$\delta_u(l + m\phi_i - k\phi_i) + \delta_l(-k\phi_i^2) = l\delta_2$$

hence $$l + b\phi_i - c\phi_i^2 = \left(\frac{l\delta_2}{W}\right)$$

or $$W = \frac{l\delta_2}{(l + b\phi_i - c\phi_i^2)} = \frac{l\delta_1}{n(l + b\phi_i - c\phi_i^2)}$$

where $l = 0.1366$; $m = 0.09014$; $k = 0.2267$; $b = -0.0265$ and $c = 0.371$

from the equation above

$$\delta_u = W(1 - \phi_i)$$

therefore $$\delta_u = \frac{l\delta_1}{n}\,\frac{1 - \phi_i}{l + b\phi_i - c\phi_i^2}$$

To obtain an expression for the boundary layer thickness δ_3 at the end of the reattachment pressure rise we assume zero entrainment in the reattachment process thus:-

$$\int_0^{\delta_u}\rho_2 u_2 dy = \int_0^{\delta_R}\rho_3 u_3 dy$$

where the integrals are evaluated in the constant pressure region just ahead of reattachment and just behind reattachment respectively.

Just upstream of reattachment

$$\int_0^{\delta u} \rho u \, dy = \rho_2 \int_0^{\delta u} u \, dY$$

$$= \rho_2 u_2 \int_0^1 \left(\phi_i + [1-\phi_i] \sin \frac{\pi \eta}{2}\right) d\eta$$

$$= \rho_2 u_2 \left[\phi_i + 2\left(\frac{1-\phi_i}{\pi}\right)\right] \delta u_2$$

$$\therefore \quad \int \rho_2 u_2 \, dy = \rho_2 u_2 \left[\phi_i + \frac{2}{\pi}(1-\phi_i)\right]\left(\frac{l}{n}\right)\left(\frac{1-\phi_i}{l + b\phi_i - c\phi_i^2}\right)\delta_1 .$$

Just downstream of reattachment

$$\int_0^{\delta_3} \rho u \, dy = \rho_3 \int u \, dY$$

$$= \rho_3 u_3 \delta_3 \int_0^1 \sin \frac{\pi \eta}{2} \, d\eta$$

$$= \rho_3 u_3 \frac{2}{\pi} \delta_3$$

For zero entrainment

$$\delta_3 = \frac{\pi \rho_2 u_2}{2 \rho_3 u_3}\left[\phi_i + \frac{2}{\pi}(1-\phi_i)\right]\left(\frac{l}{n}\right)\left(\frac{1-\phi_i}{l + b\phi_i - c\phi_i^2}\right)\delta_1$$

Where $\rho_2 u_2, \rho_3 u_3$ can be calculated from the separated flow geometry together with inviscid flow relationships. δ_1 can be deduced from equation (4.6.9.) and ϕ_i can be determined from the plot of ϕ_i versus $\log.\left(\frac{x_2 u_2 \nu_2}{x_1 u_2 \nu_1 n^2}\right)$ from Cooke.

Assuming the boundary layer to grow from an imaginary point a distance x_3 along the surface ahead of the reattachment position (see figure 56)

$$\delta_3 = 4.795 \left(\frac{\nu_3 X_3}{u_3}\right)^{1/2} = 4.795 \left(\frac{\nu_3 C_3 x_3}{u_3}\right)^{1/2}$$

thus $$x_3 = \left(\frac{u_3}{\nu_3 C_3}\right)\left(\frac{\delta_3}{4.795}\right)^{1/2}$$

An approximate value for the heat transfer to the point just downstream of the end of the compression process is then given by

$$q_3 = \frac{0.332 \rho_3^* u_3 (P_r^*)^{-2/3} (h_{AW} - h_W)}{\left(\frac{\rho_3 u_3 x_3}{\mu_3}\right)^{1/2}} \quad \ldots . \quad 4.6.10.$$

Cavity reattachment

The heat transfer distribution to the reattachment zone of a two-dimensional cavity flow was examined theoretically by Chung and Viegas (1961). They considered the inviscid incompressible but rotational flow in a cavity similar to that proposed by Chapman (1956) and with the same assumptions, namely, the boundary layer thickness at separation was zero and the depth of the cavity was much larger than the thickness of the shear layer. A potential flow solution was found for the distribution of pressure and velocity along the walls of the cavity. The viscous effects were assumed to be confined within a boundary layer which grows from the reattachment point at the shoulder of the cavity. The distribution of heat transfer to the reattachment region was calculated from Lees theory (see section 3.3.1). Since the boundary layer is assumed to grow from the shoulder, the heat transfer at this point is theoretically infinite, so to obtain a finite value for the heat transfer in the reattachment zone the average heat transfer within a distance L, which is of the order of the mixing layer, is calculated. Chung and Viegas found that the average heat transfer coefficient in the reattachment zone was given by the semi-empirical expression

$$N_{u_R} = \frac{q \cdot P_r \cdot l}{(h_e - h_w)\mu_e} = 0.463\, P_r^{1/3} R_{e_l}^{3/4} \cdot \left(\frac{\rho_e}{\rho_R}\right)^{1/2} \left(0.76 + 1.411 \frac{P_e}{P_R}\right)$$

where l is the length of the separated shear layer and conditions external to the shear layer and at that reattachment point are indicated by indices e and R respectively. The above equation is applicable in the shoulder reattachment region of an axisymmetric cavity flow if the region of reattachment is small compared with the radius of the reattachment circle.

5. CONCLUSIONS

The heat transfer instrumentation, which is based on the thin film thermometer technique together with electrical analogues, has been successfully developed to measure heat transfer rates of between 0.02 and 100 Btu.ft^{-2}sec^{-1} with an accuracy of $\pm$ 8% in a gun tunnel.

Heat transfer measurements on models in unseparated flow were compared with theoretical calculations. The stagnation point solutions of Fay and Riddell, and Cohen and Reshotko were in good agreement with experimental measurements of the stagnation point heat transfer to both two-dimensional and axisymmetric models. The distribution of heat transfer to hemispherically capped and flat ended cylinders were adequately predicted by the theories of Lees, and Kemp,Rose and Detra. Measurements of the heat transfer distribution to sharp flat plates were in close agreement with the constant pressure solutions of Van Driest and Eckert, whilst the heat transfer in the viscous interaction region near the leading edge was most accurately predicted by the theory of Hall, Cheng, Golian and Hertzberg. The constant pressure solutions were used to accurately predict the heat transfer distribution over cones with vertex semi-angles of 30 and 45 degrees.

An examination of the heat transfer profiles obtained from detailed measurements in regions of adverse pressure gradient and moderately separated flow, induced both by forward facing wedges and externally generated shocks, has shown that for these configurations the separation phenomena is independent of the mechanism by which it is induced. A separation criteria, in terms of the form of the heat transfer profiles, is suggested to distinguish between separated and unseparated flows.

Measurements of the heat transfer distribution in regions of adverse pressure gradient were compared with theoretical calculations based on the basic method of Monaghan, with modifications to account

for the variation of $\rho\mu$ through the boundary layer and for a non-unity Prandtl number. Agreement between the experimental and theoretical distributions indicates that this method is a valuable aid for the prediction of heat transfer distributions over flapped and flared junctions.

A detailed study has been made of the heat transfer distribution developed in the reattachment region of both two-dimensional and axisymmetric separated shear layers. The accurate measurement of the large heat transfer gradients in these regions required a high density of individual measurements on surfaces which did not distort the heat transfer measurements by longitudinal heat conduction. A study of the heat transfer distributions and schlieren photographs over two-dimensional models with moderately separated flow revealed that the maximum heat transfer occurred, not at the reattachment point, but at the end of the reattachment compression region at a point which was coincident with the minimum thickness of the reattached boundary layer. The heat transfer at the end of the reattachment compression rise was calculated for small angle wedges by a method based on calculating the boundary layer thickness in this region. The results of this method were in reasonable agreement with the experimental values for small wedge angles, but were increasingly inaccurate for wedge angles of greater than 35°.

The experimental measurements indicated that the distance between the reattachment point and point of maximum heat transfer decreased with increasing wedge angle, until for wedge angles of greater than 35°, these points were virtually coincident. Calculations based on the assumption that the boundary layer grows from the reattachment point were in reasonable agreement with the experimental measurements, both in two-dimensional and axisymmetric, flows, downstream of the point of face reattachment. The magnitude of the maximum heat transfer generated in the reattachment region varies approximately linearly with reattachment angle.

Heat transfer measurements in the separated flow over spiked cones at Mach numbers of 10 and 15 indicate that although the Mach number of the free stream does not greatly influence the magnitude of the non-dimensionalised maximum heat transfer, the heat transfer gradients are more severe in the higher Mach number flows.

Experimental data from tests on both the two-dimensional and axisymmetric models indicates that the boundary layer thickness at separation does not significantly influence the heat transfer generated in the reattachment region.

Theoretical calculations based on the method of Chung and Viegas were in agreement with experimental measurements in regions of shoulder reattachment. The results of the experimental work indicates that the heat transfer rates developed at the reattachment point of a reattaching laminar shear layer can be greater than those found at the stagnation point of a body, whose radius of curvature at this point is equal in length to the shear layer.

All these heat transfer measurements indicate that the heat transfer generated in the reattachment region of a separated shear layer will constitute a serious heating problem ranking in importance with that of nose and leading edge heating on hypersonic vehicles.

The total heat transfer to axisymmetric spiked bodies varies markedly with body shape, spike length and Mach number. The most important factor which influences the total heat transfer characteristics is the position of the point of shear layer reattachment. For face reattachment on a cone the maximum total heat transfer increases with reattachment angle, and for the worst case (60°cone, L/D = 0.75. at M = 10) the total heat transfer was more than doubled by the presence of the spike. For shoulder reattachment the total heat transfer to the cones decreases with increasing spike length, until for spike lengths of greater than 3 body diameter the total heat transfer is approximately constant at its minimum value. Under these conditions the total heat transfer to an axisymmetric blunt body can be substantially reduced by the promotion of flow

separation with a spike. The effectiveness of the spike in reducing the total heat transfer increases with flow Mach number and body bluntness. Under optimum conditions total heat transfer rates of less than one fifth of the basic cone value can be obtained, without the penalty of large local increases in heat transfer to the reattachment region.

Spiked body flows are extremely yaw sensitive and an asymmetry in the flow pattern will result in the generation of very large local heat transfer rates in the reattachment region. The spiked bodies which are most effective in reducing the total heat transfer, will be most adversely affected by the heat transfer generated in the reattachment region of a asymmetric flow.

REFERENCES

Author(s)	Date	Title etc.
Beastall, D.	1952	The Effect of a Spike Protruding in Front of a Bluff Body at Supersonic Speeds. R & M No.3007
Bendersky, D.	1953	A Special Thermocouple for Measuring Transient Temperatures. Mech. Engng. Vol.75. p.p.117.
Bershader, D. Allport, J.	1956	On the Laminar Boundary Layer Induced by a Trailing Shock Wave. Princeton University TR 11 - 22.
Bloom, M.H.	1961	On Moderately Separated Flows. Jour. Aero/Space Sci. Vol.28 N.4.
Bloom, M.H. Pallone, A	1958	Shroud Tests of Pressure and Heat Heat Transfer Over Short After-bodies with Separated Wakes. W.A.D.C. T.N.58 - 185, Polytechnic Inst. of Brooklyn.
Bogdon, L.	1963	High Temperature, Thin-Film Resistance Thermometers for Heat Transfer Measurements. C.A.L. Rep. No. HM-1510-Y-6.
Bogdonoff, S.M. Vas, I.E.	1955	Preliminary Investigation of Spiked Bodies at Hypersonic Speeds. Jour. Aero/Sci. Vol.26. No.2.
Bogdonoff S.M. Vas I.E.	1962	Some Experiments on Hypersonic Separated Flows. A.R.S. Jour. Vol.32. No.10. Oct.1962. p.p.1564 - 1572.
Bray, K.N.C. Gadd G.E. Woodger, M	1960	Some Calculations by the Crocco-Lees and Other Methods of Interactions between Shock Waves and Laminar Boundary Layer, including Effects of Heat Transfer and Suction. A.R.C. C.P.556
Carslaw, H.S. Jaeger, J.C.	1948	Conduction of Heat in Solids. Oxford Univ. Press, Oxford.

Carlson	1959	Heat Transfer in Laminar Separated Wake Regions. 1959 Heat Transfer and Fluid Mechanic Institute. Institute Stanford Univ. Press.
Centolanzi, F.J.	1963	Heat Transfer to Blunt Conical Bodies having Cavities to Promote Separation. N.A.S.A. T.N. D-1975, July 1963.
Chapman, D.R. Rubesin, M.W.	1949	Temperature and Velocity Profiles in the Compressible Laminar Boundary Layer with Arbitrary Distribution of Surface Temperature. Jour. Ae.Sci. Vol.16. No.9.
Chapman, D.R.	1956	A Theoretical Analysis of Heat Transfer in Regions of Separated Flow. N.A.C.A. T.N.3792
Chapman, D.R.	1949	Laminar Mixing of a Compressible Fluid. N.A.C.A. T.N.1800.
Chapman, D.R. Kuehn, D.M. Larson, H.K.	1957	Investigation of Separated Flows in Supersonic and Subsonic Stream with Emphasis on the Effect of Transition. N.A.C.A. T.N.3869
Charwat, A.F. Dewey, C.F. Roos, J.A. Hitz, J.A.	1961	An Investigation of Separated Flows. Part I. Jour. Aero/Space Sci.Vol.27. No.6. Part II. Jour Aero/Space Sci.Vol.27. No.7.
Cohen, C.B. Reshotko, E.	1955	Heat Transfer at the Forward Stagnation Point of Blunt Bodies. N.A.C.A. T.N.3513.
Chung, P.M. Viegas, J.R.	1962	Heat Transfer at the Reattachment Zone of Separated Laminar Boundary Layers. N.A.S.A. T.N. D-1072.
Cox, R.N.	1960	Hypersonic Flow. Proc Colston Sym. Butterworths, Eng.1960
Cooke, J.C.	1963	Separated Supersonic Flow. R.A.E. T.N. No. A.E.R.O.2879.

Crawford, D.H.	1959	Investigation of the Flow Over a Spiked-Nose Hemisphere-Cylinder at a Mach Number of 6.8. N.A.S.A. T.N. D-118.
Crocco, L. Lees, L.	1952	A Mixing Theory for the Interaction between Dissipative Flows and Nearly Isentropic Streams. Jour. Aero/Sci. Vol.10. No.10.
Curle, N.	1962	The Effects of Heat Transfer on Laminar Boundary Layer Separation in Supersonic Flow. A.R.C.21, 986. F.M.2965.
Curle, N.	1960	The Steady Compressible Laminar Boundary Layer with Arbitrary Pressure Gradient and Uniform Wall Temperature. Proc. Roy. Soc. A. 249. p.206.
Eckert, E.R.G.	1955	Engineering Relations for Skin Friction and Heat Transfer to Surfaces in High Velocity Flows. Jour. Aero/Space. Sci. Vol.22. No.8 p.p. 585 - 587.
Emrich, R.J. Chabai, A.J.	1955	Measurement of Wall Temperature and Heat Flow in a Shock Tube. Jour. Applied Physic. 1955.
Fay, J.A. Riddell, F.R.	1957	Theory of Stagnation Point Heat Transfer in Dissociated Air. A.V.C.O. Research Lab. Res.Rep.No.1.
Ferguson, H.F. Schaefer, J.W.	1962	Heat Transfer and Pressure Distribution Cone-Cylinder-Flare Configuration with Boundary Layer Separation. N.A.S.A. T.N. D-1436.
Gadd, G.E. Holder, D.W. Regan, J.D.	1954	An Experimental Investigation of the Interaction between Shock Waves and Boundary Layers. Proc. Royal Soc. Vol.226. No.1165 p.p.227 - 253. November 1954.

Gadd, D.W. Holder, G.E.	1955	The Interaction between Shock Waves and Boundary Layers and its Relation to Base Pressures in Supersonic Flows. Proceedings of a Symposium of Boundary Layer Effects in Aerodynamics. N.P.L. (1955)
Gadd, G.E. Holder, D.W.	1959	The Behavious of Supersonic Boundary Layers in the Presence of Shock Waves. I.A.S. Paper No.59 - 138.
Gadd, G.E. Attridge, J.L.	1961	A Note on the Effects of Heat Transfer on the Separation of a Laminar Boundary Layer. A.R.C. C.P.556.
Gadd, G.E.	1960	Boundary Layer Separation in the Presence of Heat Transfer. N.P.L./Aero./400.
Ginoux, J.J.	1960	The Existence of Three-Dimensional Perturbations in Reattachment of a Two-Dimensional Supersonic Boundary Layer after Separation. A.G.A.R.D. Rep.272.
Glick, H.S.	1960	Modified Crocco-Lees Mixing Theory for Separated Flows. Jour.Aero/Space Sci. Vol.29. No.10.
Hall, J.K. Cheng, H.K. Golian, T.C. Hertzberg, A.	1961	Boundary Layer Displacement and Leading-Edge Bluntness Effects in High-Temperature Hypersonic Flow. Jour. Aero/Space Sci. Vol.22. No.8. p.p. 585 - 587.
Hackemann, P.	1941	Method for Measuring Rapidly Changing Surface Temperature and its Application to Gun Barrels. British Theor. Res. Tr. 1/46. Armament Res. Dept.
Hakkinen, R.J. Greber, I. Trilling, L.	1959	The Interaction on an Oblique Shock Wave with a Laminar Boundary Layer. N.A.S.A. Memo 2 - 18 - 59W.
Hantzsche, W. Wendt, H.	1940	Jahrbuch deut. Luftfahr. 1, 517

Hertzberg, A. Wittliff, C.E.	1960	Summary of Shock Tunnel Development and Application to Hypersonic Research. I.A.S. Paper No.60 - 67.
Holden, M.S.	1962	Preliminary Investigation of Heat Transfer Rates in Regions of Separated Flow. Imperial Col. Aero. Dept. Rep. No.114. Sept.1962.
Johannsen, N.H.	1955	Experiments on Supersonic Flow past Bodies of Revolution with Annular Gaps of Rectangular Section. Phil. Mag. Series 7. Vol.46
Jones, J.J.	1952	Flow Separation from Rods Ahead of Blunt Noses at Mach Number 2.72. N.A.C.A. R.M.L. 52E05a.
Kemp, N.H. Rose P.H. Detra, R.W.	1958	Laminar Heat Transfer Around Blunt Bodies in Dissociated Air. Res. Rep.15 A.V.C.O.
Larson, H.K.	1958	Heat Transfer in Separated Flows. Jour. Aero/Space Sci. Vol.25. No.11.
Lawson, D.I. McGuire, J.H.	1953	The Solution of Transient Heat-Flow Problems by Analogous Electrical Networks. Proc. Inst. Mech. Eng. Vol.167 p.275.
Ledford, R.L.	1962	A Device for Measuring Heat Transfer Rates in Arc-discharge Hypervelocity Wind Tunnels. A.E.R.C. T.D.R. - 62 - 64.
Lees L.	1956	Laminar Heat Transfer over Blunt-Nosed Bodies at Hypersonic Speeds. Jet. Prop. Vol.26. No.4. p.p.259 - 269.
Lees, L.	1957	Recent Developments in Hypersonic Flow. Jet. Prop. Vol.27. No.9. p.p.1162-1177.
Liepmann, H.W. Roshko, A. Dhawan, S.	1951	On Reflection of Shock Waves from Boundary Layers. N.A.C.A. Rep. No.1100. 1952.

Lock, R.C.	1951	The Velocity Distribution in the Laminar Boundary between Parallel Streams. Quar. Jour. Mech. App. Maths. Vol.14. p.p.42.
Mair, W.A.	1952	Experiments on Separation of Boundary Layers on Probes in Front of Blunt-Nosed Bodies in a Supersonic Air Stream. The Phil. Mag. July 1952.
Maull, D.J.	1960	Hypersonic Flow over Axially Symmetric Spiked Bodies. J.F.M. Vol. 8. p.p.584 - 592.
Merritt, G.E.	1961	Velocity Measurement in the University of Southampton Hypersonic Gun Tunnel. University of Southampton. Aero.and Astro. Rep. No.172.
Meyer, R.F.	1960	A Heat Flux Meter for use with Thin-Film Surface Thermometers. N.R.C.C. Rep. L.R. - 279.
Mier, A.	1939	Recording Rapidly Changing Cylinder Wall Temperatures. T.M.1013, May 1942.
Miller, D.S. Hijman, R. Redeker, E.	1962	Shock Impingement on Boundary Layer Proc. Inst. Heat Transfer and Fluid Mechanic. Stanford Univ. Press.
Moeckel, W.E.	1951	Flow Separation Ahead of Blunt Bodies at Supersonic Speeds. N.A.C.A. T.N.2418.
Monaghan, R.J.	1960	Effects of Heat Transfer on Laminar Boundary Layer Development Under Pressure Gradients in Compressible Flow. A·G.A.R.D. Rep. No.279
Morgan, C.C. Andrews, J·C.	1960	"Morgandyne" Heat-Transfer Transducer and Flame-Torch Calibration Technique for Hypersonic Wind Tunnels. A.E.D.C.-TR-60-1.
Nash, J.F.	1962	The Effect of an Initial Boundary-Layer on the Development of a Turbulent Free Shear Layer. N.P.L. Aero.Rep. 1019. A.R.C.23847.

Naysmith, A.	1962	Measurements of Heat Transfer in Bubbles of Separated Flow in Supersonic Air Streams International Heat Transfer Conf. A.S.M.E. Publ. (Part 2. Sect. A and B).
Needham, D.A.	1963	Progress Report on the Imperial College Hypersonic Gun Tunnel. Imperial Coll. Aero. Rep. No.118.
Perls, T.A. Hartog, J.J.	1961	Pyroelectric Transducers for Heat Transfer Measurement Lock-Head Missile and Space Divison. Rept. No.L.M.S.D. - 325500.
Powers, W.E. Stetson, K.F. Adams, M.C.	1959	A Shock Tube Investigation of Heat Transfer to the Wake of a Hemisphere-Cylinder, with Applications to Hypersonic Flight. I.A.S. Rept. No.59 - 35.
Rabinowicz, J. Jessey, M.E. Bartsch, C.A.	1956	Resistance Thermometers for Transient High Temperature Studies. Jour. Applied Physic. Vol.27. p.97.
Rabinowicz, J.	1957	Measurements of Turbulent Heat Transfer Rates on an Aft - Portion and Blunt Base of a Hemisphere-Cylinder in a Shock Tube. G.A.L. C.I.T. Hypersonic Research Project. Memo No.41.
Robertson, A.F. Cross, D.	1958	An Electrical-Analogue Method for Transient Heat Flow Analysis. U.S. Bureau Standards. Jour. of Research Vol.61. No.2.
Romberg, N.F.	1956	Stagnation Point Heat Transfer for Hypersonic Flow. Jet Propulsion Vol.28 p.p.1098 - 1101.
Rose, P.H.	1958	Development of the Calorimeter Heat Transfer Gauge for Use in Shock Tubes. Review of Scientific Instruments. Vol.29. No.7.
Sabol, A.P.	1958	Stagnation Point Heat Transfer Measurement to a Hemisphere. N.A.C.A. T.N.4354.

Seban, R.A. Emery, A. Levy, A.	1958	Heat Transfer to Separated and Reattached Subsonic Flows obtained Downstream of a Surface Step. Jour. Aero. Sci. Vol.26. No.12.
Stalder, J.R. Nielson, H.V.	1954	Heat Transfer from a Hemisphere-Cylinder Equipped with Flow-Separation Spikes. N.A.C.A. T.N.3287.
Sterrett, J.R. Emery, J.C.	1960	Extension of Boundary Layer Separation Criteria to a Mach Number of 6.5 by Utilising Flat Plates and Forward Facing Steps. N.A.S.A. T.N. D-618.
Sibulkin, M	1952	Heat Transfer Near the Forward Stagnation Point of a Body of Revolution. Jour. Aero. Sci. Vol.19. No.8. p.p.570.
Skinner, G.T.	1960	Analogue Networks to Convert Surface Temperature to Heat Flux. C.A.L. Rep. No. C.A.L.-100.
Skinner, G.T.	1961	Calibration of Thin-Film Backing Materials. A.R.S. Journal. Vol.31. No.5.
Stollery, J.L.	1960	Stagnation Temperature Measurement in a Hypersonic Gun Tunnel Using the Sodium Line Reversal Method. Imperial College Aero. T.N.16.
Stollery, J.L. Maull, D.J. Belcher, B.J.	1960	The Imperial College Hypersonic Gun Tunnel. Journ. of Royal Aero. Soc. Jan.1960.
Squire, H.B.	1938	Modern Developments in Fluid Dynamics Vol.II. p.p. 631.
Thomann, H.	1958	Measurements of Heat Transfer and Recovery Temperature in Regions of Separated Flow at a Mach Number of 1.8. F.F.A. Rep.82.
Van Driest, E.R.	1952	Investigation of the Laminar Boundary Layer in Compressible Fluids using the Crocco Method. N.A.C.A. T.N.2597.

Vidal, R.J.	1956	Model Instrumentation Techniques for Heat Transfer and Force Measurements in a Shock Tunnel. Wright Air. Dev. Cent. T.N.56-315 A.D.-97238.
Wagner, R.D. Pine, C.P.	1961	Laminar Heat Transfer and Pressure Distribution Studies on a Series of Re-Entry Nose Shapes at a Mach Number of 19.4. in Helium. N.A.S.A. T.N. D-891.
Winding, C. Topper, L. Baus, B.	1956	Metal Film Resistance Thermometers for Measuring Surface Temperatures. Inst. Engng. Chem. Vol.47. p.p.386.
Wood, C.J.	1962	Hypersonic Flow over Spiked Cones. J.F.M. Vol.12. Part 4. p.p.614-624.
Young, A.D.	1949	Modern Developments in Fluid Dynamics (High Speed Flow) Vol.I.p.p.422.
Young, A.D. Kirkby, S.	1955	The Profile Drag of Biconvex and Double Wedge Wing Sections at Supersonic Speeds. Proceedings of a Symposium on Boundary Layer Effects. in Aerodynamic. N.P.L.
Zakkay, V.	1961	Preliminary Experimental Investigation of the Flow about a Blunt Body with Flow-Separation Spikes at M = 7.9. P.I.B.A.L. Rep. No.631

APPENDIX 1

GAUGE AND MODEL PREPARATION

Preparation of thin film gauges

The preparation of the thin film gauges was the single most important factor in experimental technique.

Application The resistance element was deposited using the "painting technique", in which a metallic alloy of platinum and gold which is held in suspension in an organic solvent, is applied in a thin film to the pyrex substrate. The paint used in this work was Hanovai X-05. Application of the paint using a ruling pen, an air spray and a hand brush were all tried. The ruling pen did not give sufficient control over the gauge thickness, which was generally too thick. The air-spray could be used to give a film of finely controlled thickness, but the masking of the model was difficult, particularly on curved surfaces. All the films used in the experiments were applied with a sable brush, and with practice the resistance could be reproduced with an accuracy approaching 5%. After the model had been cleaned thoroughly with acetone, a thin coating of the paint was applied, which was just thick enough for the brush marks to flow out. It was found that when the paint was applied too liberally, films of poor quality were produced, and when thick films were required it was found more satisfactory to build up the film thickness by a series of painting and baking cycles rather than increase the quantity of metal to the surface in a single application.

Baking Cycle The baking process is of critical importance in the production of thin film gauges with the optimum abrasion properties. A series of carefully controlled experiments were made to examine the mechanism of the metal glass bond and to determine the baking

cycle which produced films of optimum quality. A number of tests were made in which the film thickness, maximum baking temperature and length of baking cycle was varied independently. The films were examined using interferometer techniques, and by subjecting the films to abrasion. From the interferometer examination it was found that after the organic solvent had been driven off, at approximately 480°C, uniform films of between one half and one tenth of a micron in thickness were deposited on the surface of the pyrex. At a temperature of approximately 600°C the pyrex substrate begins to soften and the metal begins to sink (but not necessarily diffuse) into the surface, until at a temperature of 680°C only about one-quarter of the film thickness remains above the surface of the surrounding pyrex. The surface tension of the platinum caused the surface of the films to be approximately parabolic in form as shown in figure 2. The abrasion properties of the films were tested by examing them under a microscope whilst they were scratched with a sharp instrument. For films baked to a maximum temperature of between 480°C, and 600°C (at which temperature the pyrex starts to soften), the platinum films can be easily removed by mild abrasion. The tenacity of the film increases with maximum baking temperature between 640°C and 680°C. The maximum baking temperature is controlled by the structural strength of the models and the amount of diffusion of the film material allowed into the pyrex. Since the calibration factor of the gauge may depend upon the amount of diffusion of the gauge material into the substrate, a common baking and annealing cyle was used for all models. An automatic baking apparatus was used to control the baking cycle of each model. The baking cycle used is shown in figure 15. It is important that gaseous products from the organic solvent should be allowed to escape from the oven otherwise dull fragile films will result.

Abrasion Properties Considerable experience was gained on abrasion problems encountered in tunnel operation. Although the subject is extremely complicated, in a rough way we can classify flow abrasion into two types; tangential abrasion, and pitting abrasion. While for tangential abrasion, the thinnest practical gauge proved to give the best performance, thick gauges were found to be the most satisfactory for resisting pitting abrasion. The gauge thickness on the models in the experiments were varied in accordance with these observations.

Silver Connecting Leads All the connections to the platinum gauges were made with painted silver connecting leads of Hanovia silver paste No.25. The leads had a resistance of less than one percent of the gauge resistance and were approximately two orders of magnitude smaller than the thickness of the boundary layer. The soldered connections to the silver leads were made in positions so that they did not create a disturbance to the airflow over the models. Soldering directly to the platinum, while perfectly easy, was found to locally weaken the gauge close to the junction, as well as creating a local disturbance to the air flow. The silver paste was applied to the models using a "Standograph Stencil Pen", with the paste thinned with turpentine to the optimum consistency. The baking cycle for the silver paste was exactly the same as for the film material but with the maximum temperature reduced to 640°C. All the electrical connections to the models were made with wiring leads covered with special teflon insulation material. This covering enabled the models to be calibrated up to 100°C without rewiring and was particularly useful when a series of very closely spaced connections were made, where the insulation could be maintained right up to the soldered junction.

Preparation of Glass Models All the surfaces upon which aerodynamic measurements were taken were made from pyrex glass. This glass was found to be best suited for the process of blowing, forming a grinding together with the other operations involved in the production of a finished model. Since the models could not be produced by conventional machining processes, special problems were involved in the production of models with accurate dimensions. The axisymmetric models represented the greatest problem for these were made by hand. Although the obvious method was to construct the models by grinding down a solid bar of glass to the required shape, the large cost involved ruled out this technique. After a number of techniques had been tried without success, a method was developed in which a stainless steel tool in the shape of the model was used to form a molton cylinder of pyrex rotating in a glass lathe. The shoulder of the cone models which were slightly rounded by the forming process were sharpened by grinding the cylindrical section of the models. The models were checked with specially prepared templates and a tolerance of 2% of the nominal dimensions was specified.

It is important that the models should be polished to give a good surface finish to prevent excessive and irregular diffusion of the gauge material into the substrate during the baking process. It is also important that after the models have been polished and before the platinum gauges are applied the model should be taken through the baking cycle. Careful microscopic examination on polished glass which had not been annealed before the films were applied, revealed that microscopic cracks invisable to the naked eye, which had been "welded over" in the polishing process would sometimes re-open causing a partical fracture and weakening of the gauge. This difficulty was completely overcome by baking and annealing the models directly after they had been polished.

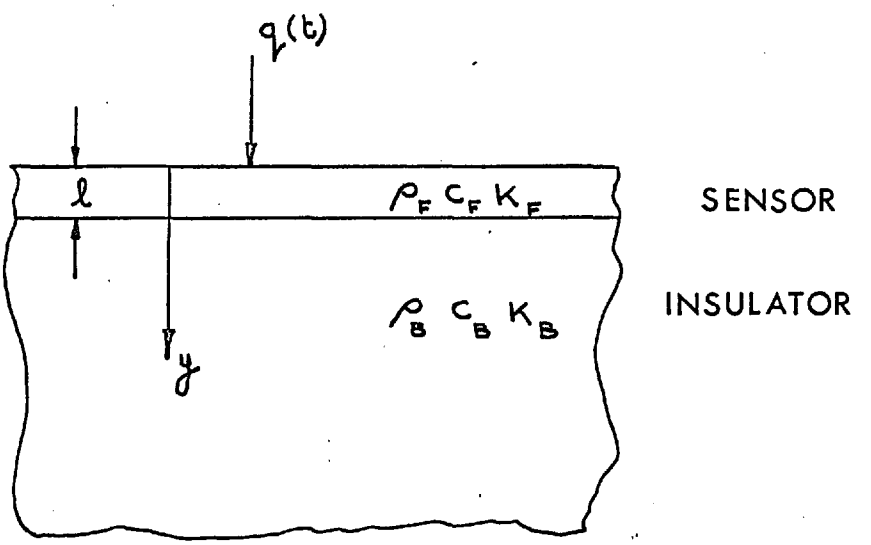

Figure 1 ONE DIMENSIONAL HEAT CONDUCTION MODEL

Figure 2 ACTUAL CROSS-SECTION OF THIN FILM

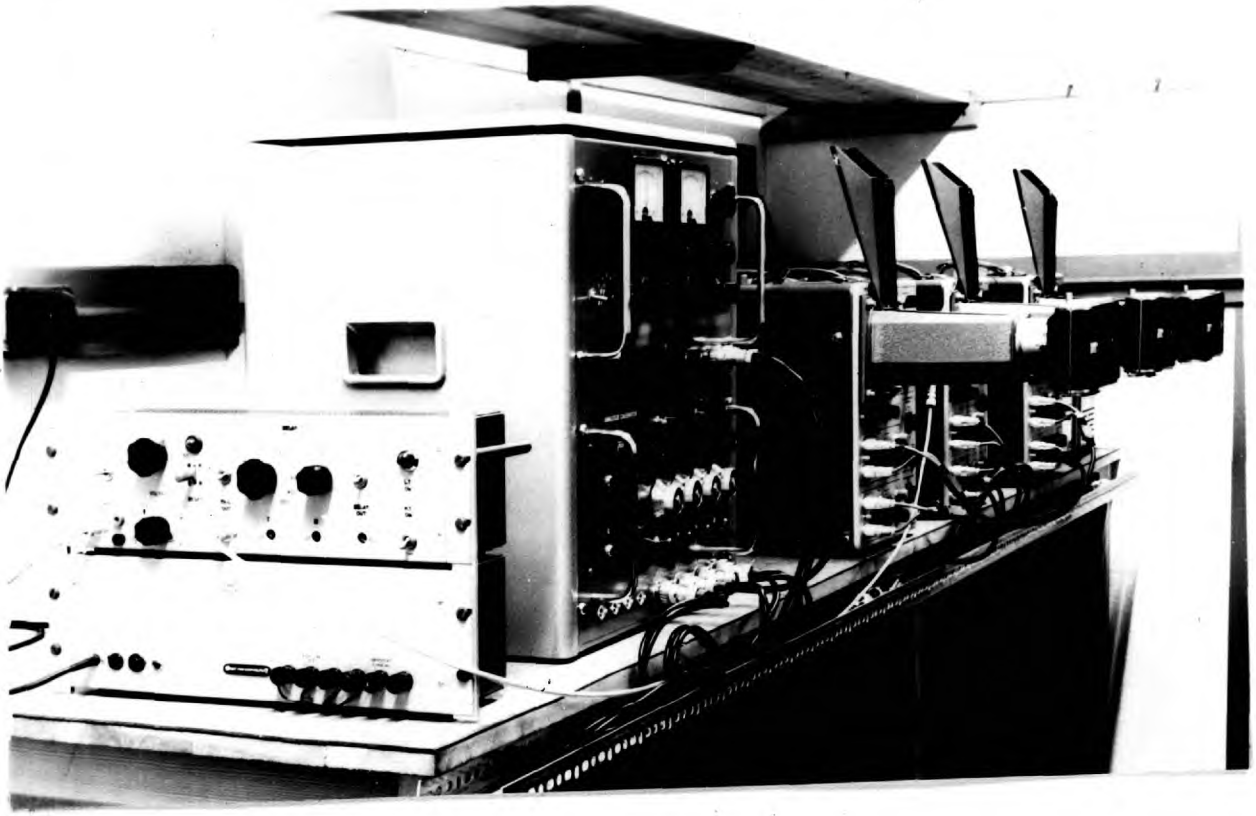

Figure 3 THE HEAT TRANSFER RECORDING APPARATUS

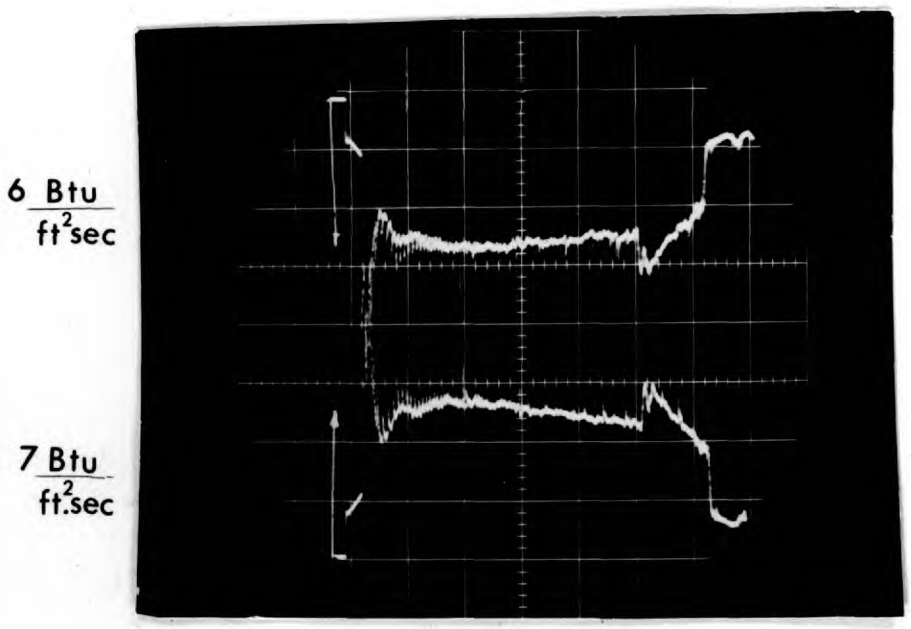

Figure 4 TYPICAL ANALOGUE TRACES

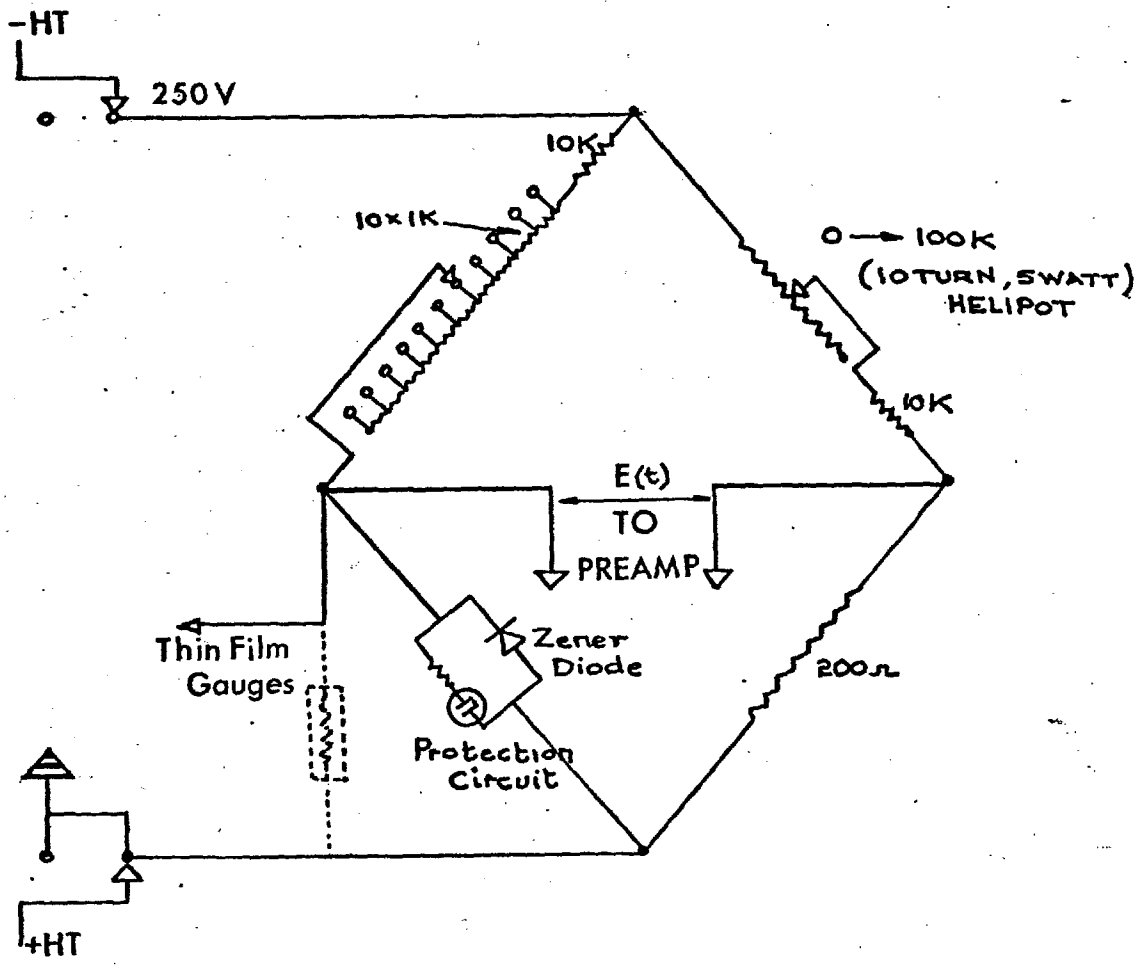

Figure 5 SIGNAL BRIDGE CIRCUIT

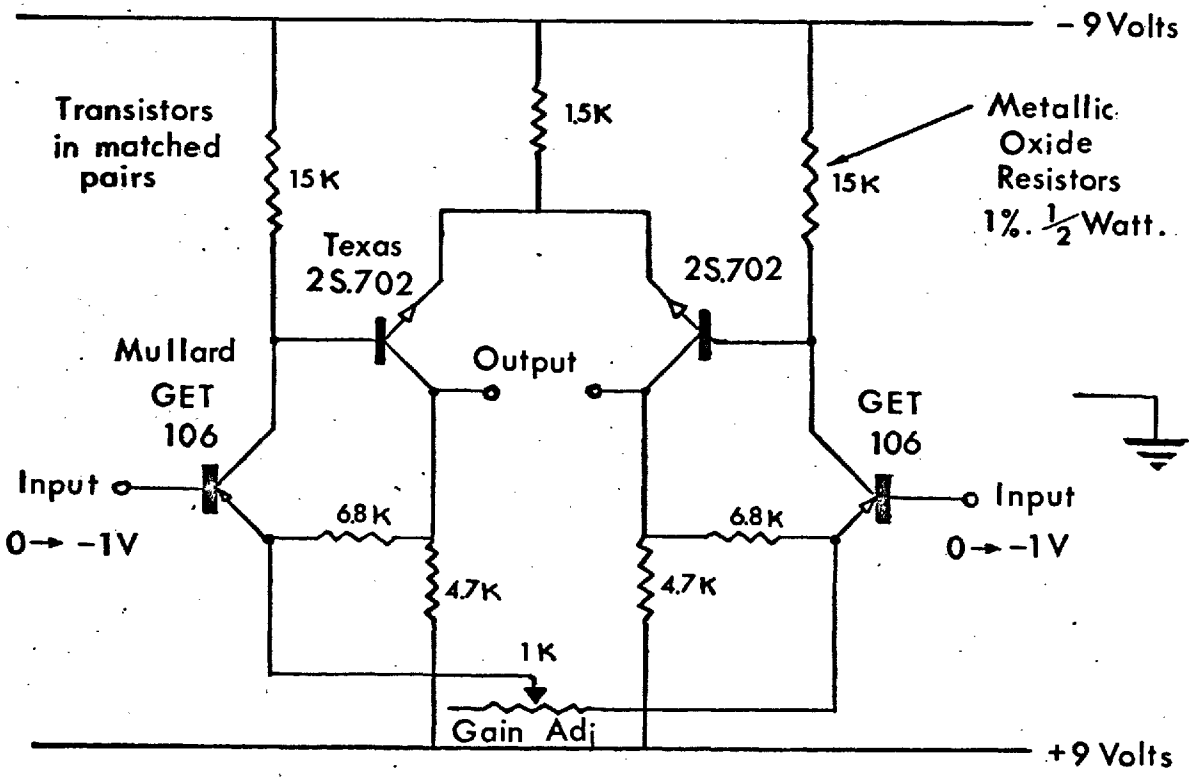

Figure 6. TRANSISTOR DIFFERENTIAL AMPLIFIER

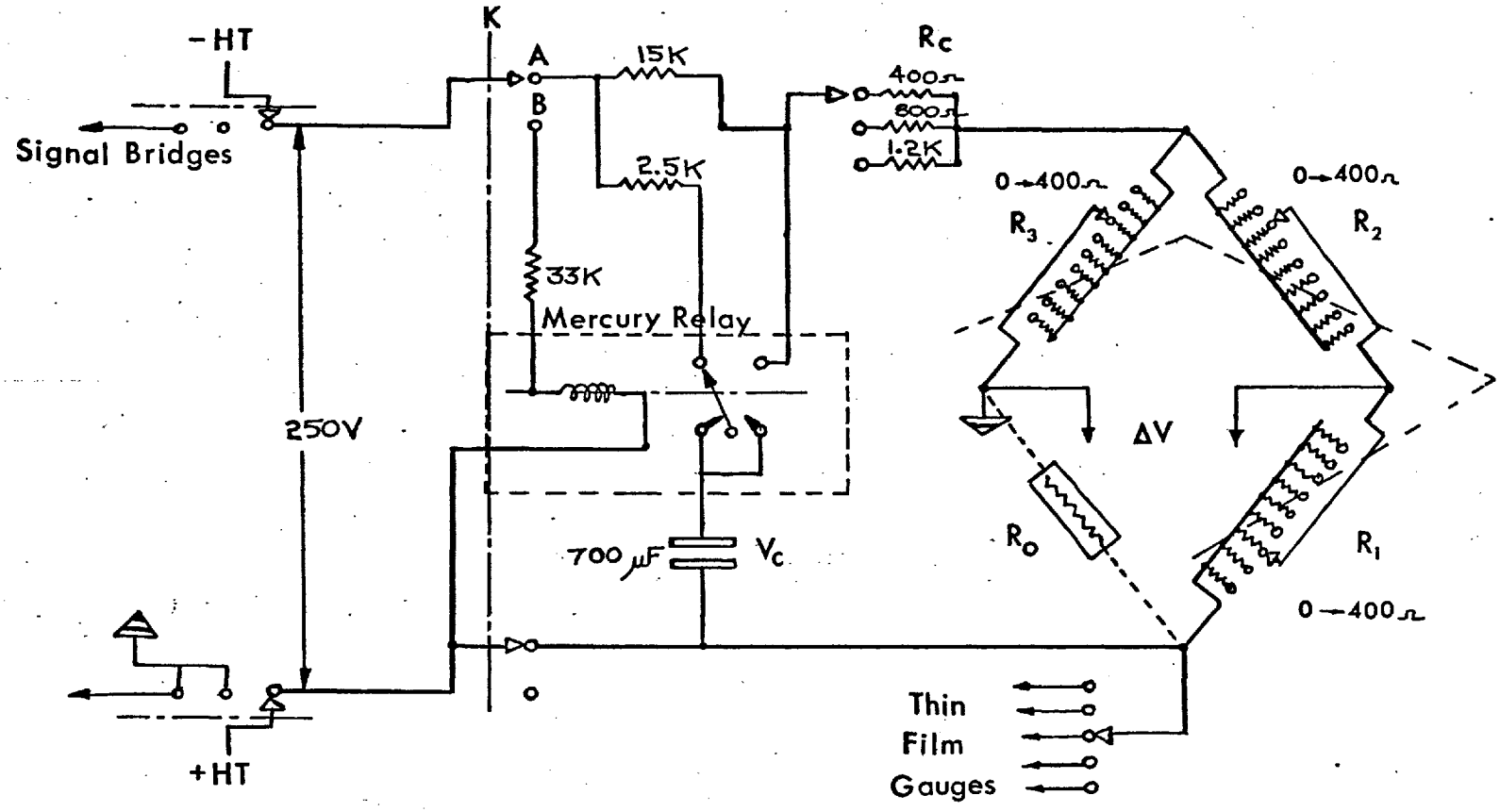

Figure 7 PULSE CALIBRATOR

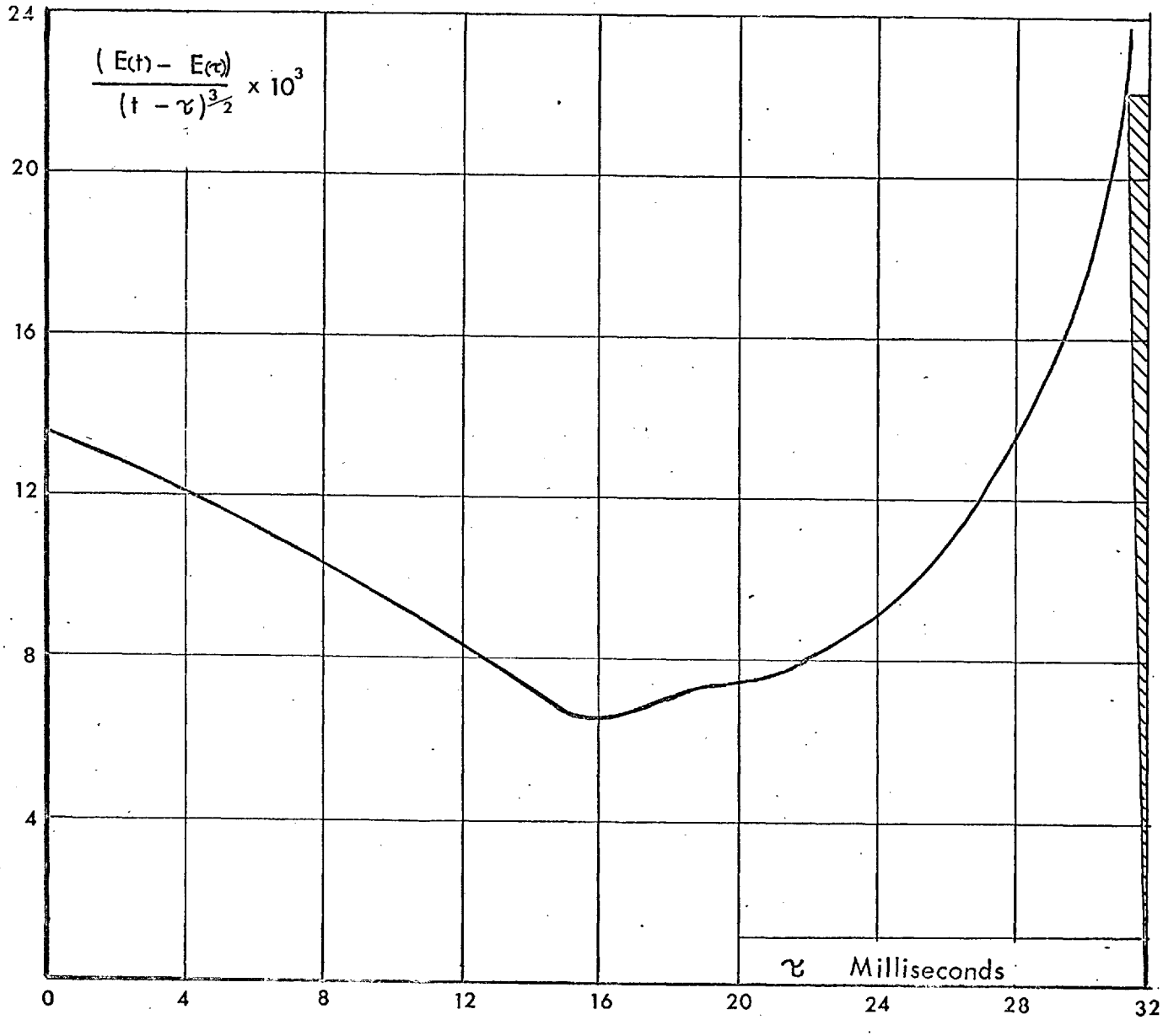

Figure 8 TYPICAL INTEGRATION OF THE GAUGE OUTPUT

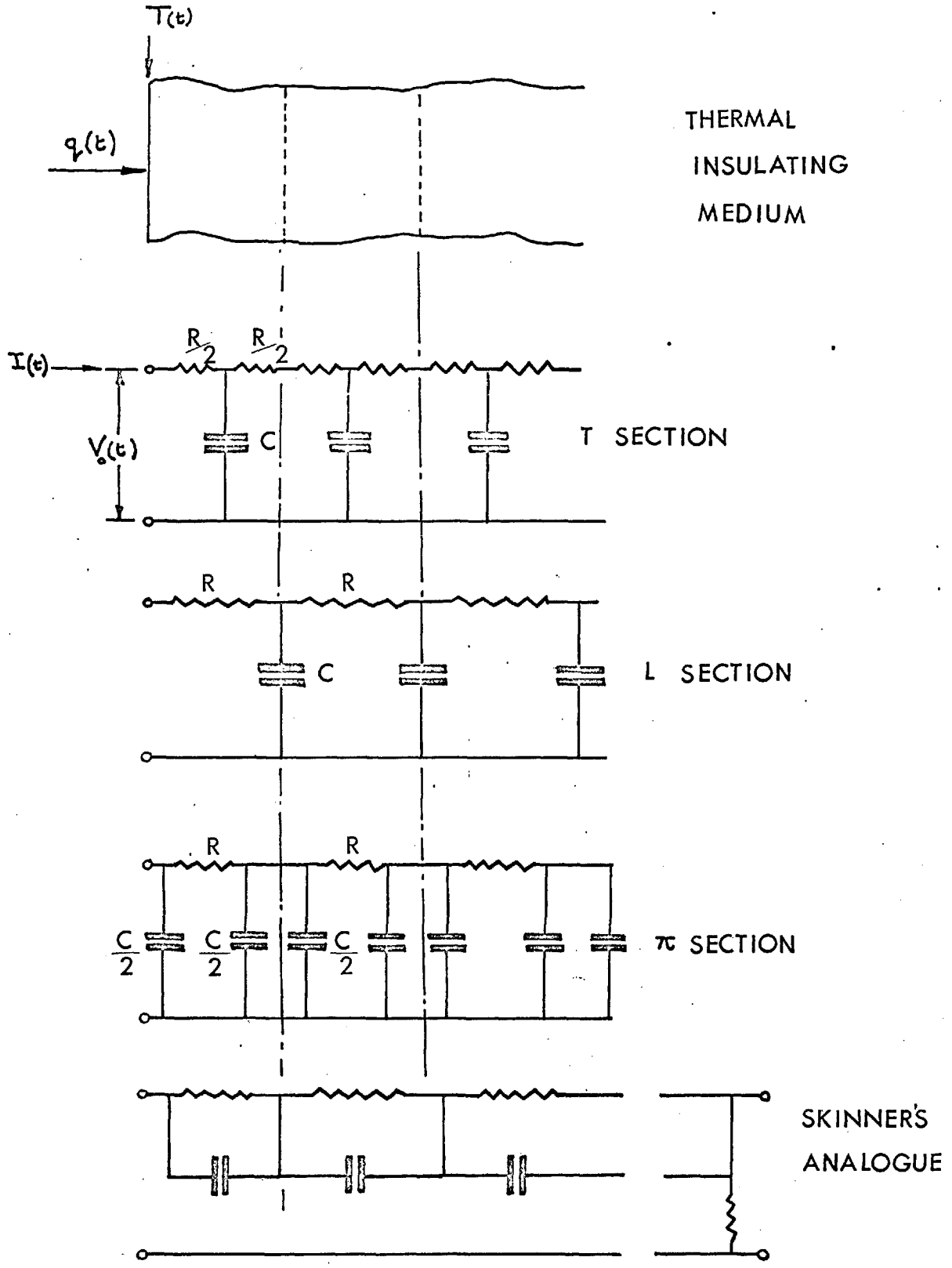

Figure 9 ANALOGUE SECTIONS

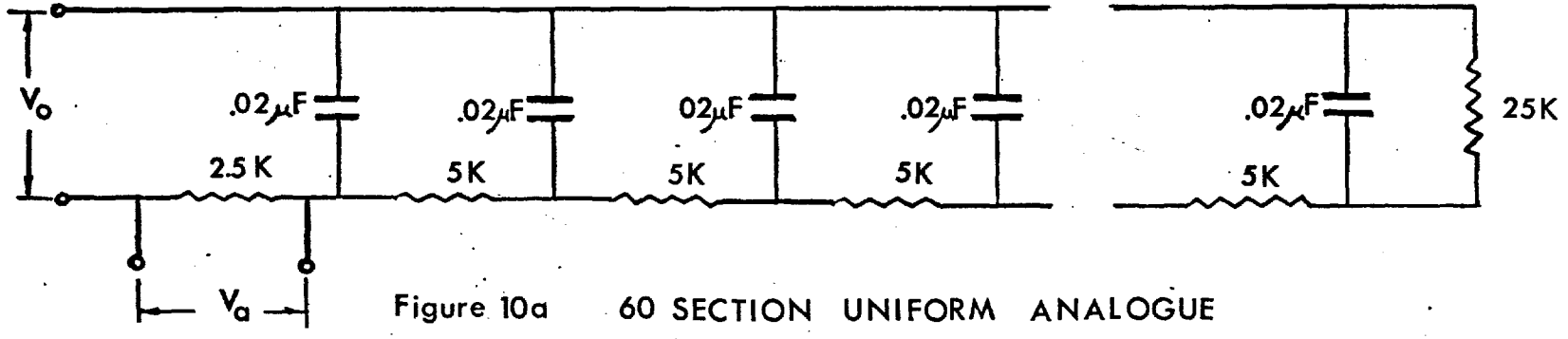

Figure 10a 60 SECTION UNIFORM ANALOGUE

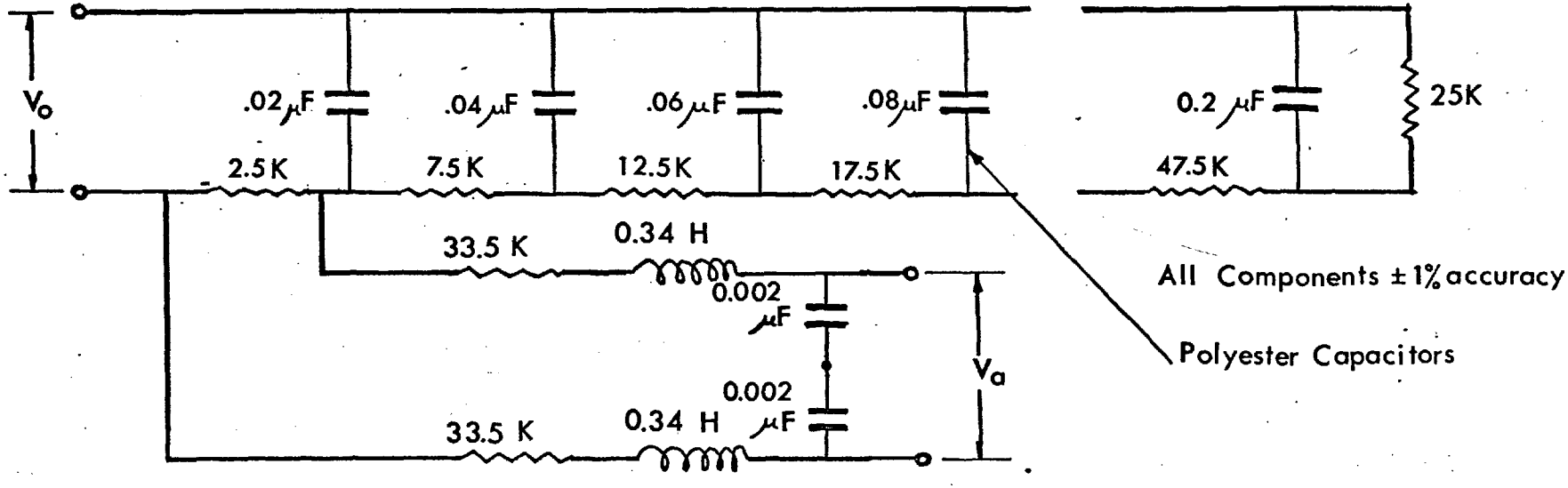

Figure 10b 10 SECTION ARITHMETIC ANALOGUE + L.R.C NETWORK

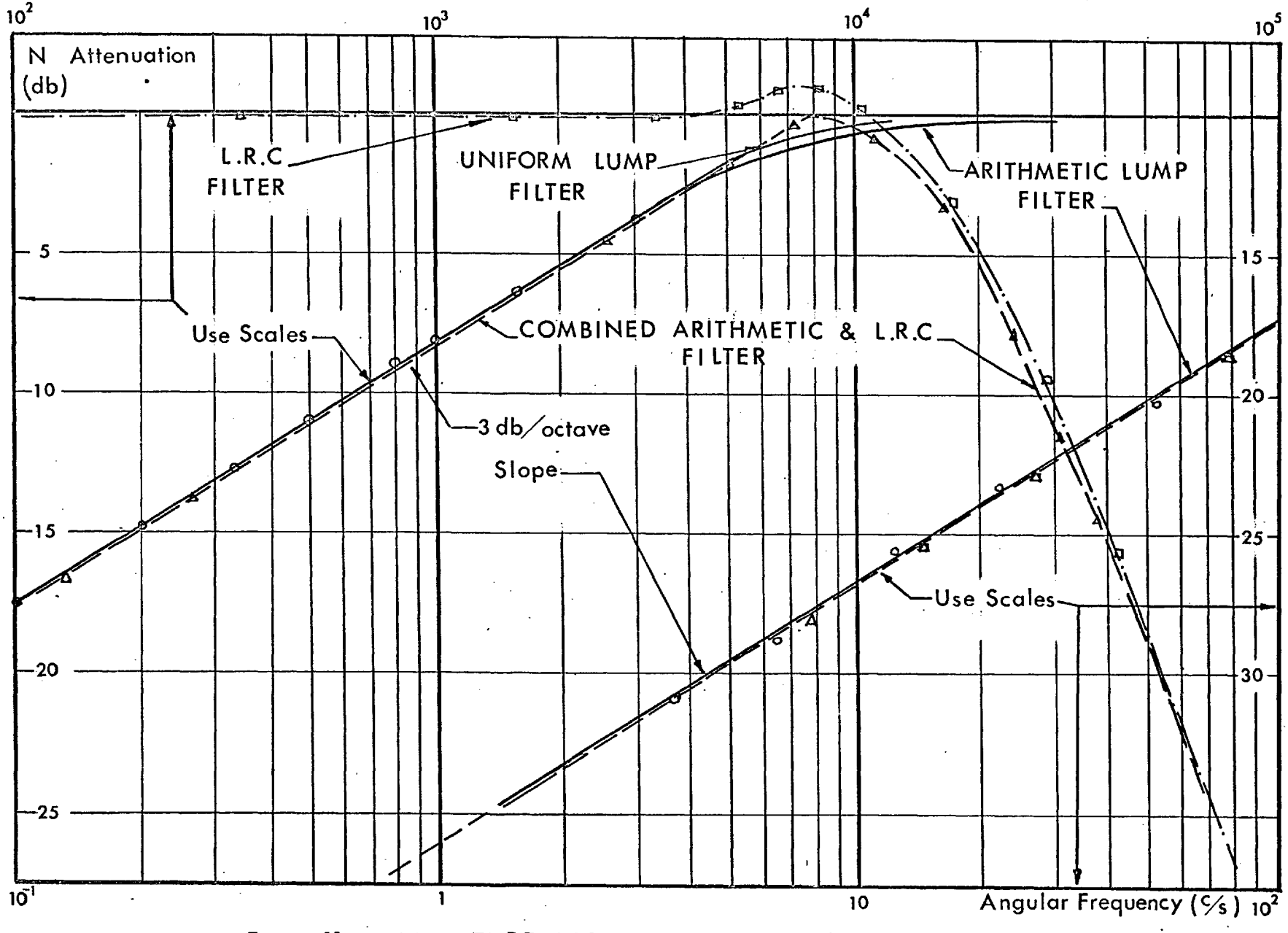

Figure 11 AMPLITUDE RESPONSE OF ANALOGUE NETWORKS

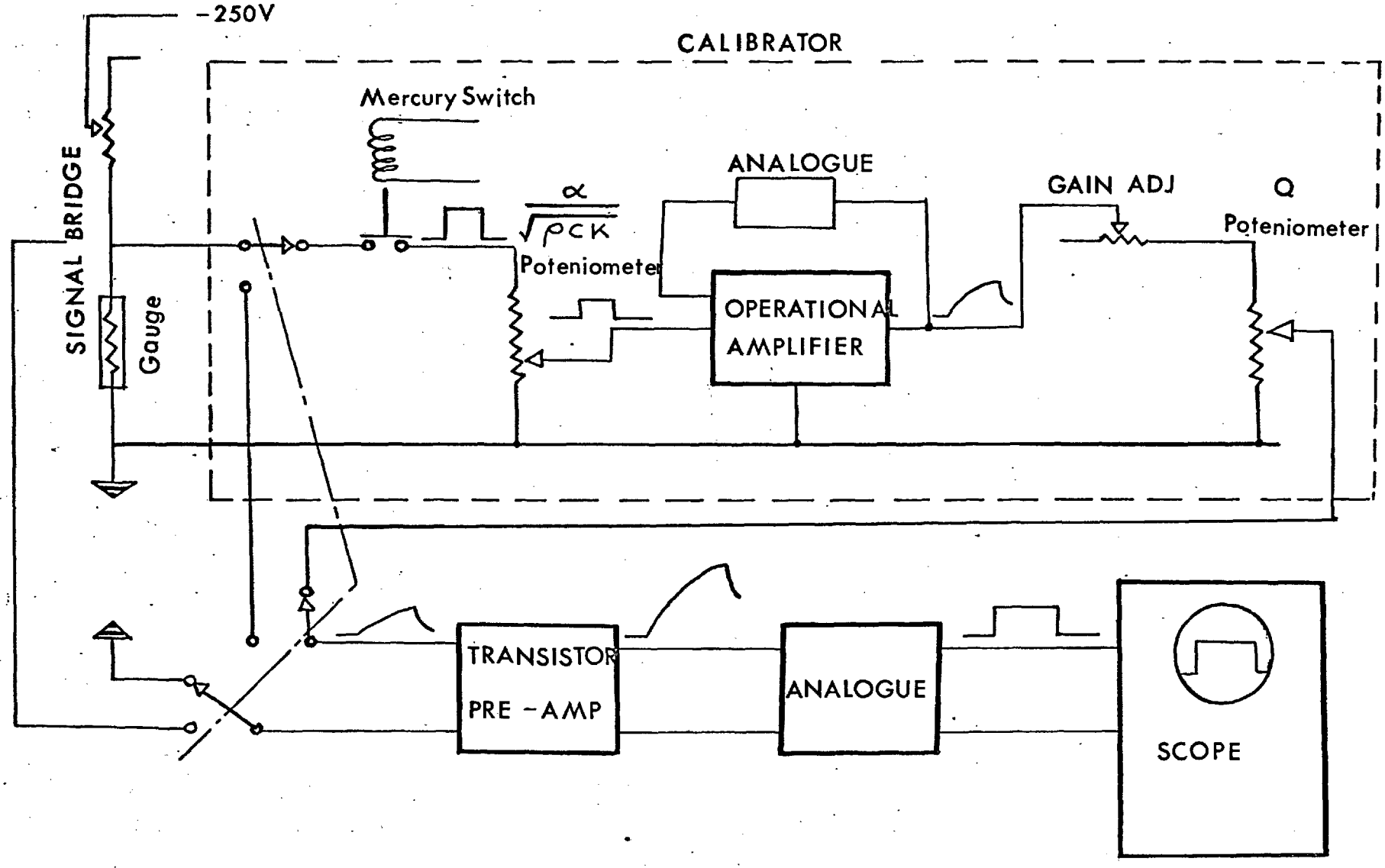

Figure 12 BLOCK DIAGRAM SHOWING THE OPERATION OF THE ELECTRONIC CALIBRATOR

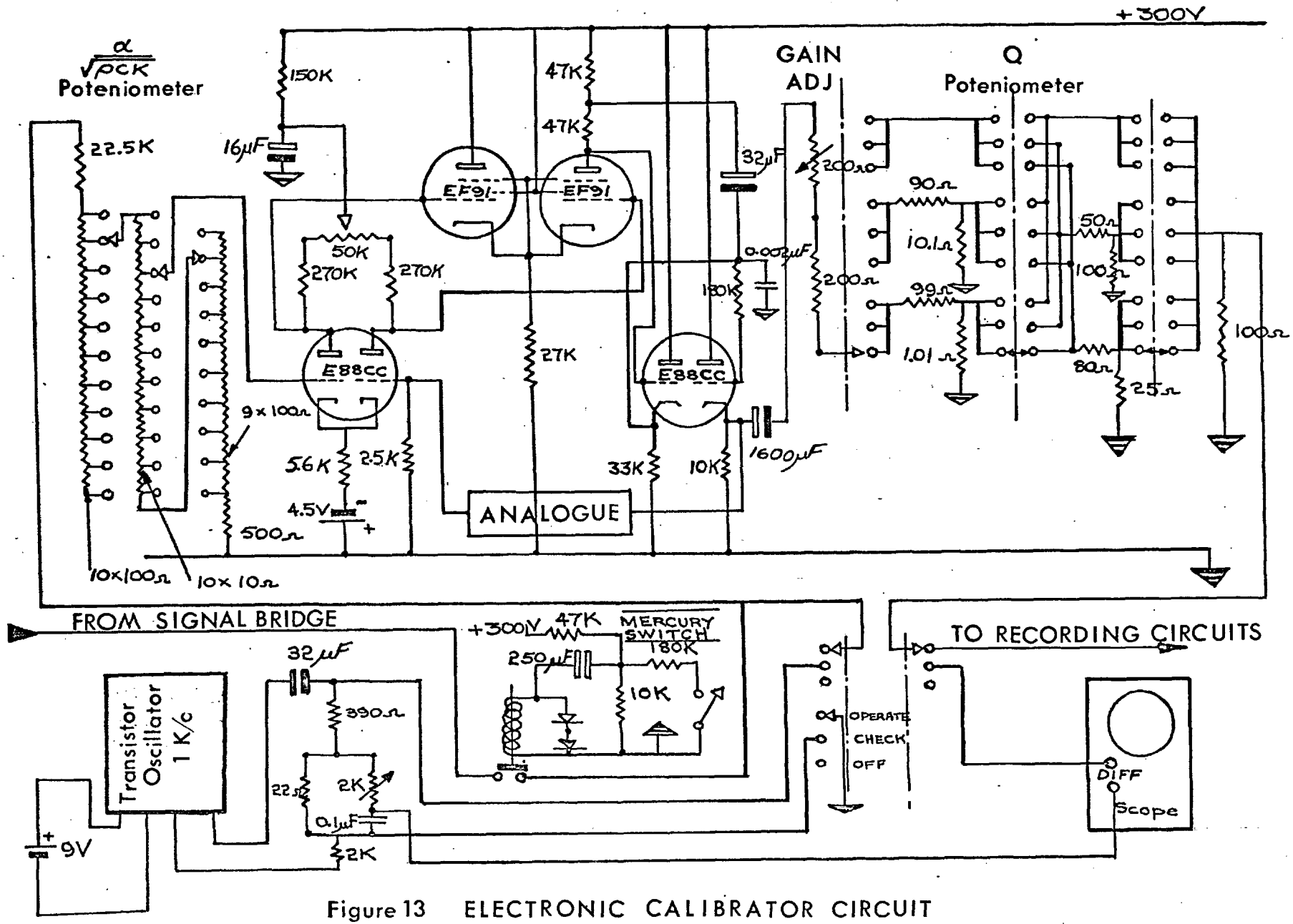

Figure 13 ELECTRONIC CALIBRATOR CIRCUIT

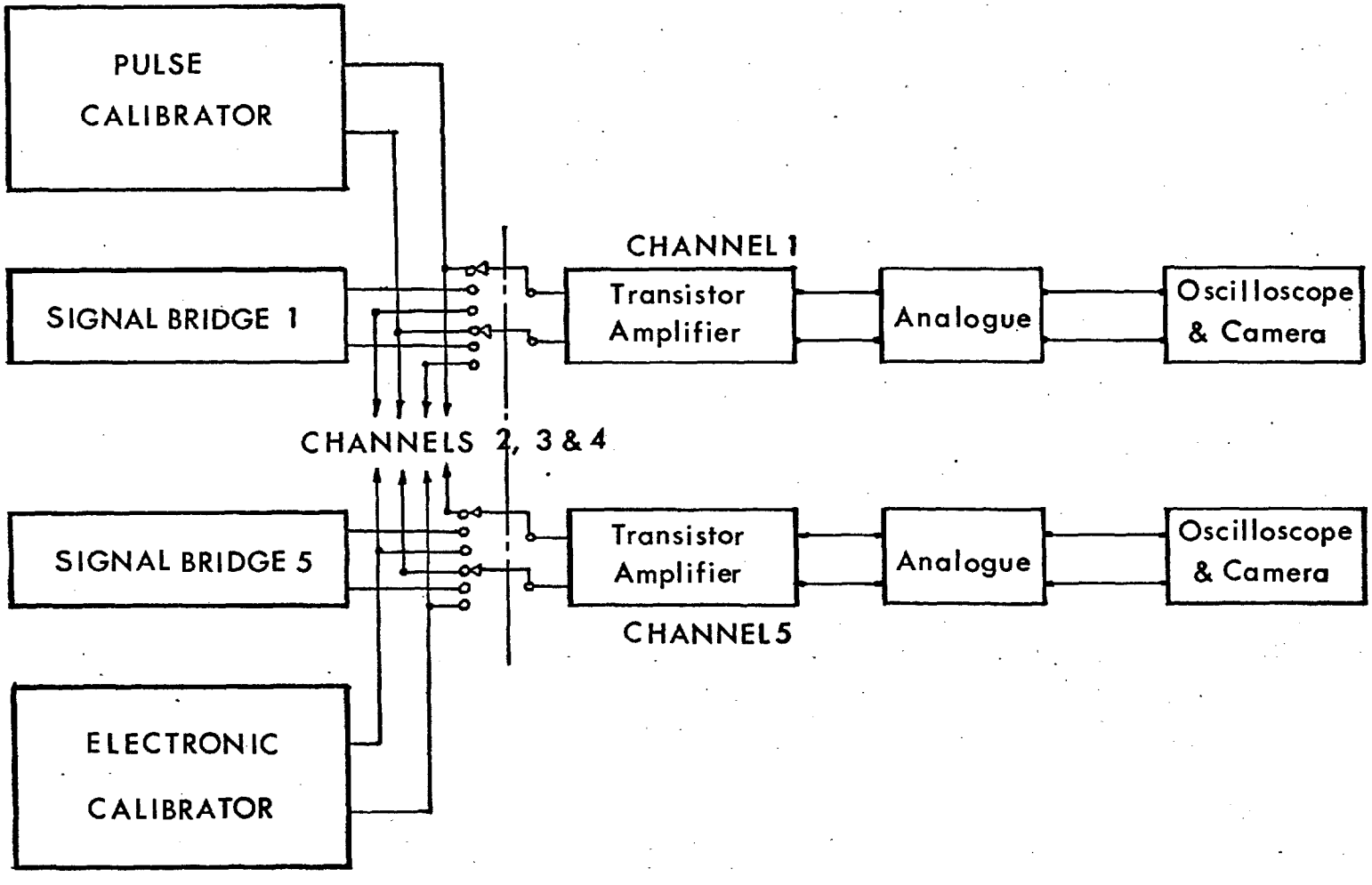

Figure 14 GENERAL LAYOUT OF ELECTRONIC APPARATUS

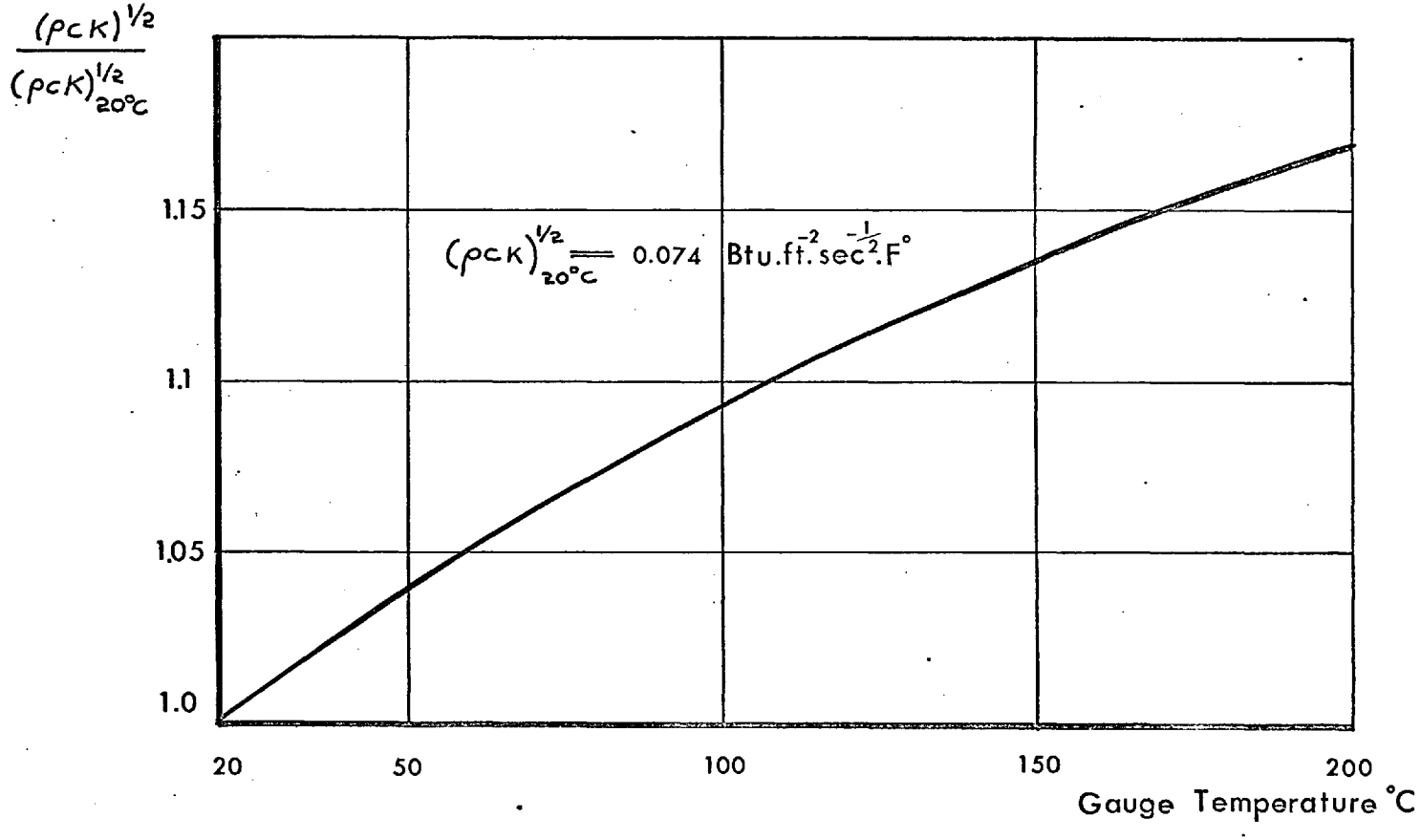

Figure 15 VARIATION OF $(\rho c K)^{1/2}_{Pyrex}$ WITH TEMPERATURE

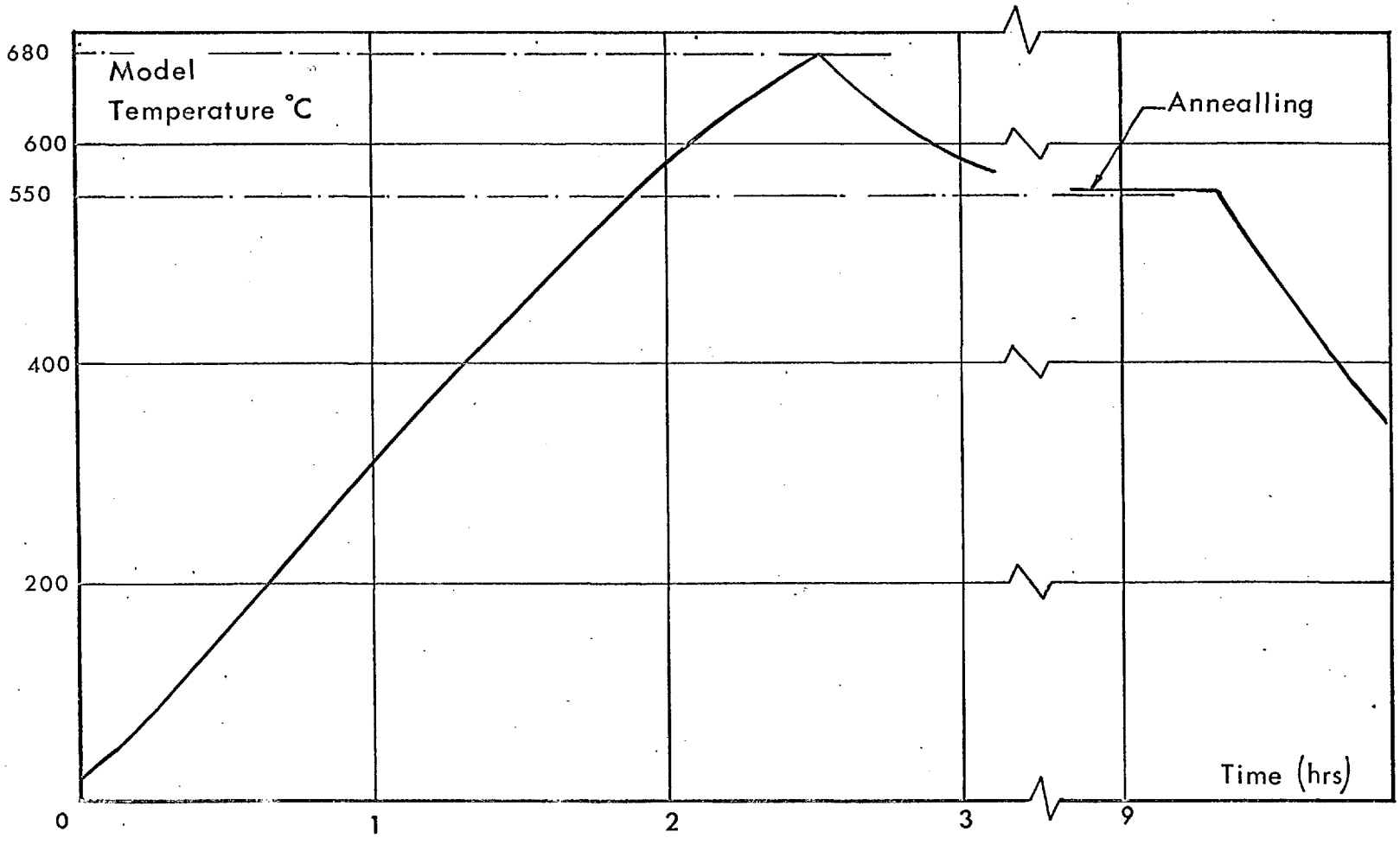

Figure 16 BAKING CYCLE FOR THIN FILM GAUGE (Platinum — Pyrex)

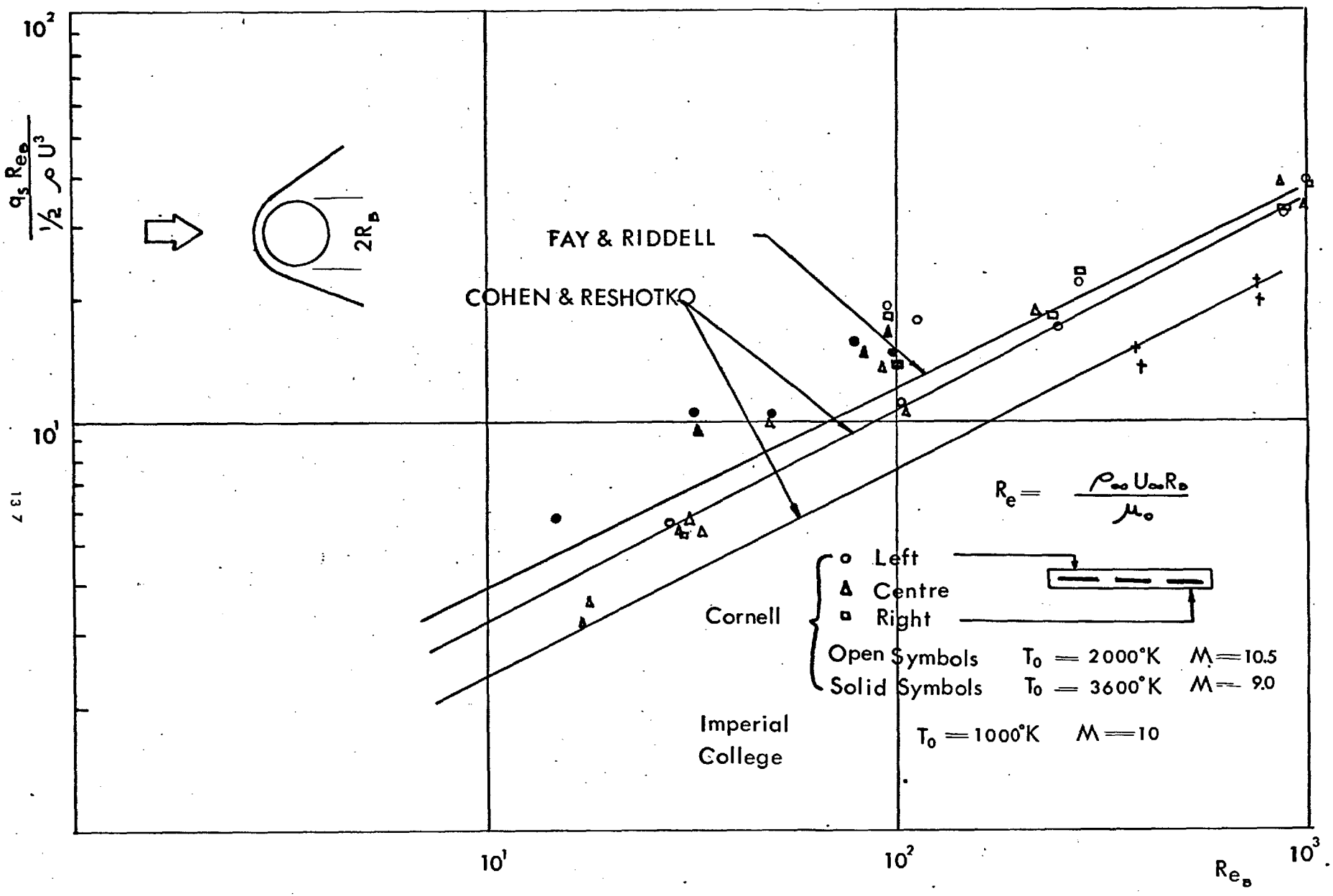

Figure 17 STAGNATION POINT HEAT TRANSFER TO A CYLINDER

Figure 18a HEMISPHERE CYLINDERS

Figure 18b FLAT ENDED CYLINDERS

Figure 18c CYLINDER MODEL

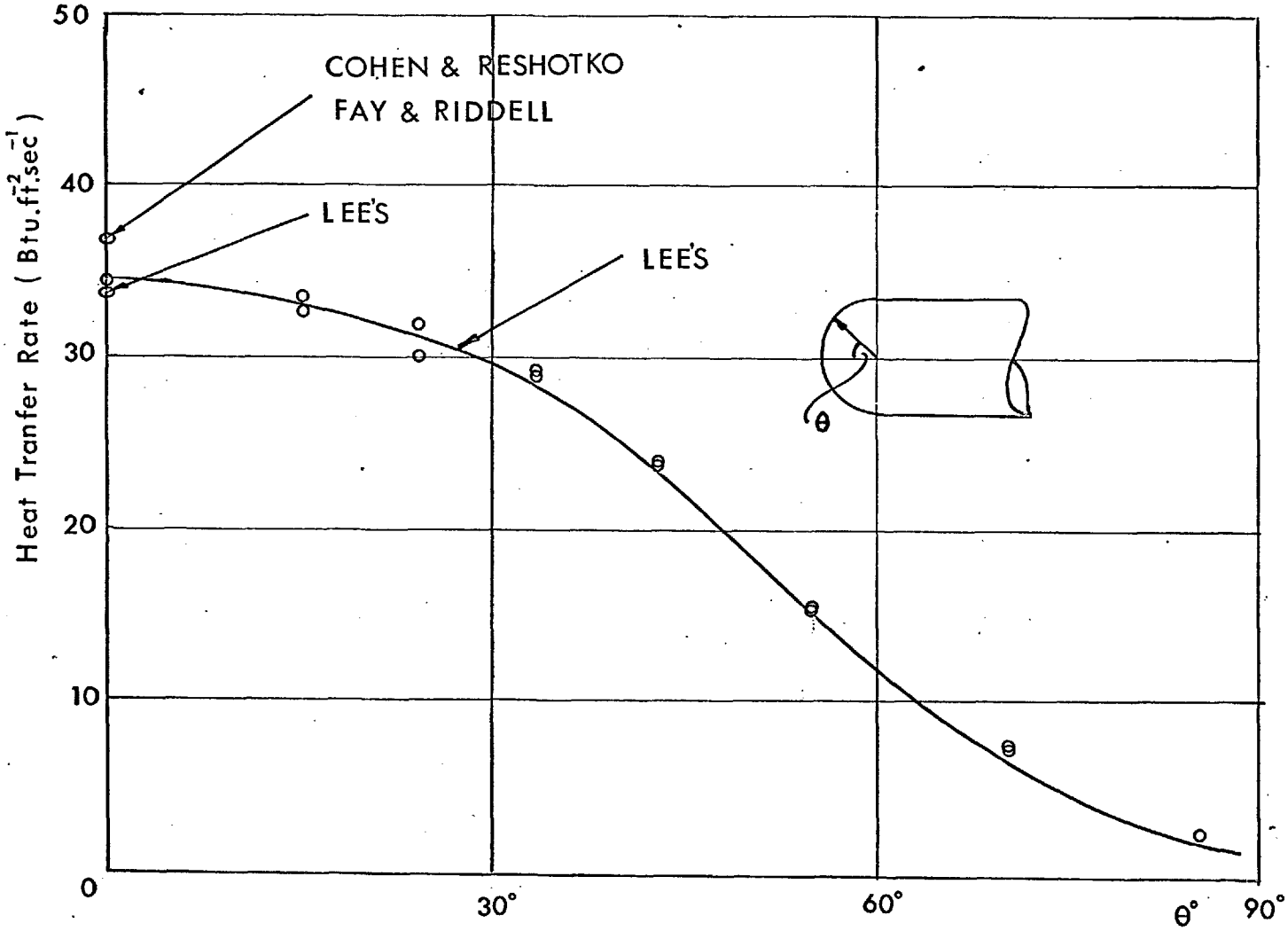

Figure 19 HEAT TRANSFER TO A HEMISPHERICALLY CAPPED CYLINDER

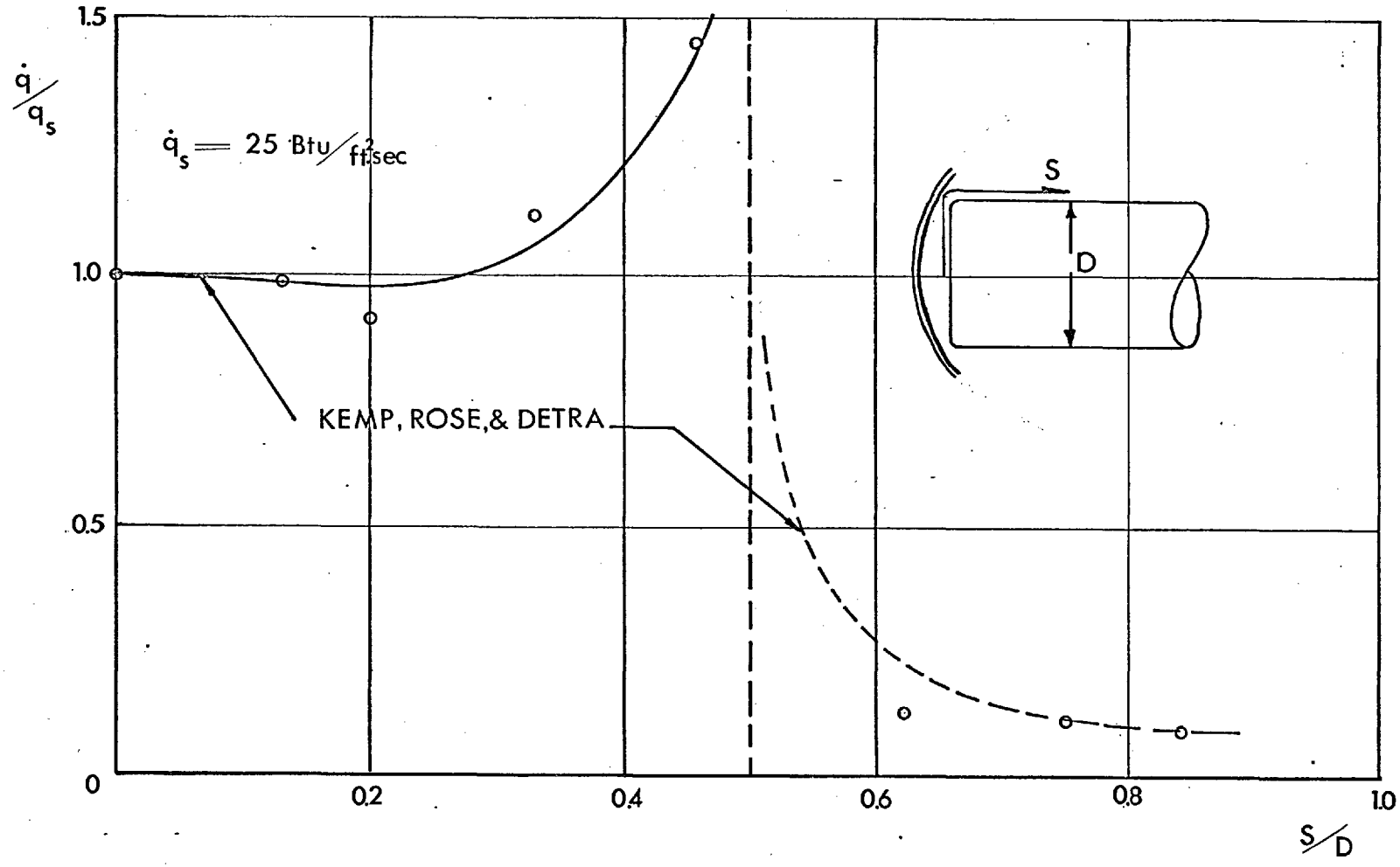

Figure 20 HEAT TRANSFER TO A FLAT ENDED CYLINDER

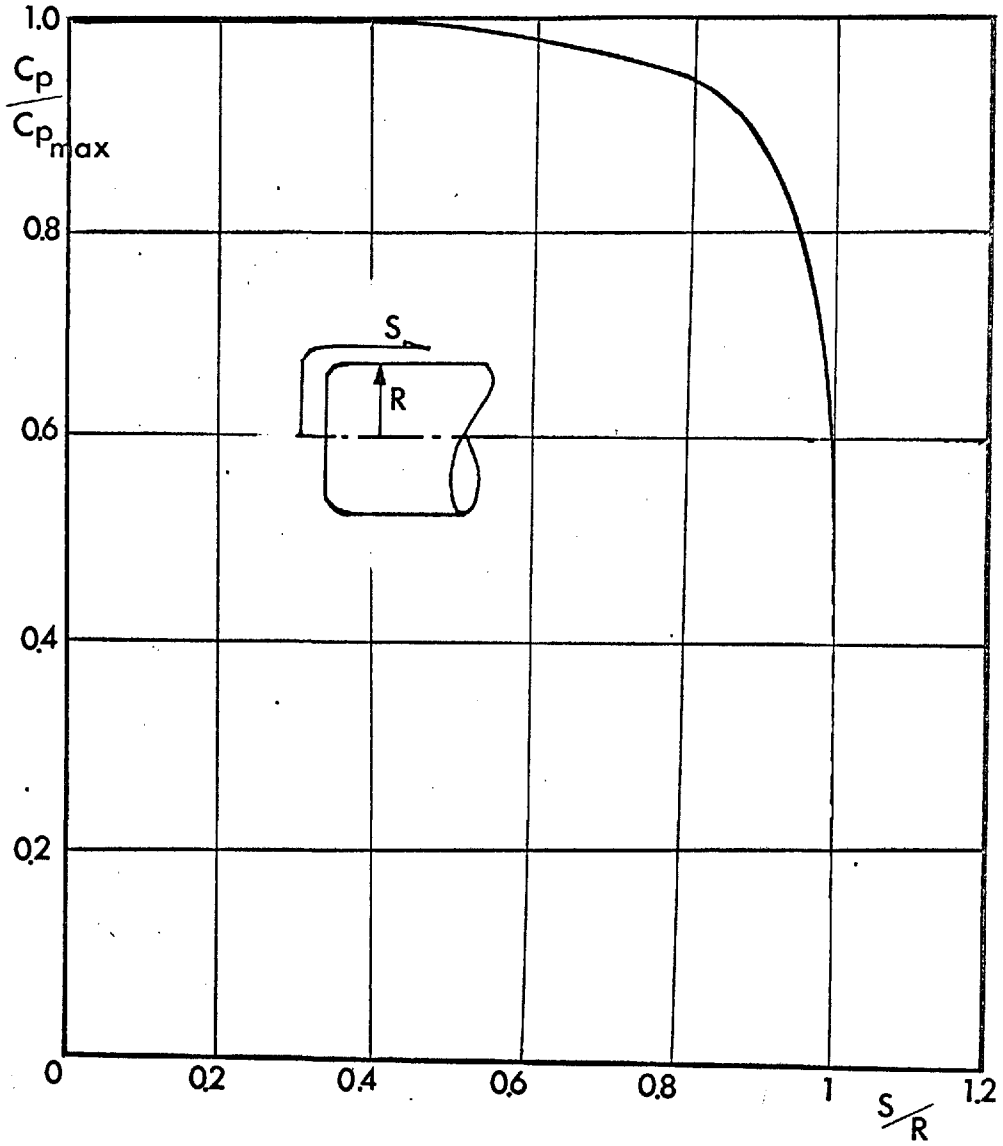

Figure 21 PRESSURE DISTRIBUTION ON A FLAT—ENDED CYLINDER

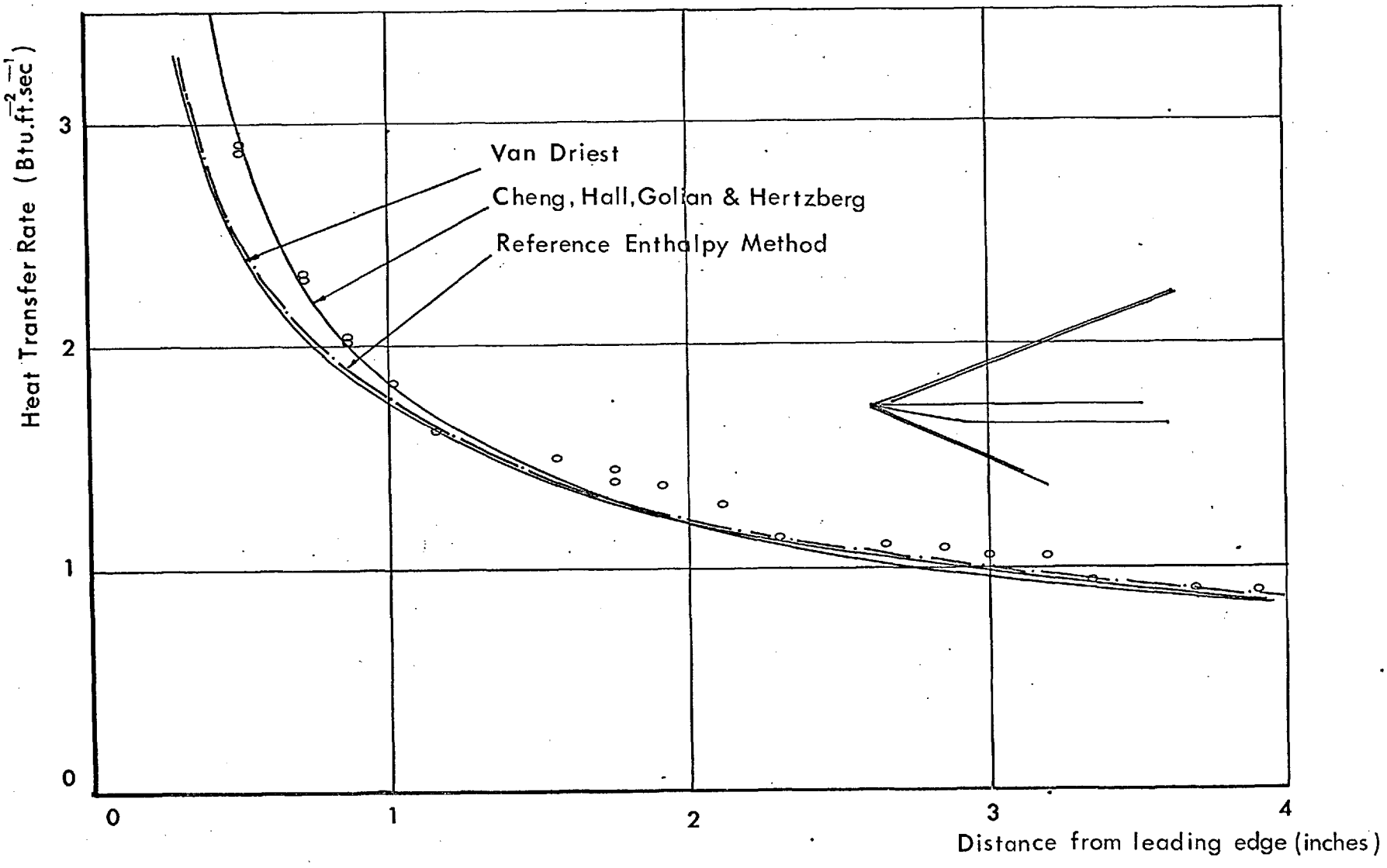

Figure 22 HEAT TRANSFER TO A FLAT PLATE

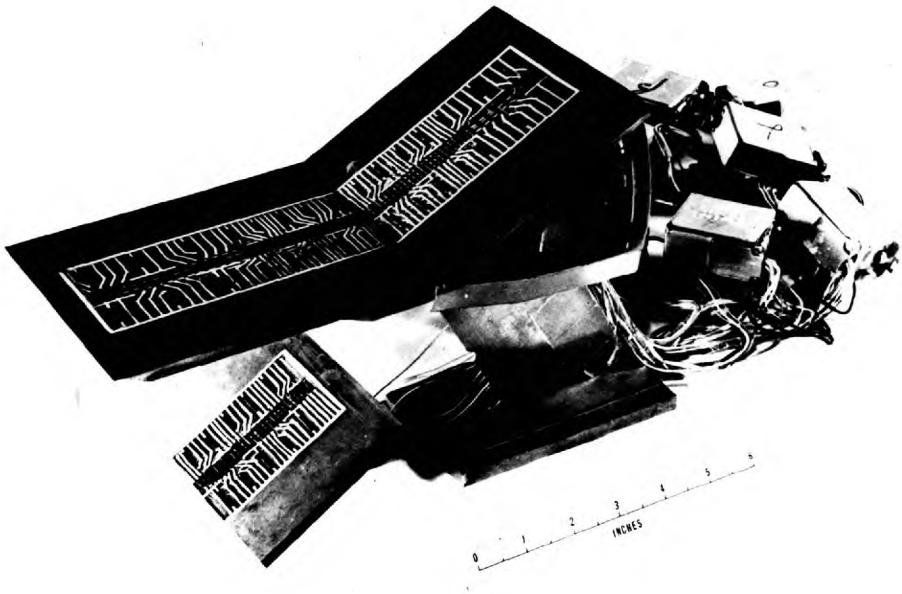

Figure 23 VARIABLE ANGLE WEDGE MODEL

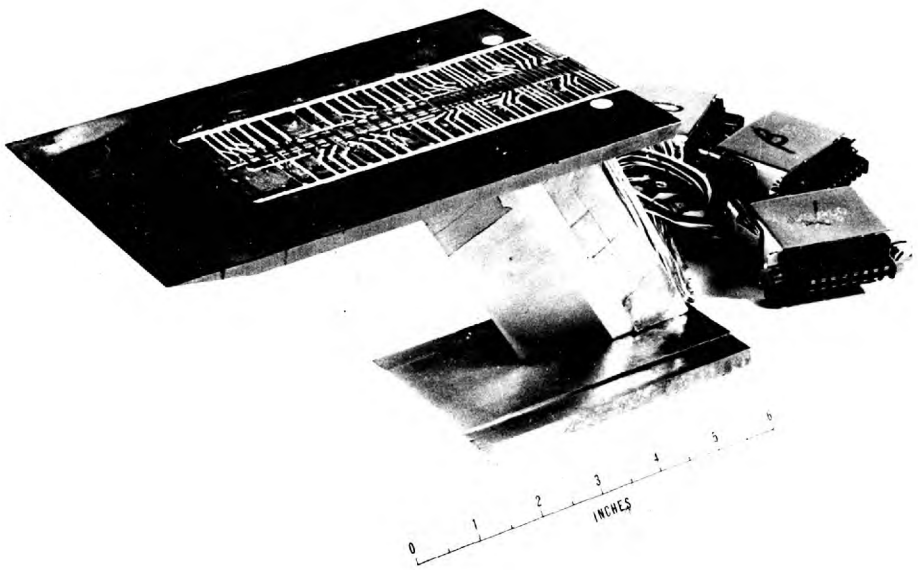

Figure 24 FLAT PLATE MODEL

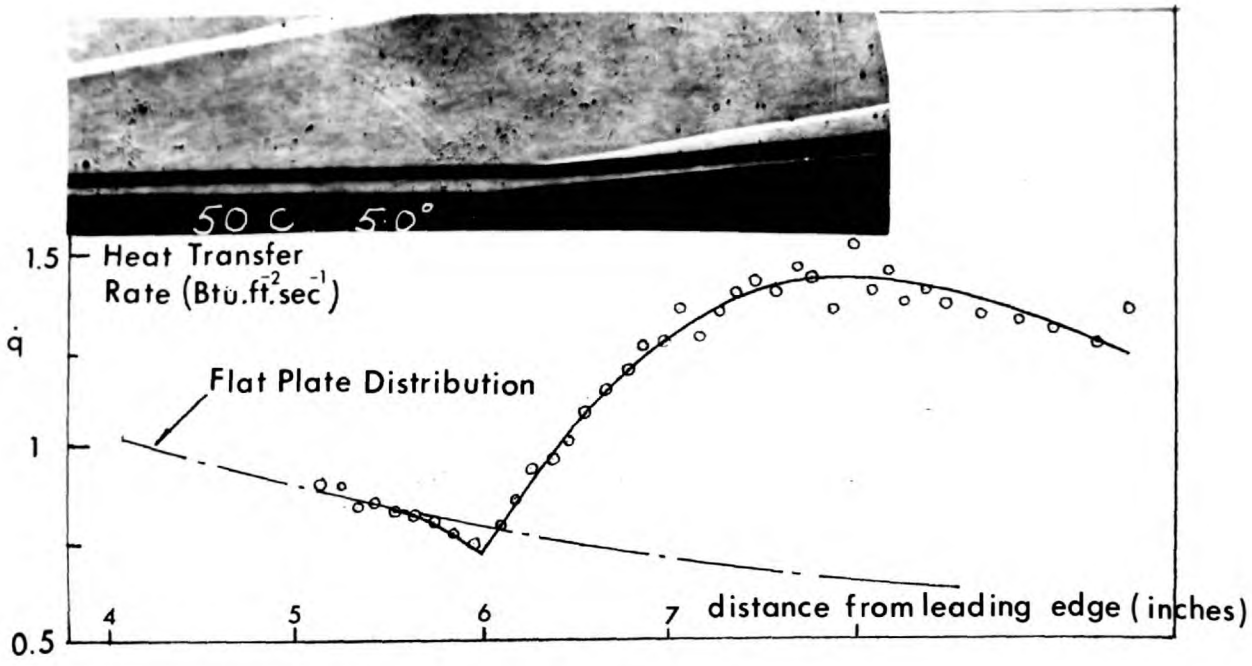

Figure 25a 5° WEDGE

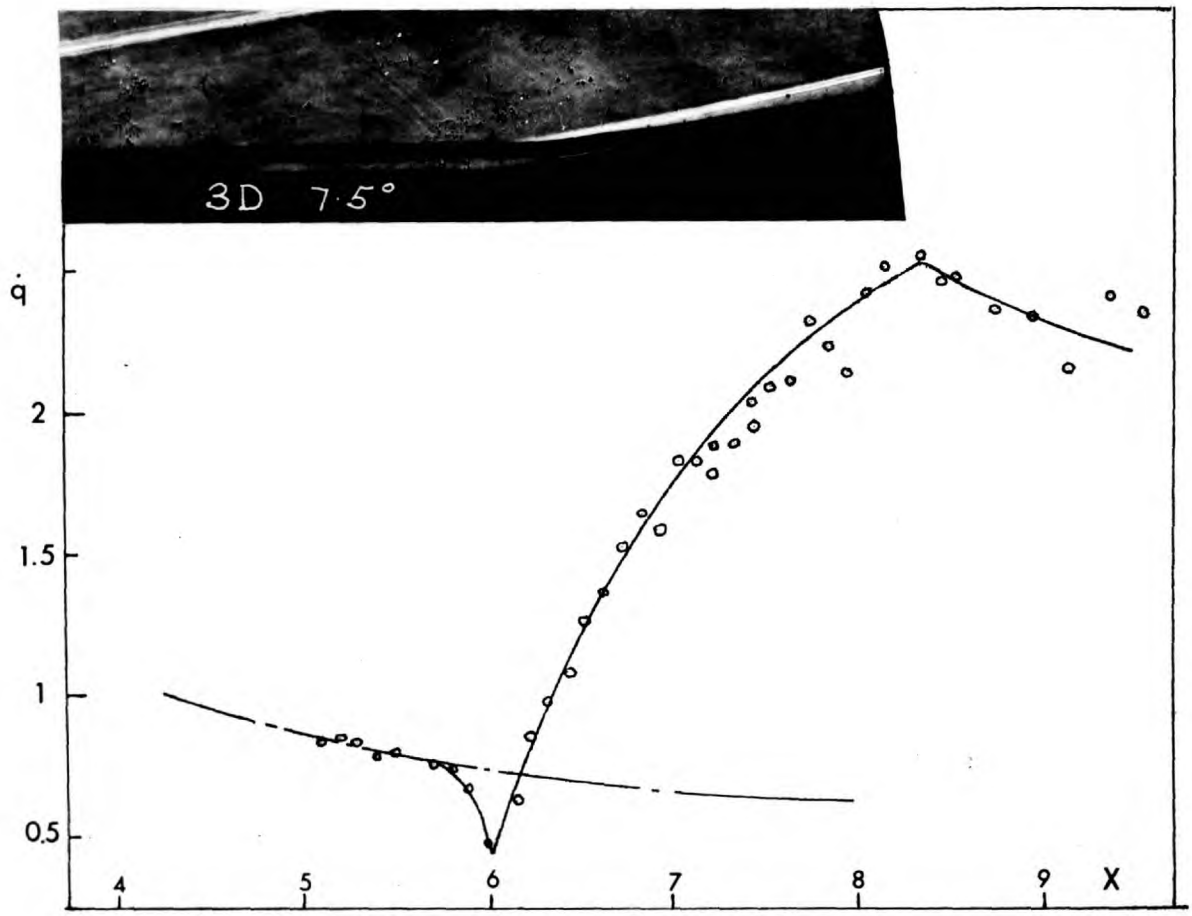

Figure 25b 7.5° WEDGE

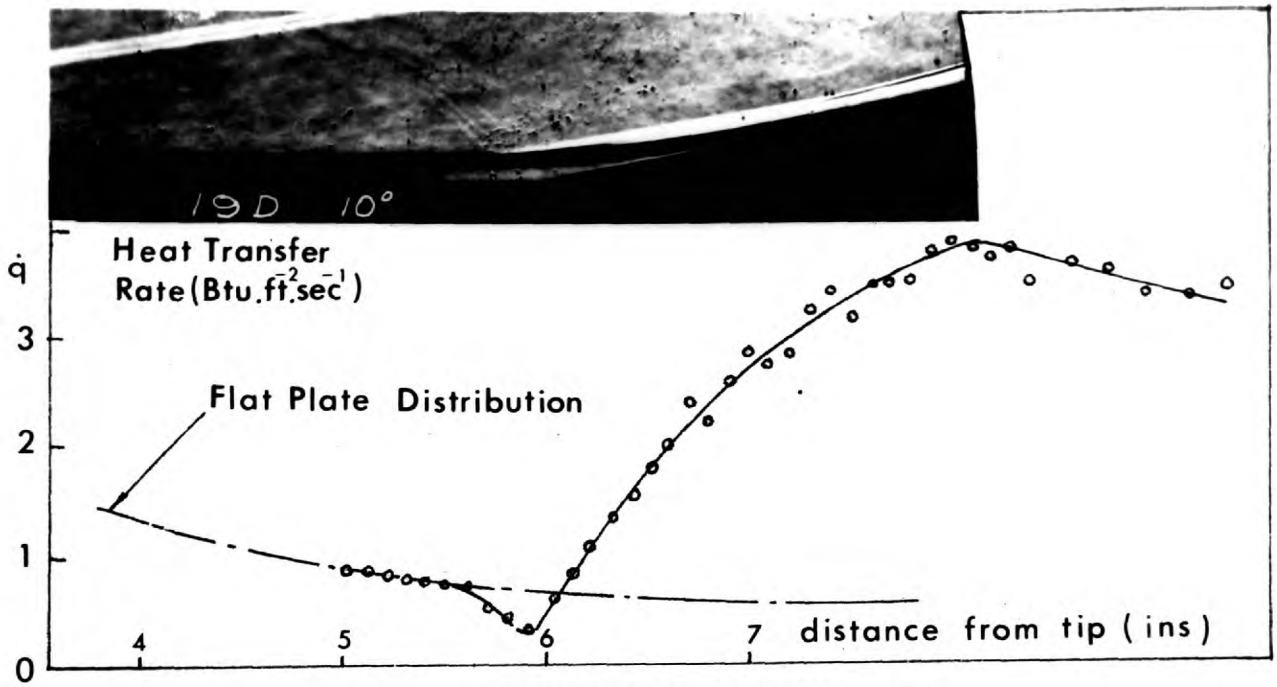

Figure 25c 10° WEDGE

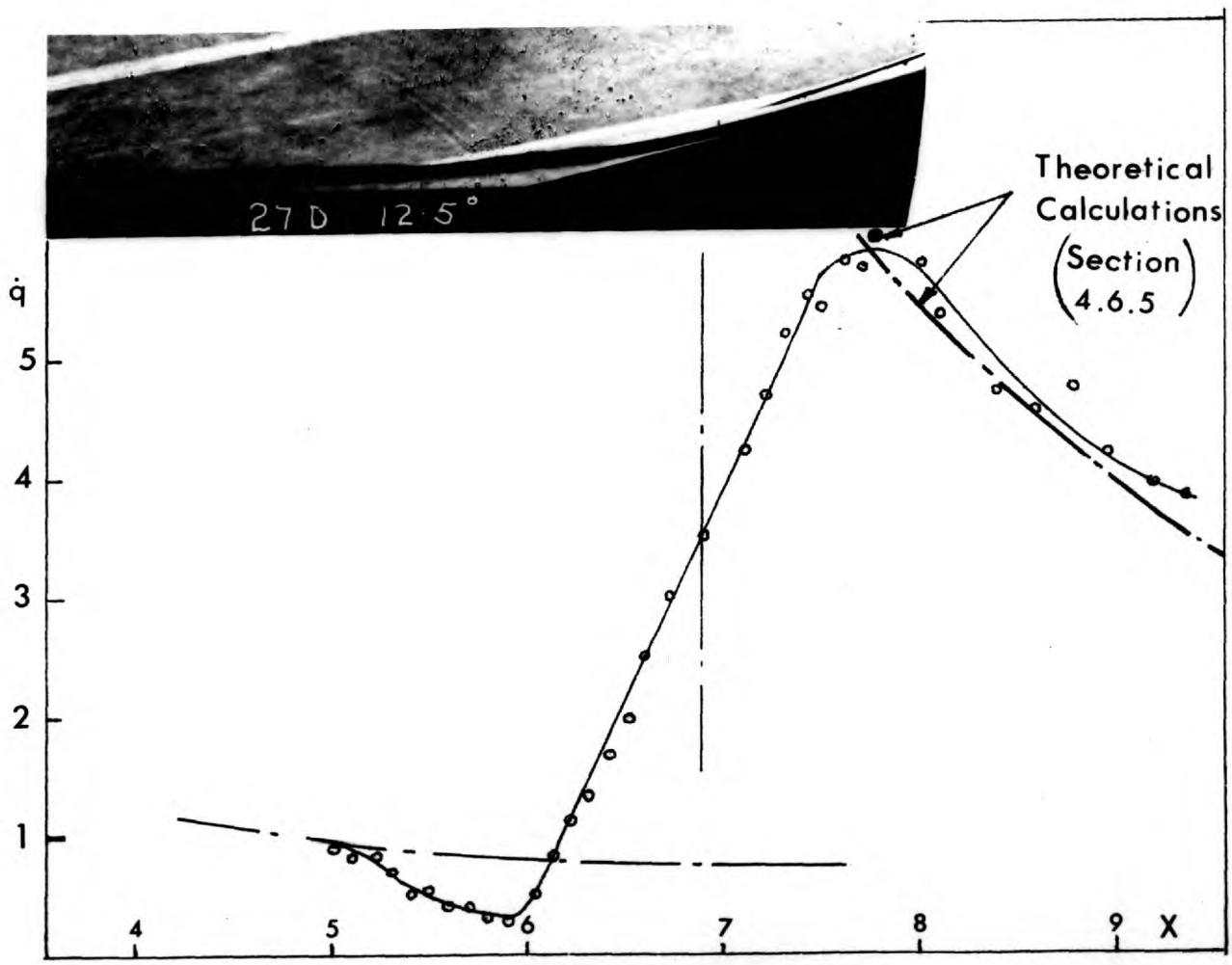

Figure 25d 12.5° WEDGE

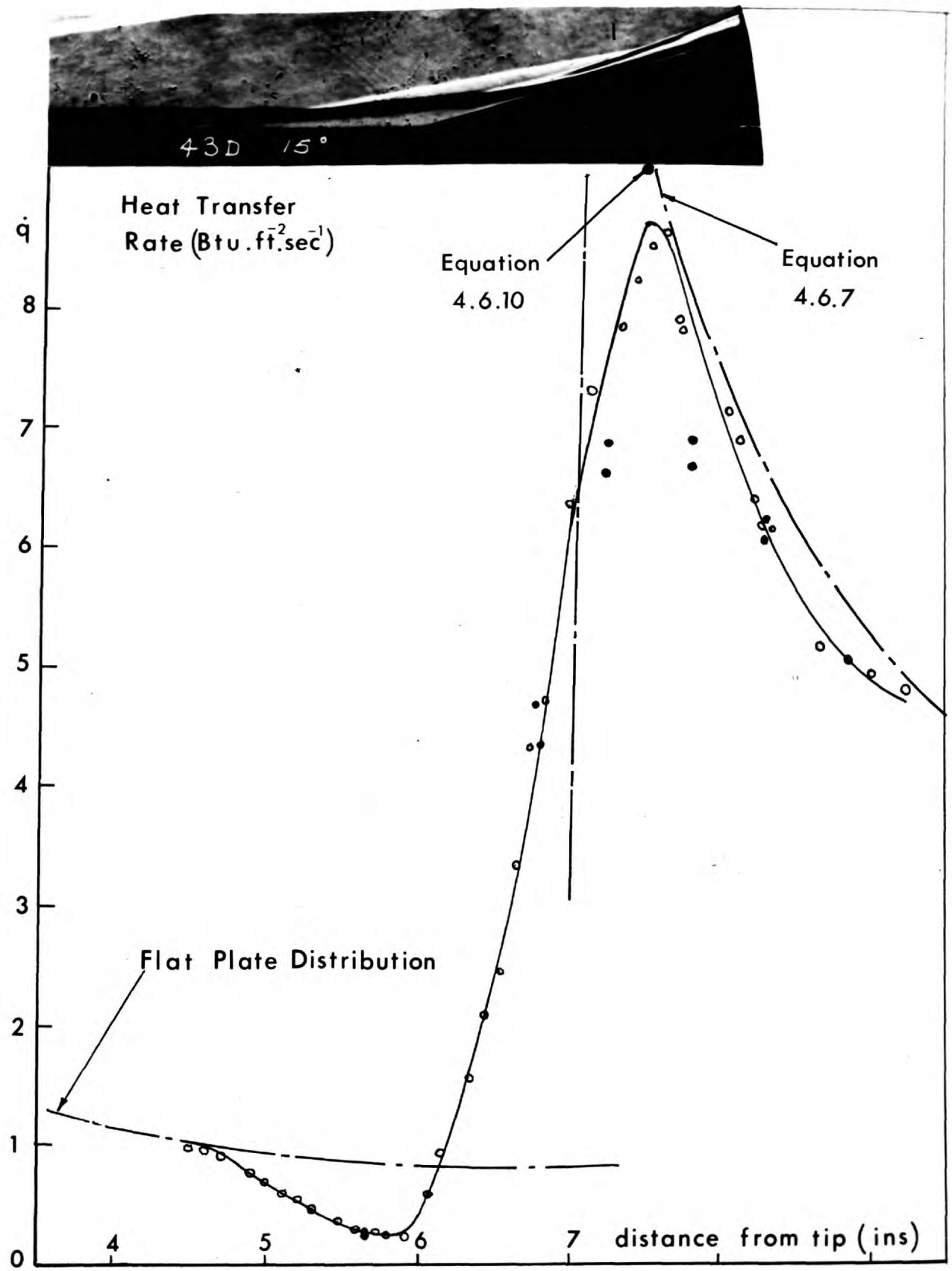

Figure 25e 15° WEDGE

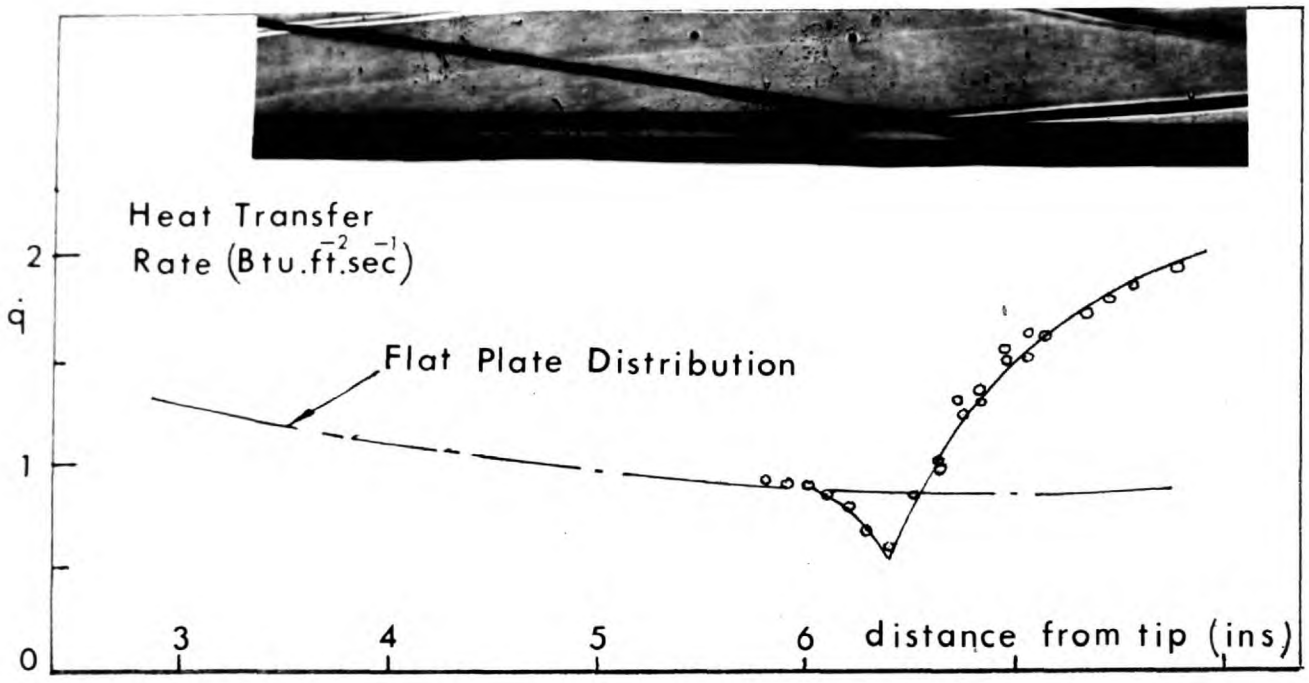

Figure 26a SHOCK ANGLE 2.1°

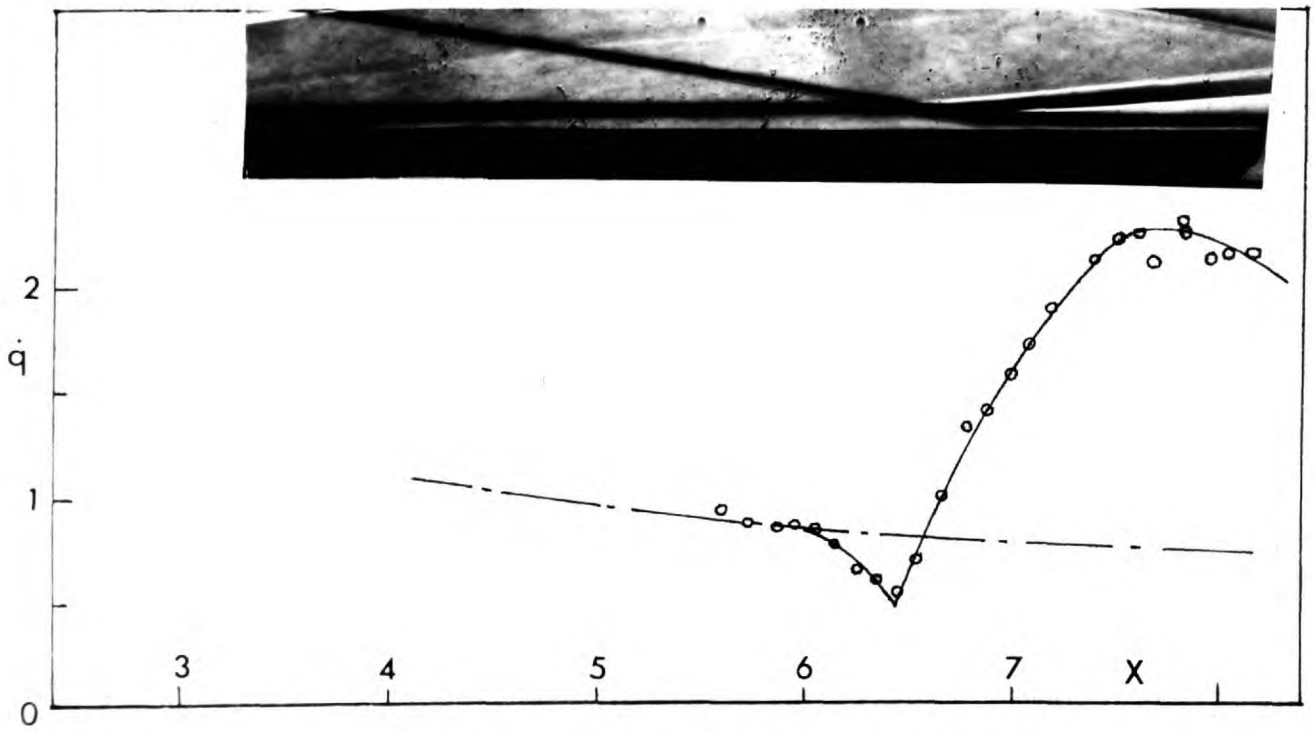

Figure 26b SHOCK ANGLE 3.2°

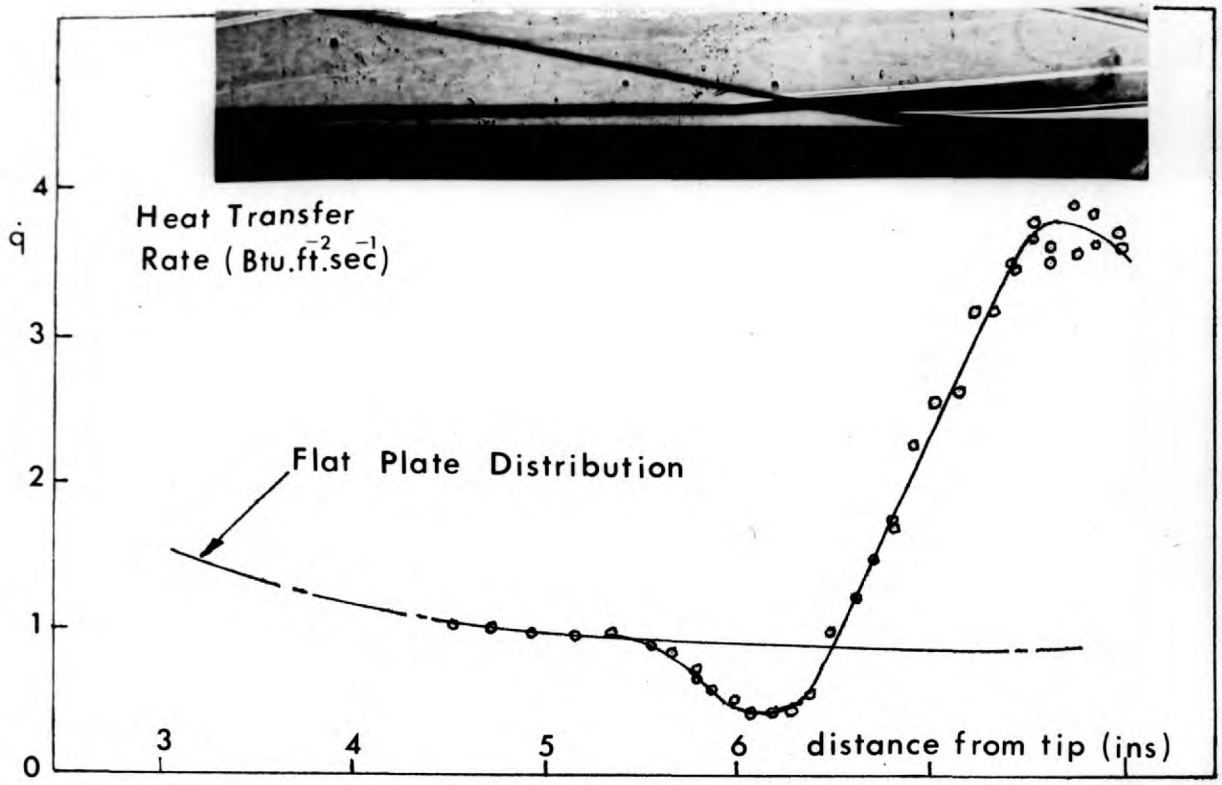

Figure 26c SHOCK ANGLE 5.2°

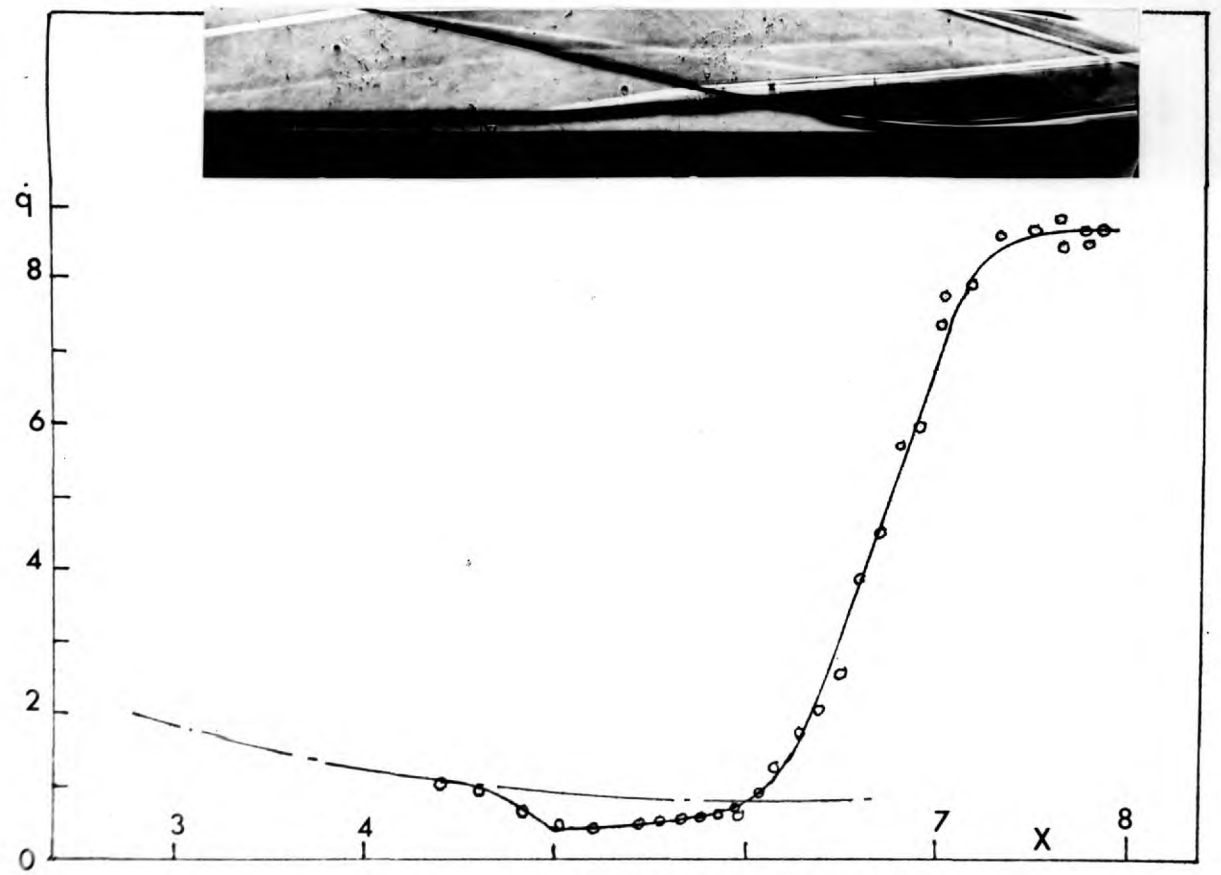

Figure 26d SHOCK ANGLE 8.3°

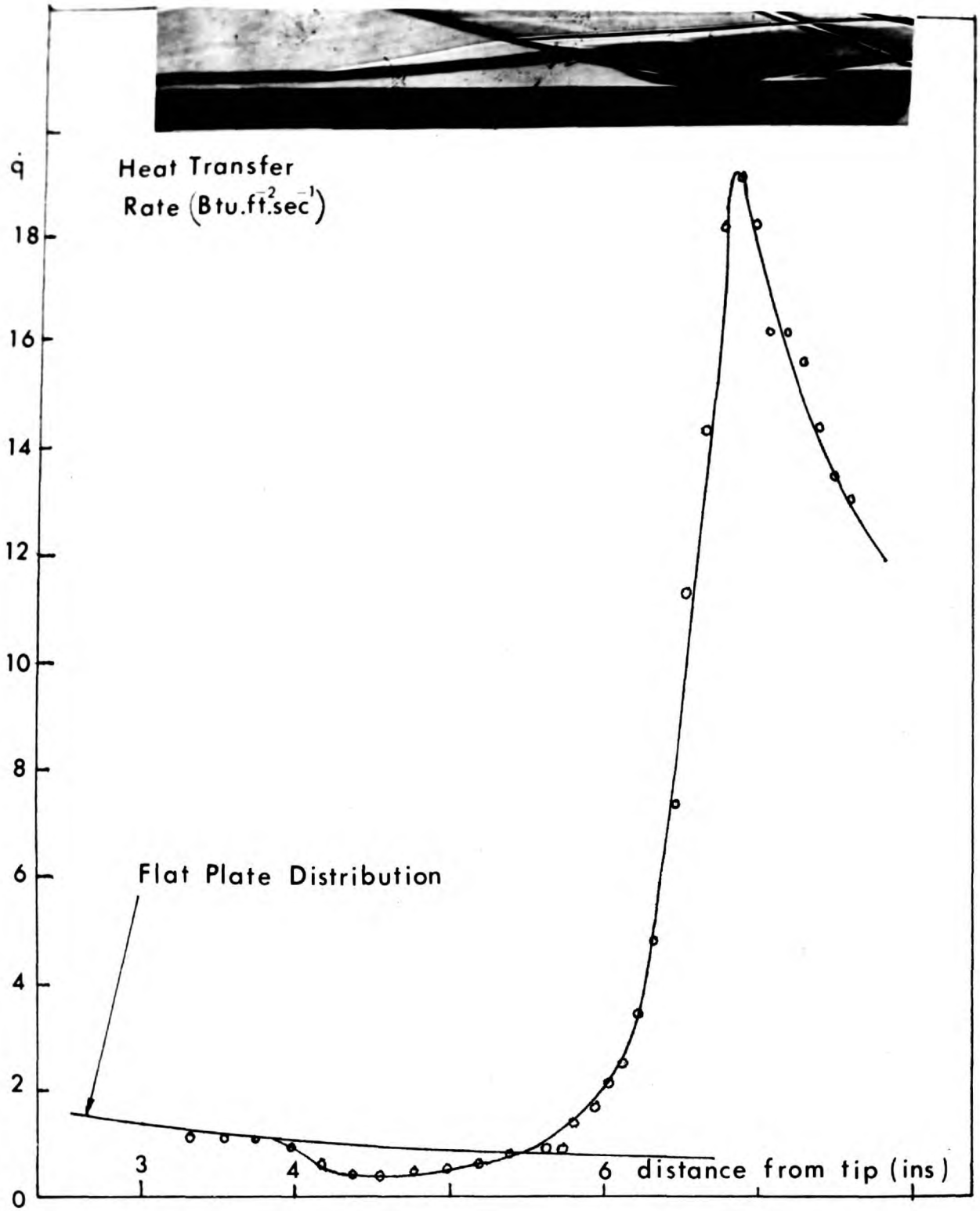

Figure 26e SHOCK ANGLE 10.4°

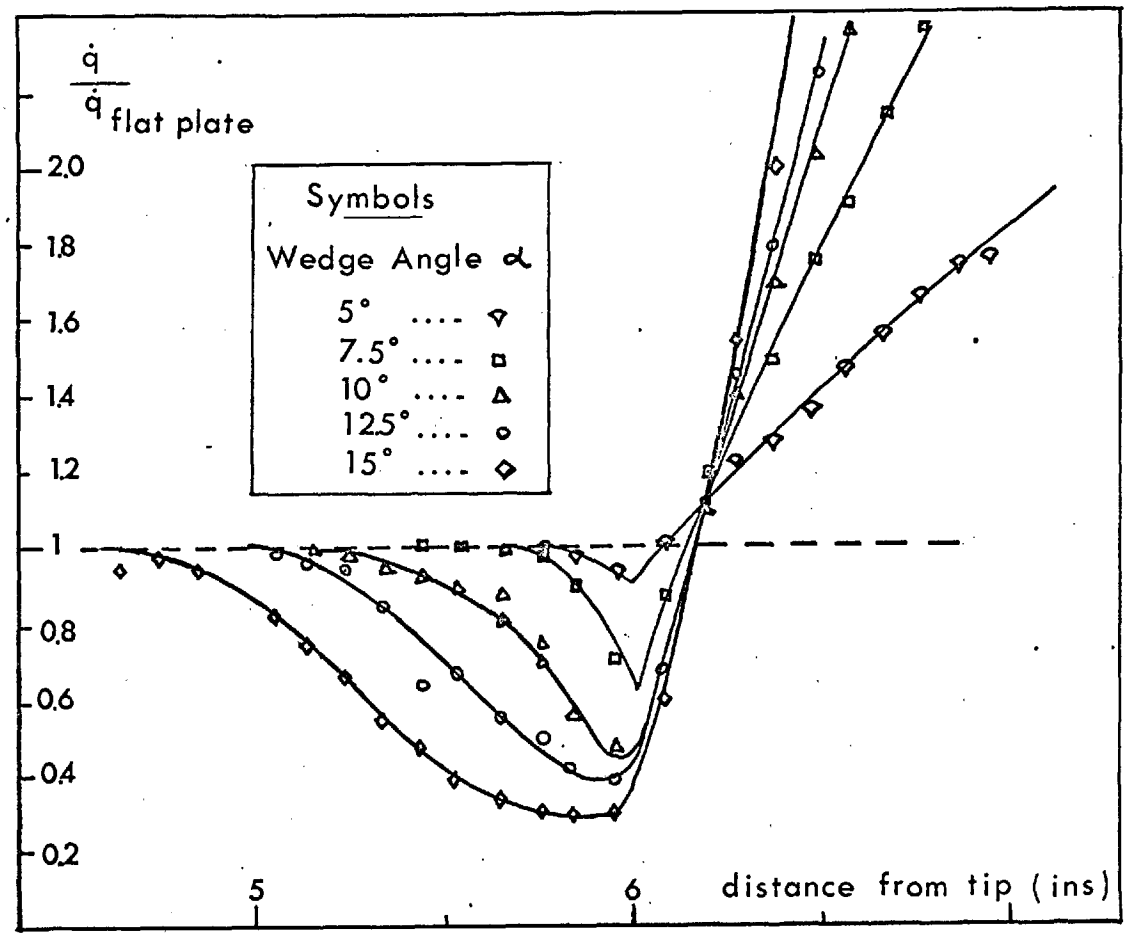

Figure 27 WEDGE INDUCED SEPARATION

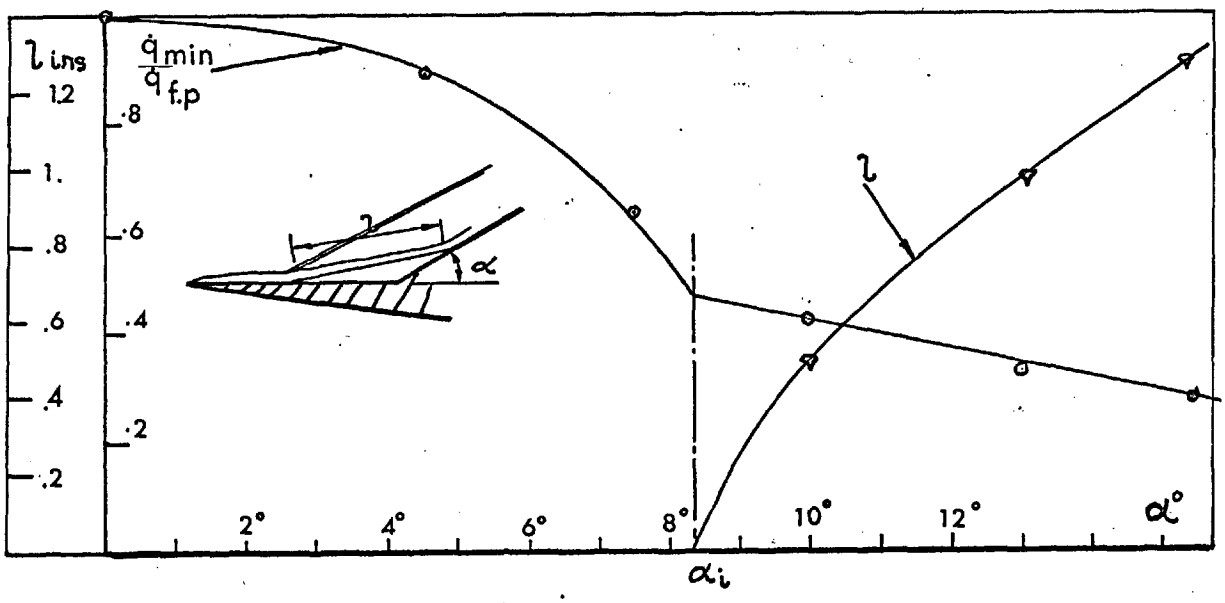

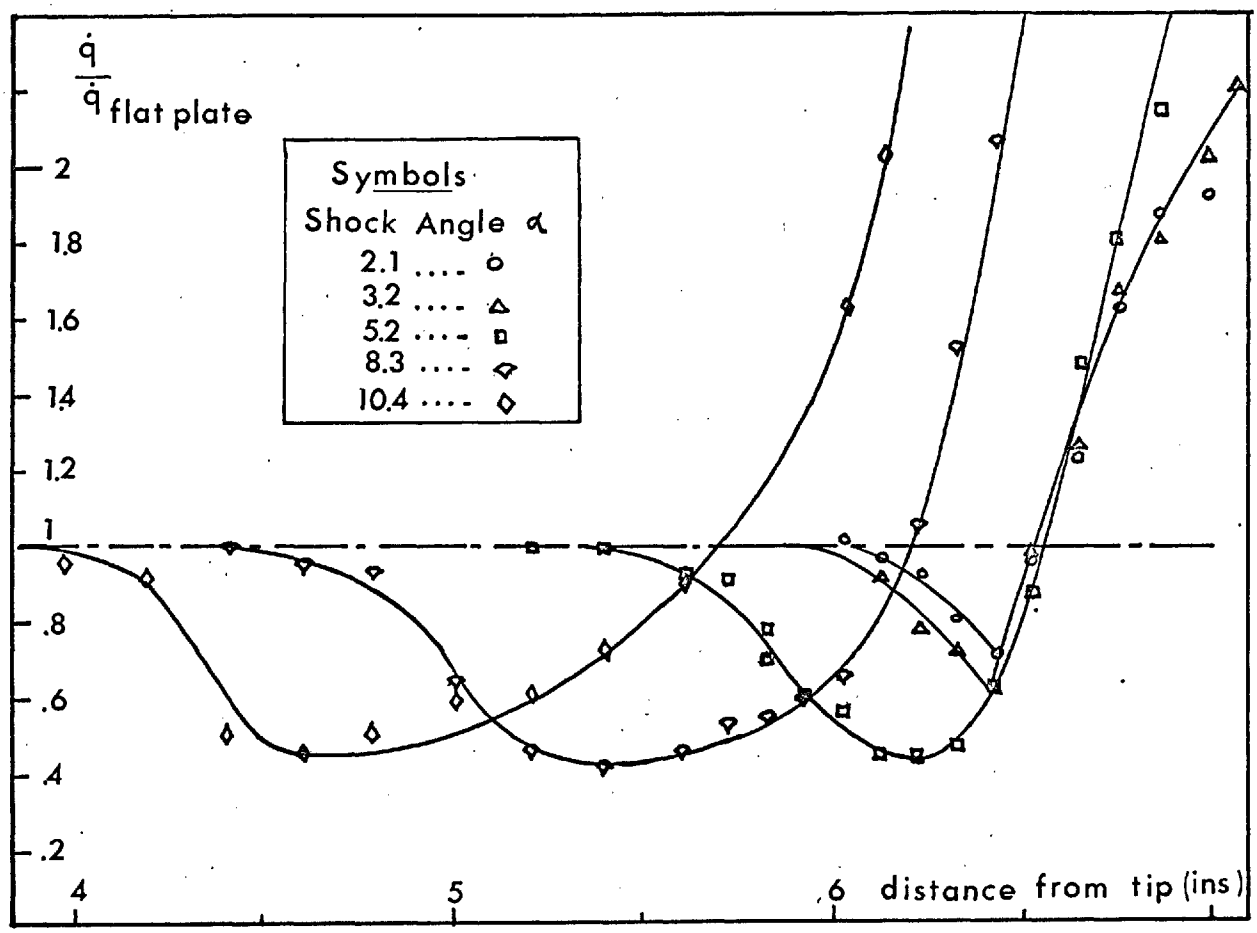

Figure 28 EXTERNALLY GENERATED SHOCK INDUCED SEPARATION

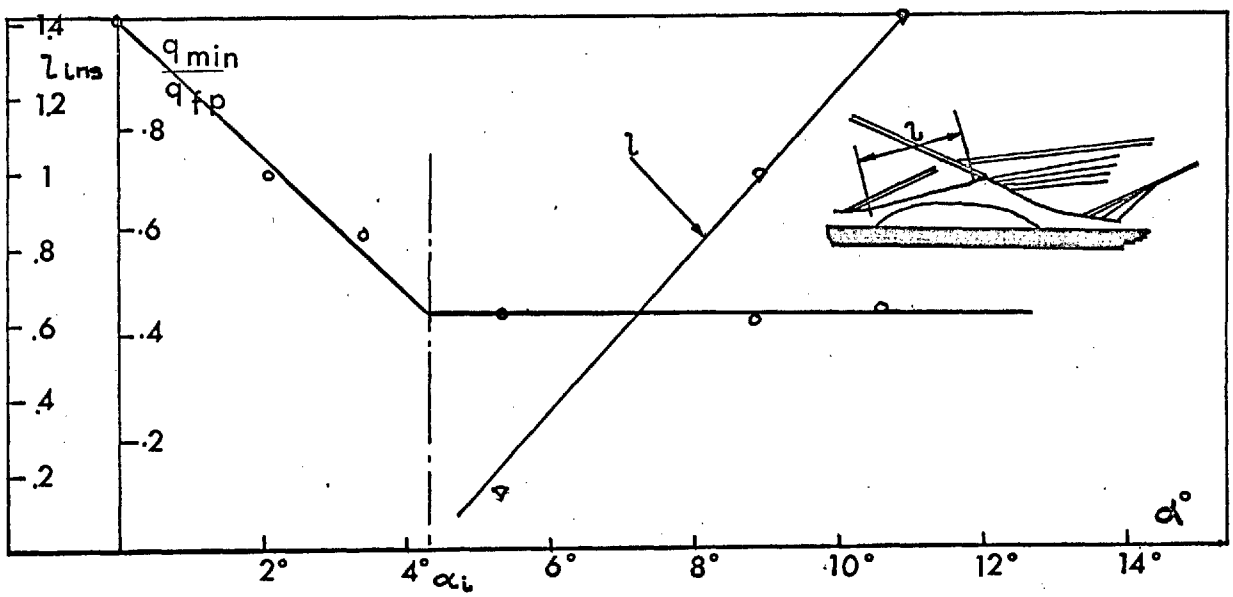

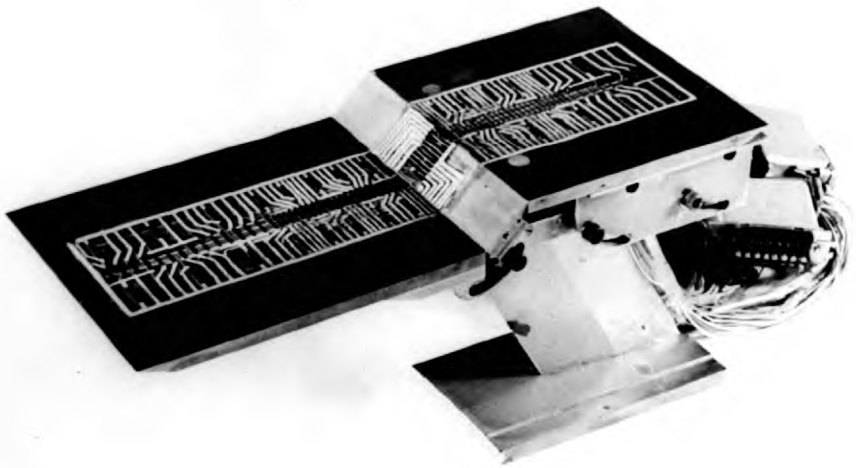

Figure 29 VARIABLE ANGLE STEP MODEL

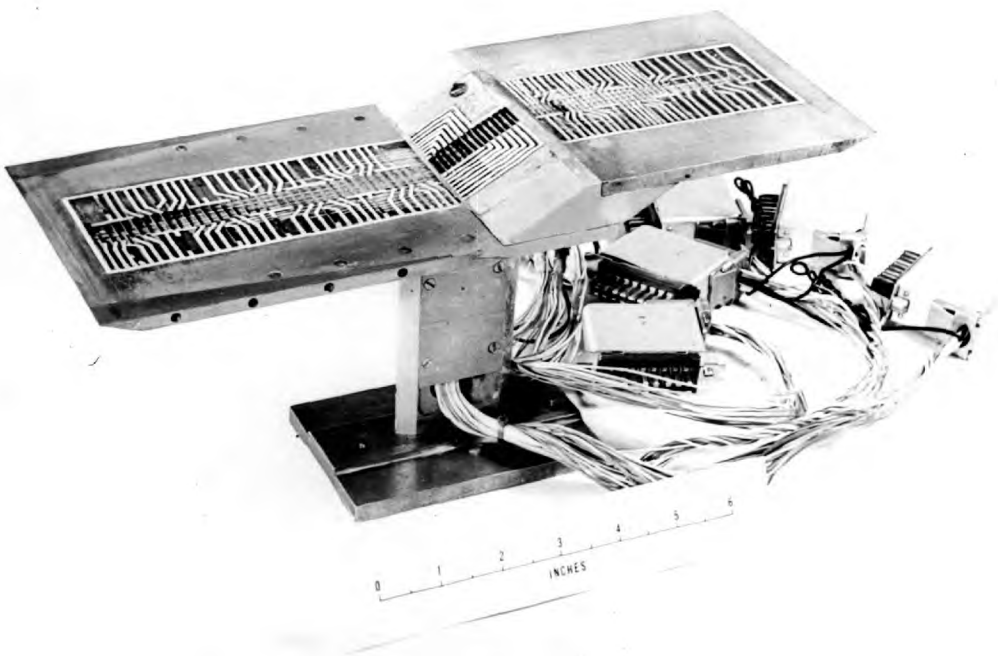

Figure30 a 30° FIXED ANGLE STEP MODEL

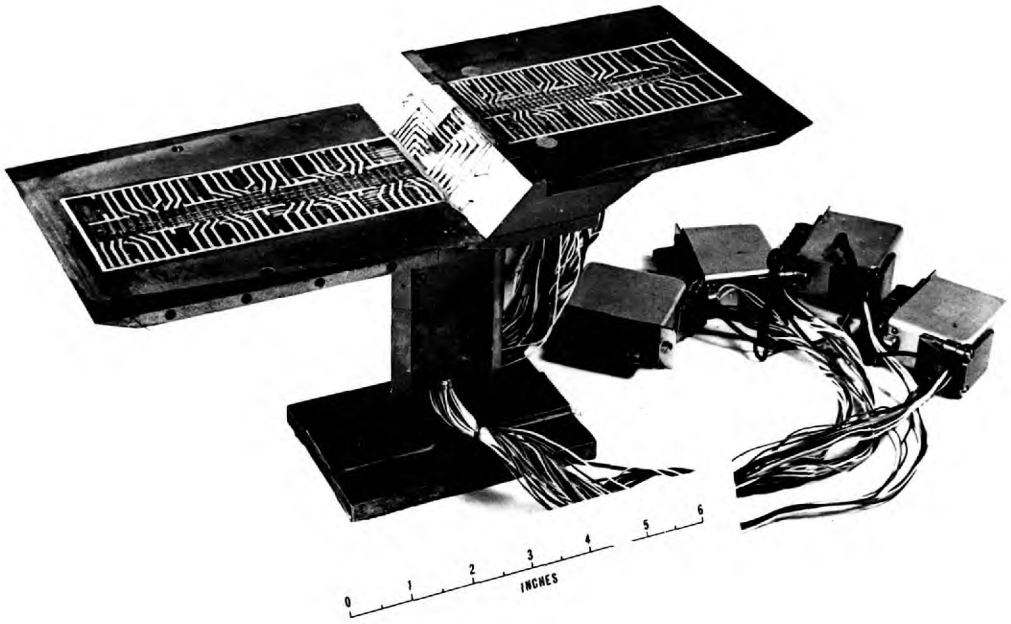

Figure 30b 45° STEP

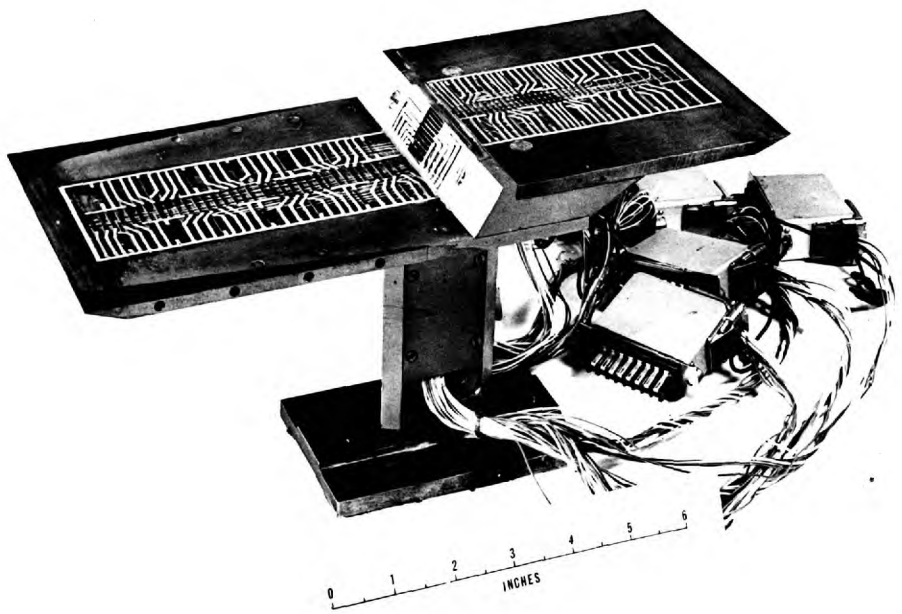

Figure 30c 60° STEP

Figure 30d 75°STEP

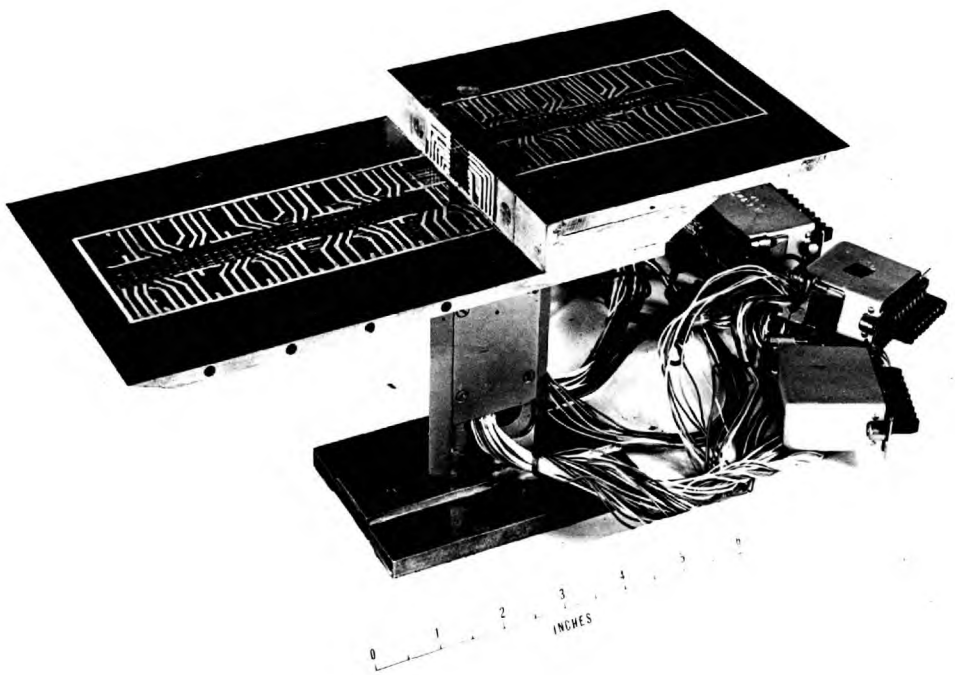

Figure 30e 90° STEP

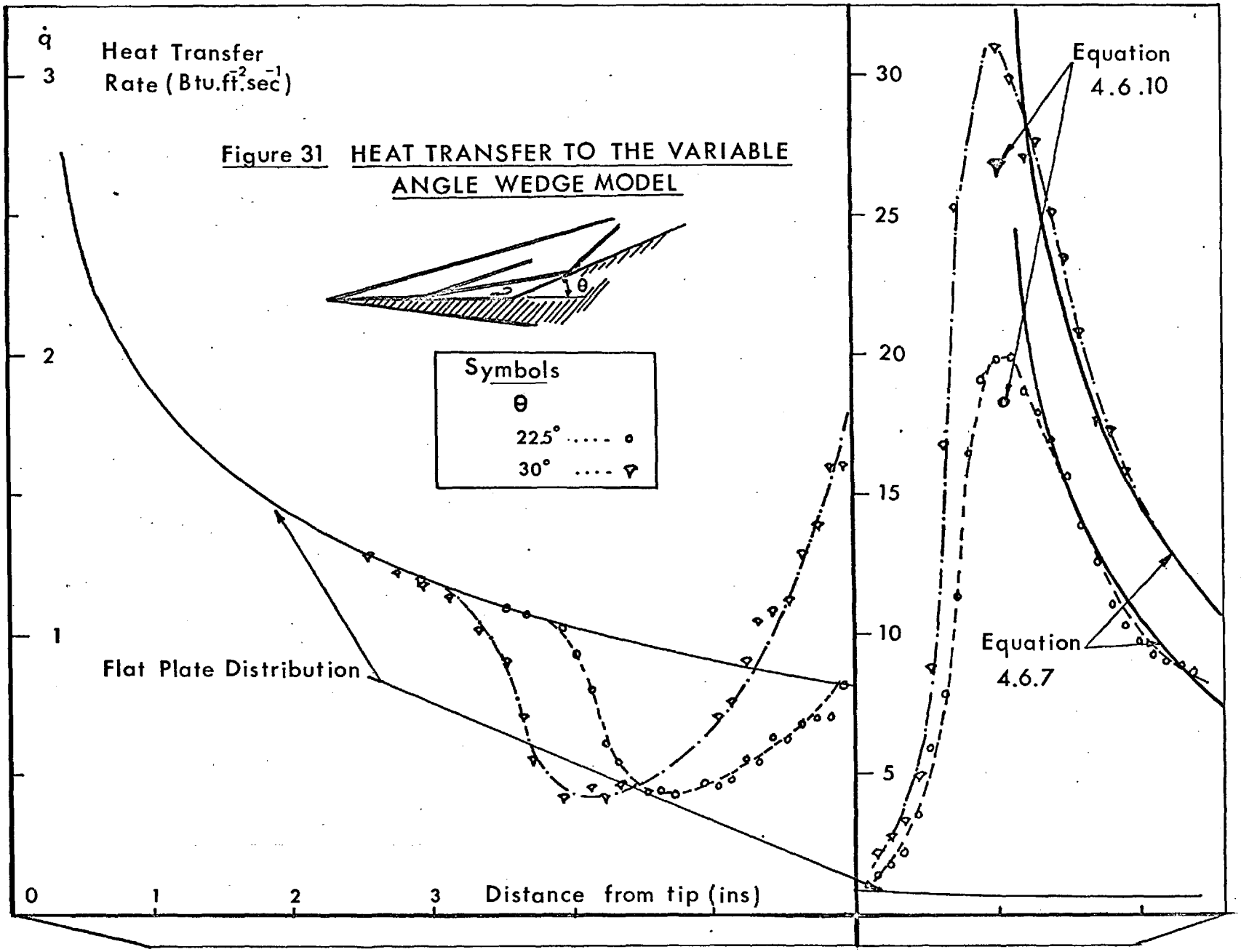

Figure 31 HEAT TRANSFER TO THE VARIABLE ANGLE WEDGE MODEL

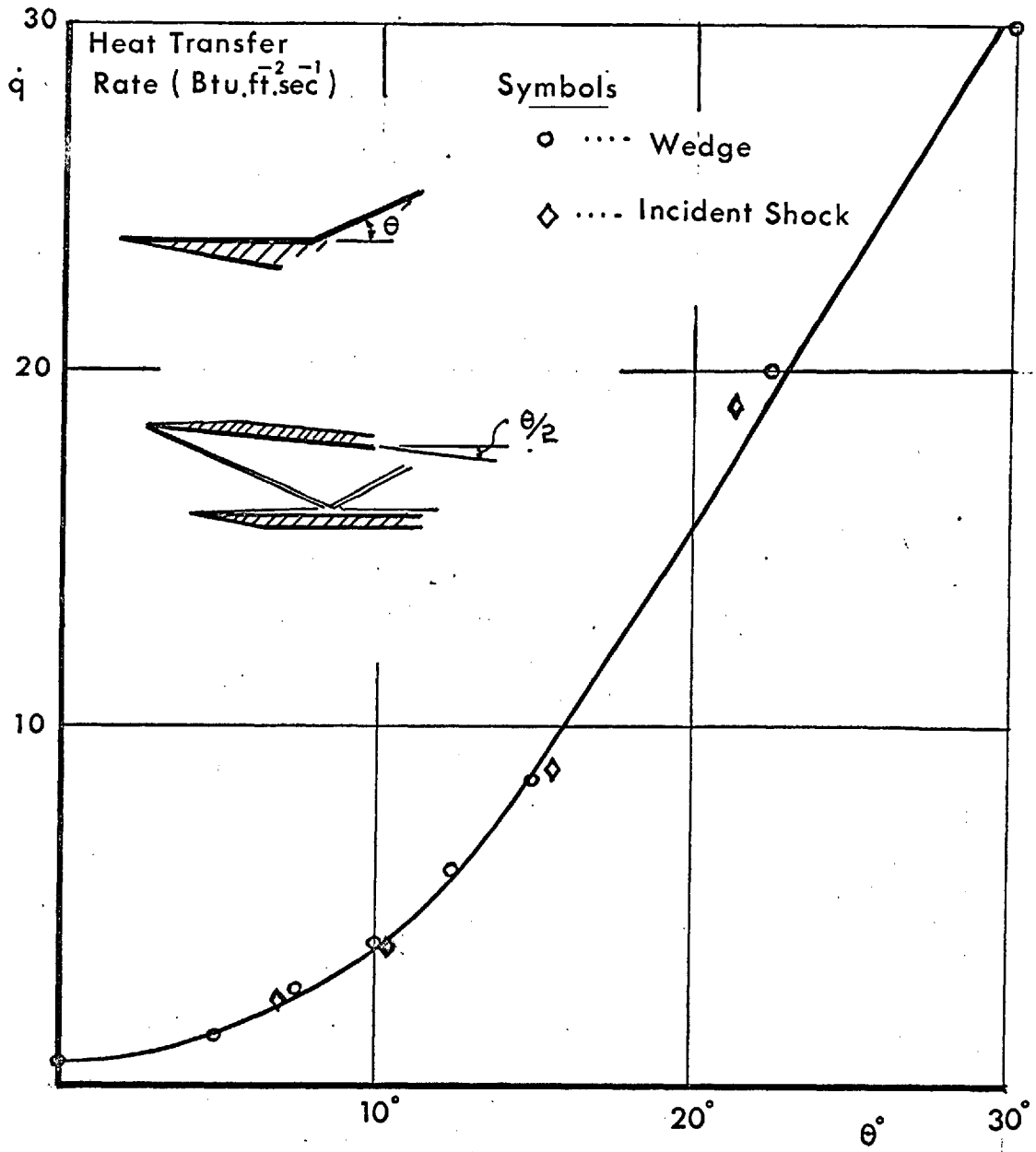

Figure 32 MAXIMUM HEAT TRANSFER IN REGIONS OF SHOCK WAVE BOUNDARY LAYER INTERACTION

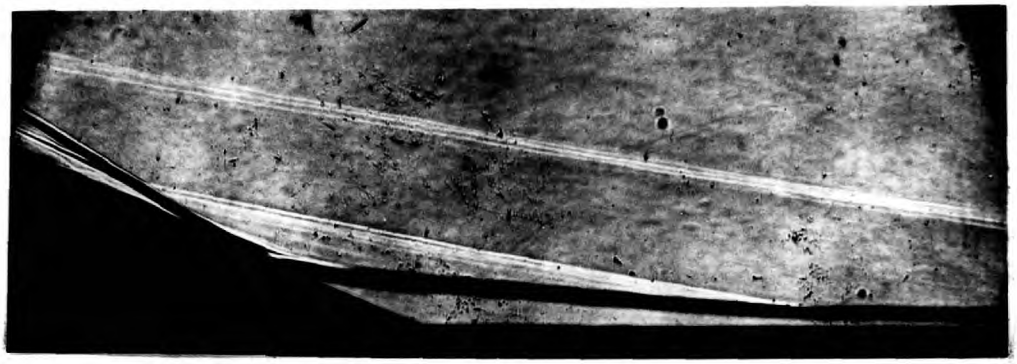

Figure 33a 22 5° WEDGE

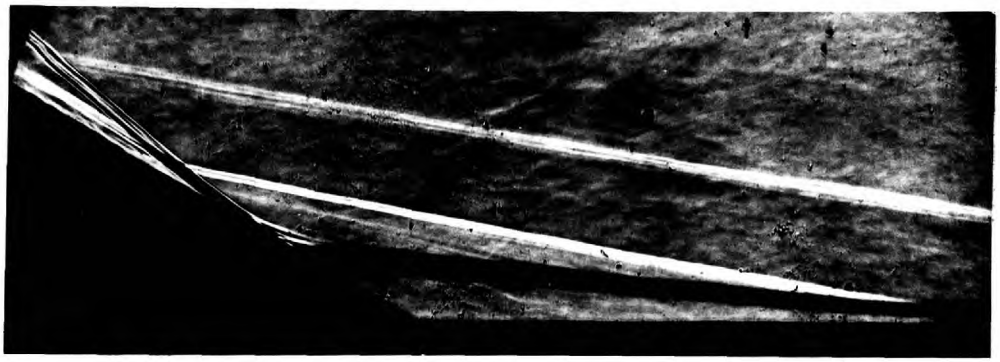

Figure 33b 30° WEDGE

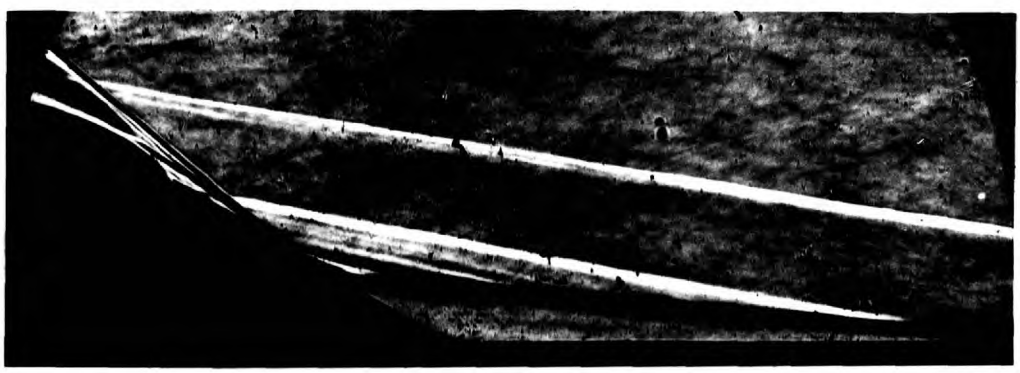

Figure 33c 30° STEP

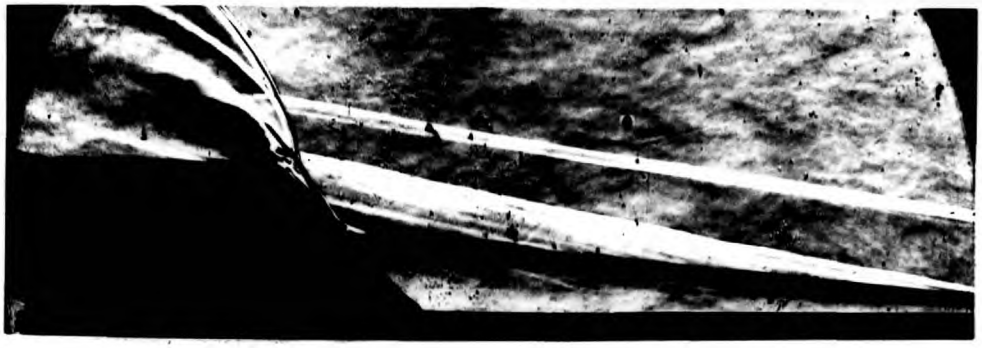

Figure34b 45° STEP

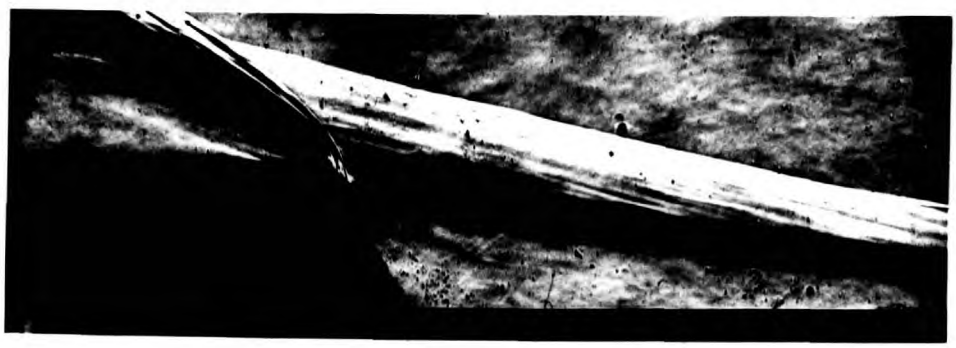

Figure34c 60° STEP

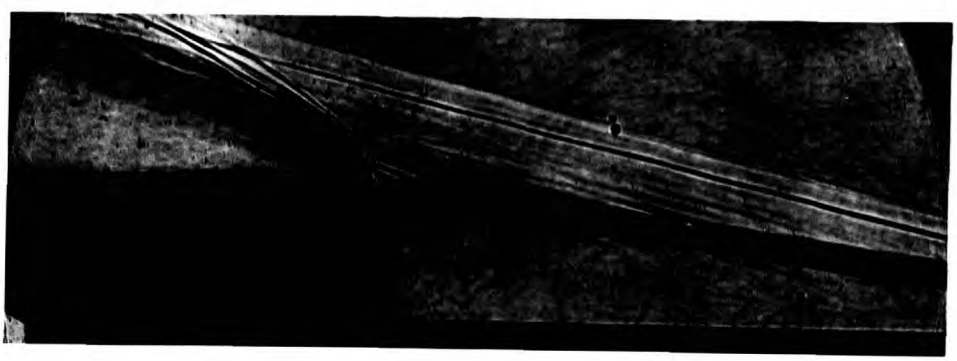

Figure34d 75° STEP

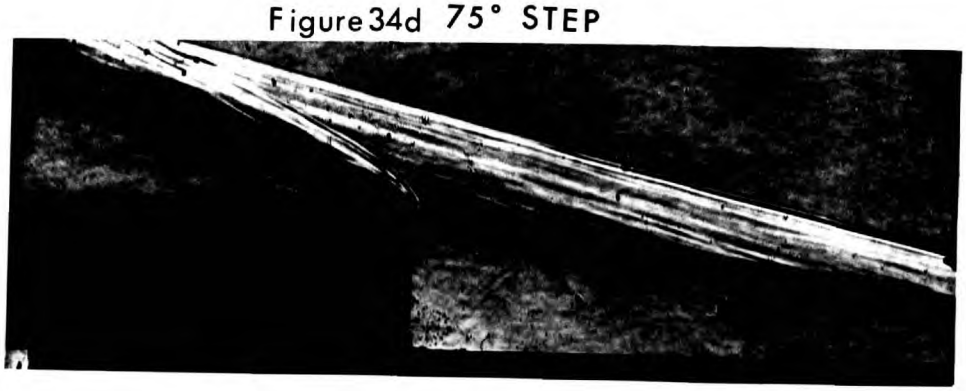

Figure34e 90° STEP

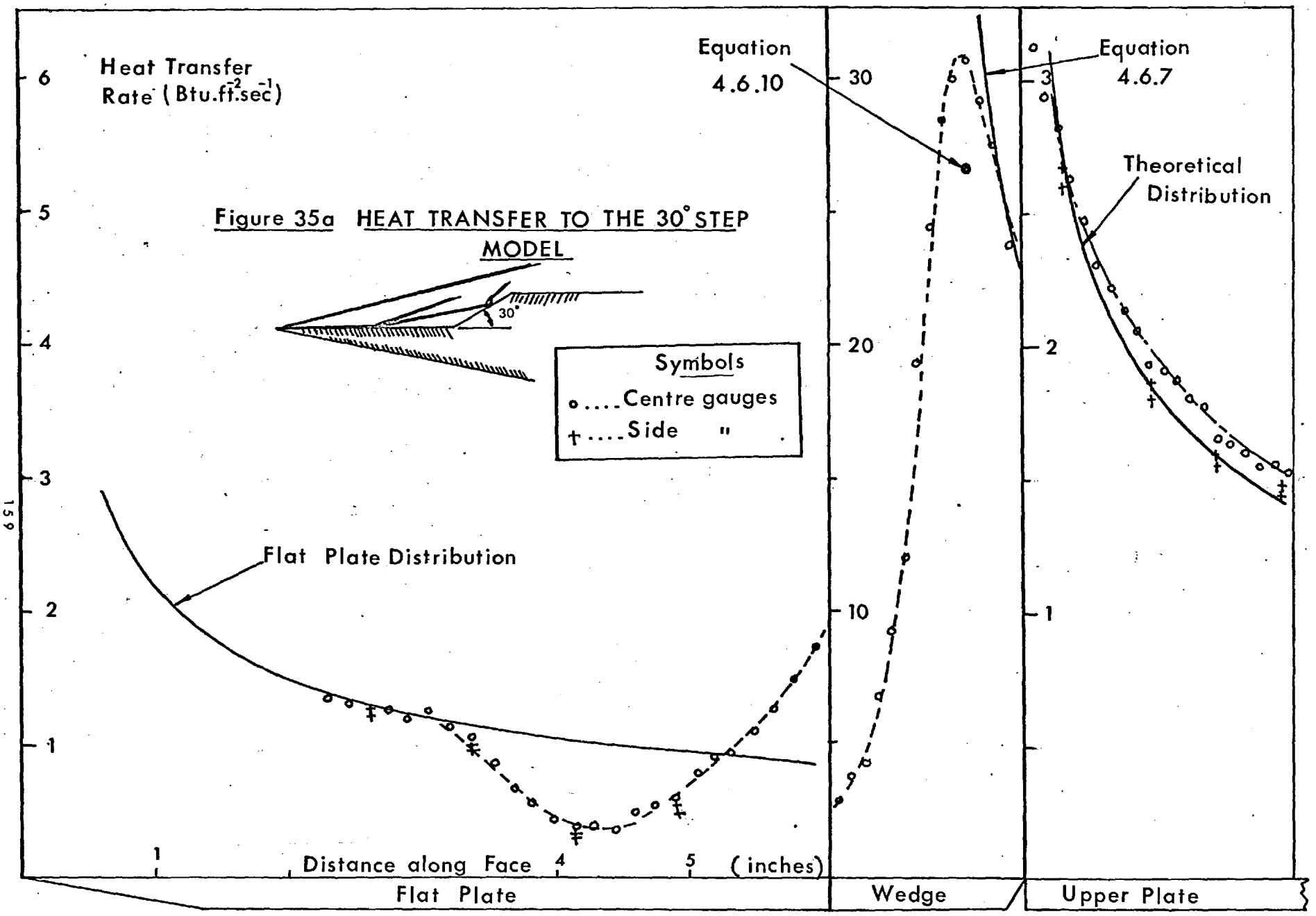

Figure 35a HEAT TRANSFER TO THE 30° STEP MODEL

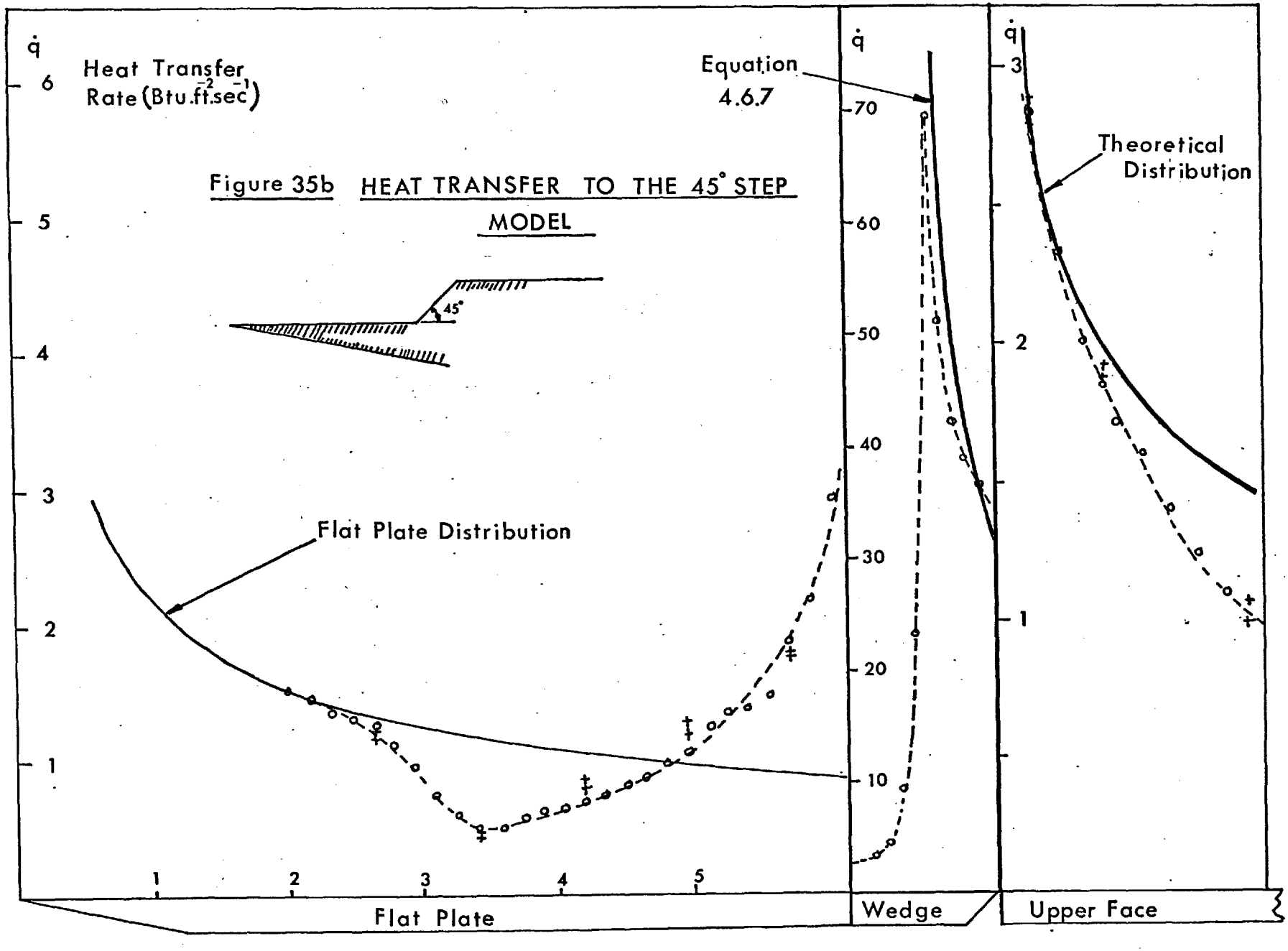
q̇
Heat Transfer Rate (Btu.ft.sec)
Equation 4.6.7
Figure 35b HEAT TRANSFER TO THE 45° STEP MODEL
45°
Flat Plate Distribution
Theoretical Distribution
Flat Plate
Wedge
Upper Face

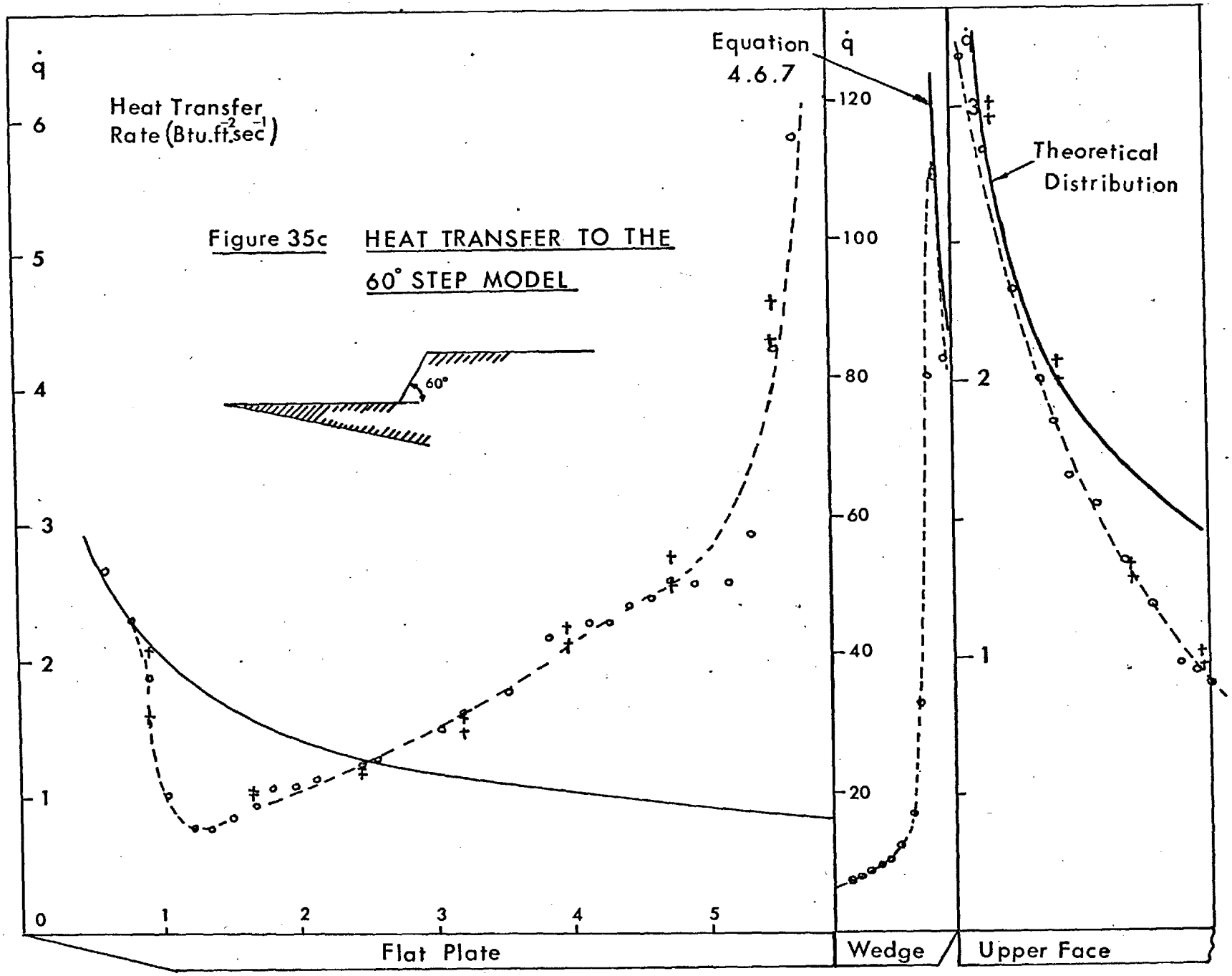

Figure 35c HEAT TRANSFER TO THE 60° STEP MODEL

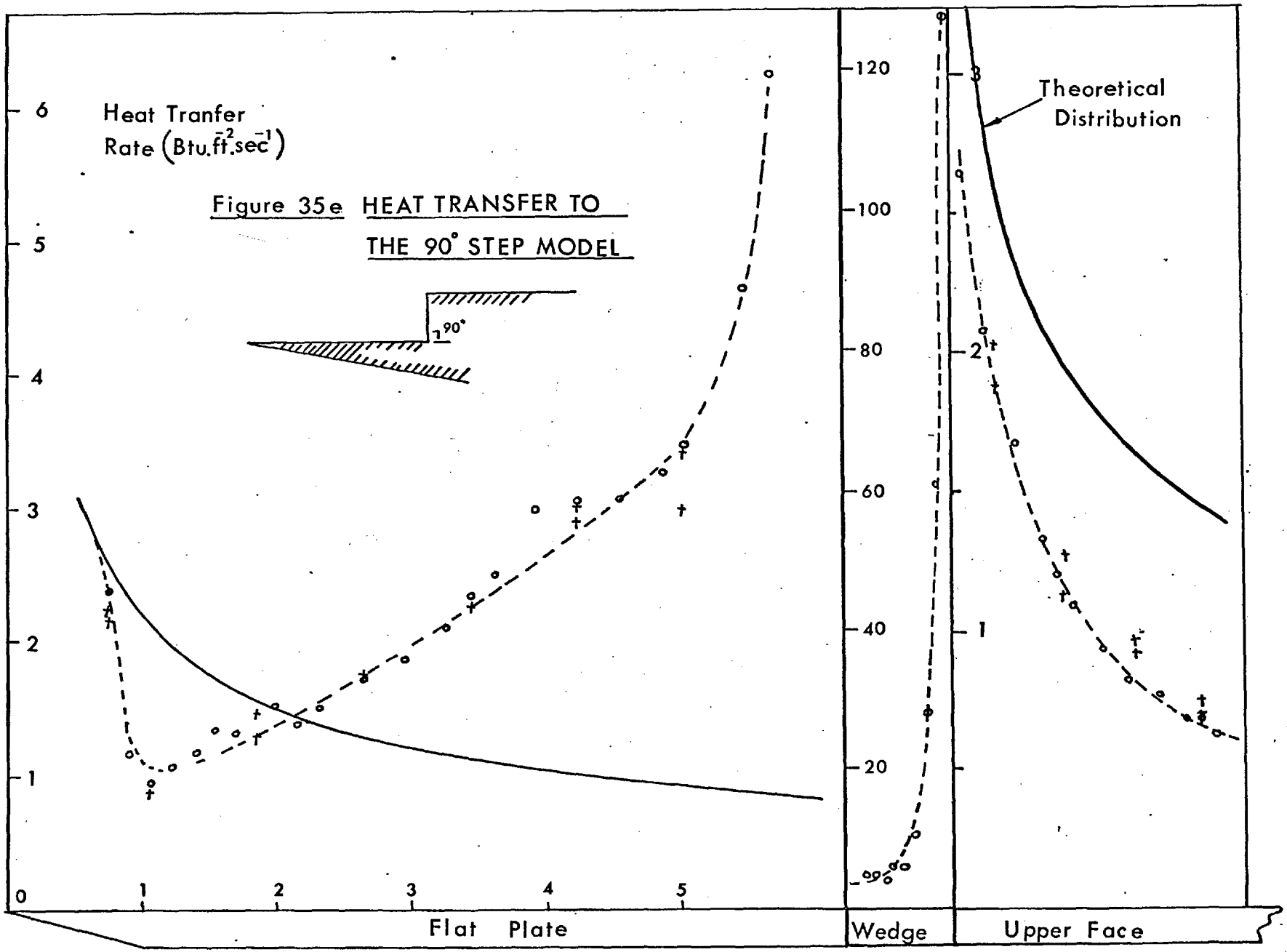
Heat Tranfer
Rate (Btu.ft.$^{-2}$sec^{-1})
Figure 35e HEAT TRANSFER TO
THE 90° STEP MODEL
90°
Theoretical
Distribution
Flat Plate
Wedge
Upper Face

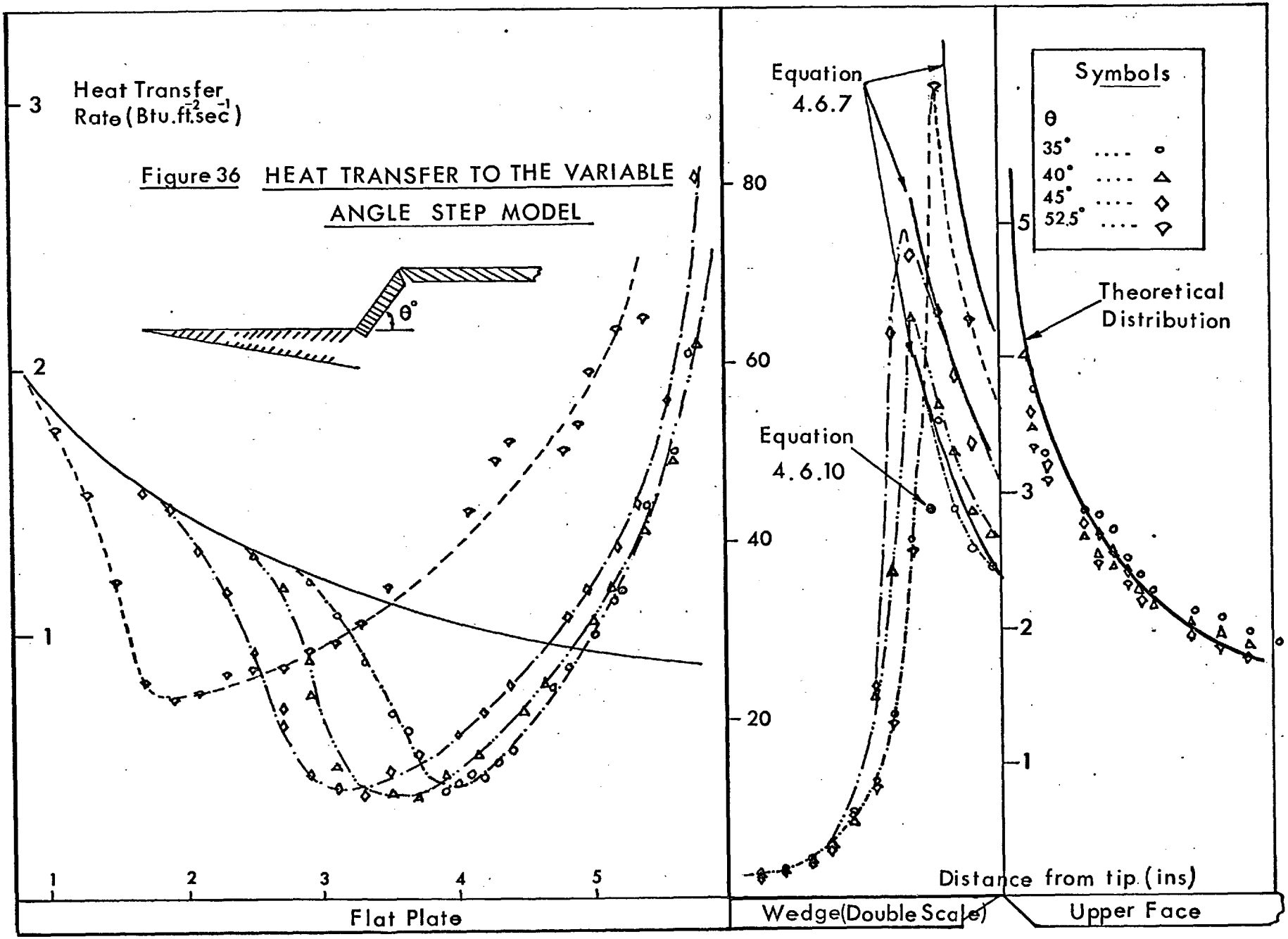

Figure 36 HEAT TRANSFER TO THE VARIABLE ANGLE STEP MODEL

Figure 37a 35° WEDGE

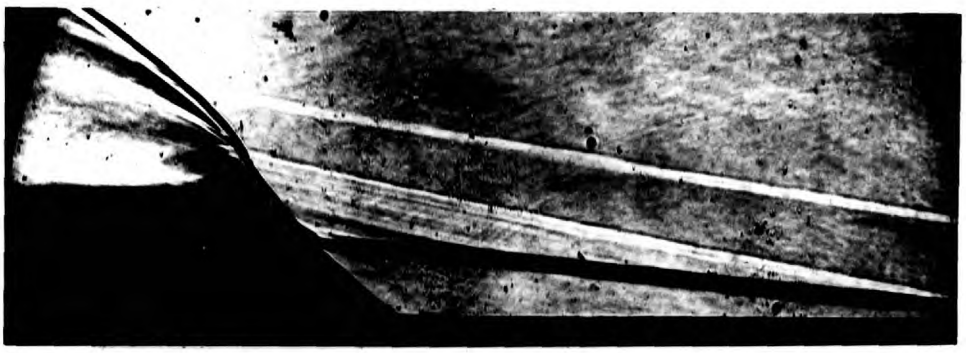

Figure 37b 40° WEDGE

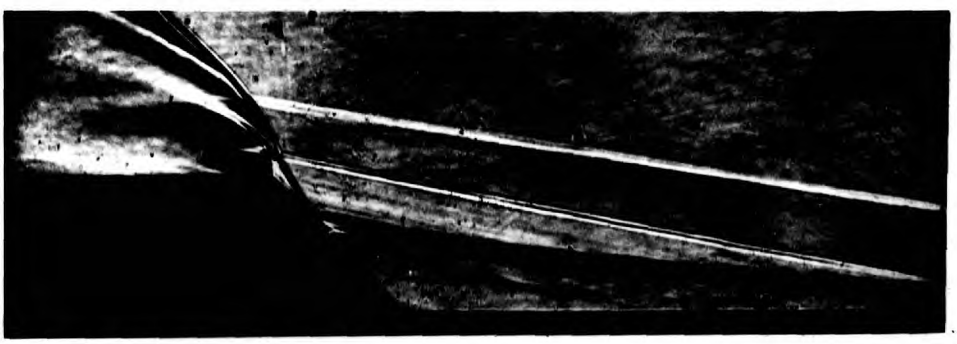

Figure 37c 45° WEDGE

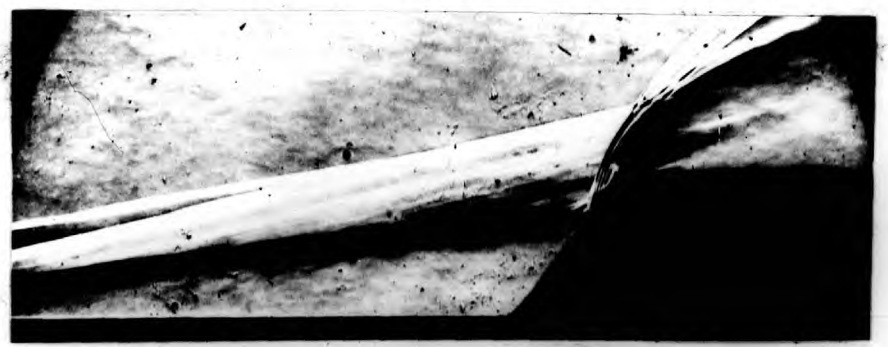

Figure 37d 52.5° WEDGE

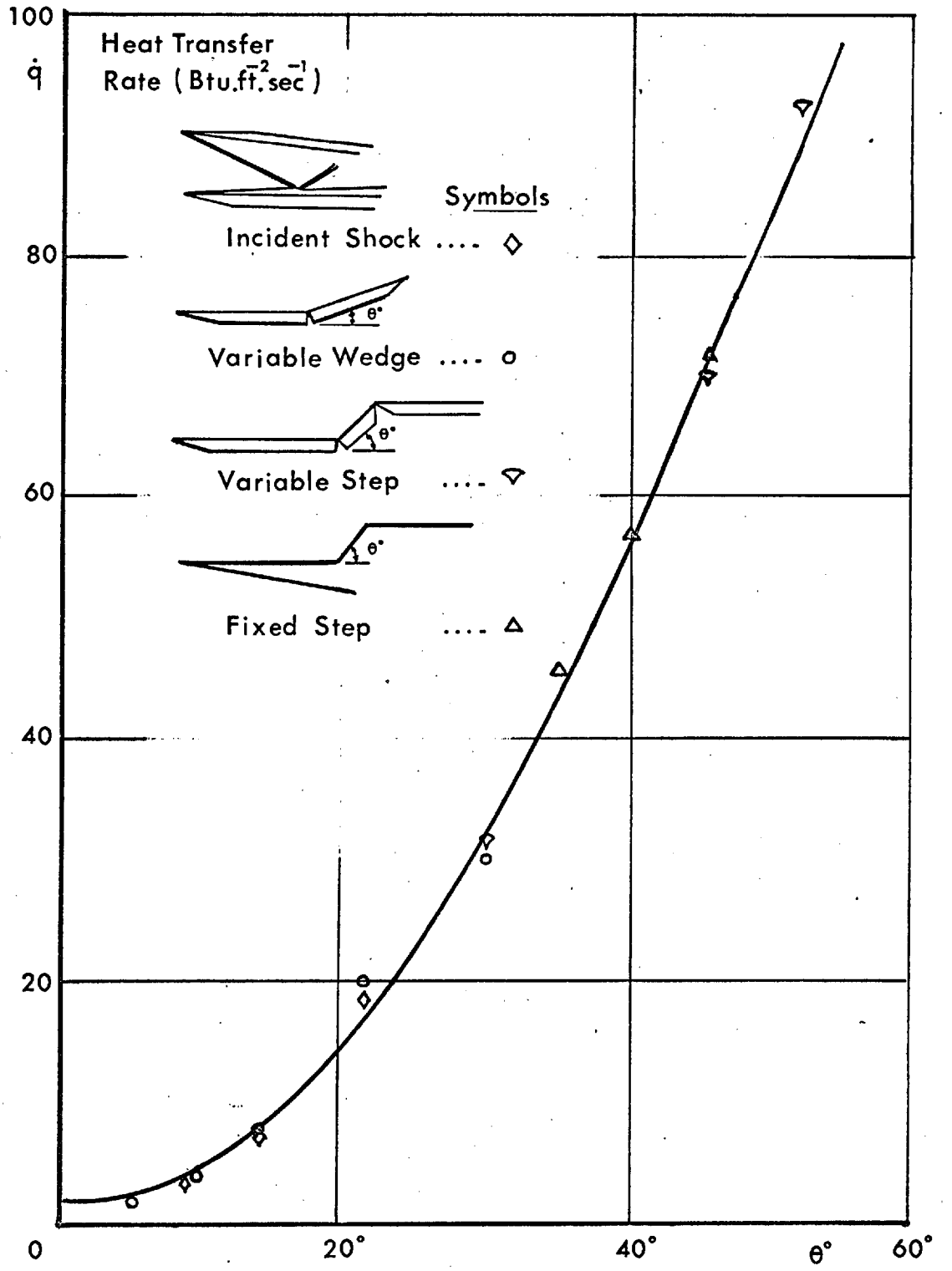

Figure 38a VARIATION OF REATTACHMENT HEAT TRANSFER WITH WEDGE ANGLE

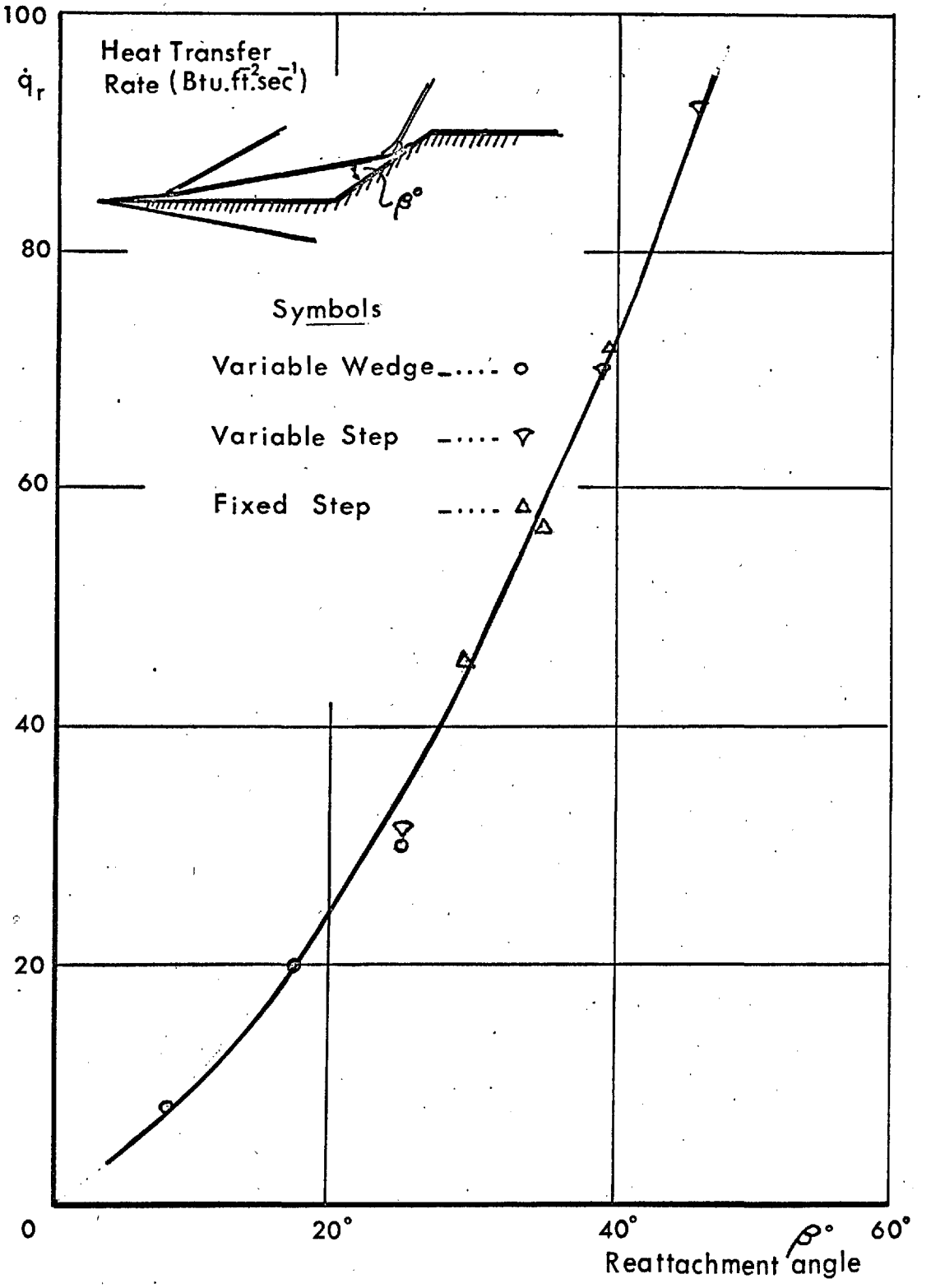

Figure 38b VARIATION OF REATTACHMENT HEAT TRANSFER WITH REATTACHMENT ANGLE

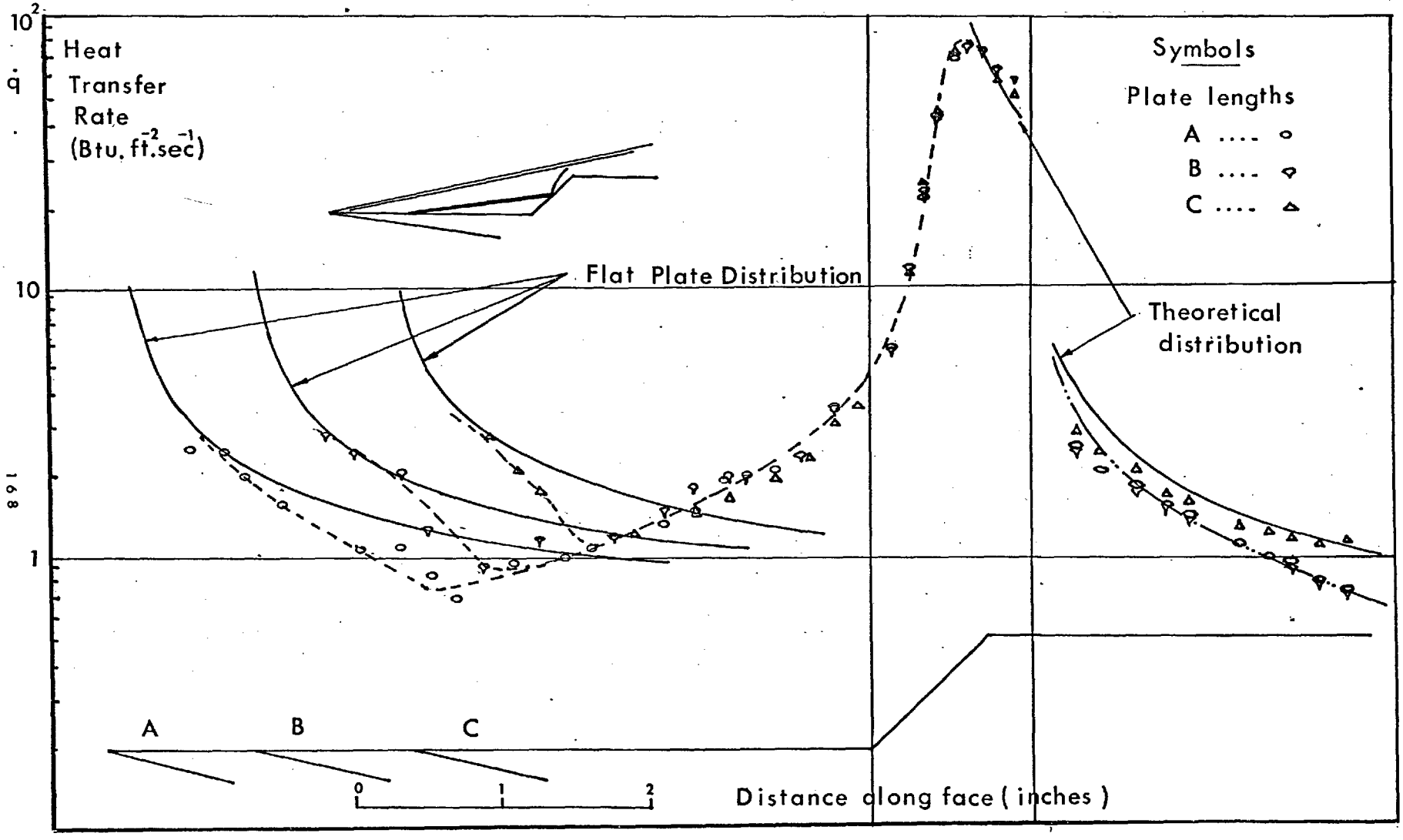

Figure 39 HEAT TRANSFER TO THE 45° STEP MODEL

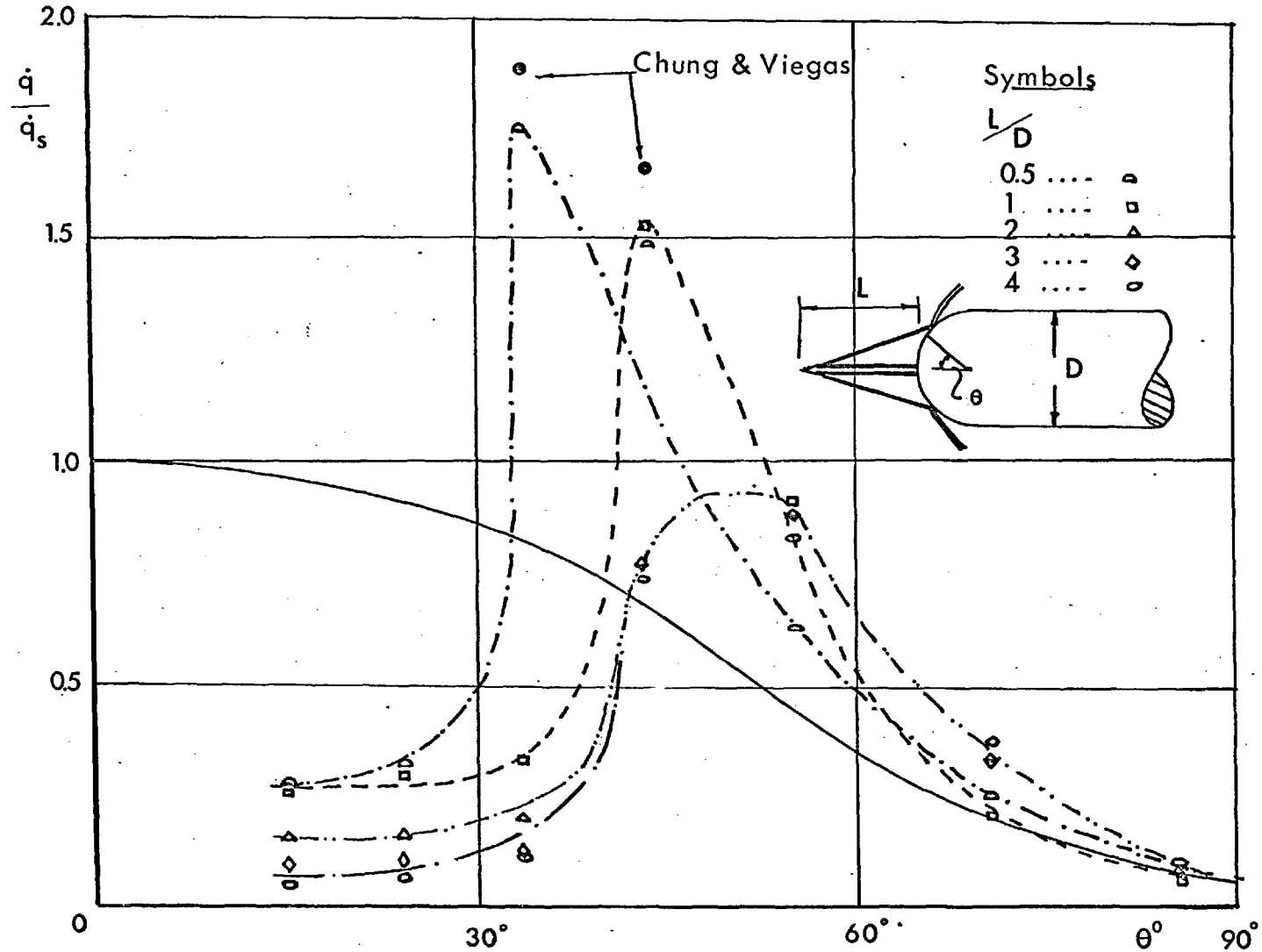

Figure 40 HEAT TRANSFER TO A SPIKED HEMISPHERE

$\frac{l}{d} = 0$

$\frac{l}{d} = 0.5$

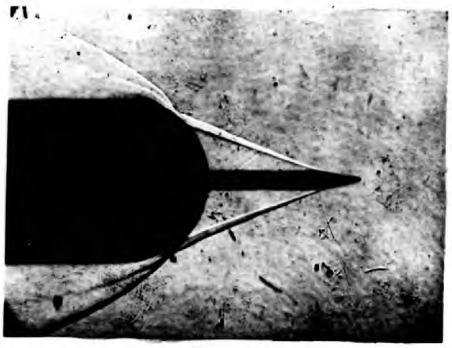

$\frac{l}{d} = 1$

$\frac{l}{d} = 2$

$\frac{l}{d} = 3$

$\frac{l}{d} = 4$

FIG.41 Flow over Spiked Hemispheres

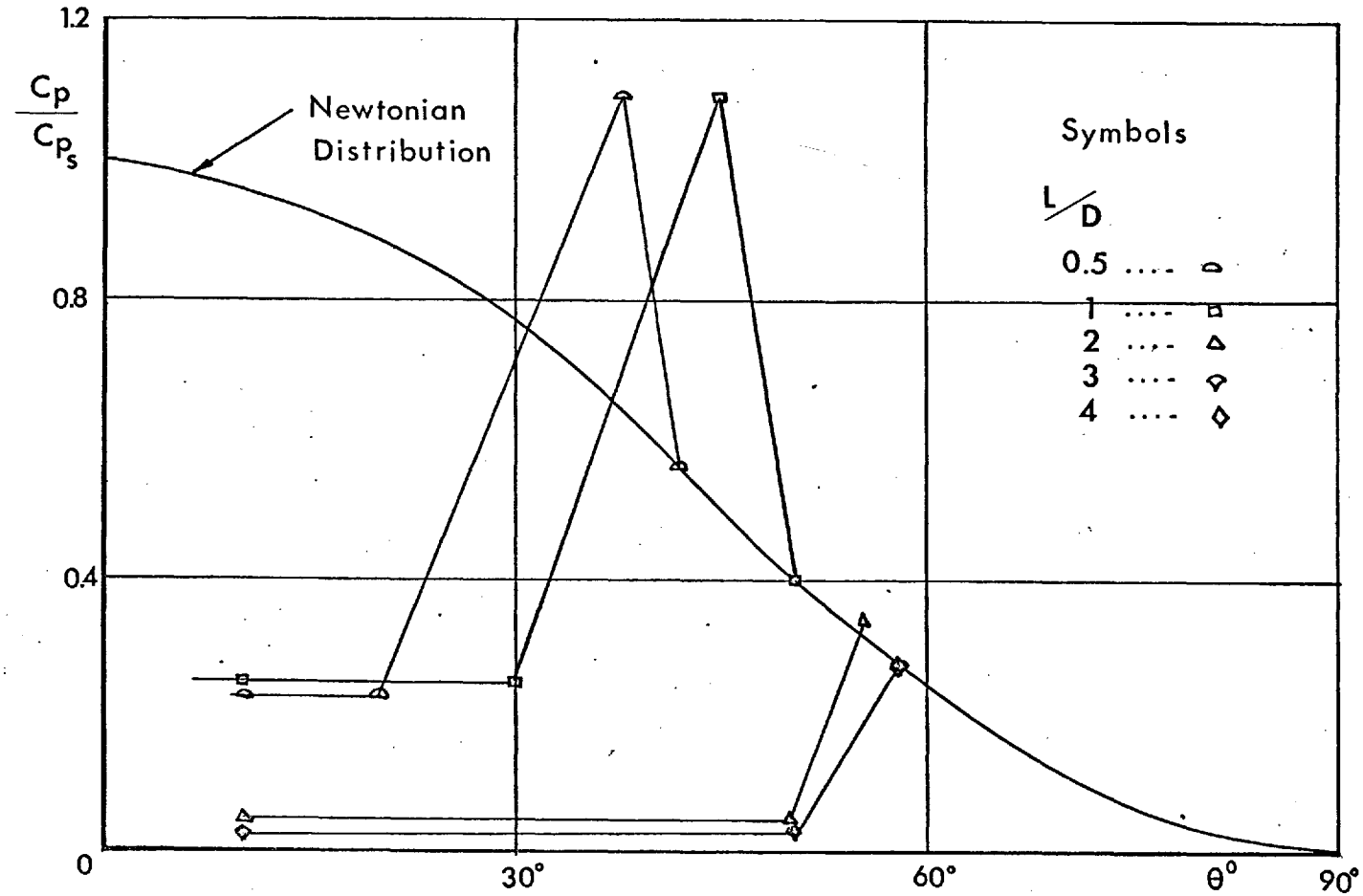

Figure 42 CALCULATED PRESSURE DISTRIBUTION TO SPIKED SPHERE

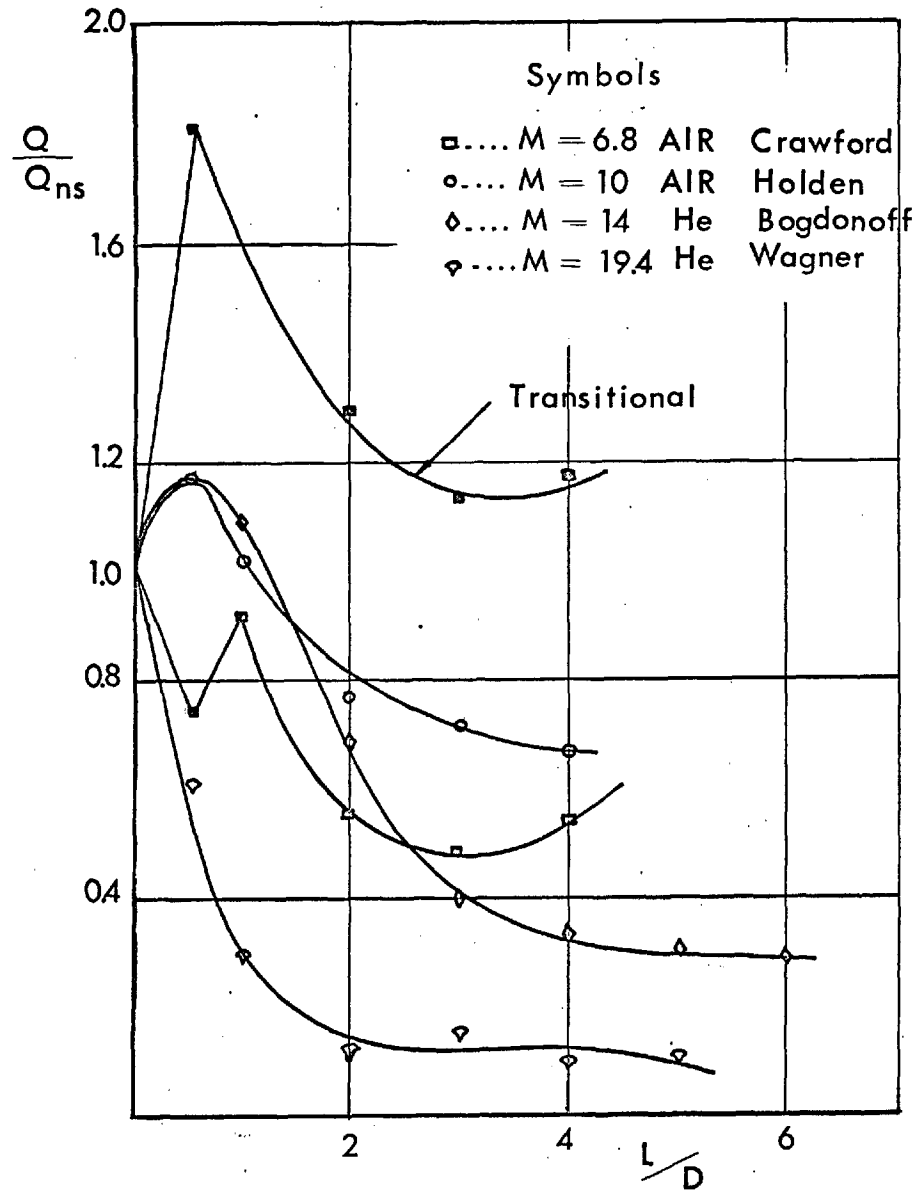

Figure 43 TOTAL HEAT TRANSFER TO A SPIKED HEMISPHERE

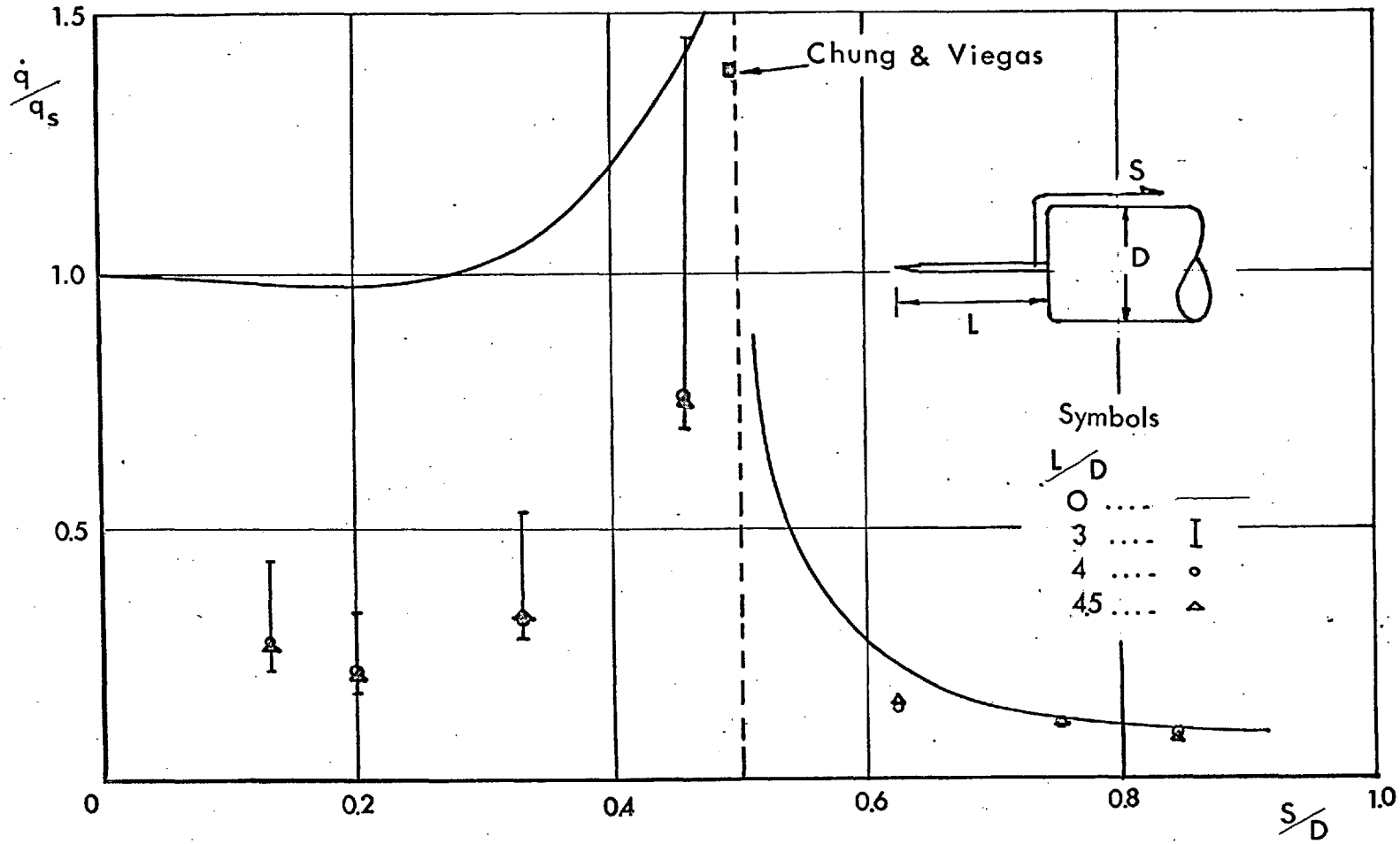

Figure 44 HEAT TRANSFER TO A SPIKED FLAT ENDED CYLINDER

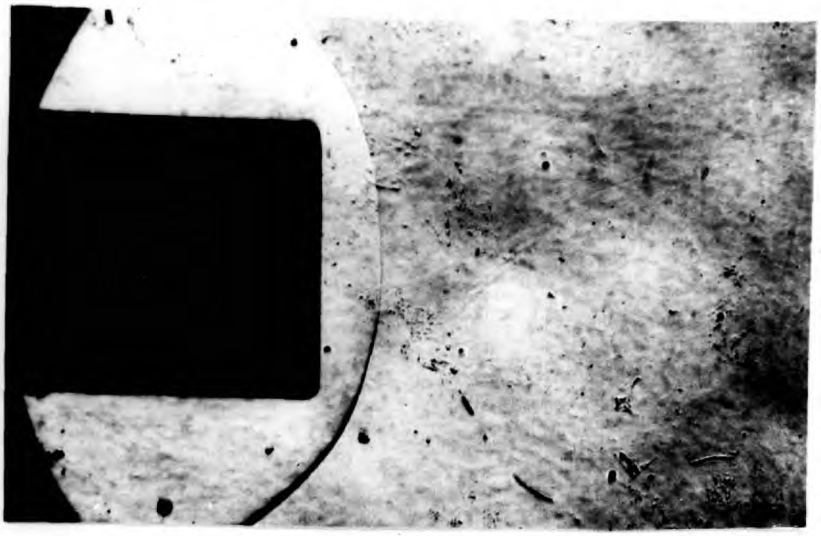

$\frac{L}{D} = 0$

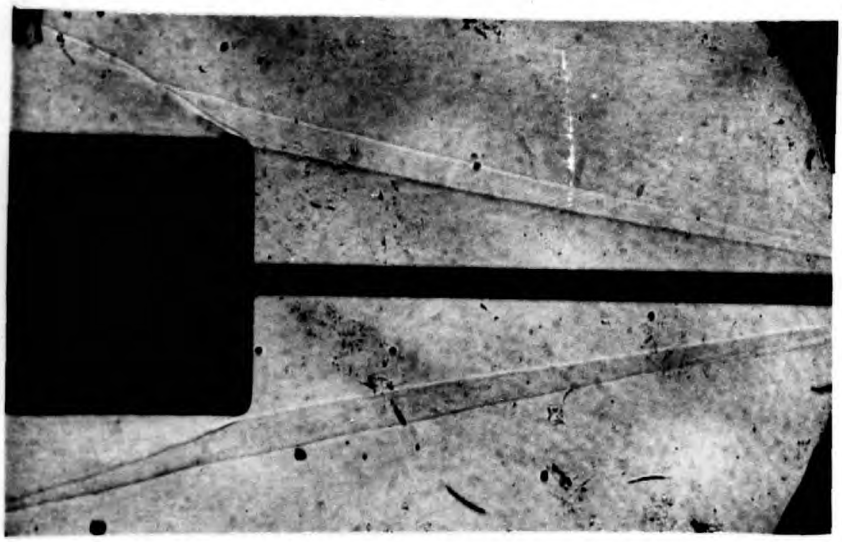

$\frac{L}{D} = 3$

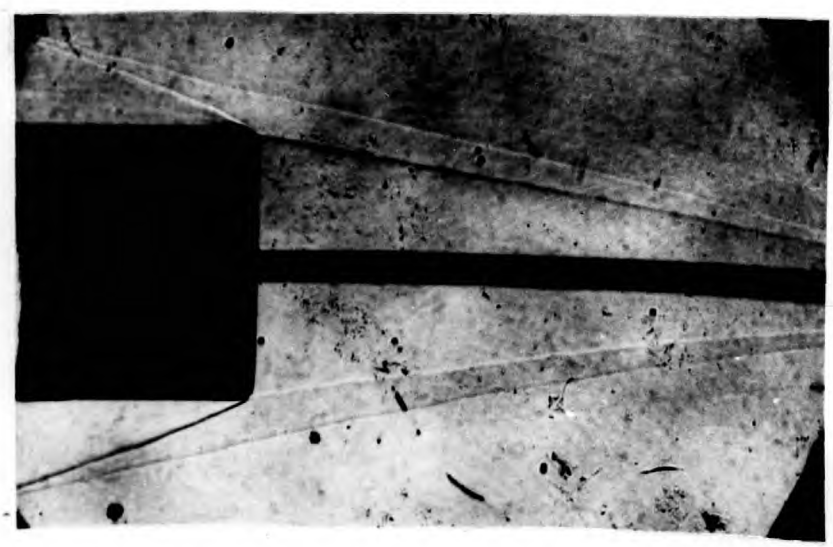

$\frac{L}{D} = 4$

Figure 45 FLOW OVER FLAT—ENDED CYLINDERS

Figure 46a 30° CONE MODEL

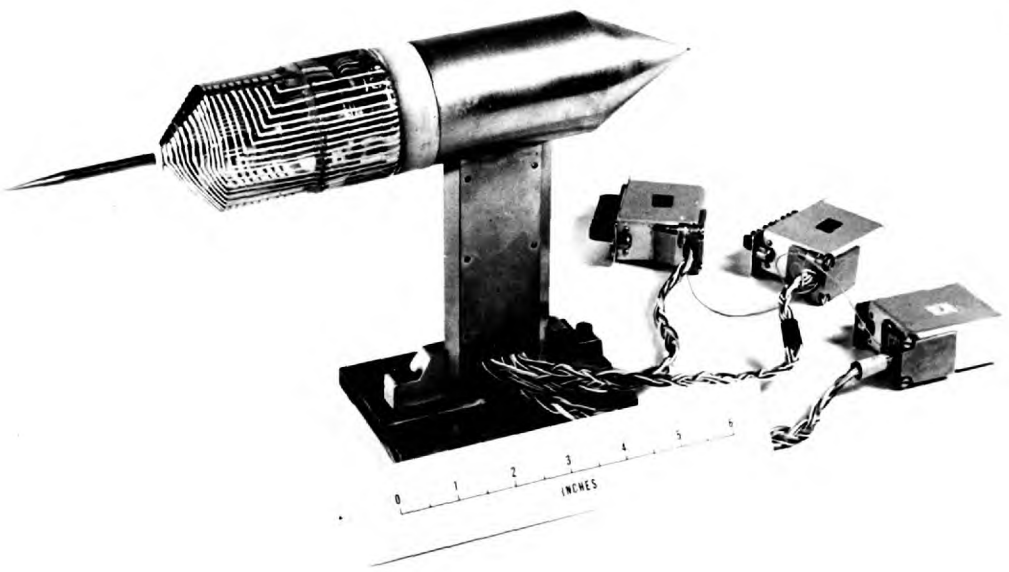

Figure 46b 45° CONE MODEL

Figure 46d 60° CONE MODEL

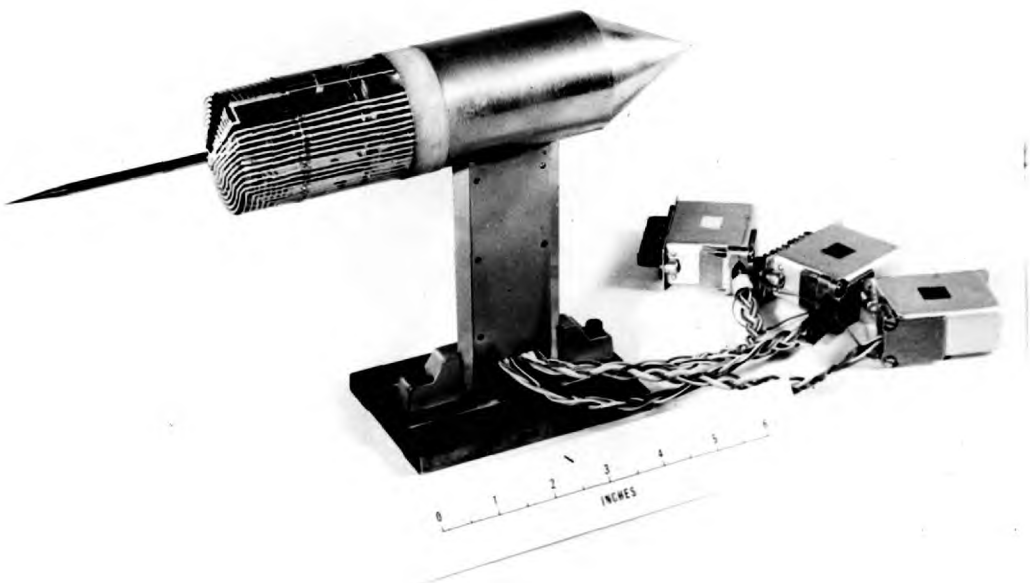

Figure 46e 75° CONE MODEL

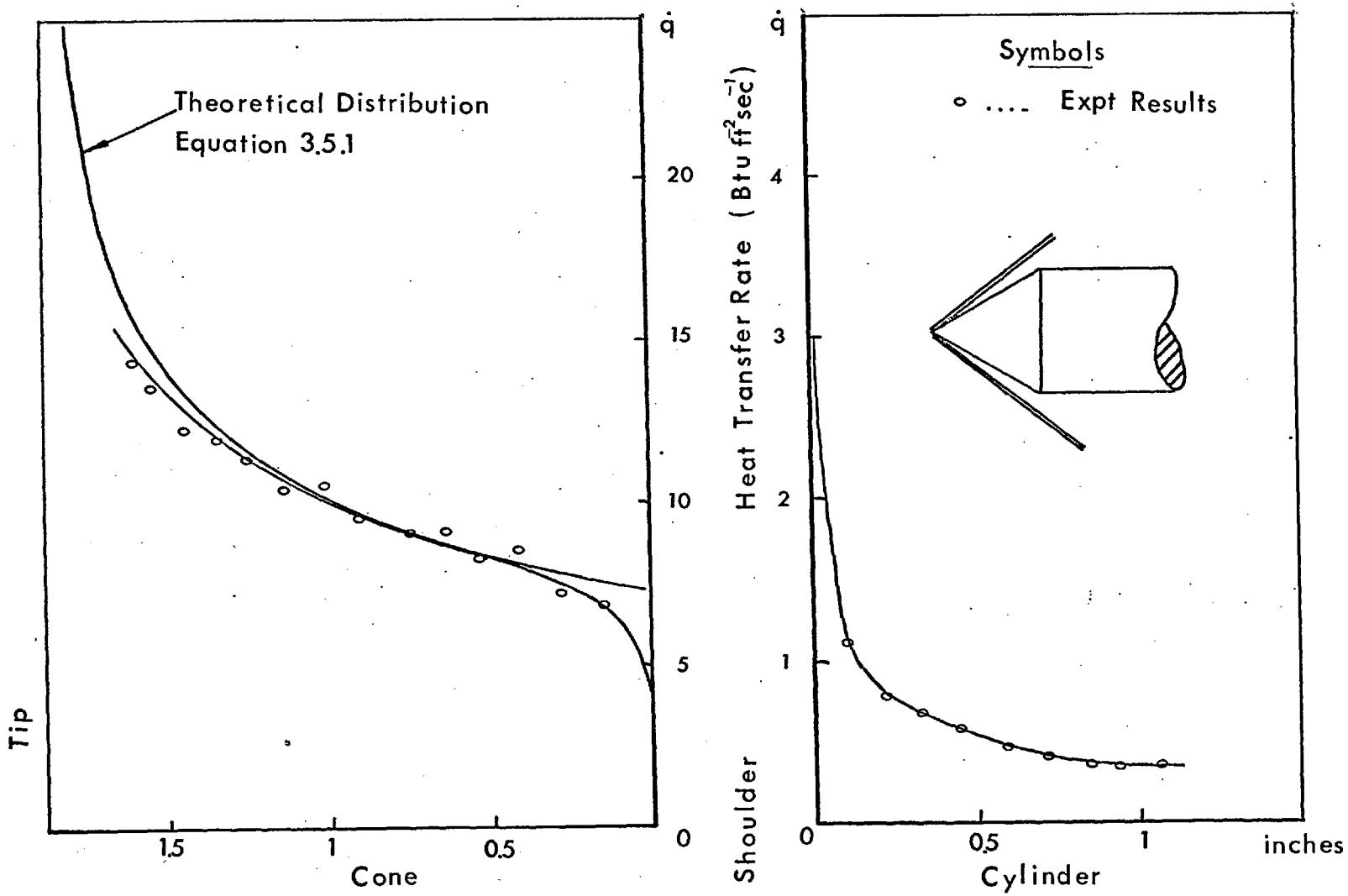

Figure 47a HEAT TRANSFER TO A 30° CONE (M = 10)

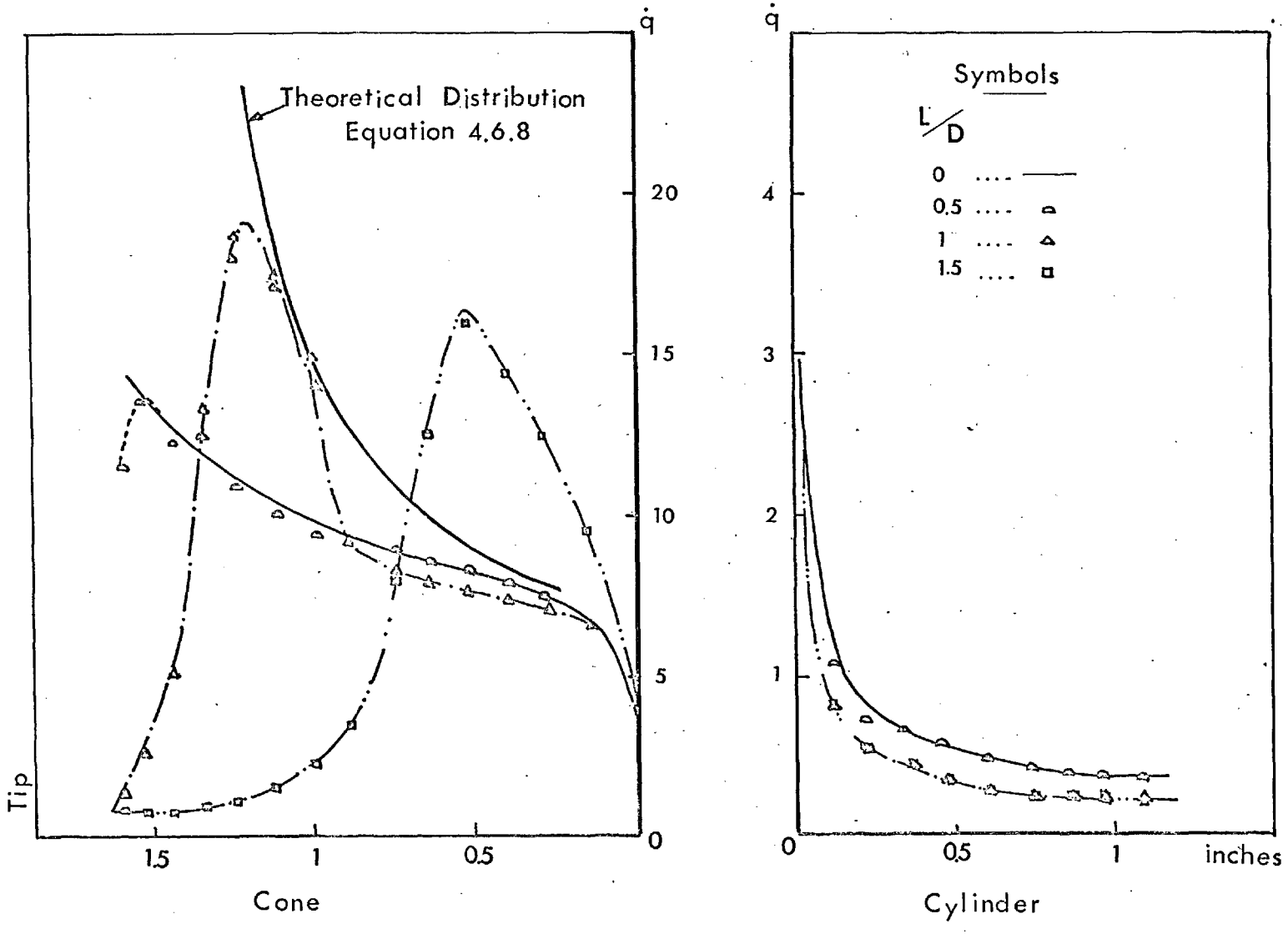

Figure 47a SPIKED 30° CONE MODEL (M = 10)

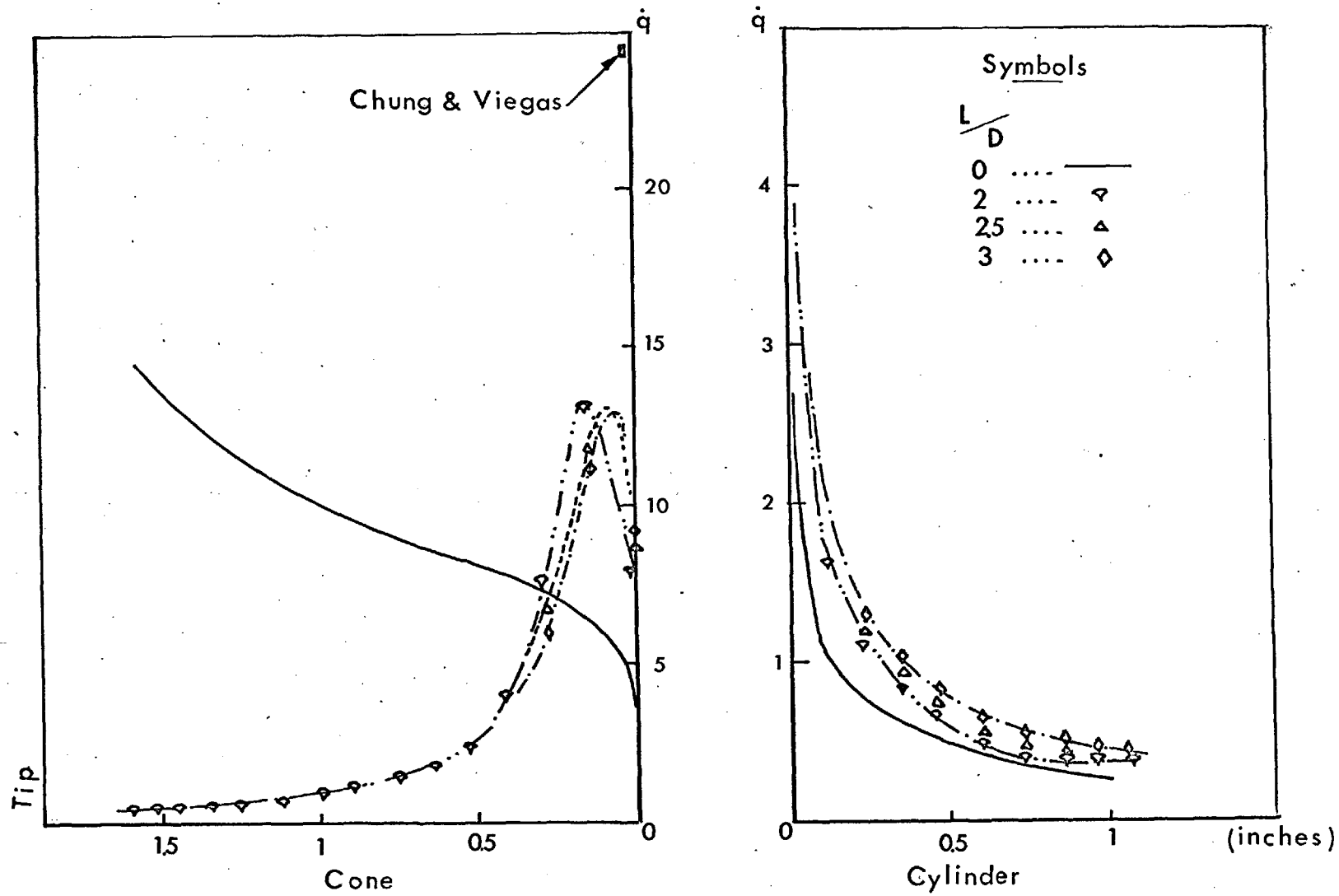

Figure 47a SPIKED 30° CONE (M = 10)

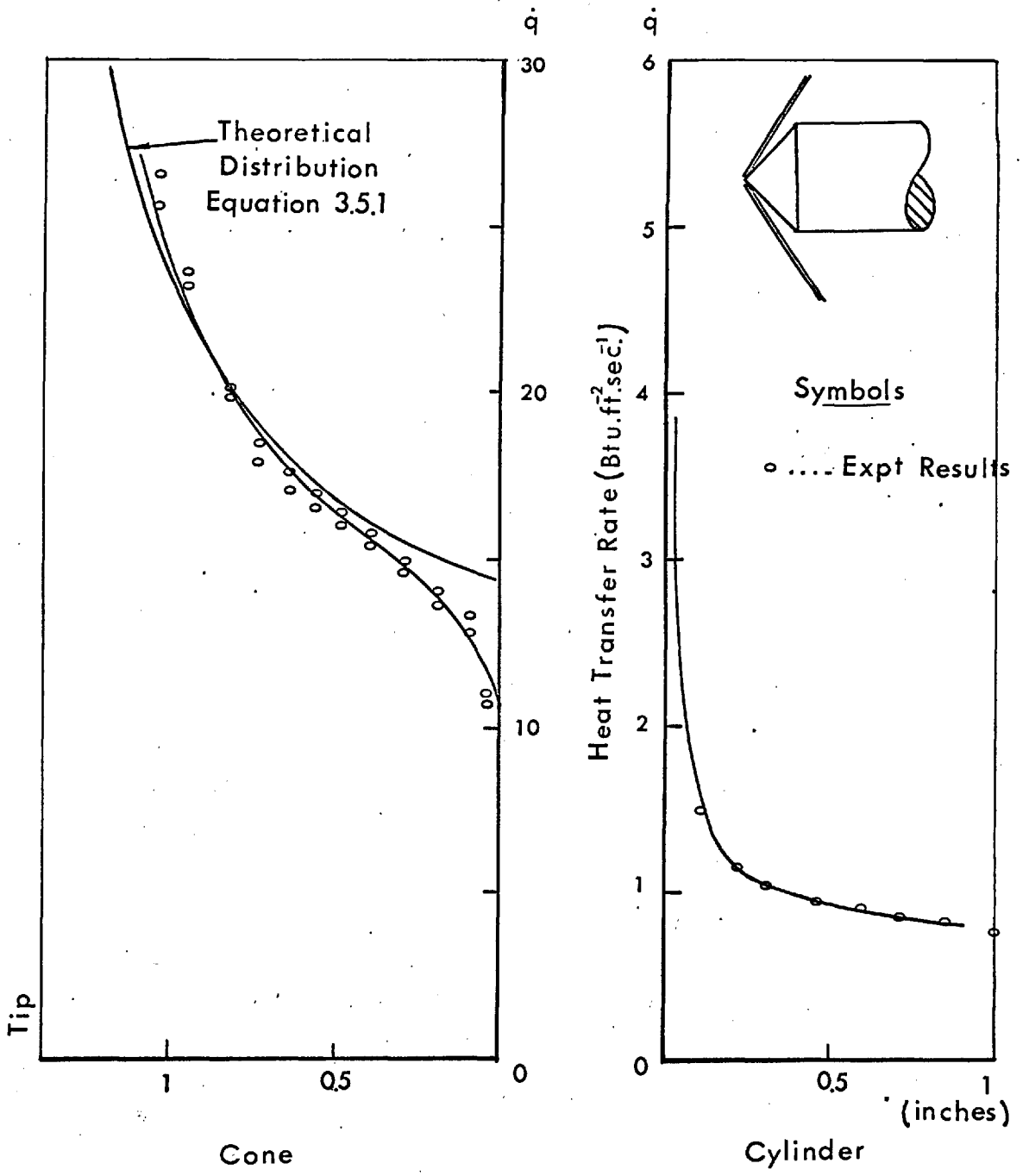

Figure 47b HEAT TRANSFER TO A 45^0 CONE ($M = 10$)

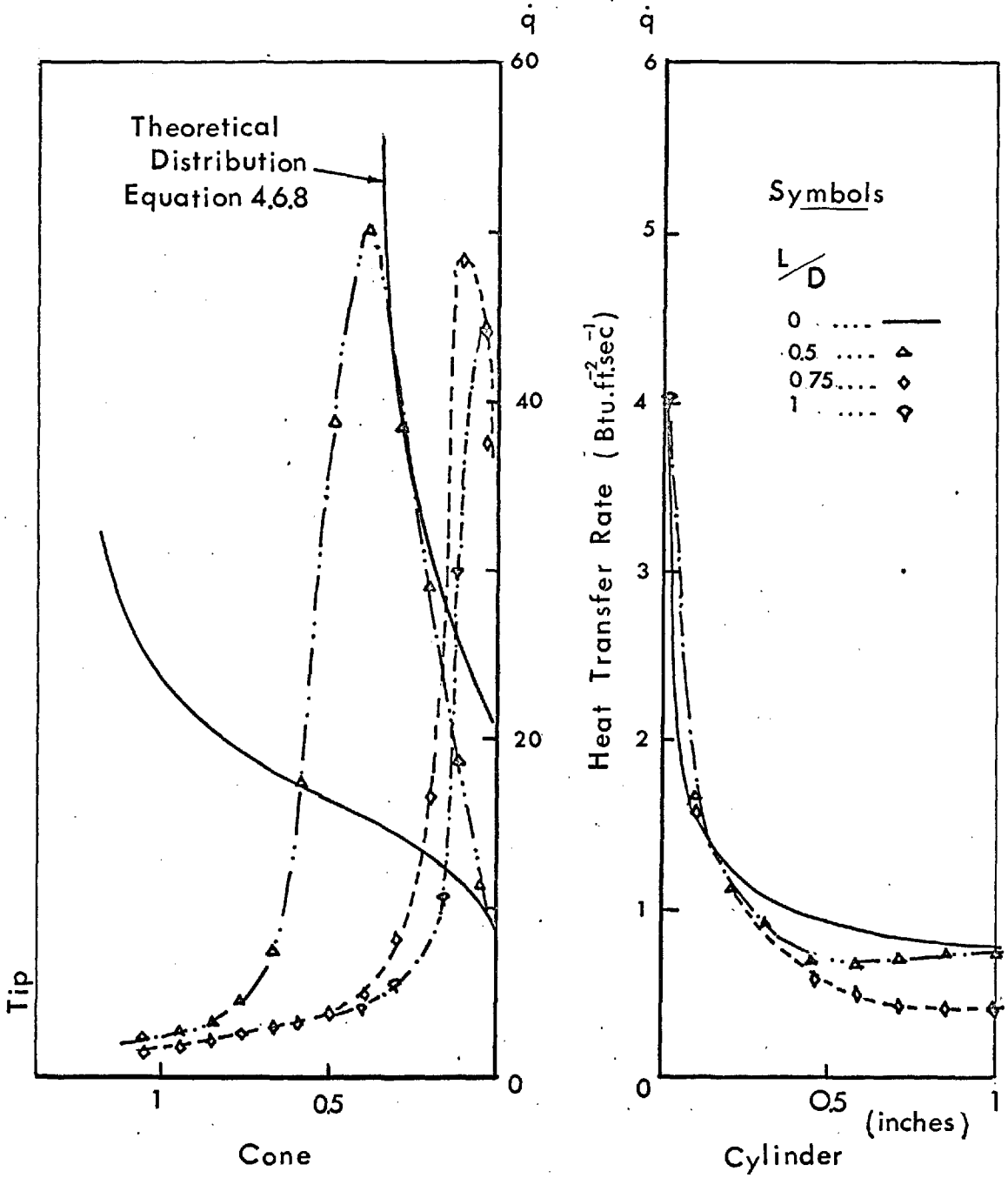

Figure 47b SPIKED 45° CONE (M = 10)

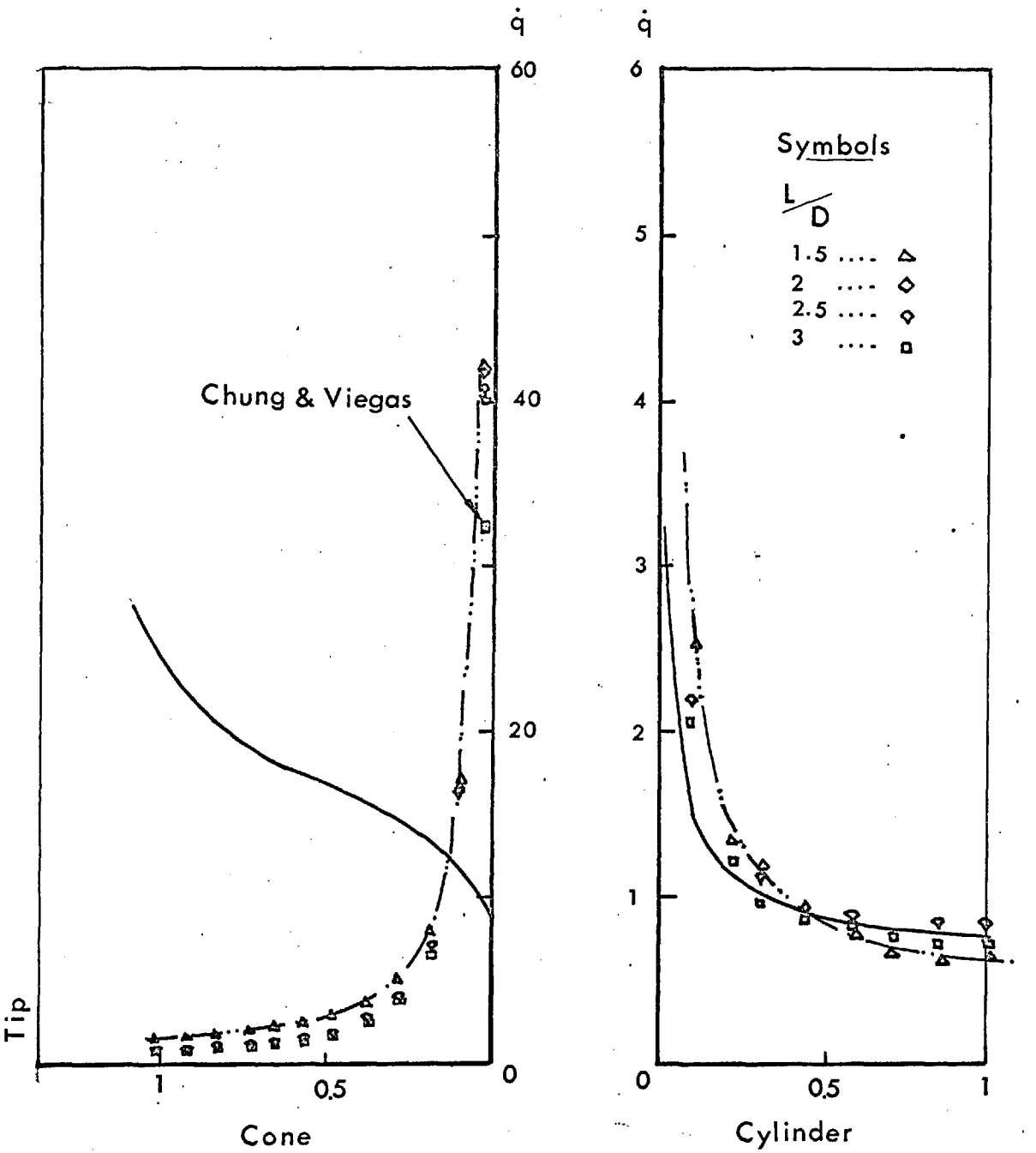

Figure 47b SPIKED 45° CONE (M = 10)

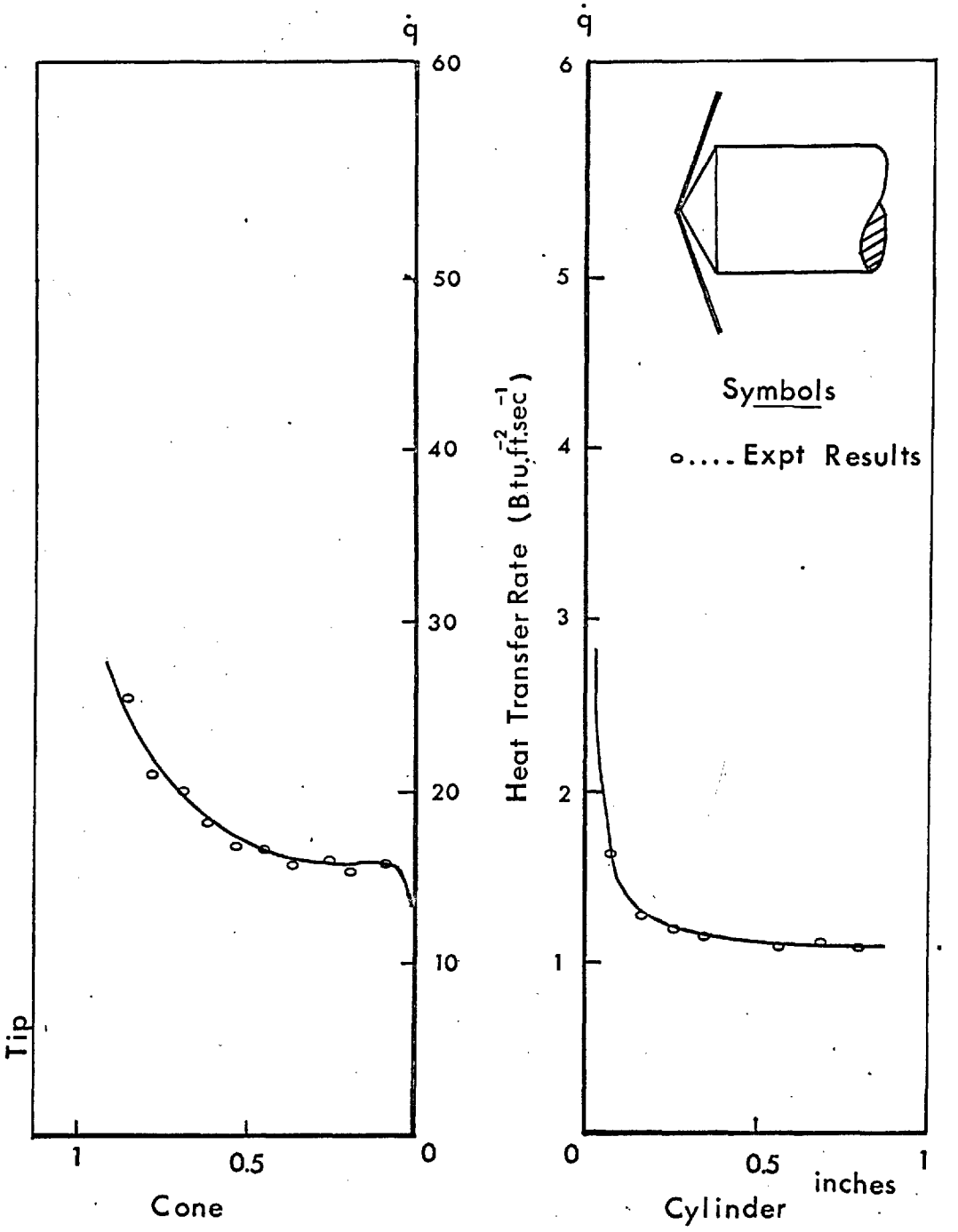

Figure 47c HEAT TRANSFER TO A 60° CONE (M = 10)

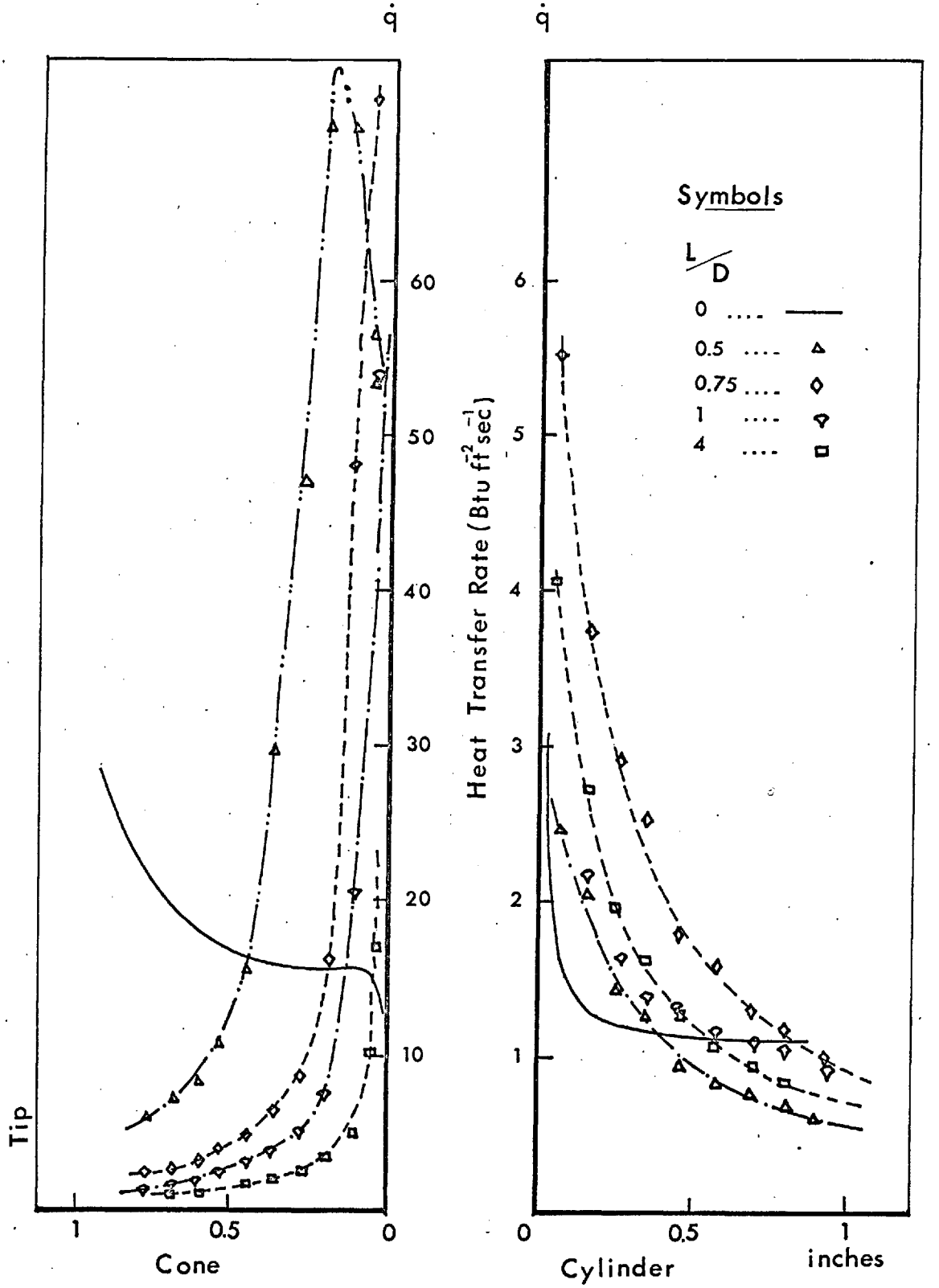

Figure 47c SPIKED 60° CONE (M = 10)

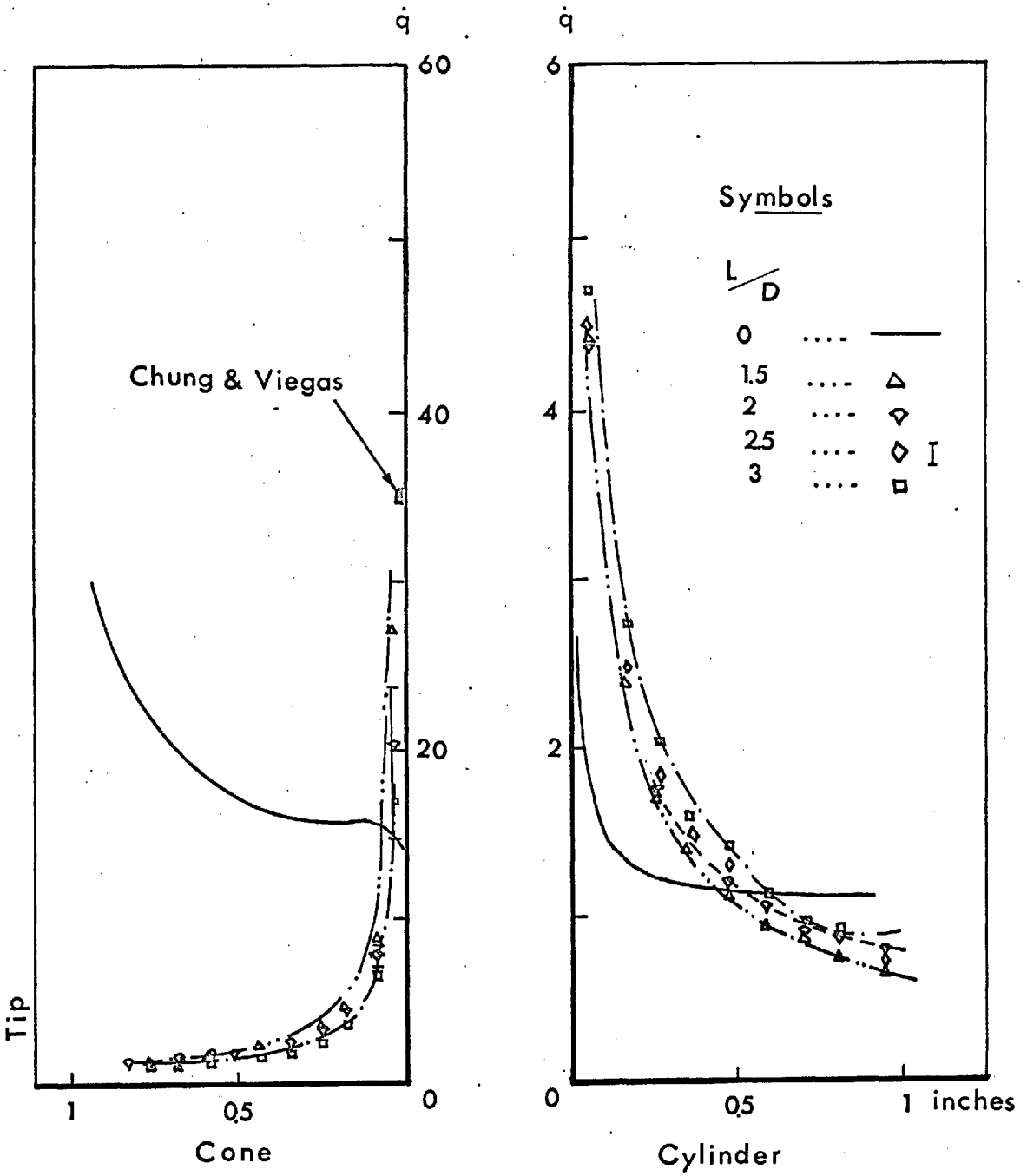

Figure 47c SPIKED 60° CONE (M = 10)

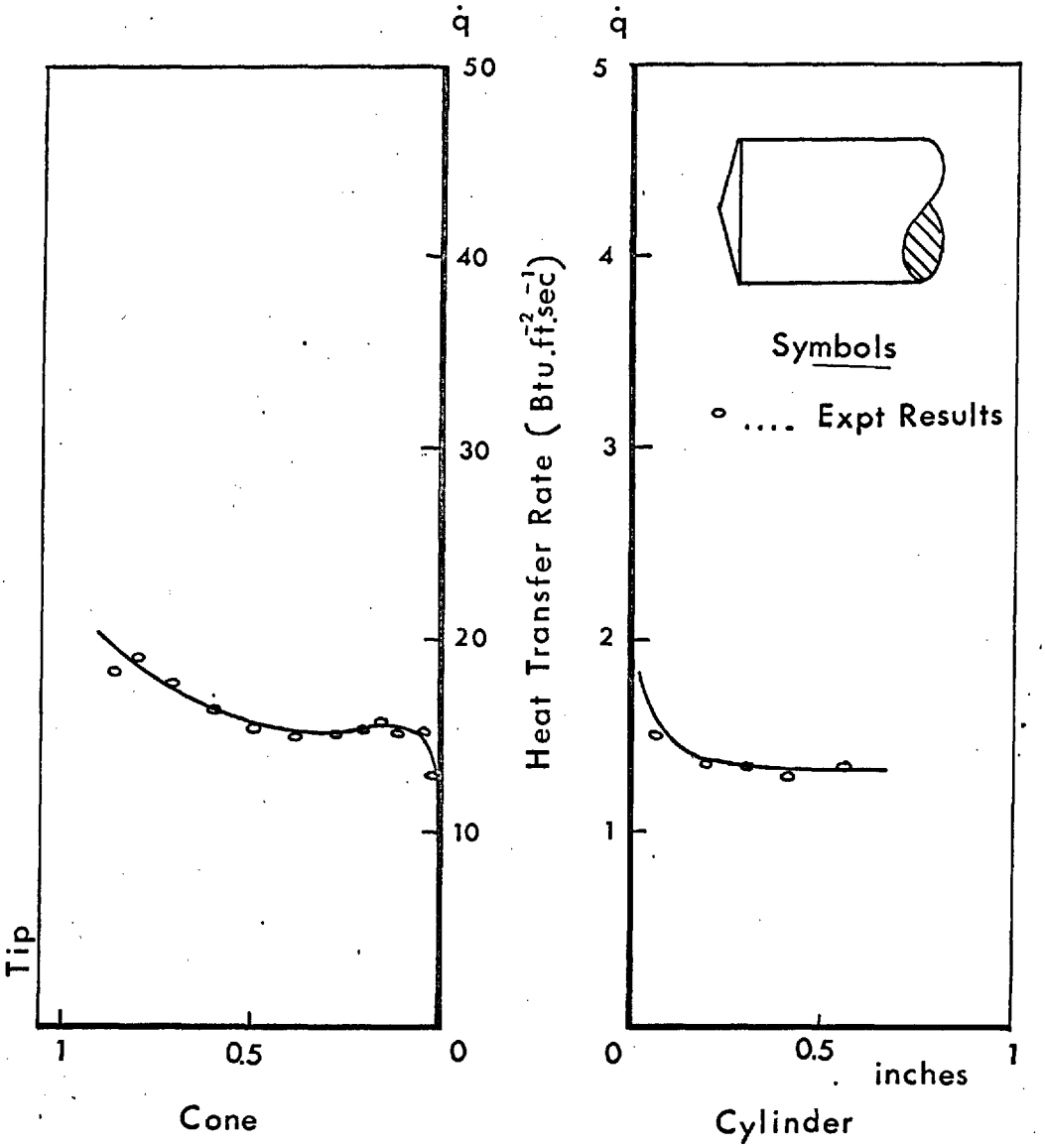

Figure 47d HEAT TRANSFER TO A 75° CONE (M = 10)

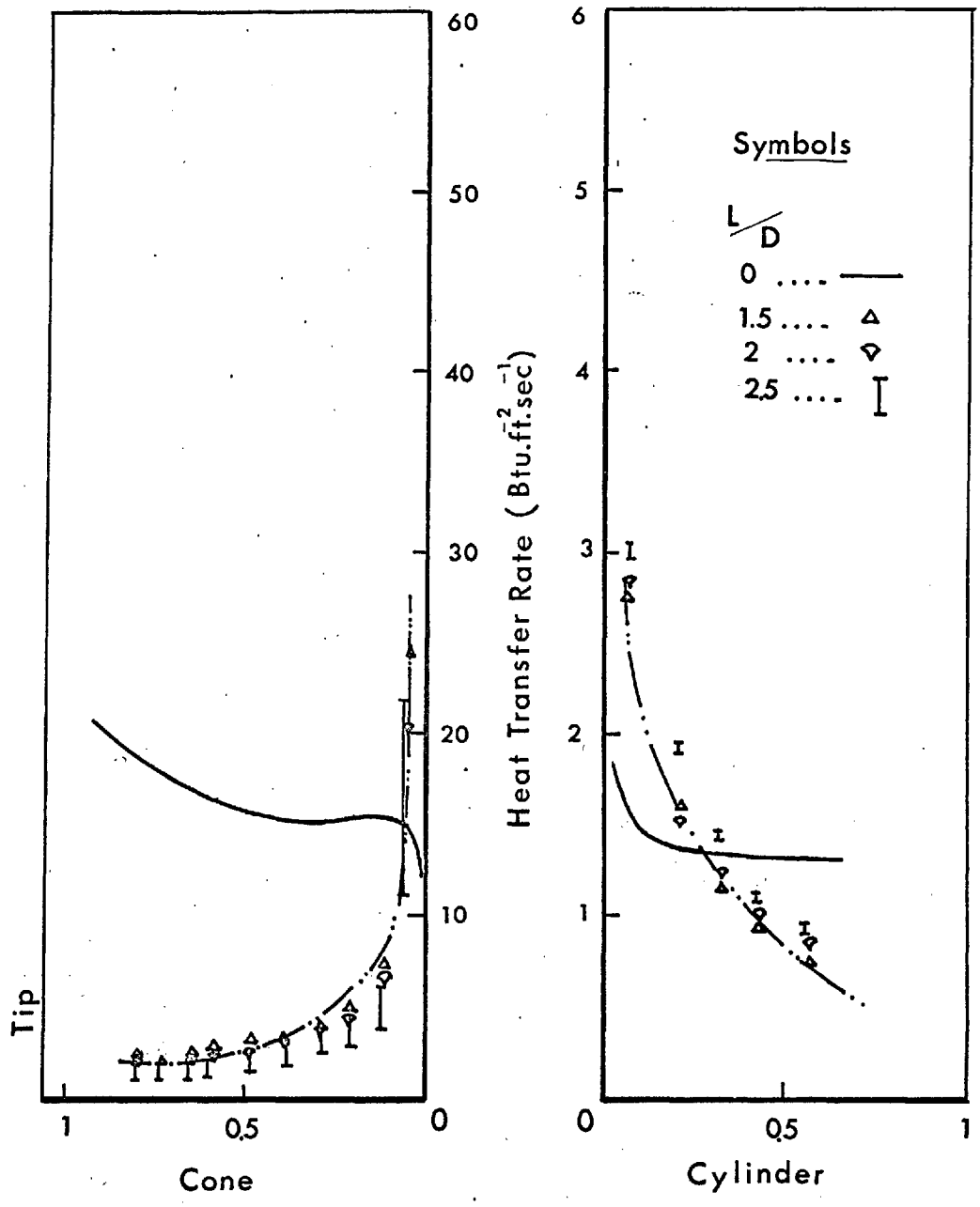

Figure 47d SPIKED 75° CONE (M = 10)

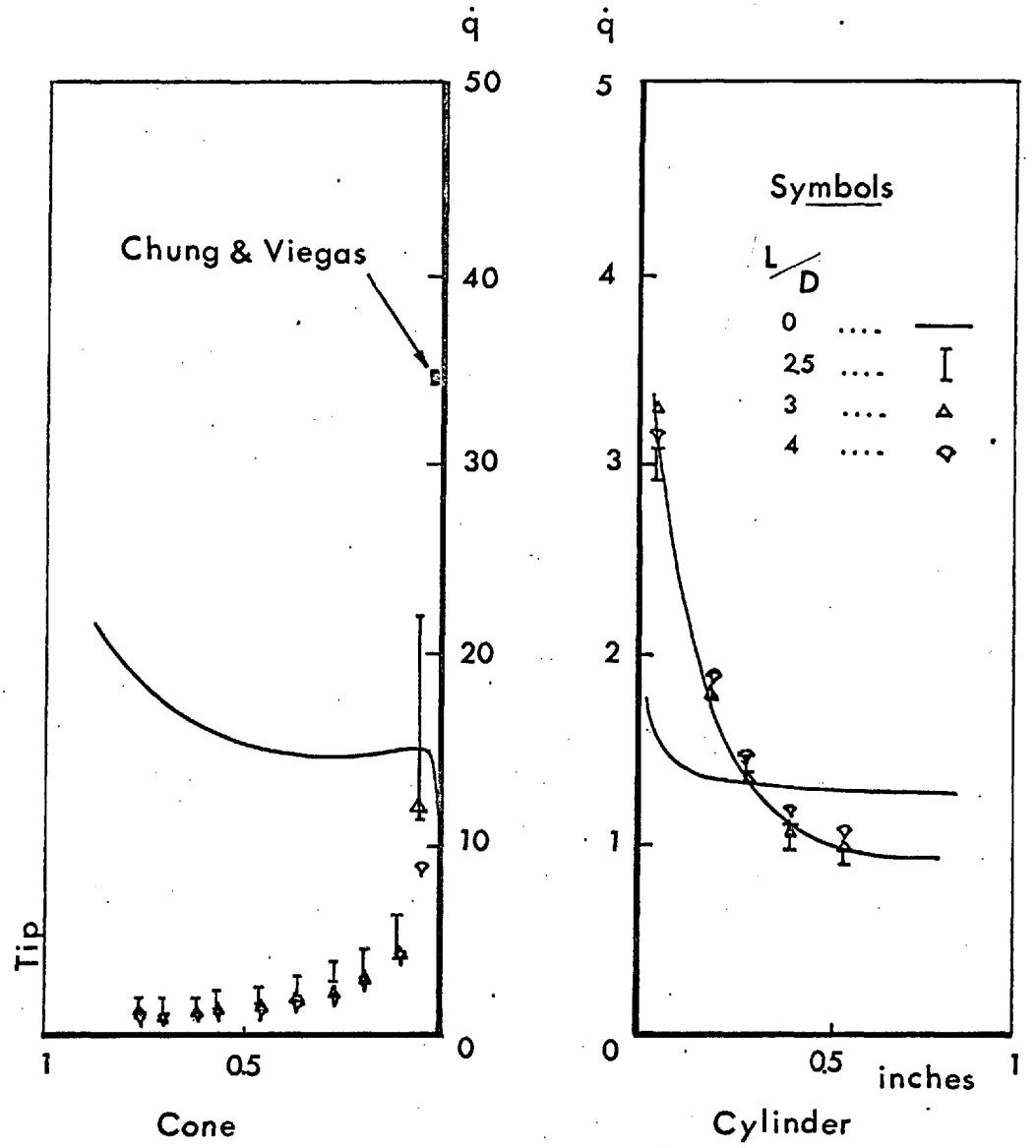

Figure 47d SPIKED 75° CONE (M = 10)

$\frac{L}{D}' = 0$

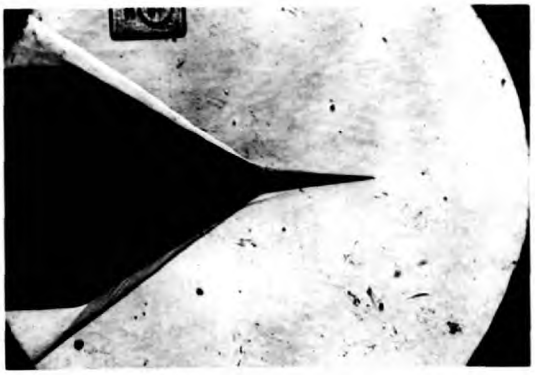

0.5

1

1.5

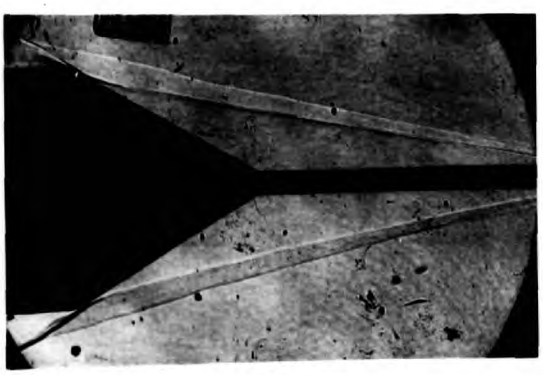

2

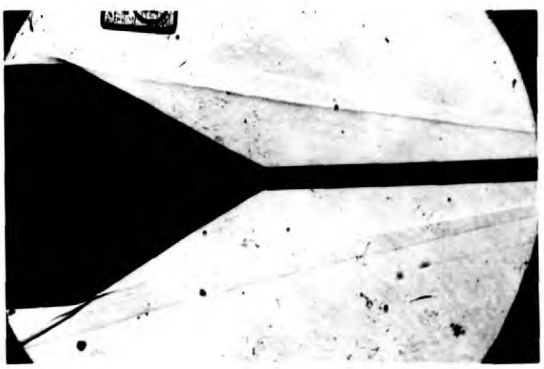

3

. Figure 48a 30 CONE (M 10)

$\frac{L}{D} =$ 0

0.5

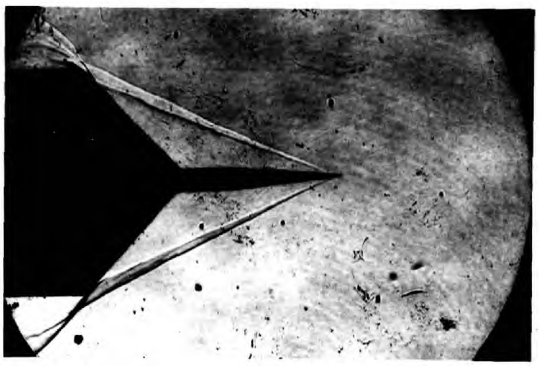

0.75

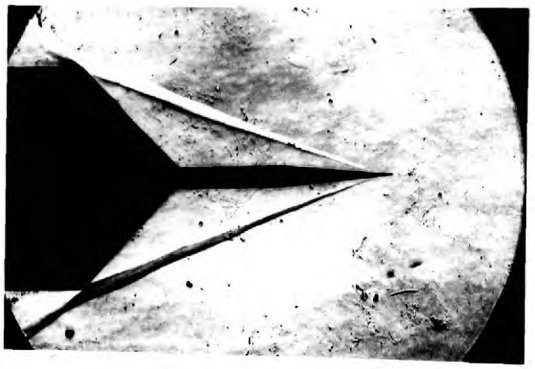

1

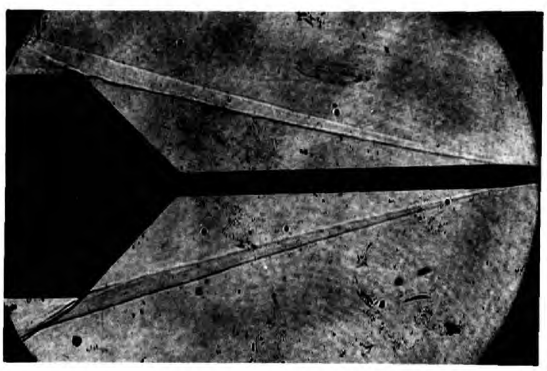

2

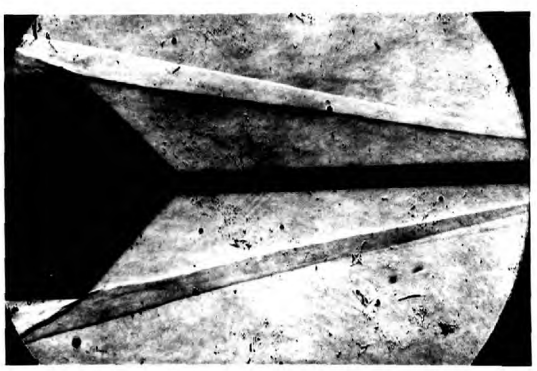

3

Figure 48b 45° CONE (M = 10)

$\frac{L}{D} =$ 0

0.75

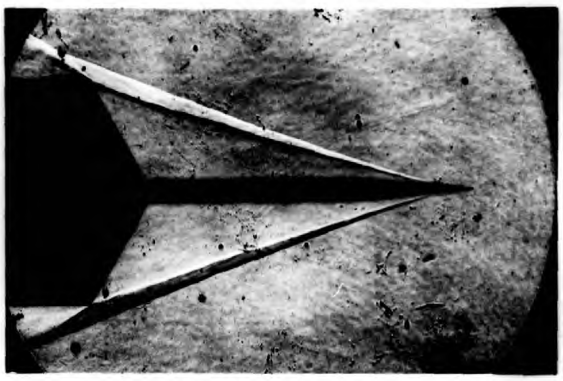

1.5

2

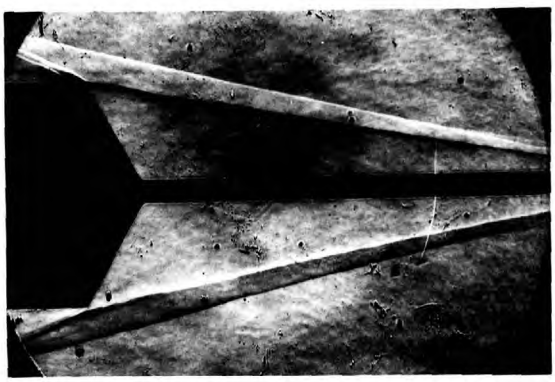

3

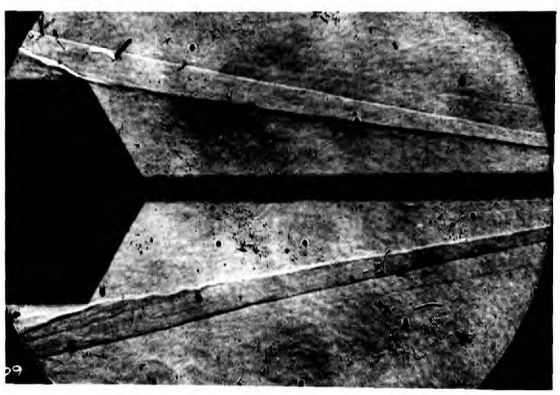

4

Figure 48c 60° CONE (M = 10)

0

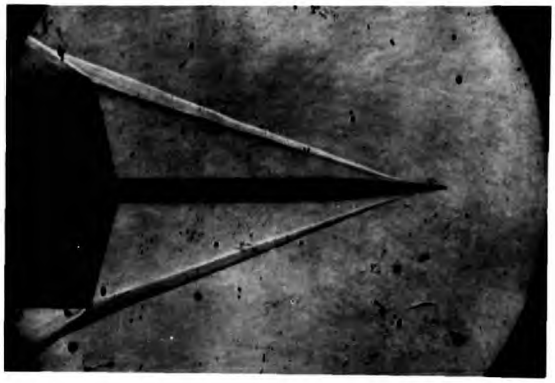

1.5

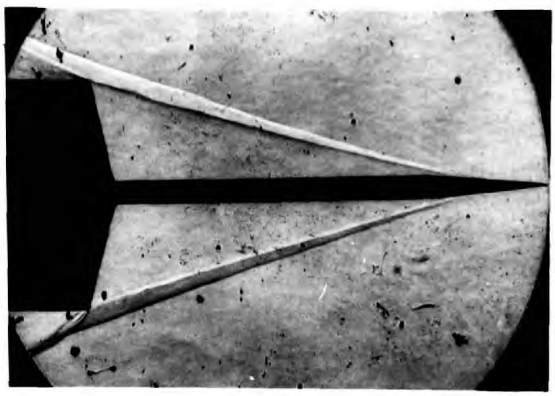

2

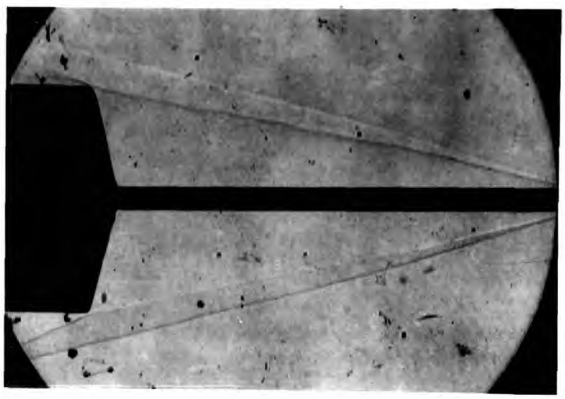

2.5

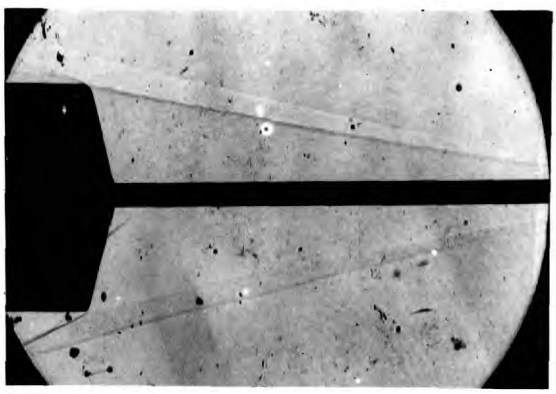

3

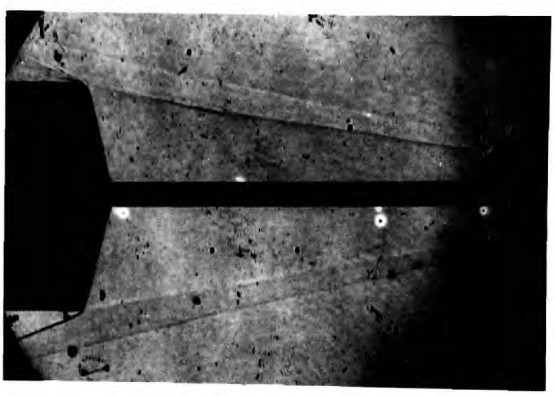

4

Figure 48 d 75° CONE $M = 10$

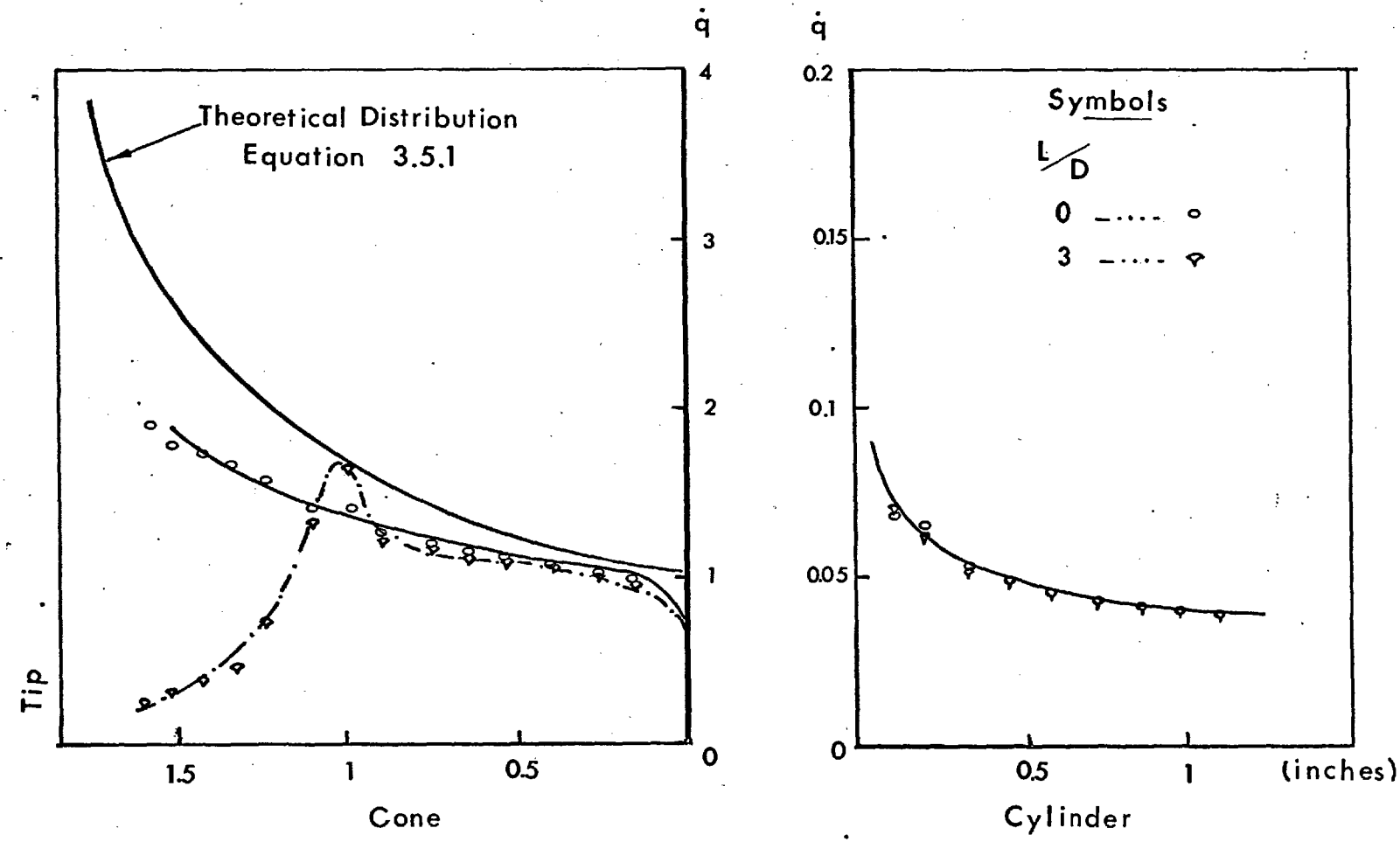

Figure 49a HEAT TRANSFER TO A SPIKED 30° CONE (M=15)

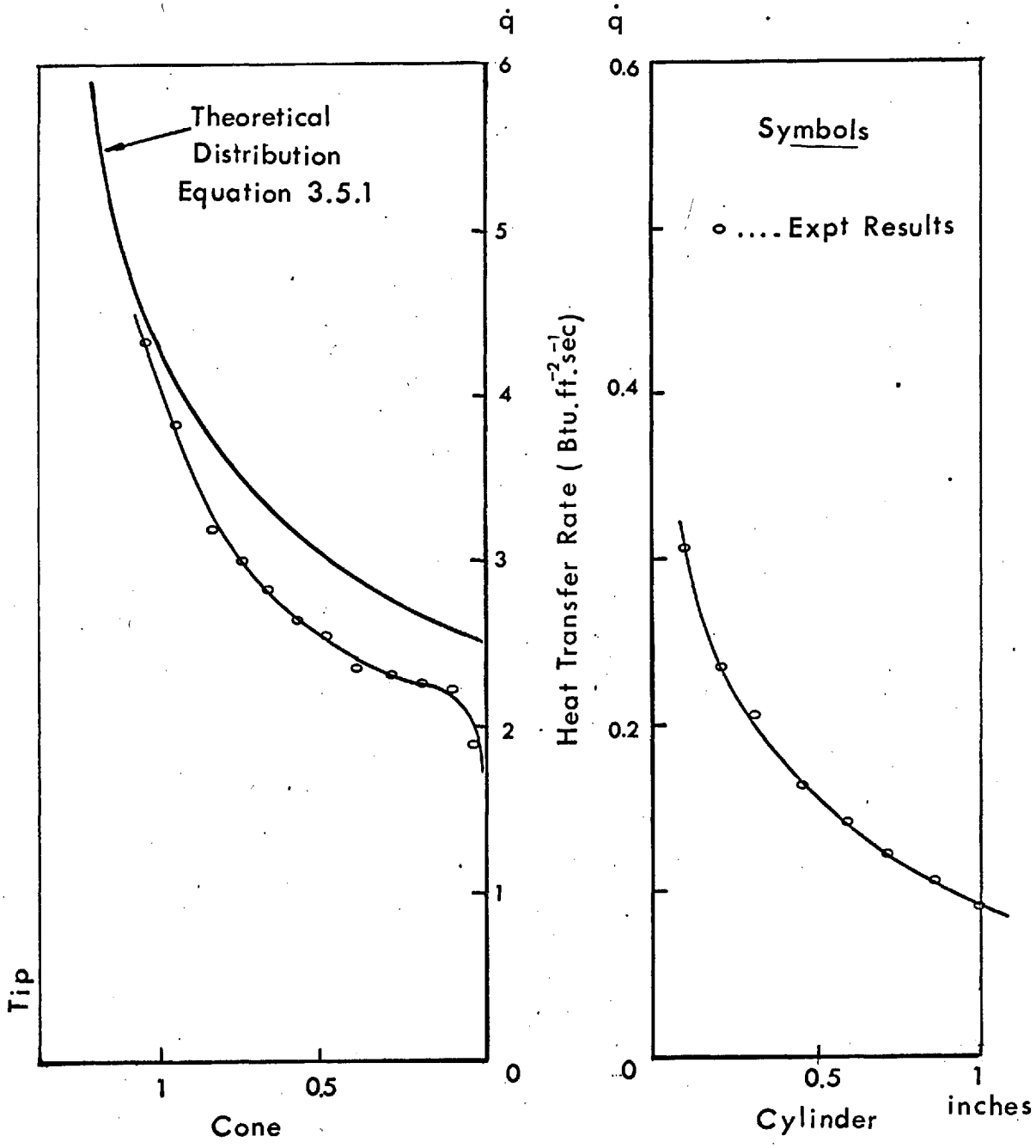

Figure 49b HEAT TRANSFER TO A 45° CONE (M = 15)

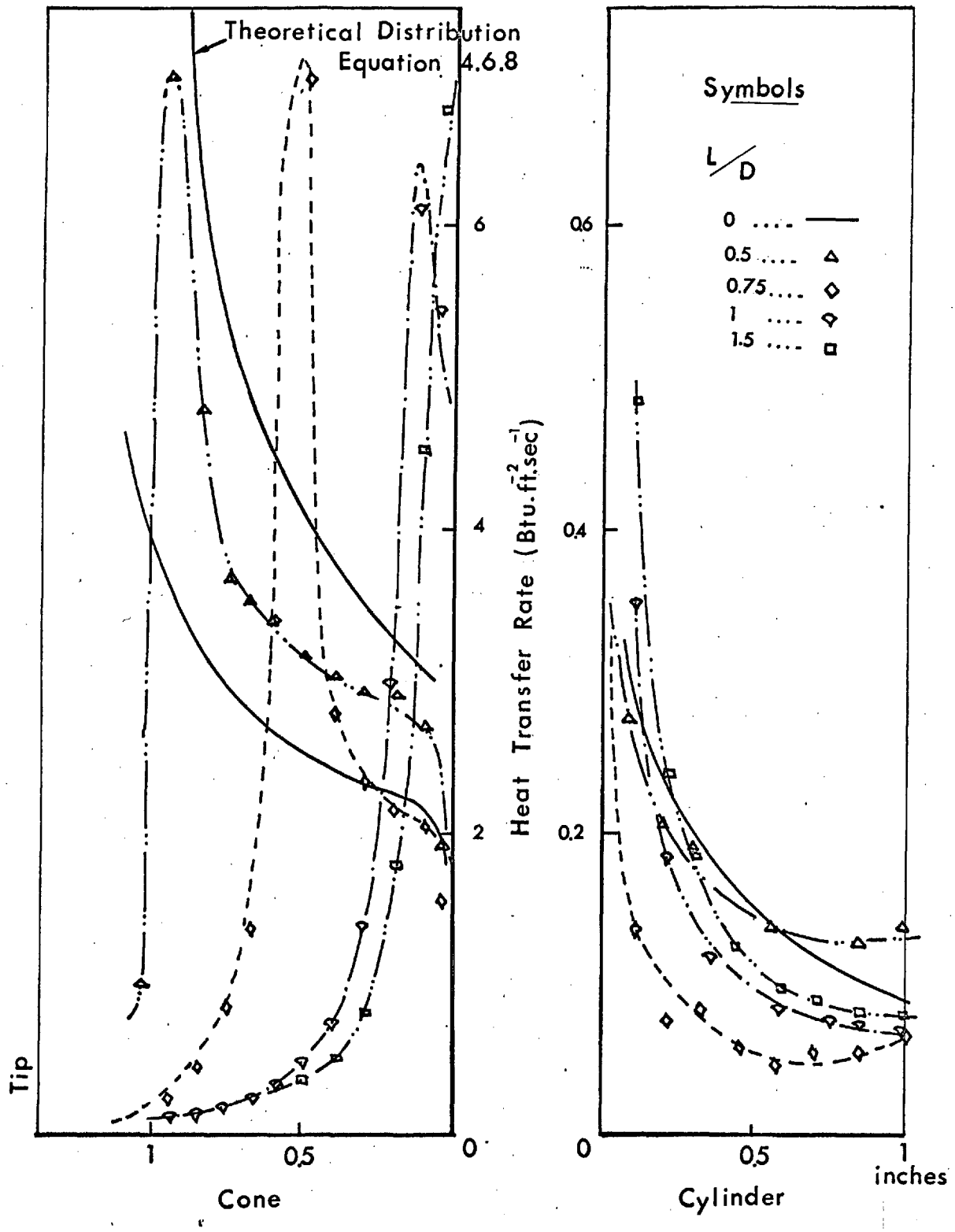

Figure 49b SPIKED 45° CONE (M = 15)

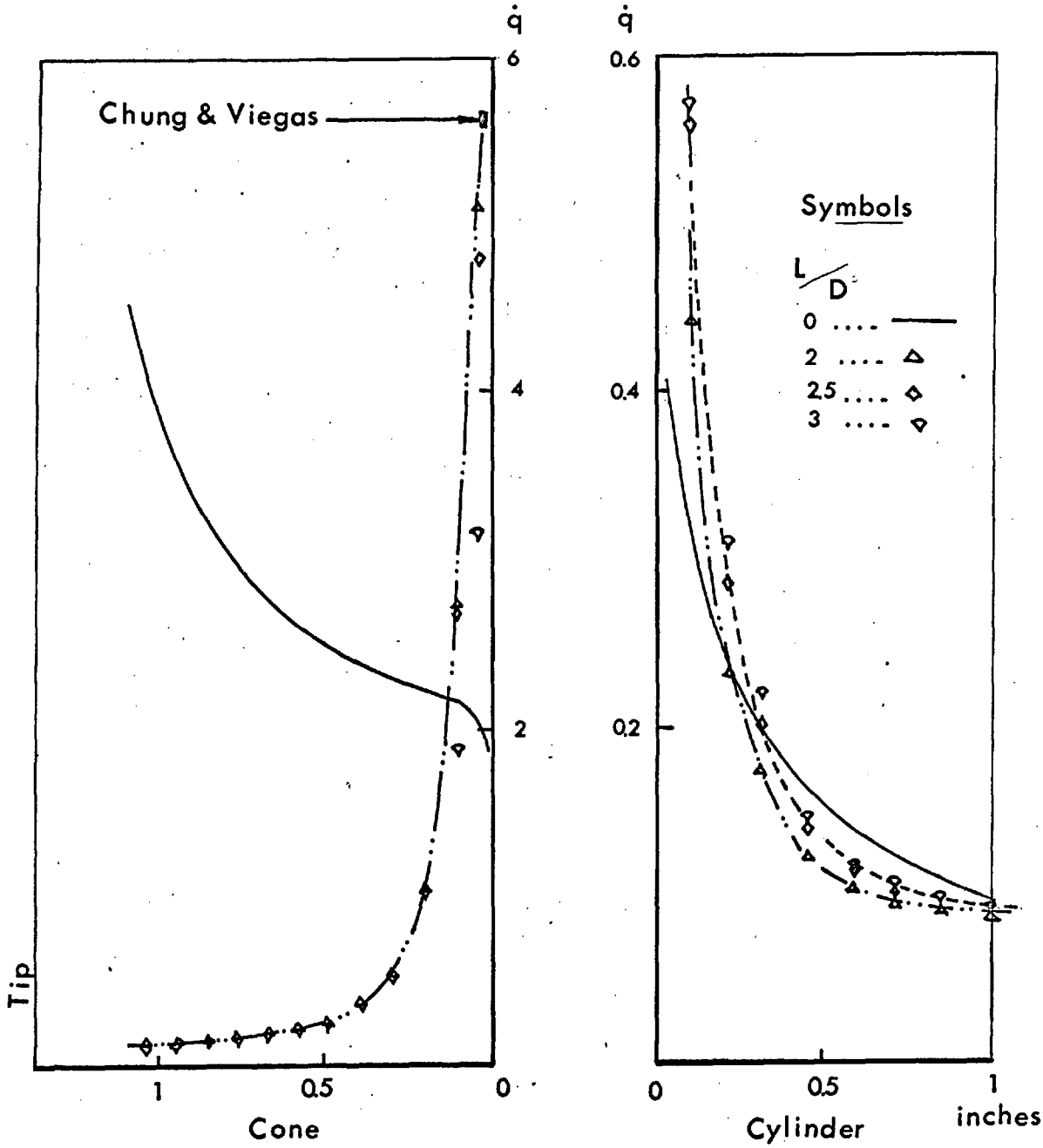

Figure 49b SPIKED 45° CONE (M = 15)

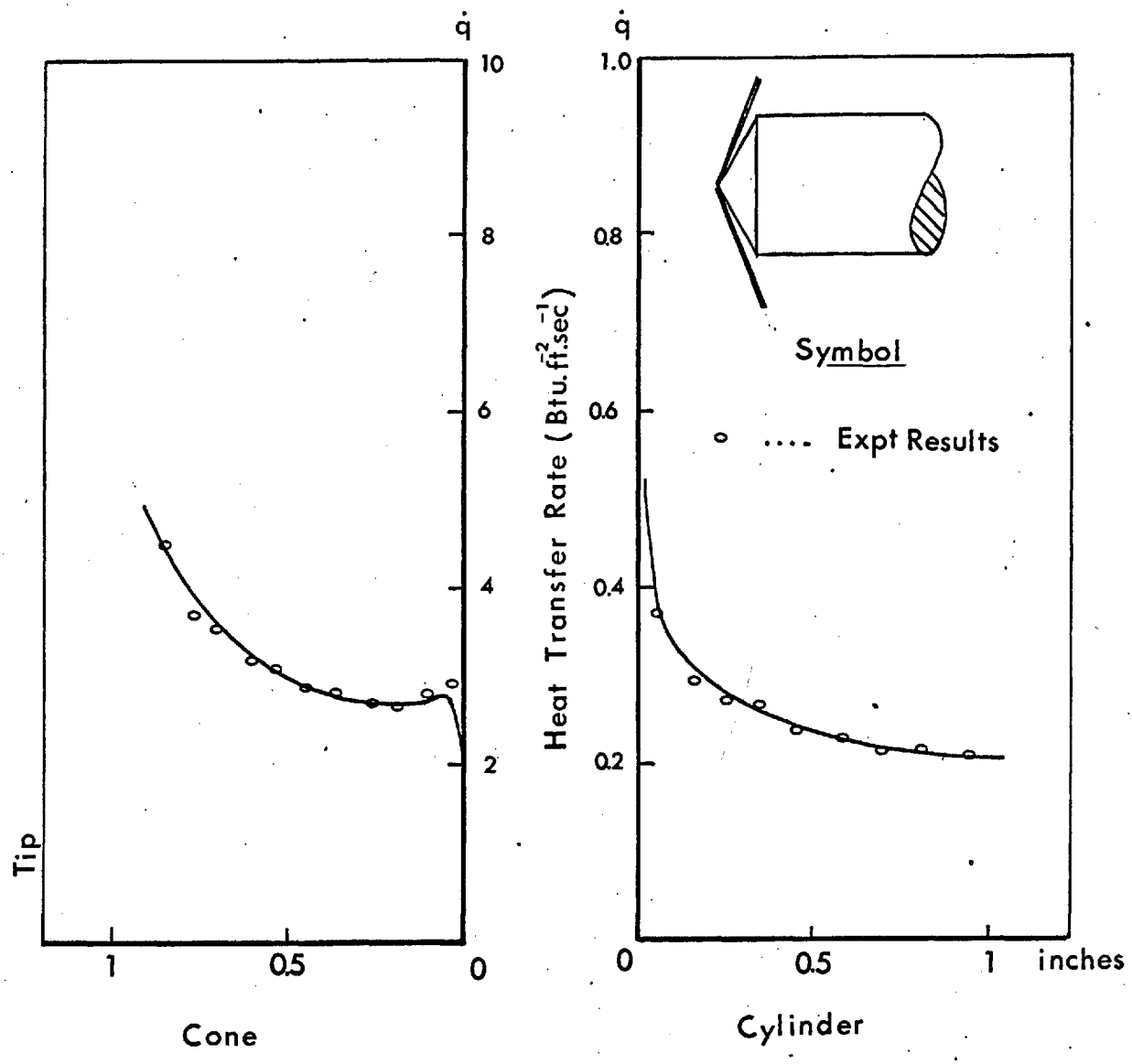

Figure 49c HEAT TRANSFER TO A 60° CONE (M = 15)

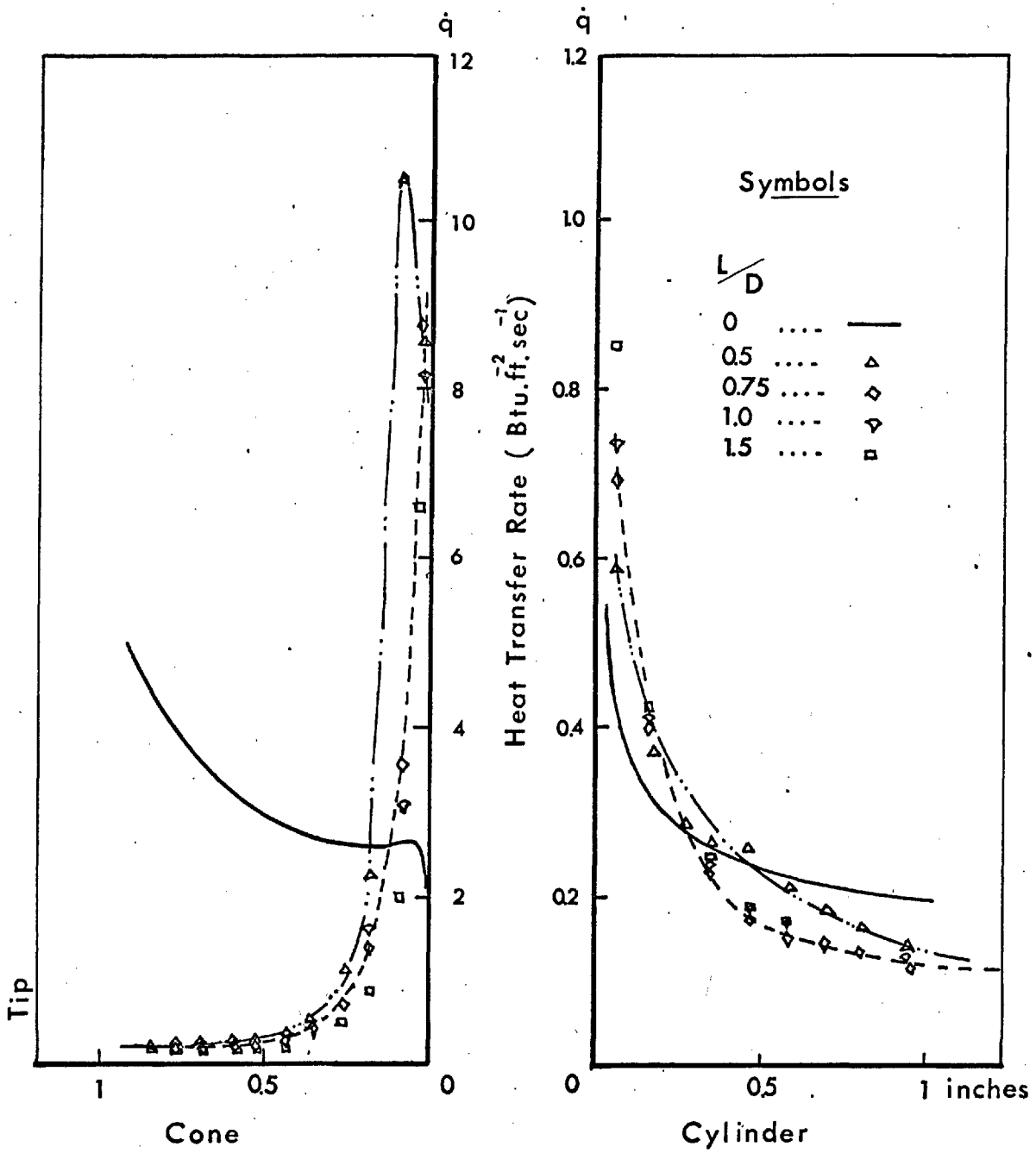

Figure 49c SPIKED 60° CONE (M = 15)

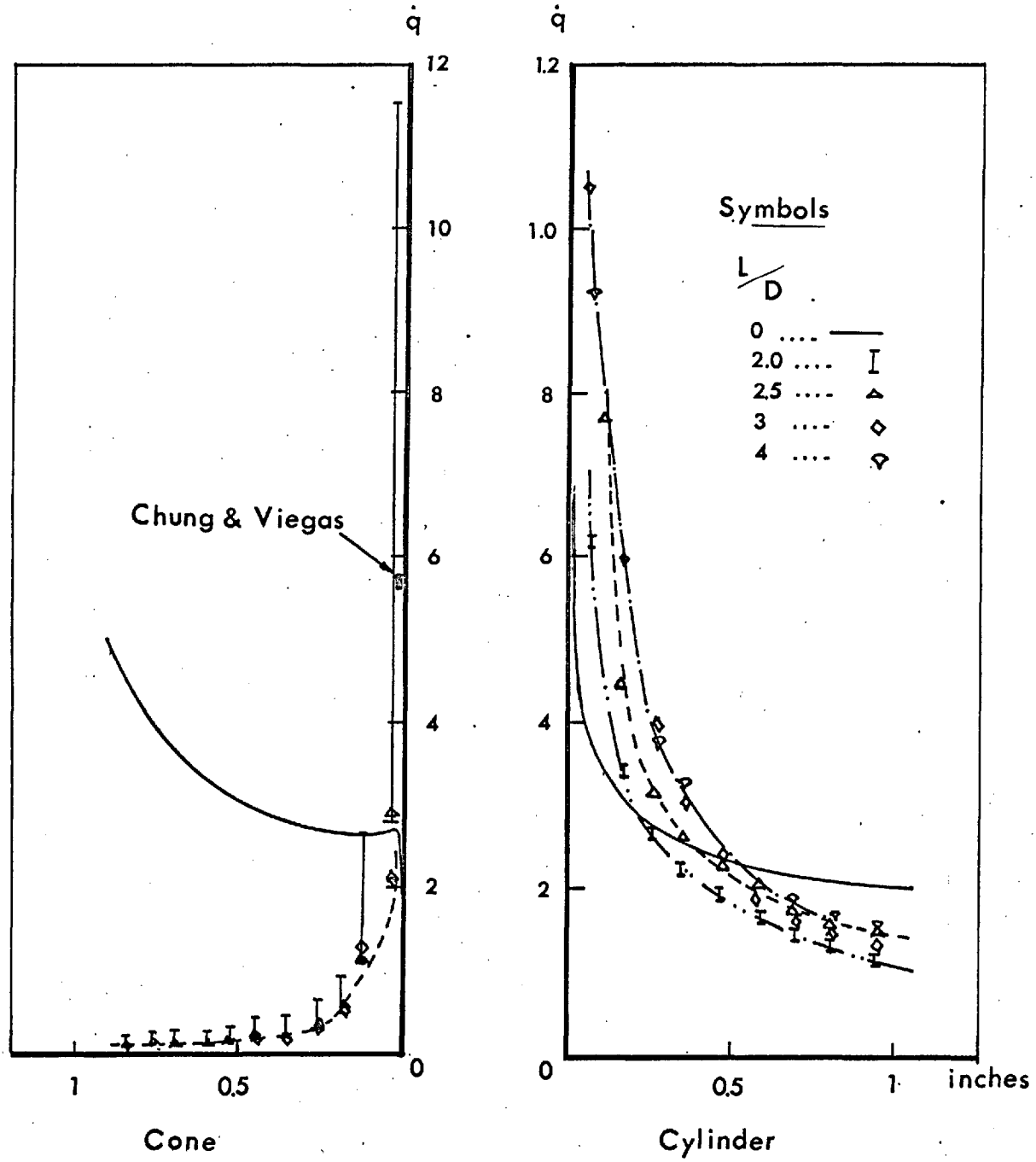

Figure 49c SPIKED 60° CONE (M — 15)

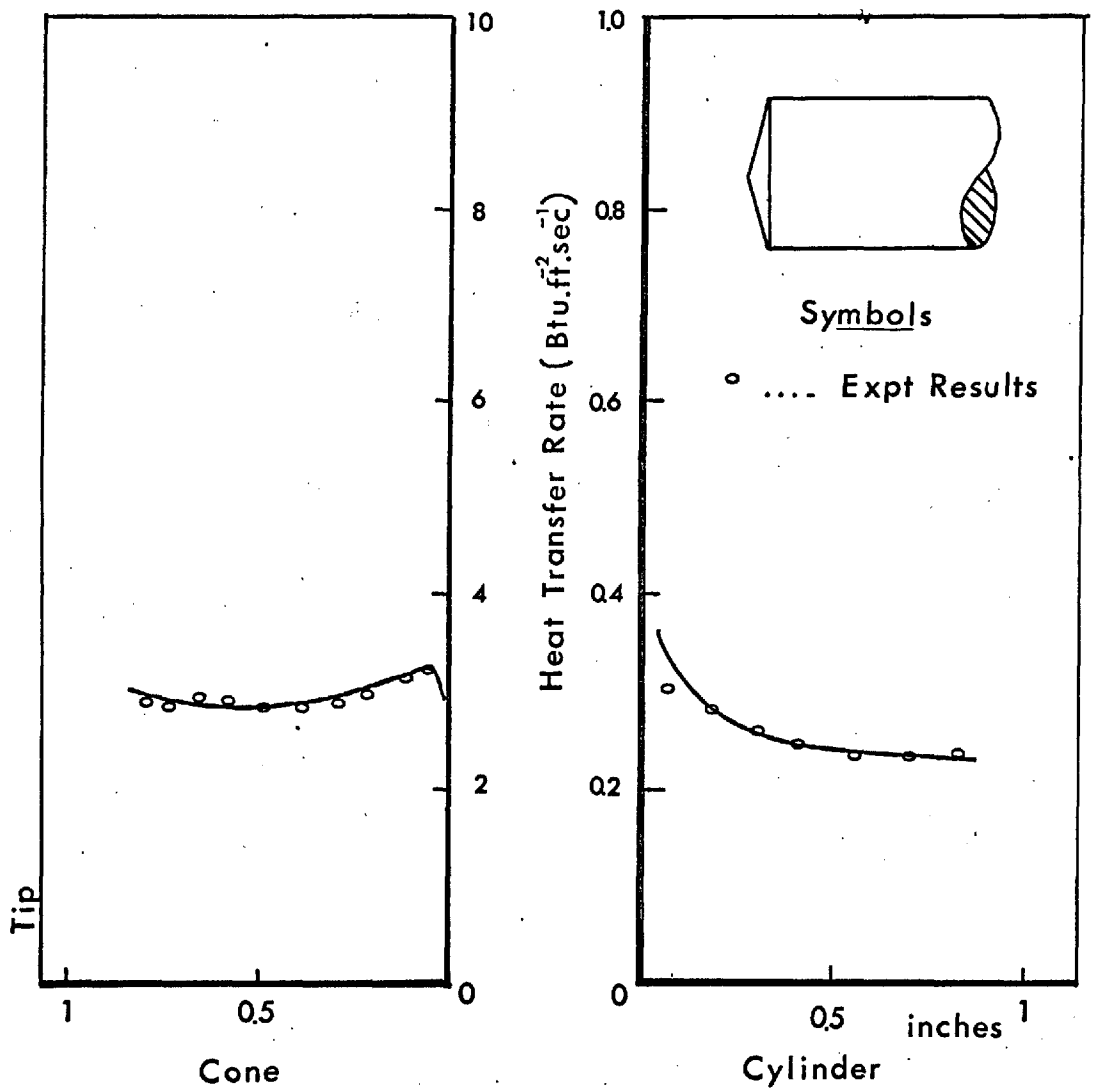

Figure 49d HEAT TRANSFER TO A 75° CONE (M=15)

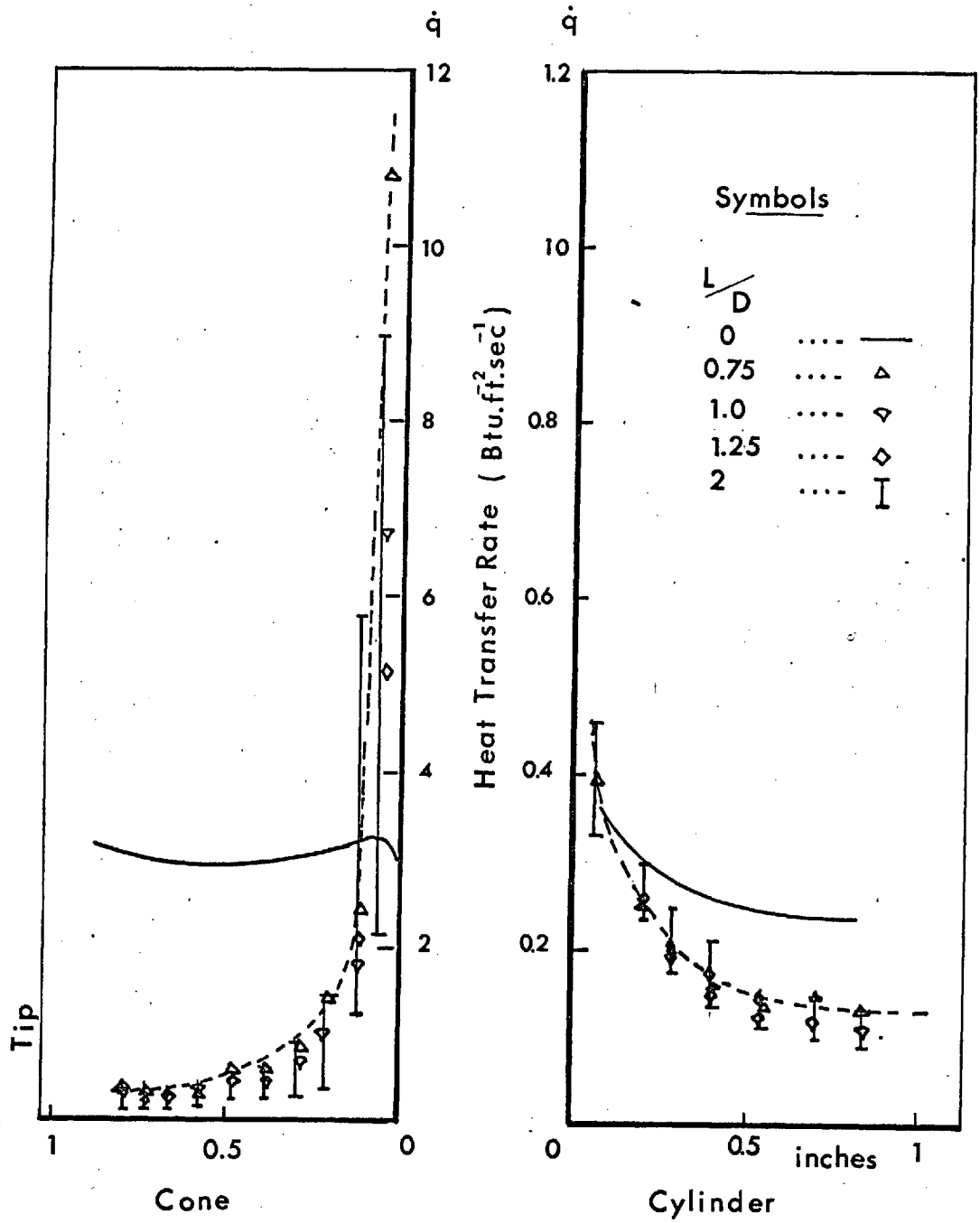

Figure 49d SPIKED 75° CONE (M = 15)

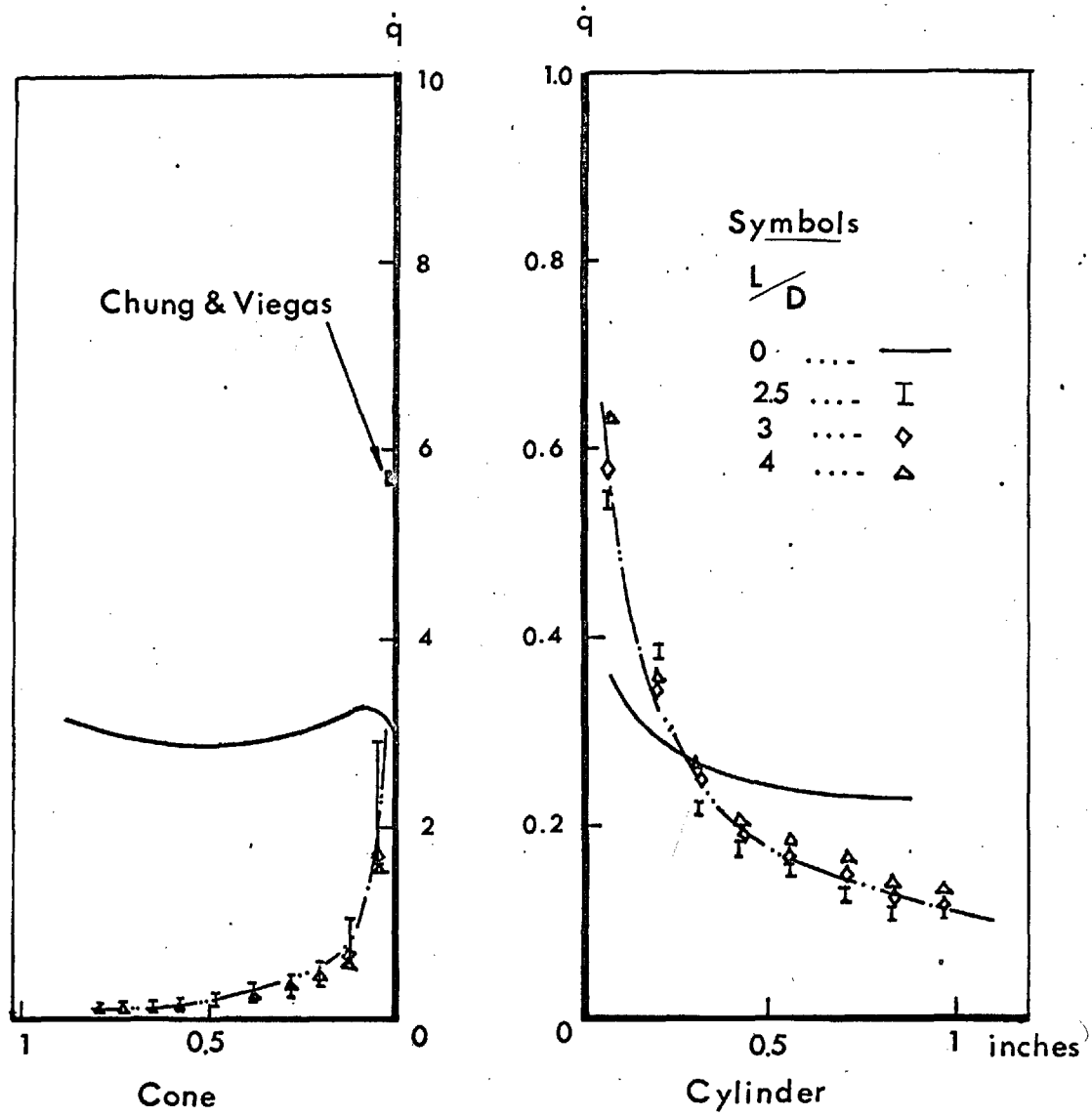

Figure 49d SPIKED 75^0 CONE (M = 15)

$\frac{L}{D}$ 0

1

3

Figure 50a 30° CONE M = 15

$\frac{L}{D} =$ 0

0.5

0.75

1

2

3

Figure 50b 45° CONE (M = 15)

$\frac{L}{D} =$ 0

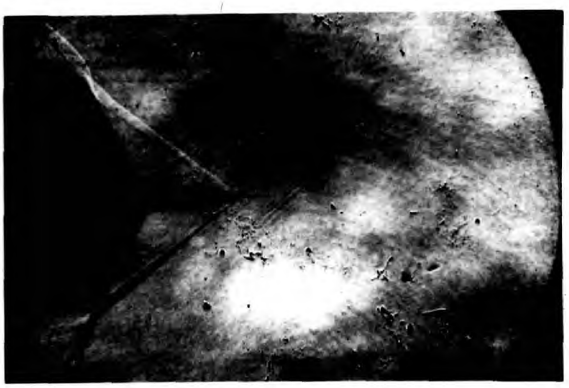

0.5

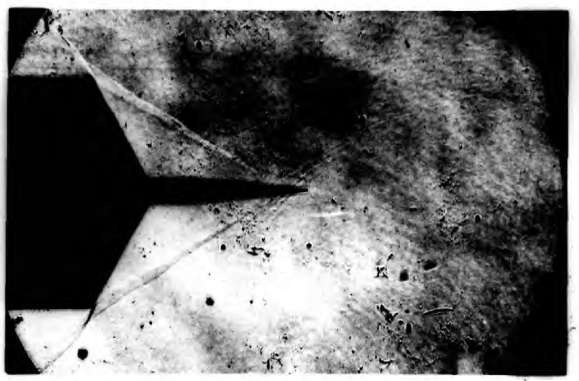

0.75

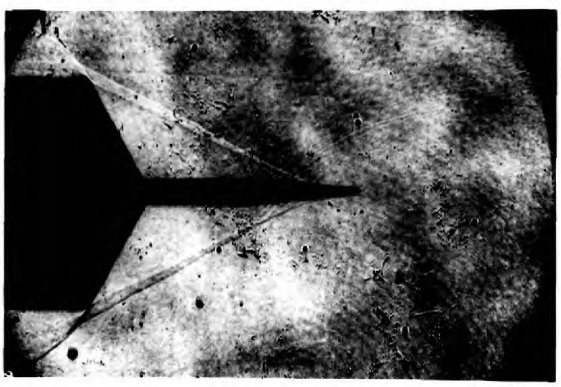

1

2

3

Figure 50c 60° CONE (M = 15)

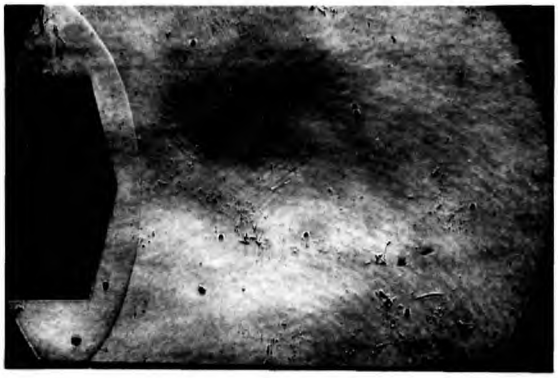

$\frac{L}{D}$ = 0

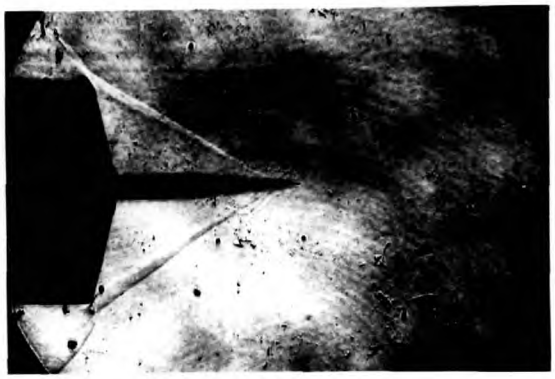

0.75

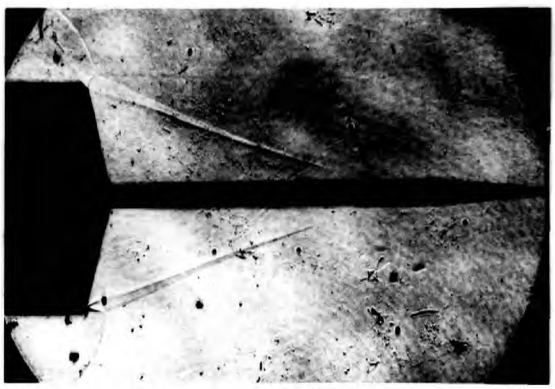

2 a

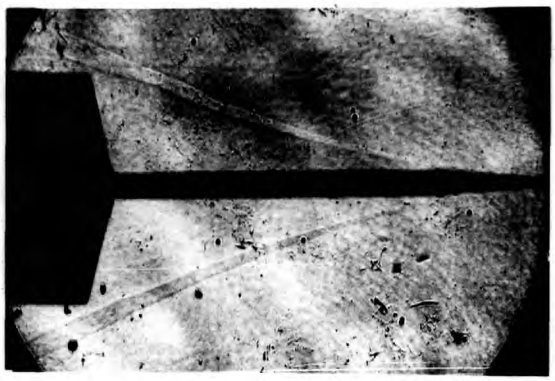

2 b

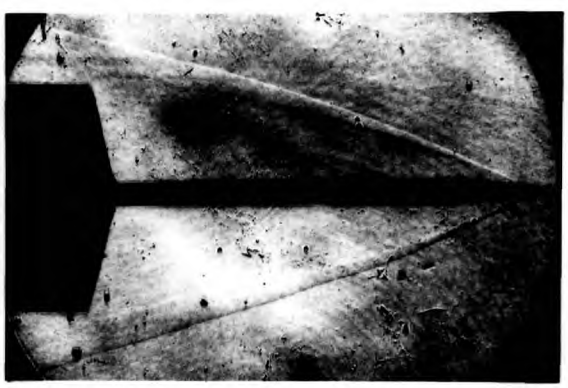

2 c

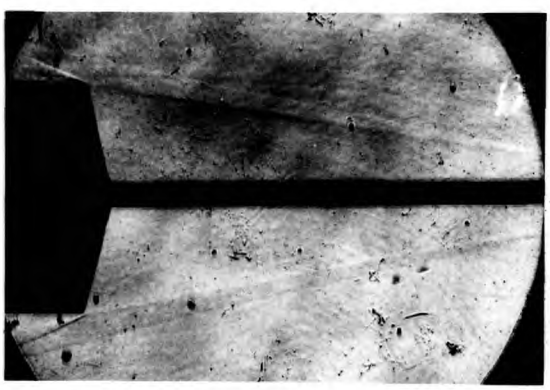

4

Figure 50d 75° CONE (M = 15)

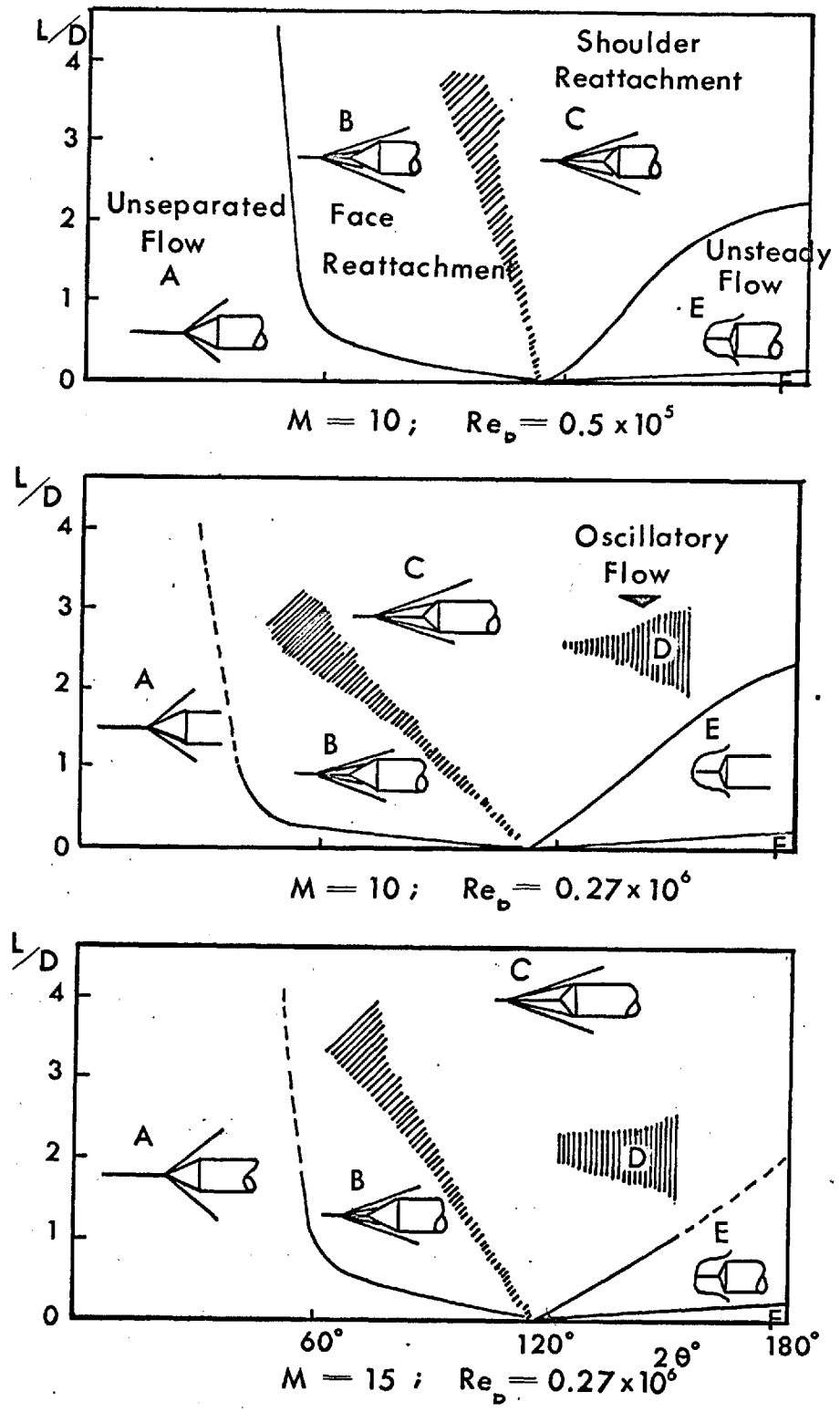

Figure 51 FLOW REGIONS OVER SPIKED CONES

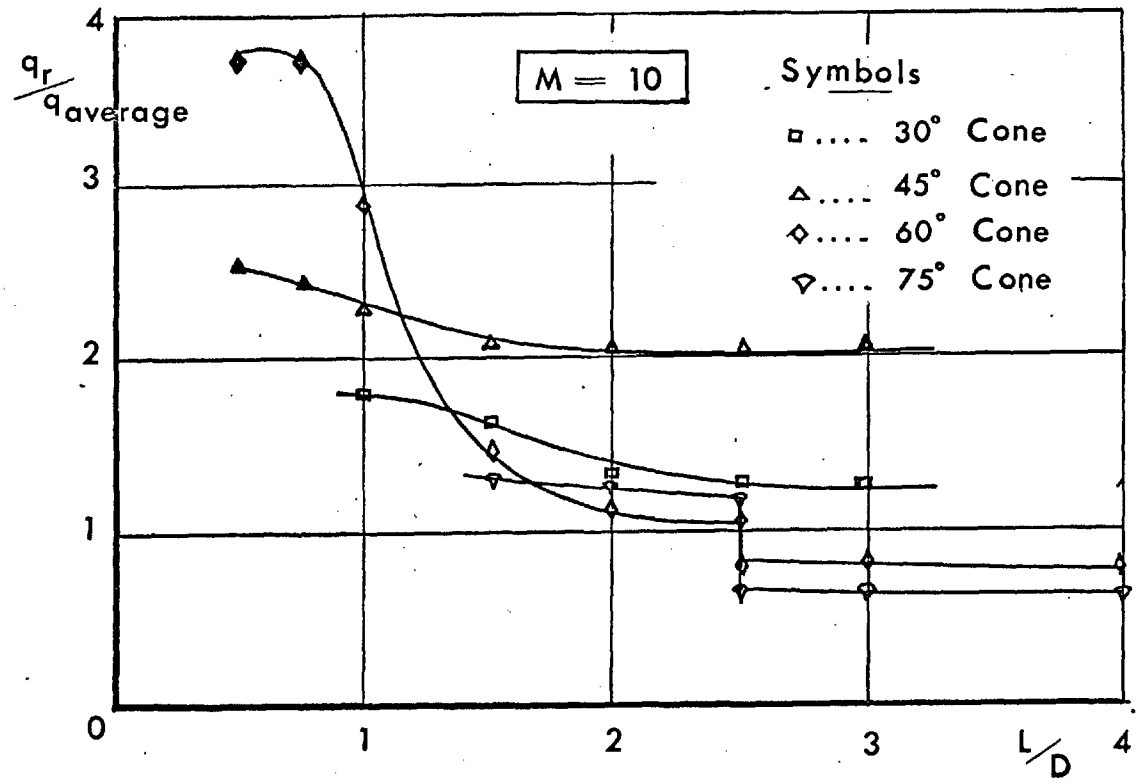

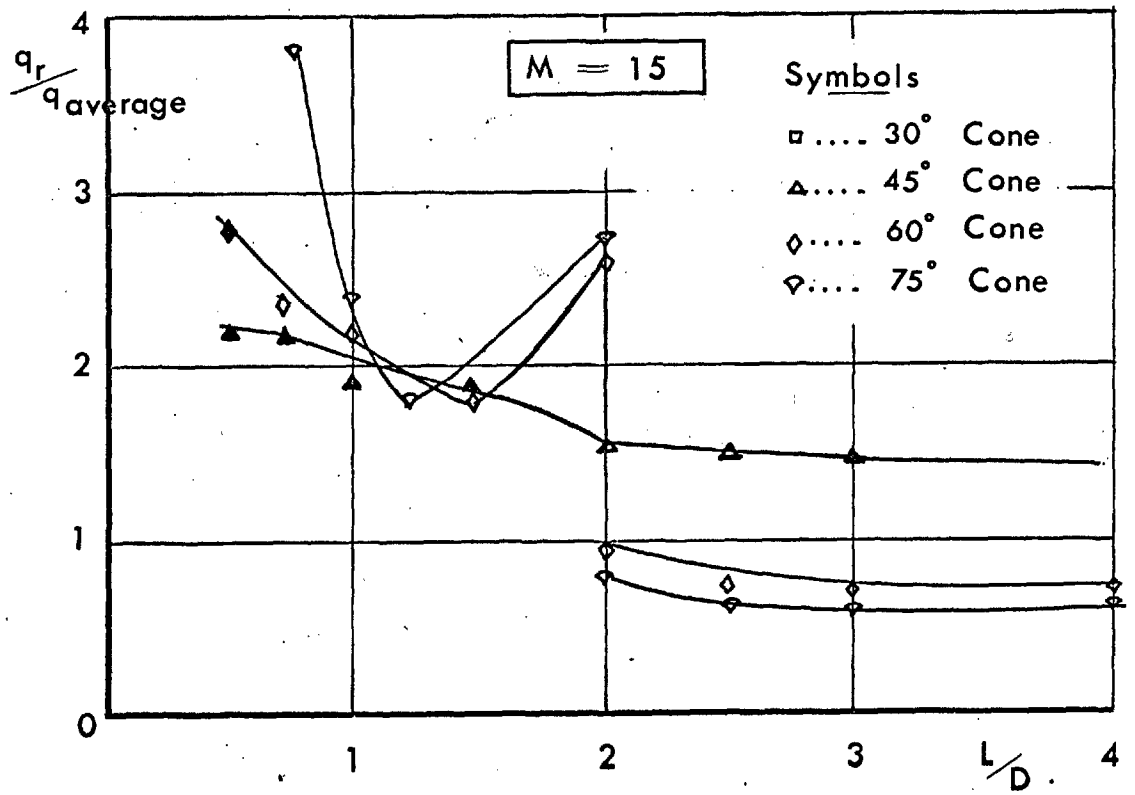

Figure 52 NON DIMENSIONISED REATTACHMENT HEAT TRANSFER

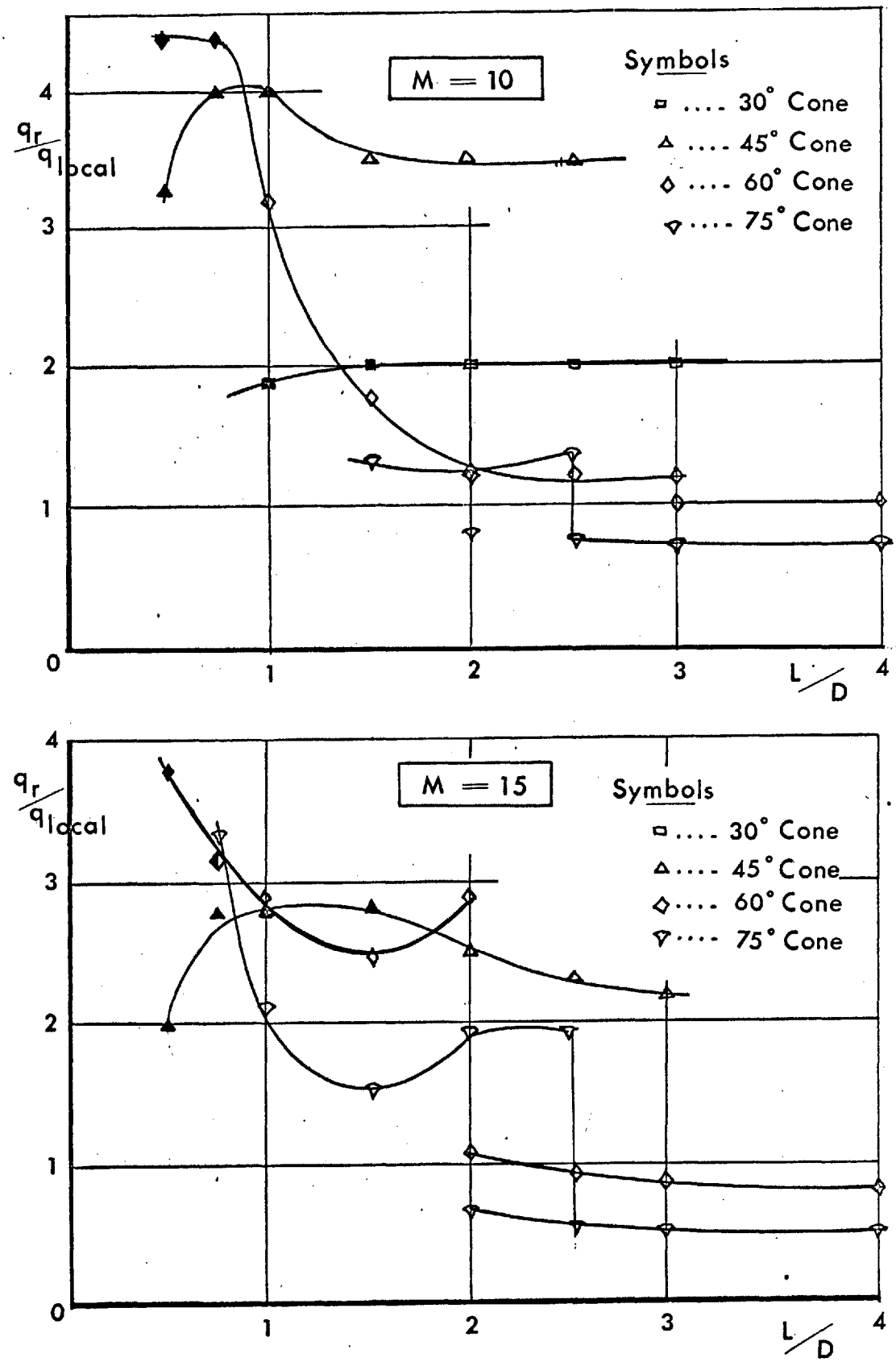

Figure 53 NON DIMENSIONISED REATTACHMENT HEAT TRANSFER

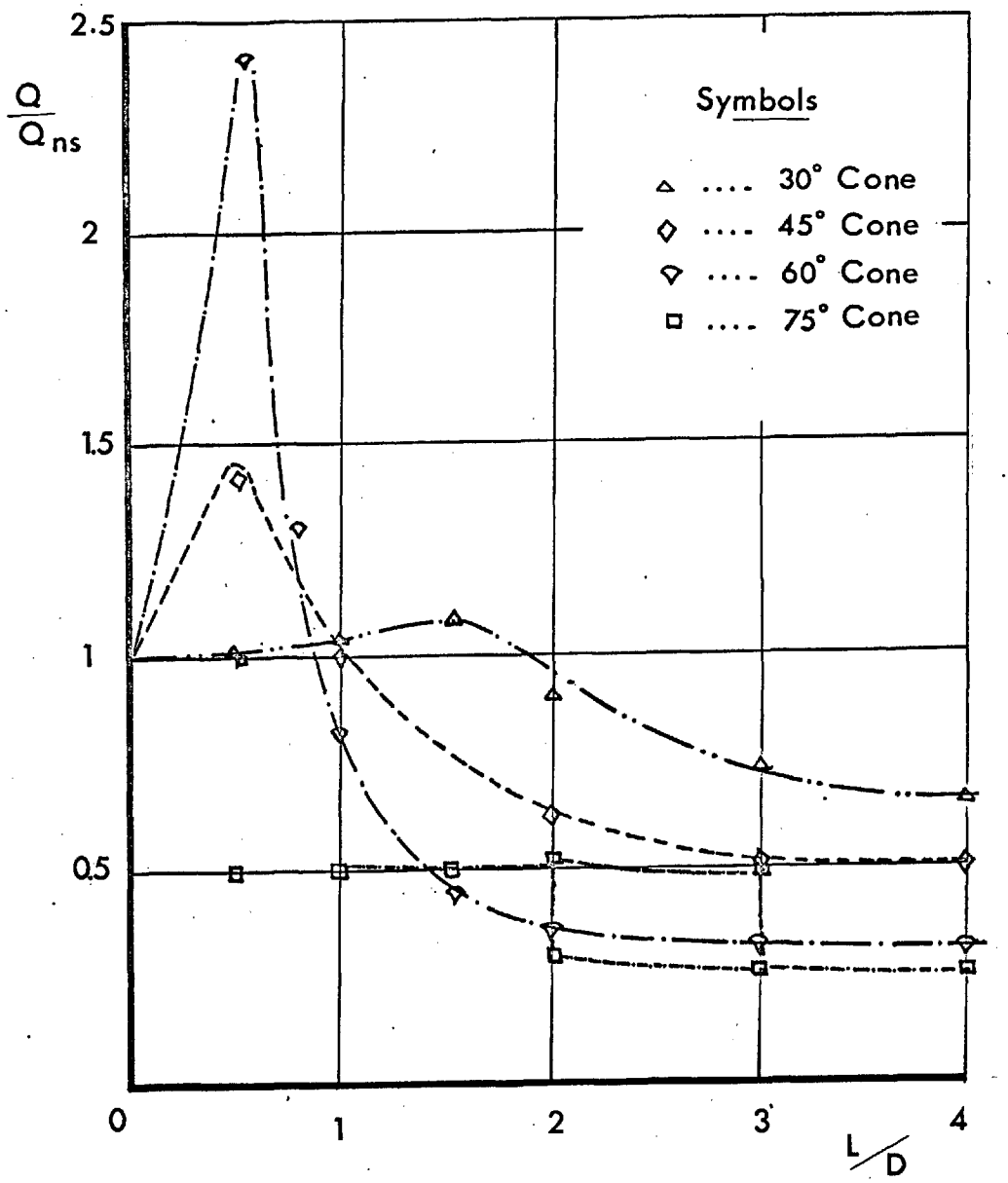

Figure 54a TOTAL HEAT TRANSFER TO SPIKED CONES (M=10)

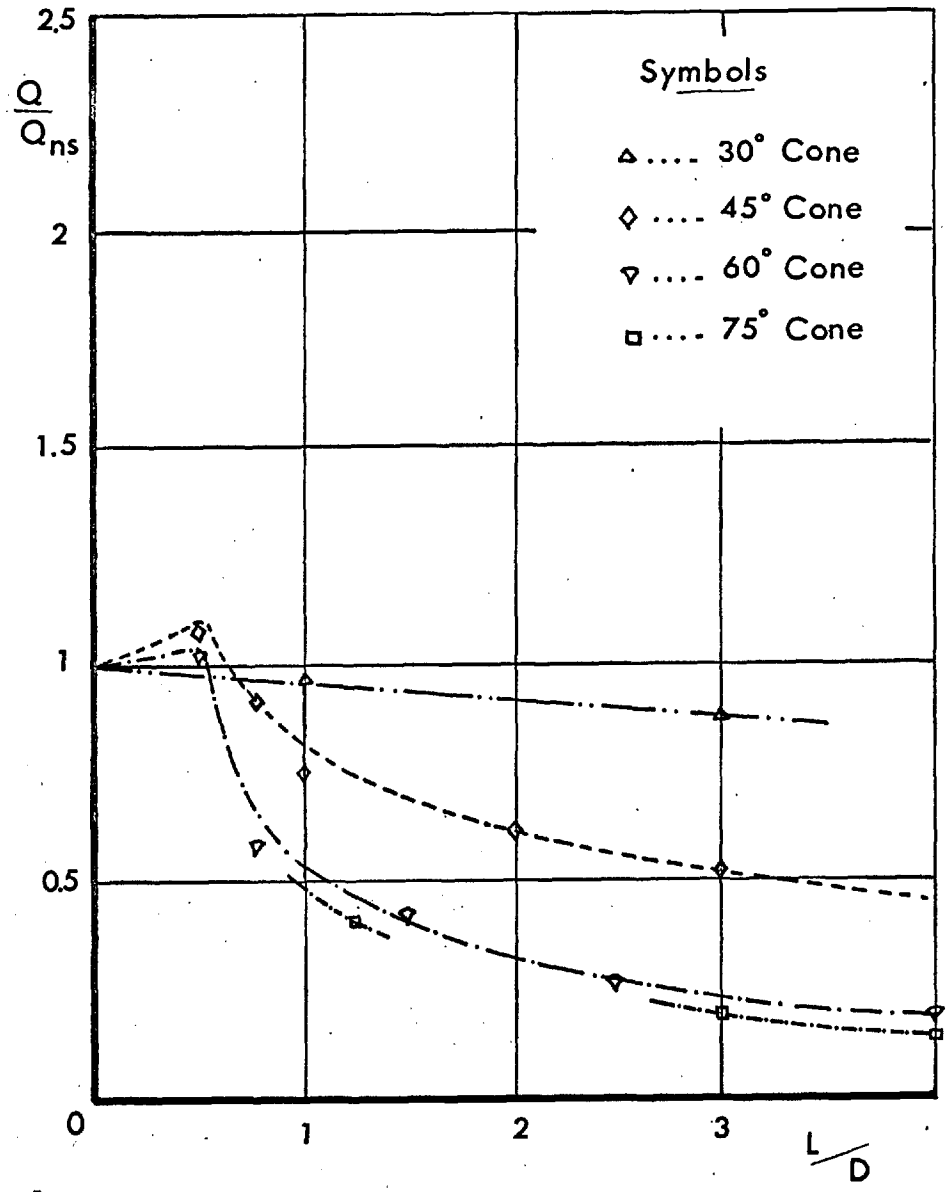

Figure 54b TOTAL HEAT TRANSFER TO SPIKED CONES (M=15)

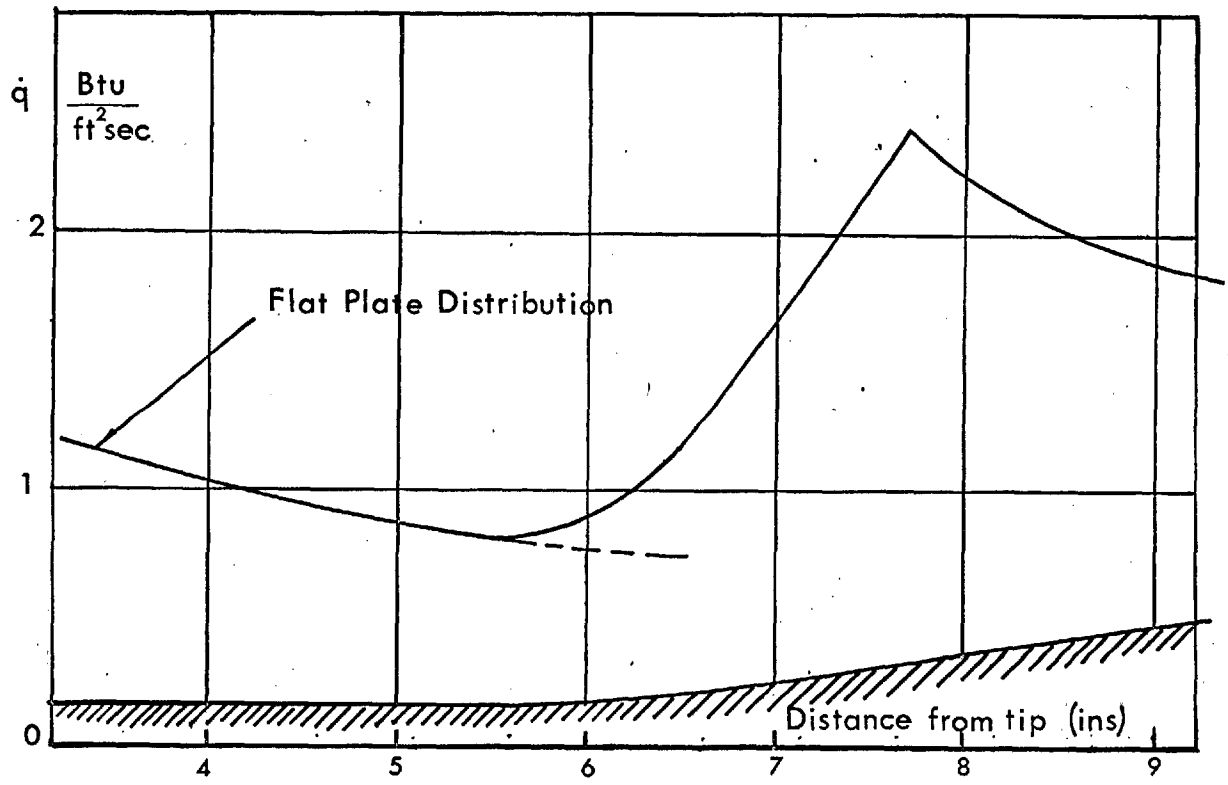

Figure 55a CALCULATED HEAT TRANSFER TO A 7.5° WEDGE

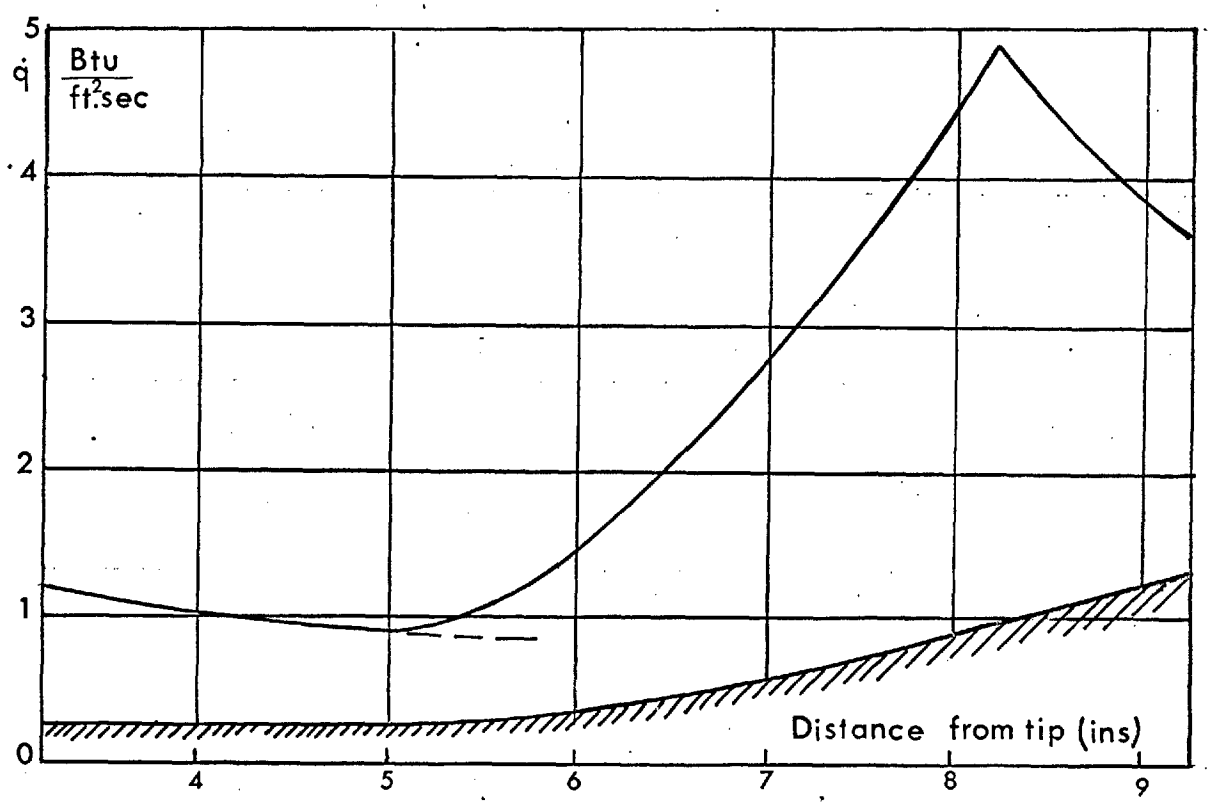

Figure 55b CALCULATED HEAT TRANSFER TO A 12.5° WEDGE

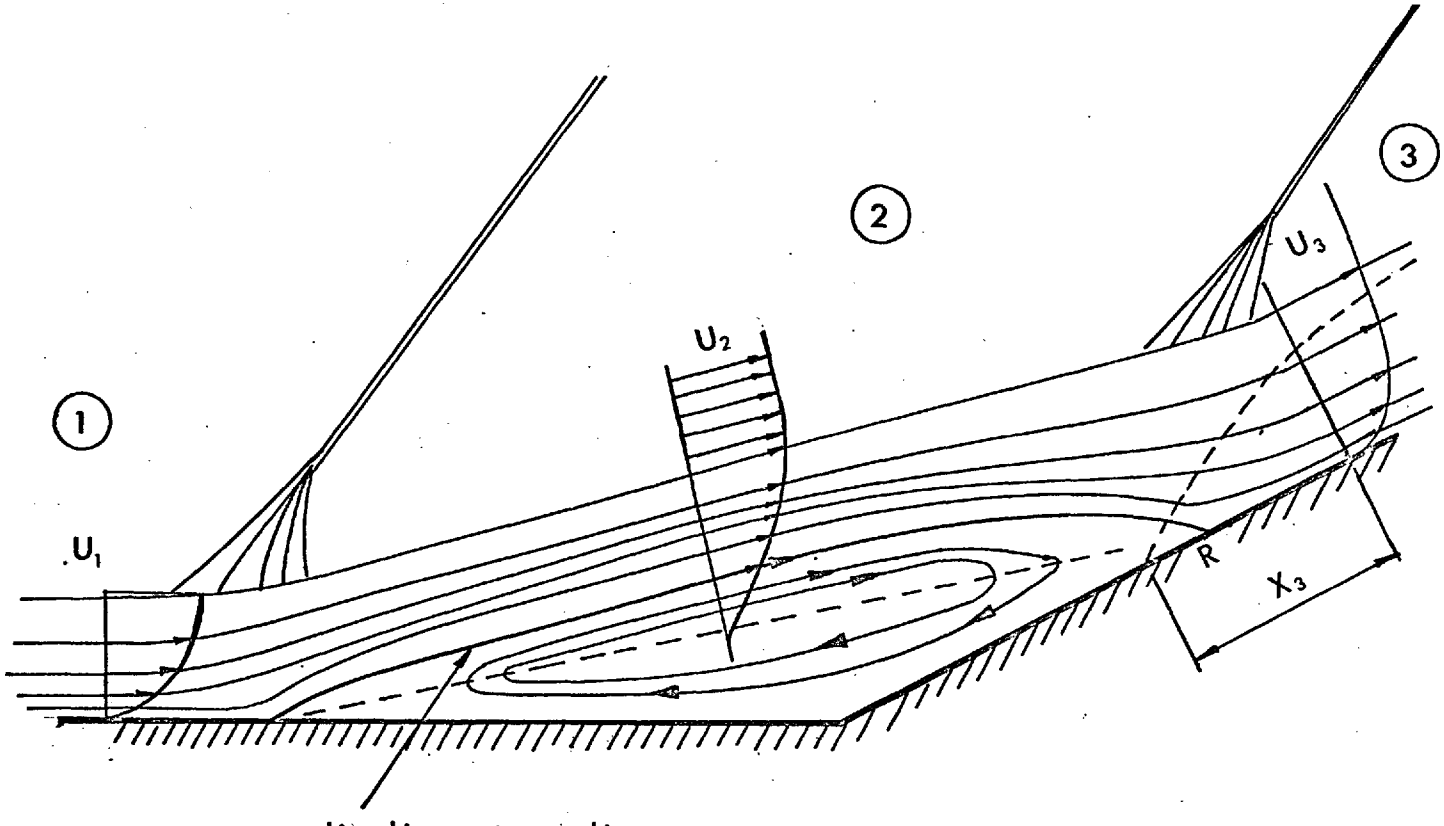

Figure 56 WEDGE SEPARATED FLOW MODEL

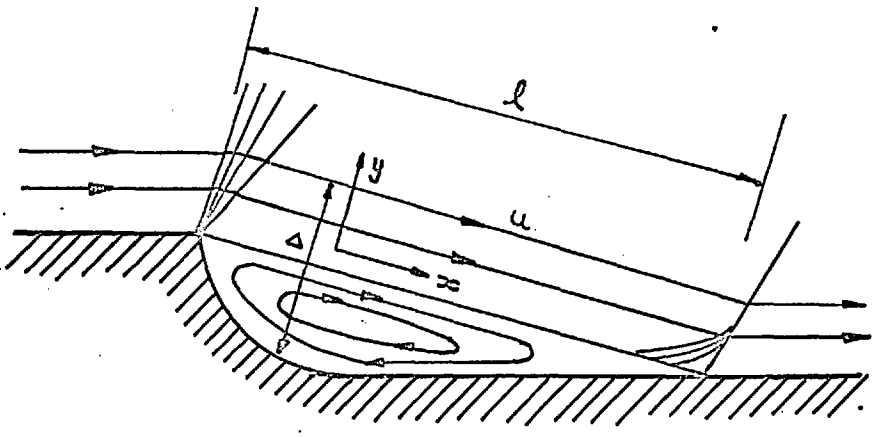

Figure 57 CARLSON'S MODEL FOR HEAT TRANSFER TO CONSTANT PRESSURE SEPARATED FLOW